Doctoral Thesis
Stockholm, Sweden 2014

Large Scale Solar Power Integration in Distribution Grids

PV Modelling, Voltage Support and Aggregation Studies

Afshin Samadi

Large Scale Solar Power Integration in Distribution Grids

PV Modelling, Voltage Support and Aggregation Studies

Afshin Samadi

Doctoral thesis supervisors:

Prof. Lennart Söder, Kungliga Tekniska Högskolan

Members of the Examination Committee:

Prof. Lars Nordström,	Kungliga Tekniska Högskolan
Prof. Luis Rouco,	Universidad Pontificia Comillas
Dr. Marjan Popov,	Technische Universiteit Delft
Prof. Hans-Peter Nee,	Kungliga Tekniska Högskolan
Dr. Stefan Arnborg,	Svenska kraftnät

This research was funded by the European Commission through the Erasmus Mundus Joint Doctorate Program, and also partially supported by the KTH Royal Insititute of Technology.

TRITA-EE 2014:050
ISSN 1653-5146
ISBN 978-91-7595-303-8

Printed by: US-AB 2014

Large Scale Solar Power Integration in Distribution Grids

PV Modelling, Voltage Support and Aggregation Studies

PROEFSCHRIFT

ter verkrijging van de graad van doctor
aan de Technische Universiteit Delft,
op gezag van de Rector Magnificus prof. ir. K.C.A.M. Luyben,
voorzitter van het College voor Promoties,
in het openbaar te verdedigen
op donderdag 13 november 2014 om 10:00 uur

door

Afshin Samadi

geboren te Hamedan, Iran

Dit proefschrift is goedgekeurd door de promotoren:

Prof.dr. Lennart Söder,	Kungliga Tekniska Högskolan
Prof.dr.ir. Paulien M. Herder,	Technische Universiteit Delft, promotor

Samenstelling promotiecommissie:

Prof.dr. Lars Nordström,	Kungliga Tekniska Högskolan
Prof.dr. Luis Rouco,	Universidad Pontificia Comillas
Dr. Marjan Popov,	Technische Universiteit Delft
Prof.dr. Hans-Peter Nee,	Kungliga Tekniska Högskolan
Dr. Stefan Arnborg,	Svenska kraftnät

Keywords: Photovoltaic systems, PV system modelling, reactive power control, droop control, voltage sensitivity analysis, German Grid Codes, relative gain array (RGA), singular value decomposition (SVD), load modeling, system identification.

ISBN 978-91-7595-303-8

Printed by: US-AB 2014

SETS Joint Doctorate

The Erasmus Mundus Joint Doctorate in **Sustainable Energy Technologies and Strategies**, SETS Joint Doctorate, is an international programme run by six institutions in cooperation:

- Comillas Pontifical University, Madrid, Spain
- Delft University of Technology, Delft, the Netherlands
- Florence School of Regulation, Florence, Italy
- Johns Hopkins University, Baltimore, USA
- KTH Royal Institute of Technology, Stockholm, Sweden
- University Paris-Sud 11, Paris, France

The Doctoral Degrees issued upon completion of the programme are issued by Comillas Pontifical University, Delft University of Technology, and KTH Royal Institute of Technology.

The Degree Certificates are giving reference to the joint programme. The doctoral candidates are jointly supervised, and must pass a joint examination procedure set up by the three institutions issuing the degrees.

This Thesis is a part of the examination for the doctoral degree.

The invested degrees are official in Spain, the Netherlands and Sweden respectively.

SETS Joint Doctorate was awarded the Erasmus Mundus **excellence label** by the European Commission in year 2010, and the European Commission's **Education, Audiovisual and Culture Executive Agency**, EACEA, has supported the funding of this programme.

The EACEA is not to be held responsible for contents of the Thesis.

Abstract

Long term supporting schemes for photovoltaic (PV) system installation have led to accommodating large numbers of PV systems within load pockets in distribution grids. High penetrations of PV systems can cause new technical challenges, such as voltage rise due to reverse power flow during light load and high PV generation conditions. Therefore, new strategies are required to address the associated challenges.

Moreover, due to these changes in distribution grids, a different response behavior of the distribution grid on the transmission side can be expected. Hence, a new equivalent model of distribution grids with high penetration of PV systems is needed to be addressed for future power system studies.

The thesis contributions lie in three parts. The first part of the thesis copes with the PV modelling. A non-proprietary PV model of a three-phase, single stage PV system is developed in PSCAD/EMTDC and PowerFactory. Three different reactive power regulation strategies are incorporated into the models and their behavior are investigated in both simulation platforms using a distribution system with PV systems.

In the second part of the thesis, the voltage rise problem is remedied by use of reactive power. On the other hand, considering large numbers of PV systems in grids, unnecessary reactive power consumption by PV systems first increases total line losses, and second it may also jeopardize the stability of the network in the case of contingencies in conventional power plants, which supply reactive power. Thus, this thesis investigates and develops the novel schemes to reduce reactive power flows while still keeping voltage within designated limits via three different approaches:

1. decentralized voltage control to the pre-defined set-points
2. developing a coordinated active power dependent (APD) voltage regulation Q(P) using local signals
3. developing a multi-objective coordinated droop-based voltage (DBV) regulation Q(V) using local signals

In the third part of the thesis, furthermore, a gray-box load modeling is used to develop a new static equivalent model of a complex distribution grid with large numbers of PV systems embedded with voltage support schemes. In the proposed model, variations of voltage at the connection point simulate variations of the model's active and reactive power. This model can simply be integrated into load-flow programs and replace the complex distribution grid, while still keeping the overall accuracy high.

The thesis results, in conclusion, demonstrate: i) using rms-based simulations in PowerFactory can provide us with quite similar results using the time domain instantaneous values in PSCAD platform; ii) decentralized voltage control to specific set-points through the PV systems in the distribution grid is fundamentally impossible due to the high level voltage control interaction and directionality among the PV systems; iii) the proposed APD method can regulate the voltage under the steady-state voltage limit and consume less total reactive power in contrast to the standard characteristic $Cos\phi(P)$ proposed by German Grid Codes; iv) the proposed optimized DBV method can directly address voltage and successfully regulate it to the upper steady-state voltage limit by causing minimum reactive power consumption as well as line losses; v) it is beneficial to address PV systems as a separate entity in the equivalencing of distribution grids with high density of PV systems.

Sammanfattning

Genom att man under lång tid har givit ekonomiska incitament till system med solceller (PV), så har mängden solcellssystem ökat kraftigt i en del distributionsnät. Större mängder solcellsanläggningar kan orsaka nya tekniska utmaningar, såsom spänningsökning. Därför behövs nya strategier till att möta dessa utmaningar.

På grund av dessa förändringar i distributionsnäten, kan man förvänta sig en annan respons från distributionsnäten vid spänningsändringar på transmissionssidan. Därför behövs även en ny modellering av distributionsnät vid hög andel solcellssystem för att kunna genomföra analyser av framtida kraftsystem.

Avhandlingen bidrag ligger inom tre områden. Den första delen av avhandlingen avser PV-modellering. En generisk PV-modell av ett trefas, enstegs solcellssystem har utvecklats i PSCAD/EMTDC och PowerFactory. Tre olika strategier för reaktiv effektreglering har integrerats i modellerna och deras beteende har undersökts i båda simulerings-plattformarna för distributionssystem med stor andel solcellssystem.

I den andra delen av avhandlingen åtgärdas höga spänningar med hjälp av reaktiv effekt. Men man måste även beakta att med många solcellssystem i distributionsnät, kan onödig reaktiv effektförbrukning i solcellssystem för det första öka de totala ledningsförlusterna, och för det andra även äventyra stabiliteten i nätet när det gäller oförutsedda bortfall i konventionella kraftverk, vilka utnyttjas för försörjning av reaktiv effekt. Således undersöker denna avhandling, samt utvecklar nya systemen för, minskning av reaktiva effektflöden samtidigt som man fortfarande ska hålla spänningen inom angivna gränser. Detta studeras med tre olika metoder:

1. decentraliserad spänningsstyrning till fördefinierade börvärden
2. utveckling av en samordnad aktiv effektbaserad (APD) spänningsreglering Q (P) med hjälp av lokala signaler
3. utveckling av en multi-objective spänningsbaserad (DBV) reaktiv effektreglering Q (V) med hjälp av lokala signaler

I den tredje delen av avhandlingen används en gray-box-modellering till att utveckla en ny statisk ekvivalent av ett komplext distributionsnät med många solcellssystem med integrerad spänningsreglering. I den föreslagna modellen varieras spänningen vid anslutningspunkten för att den erhållna ekvivalenten ska ge bra resultat vid olika situationer gällande aktiv och reaktiv effekt. Denna modell kan enkelt integreras i belastningsfördelnings-program och därmed ersätta det komplexa distributionsnätet, men ändå behålla en hög noggrannheten.

Avhandlingen visar att: i) RMS-baserade simuleringar i PowerFactory kan ge liknande resultat som simuleringar med momentan-värden i PSCAD-plattformen; ii) decentraliserad spänningskontroll till specifika börvärden genom solcellssystem i distributionsnät är i grunden omöjligt på grund av den höga interaktionen mellan spänningsregleringen i de olika PV-system; iii) den föreslagna APD-metoden kan reglera spänningen under en statisk spännings-gräns och förbrukar mindre total reaktiv effekt till skillnad mot den vanliga karakteristiska $Cos\phi(P)$ som ingår i German Grid Codes; iv) den föreslagna optimerade DBV-metoden kan direkt åtgärda spänningen och reglera den till den övre statiska spänningsgränsen till ett minimum av reaktiv effektförbrukning och ledningsförluster; v) det är fördelaktigt att beakta solcellssystem som en separat enhet när man gör ekvivalenter av distributionsnät med hög koncentration av solcellssystem.

Acknowledgment

This project was funded by SETS Erasmus Mundus Joint Doctorate and KTH. I would like to express my gratitude towards all partner institutions within the program as well as the European Commission for their support.

There are many people who helped me in various ways to accomplish this work, for which I am grateful. First of all I would like to deeply thank my supervisor Professor Lennart Söder for giving me the opportunity to carry out this PhD as well as supporting me during the program. I am truly grateful to Associate Professor Robert Eriksson for kindly helping me to direct my research in a fruitful direction and providing me valuable feedback. My special thanks to Dr. Barry Rawn for his generous hospitality, valuable feedback and constructive comments during and after my mobility period in TU Delft. I would like to thank Ebrahim Shayesteh for all fruitful discussions and his contribution in some of my papers. I would also like to acknowledge Professor Mehrdad Ghandhari for his kind support.

I would like to thank my colleagues at KTH and TU Delft for fun and interesting discussions that we had during lunch and coffee breaks.

Above all, I would like to express my heartfelt gratitude to my mother, brothers and sister, as ever, for their generous love, support and encouragement.

Science... never solves a problem without creating ten more.
— George Bernard Shaw

Contents

Contents

Chapter 1

Introduction

This chapter introduces the background of the photovoltaic systems integration into grids, presents the associated challenges with high PV penetration, discusses the necessity of the presented research in thesis, defines objectives and scope, demonstrates the scientific contributions and publications, and finally provides the general outline of the thesis.

1.1 Background

Steadily diminishing fossil fuel resources in Europe, on the one hand, and long term planning for decreasing green house gas emissions, on the other hand, have promoted use of renewable energy resources in the European Union's policies. For instance, the European Directive 2009/28/ EC obliges the state members to the predefined renewable energy targets by 2020 [1, 2]. Deploying renewable energy resources not only environmentally helps the CO2 balance but also positively affects the trade deficit of the EU due to energy imports. There is currently a hot discussion regarding the renewable energy targets for 2030 and it is expected to roughly have 70% new installed renewable power capacity out of the total new installed power capacity between 2013 and 2030 [1].

Photovoltaic systems are a key option among the available renewable energy sources. The abundant availability of the sun power in each country provides a better ground for deployment of PV systems as a potential energy resource. Moreover, distributed PV systems, in contrast to the other renewable energy sources such as wind power generators, are more easily integrated into the distribution grids at any point, for instance by installing at rooftops of buildings. Furthermore, the ever-decreasing cost of PV systems installations along with encouraging feed-in tariffs have even more put PV systems in the limelight. The focus on more integration of PV systems along with a maturity in their technology and market have led to a huge drop in PV systems electricity cost in recent years, roughly 60% from 2008 to the second quarter of 2013 [1]. It is worth mentioning that during the same period, the module prices, which used to be the dominant factor in the total PV cost, have dropped even more, around 80%, and now represents less than 40% of the total cost of a PV system [1]. Consequently, the PV-generated electricity price in some residential

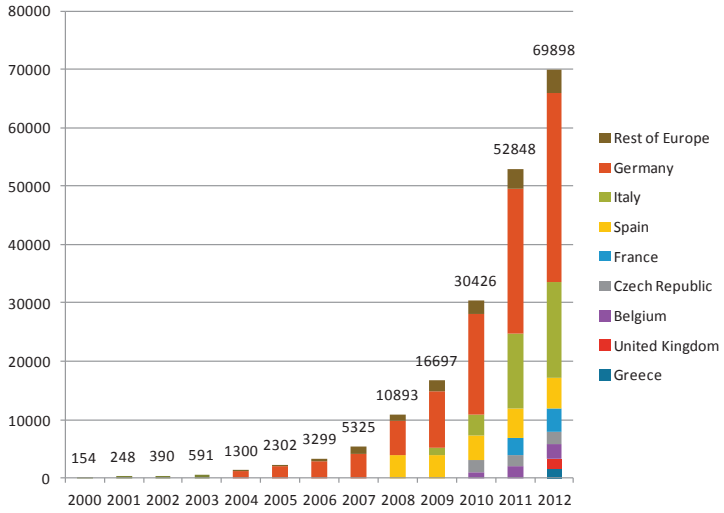

Figure 1.1: Installed PV capacity by the end of 2012 in the Europe states (in MWp) [2].

regions is already cheaper than the retail price. Therefore, the grid parity, defined as the moment when the cost of electricity generated by PV is competitive with the retail price, is already met [1, 3–6]. The falling cost of PV systems and the associated residential grid parity will steadily open new markets for PV systems.

PV industry has been one of the fastest growing industry based on the compound annual growth rate of PV systems, which has been around 55% over the last decade [1]. Fig. 1.1 depicts the evolution of cumulative PV electricity generation capacity in the European states by the end of 2012 in which about 70 GWp[1] was installed and contributed to the 2.5% of the final consumption [2]. The cumulative PV generation capacity has increased 373 times from 185 MWp in 2000 to roughly 70 GWp in 2012 shown in Fig. 1.1. Installed PV generation capacity in 2012 scored the first rank among all other installed power generation units, 51.7% of the net new power capacity. Fig. 1.2 shows the global market share of the cumulative installed PV capacity; Germany and Italy scored the first place and the second place in the global market share [7]. Though Europe has dominated the global PV market, more than 50%, an emerging secondary market outside Europe is growing [7]. For instance, PV market in China grew by 3.7 GWp in 2012, which shows 300% increase compared to 2010, and followed by 12 GWp in 2013, which was above the expected government's stated number 10 GWp [1, 8]. In addition to that, in China, an ambitious target of 100 GWp by 2020 is under discussion. There is also a big growth in Japan's PV market in 2012 by connecting 1.7 GWp to reach about 6.6 GWp that in turn followed in 2013 by a boom of 6.9 GWp new installed capacity [1, 8].

[1]The size of PV systems is typically expressed in watt-peak (Wp).

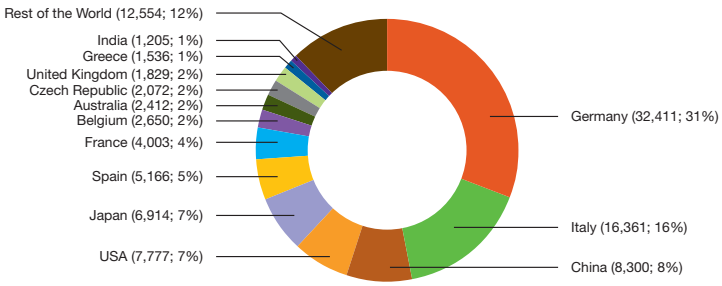

Figure 1.2: Global market shares of cumulative installed PV capacity by the end of 2012 (in MWp) [7].

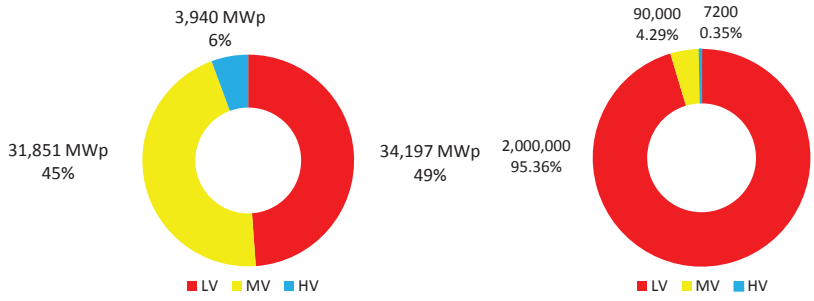

Figure 1.3: Estimation of installed PV systems per voltage level in Europe by the end of 2012: (a) cumulative capacity (b) number of connections [2].

Though PV systems can be integrated into high, medium and low voltage grids, they are mainly connected to the medium and the low voltage grids. Fig. 1.3a shows the estimated installed PV capacity per voltage level in Europe by the end of 2012 [2]. The estimated numbers of the installed PV systems per voltage level are illustrated in Fig. 1.3b [2]. Nevertheless, PV systems have unevenly been spread out within different European countries and even more uneven within the voltage levels and different regions of a country. In Germany, for instance, there are more than 33 GW of installed PV systems by end of March 2013, of which 70% have been connected to the low voltage (LV) grids and about 25% to the medium voltage (MV) grids [2]. Besides, regional differences are also comparatively significant and some regions in Germany, for example, have already encountered high local penetration of more than 200 kW/km^2 compared to the national average, which is 39 kW/km^2 [9, 10]. Accordingly, the LV grids have been more prone to experience the high density of PV connections.

The focus in this thesis is on the LV distribution grids. For many years power was only generated at large-scale conventional power plants at the high voltage levels and then delivered to consumers located mainly in distribution grids at the medium and the low voltage levels. Nevertheless, the presented statistics demonstrate how drastically this model in mind has changed during the last decade and now pure consumers in the distribution grids have changed to prosumers, which not only consume but also produce power via small-scale PV systems (or other distributed sources). This evolution in the nature of the power system operation, likewise other evolution phenomena in the nature, needs adaptations for survival.

1.2 Challenges and motivations

High penetrations of PV systems within load pockets in distribution grids have led to technical challenges such as reverse power flow and overvoltage [2, 9, 11–19]. One of the main challenges for distribution system operators (DSO) is keeping the voltage profile within an acceptable band designated by standards. Voltage violations due to the surplus flow of PVs power would have a negative impact on the stable operation of both supply-side units and demand-side appliances. Overvoltage may also shorten the life time of equipment. In this regard, integration of more PV systems in grids may be delayed if no proper action is taken. It is therefore required to contrive remedies to resolve the aforementioned consequences of high PV power penetrations and in the meantime increase the grid hosting capacity of PV systems.

Different remedies have been proposed to deal with the unwanted voltage problem associated with high PV systems penetrations that can generally be divided into three categories, namely system level, plant level and interactive level.

The system level has to do with remedies that target the grid side rather than costumers or PV plants. Plant level remedies focus on PV plants and are installed before the point of common coupling (PCC). The interactive level includes solutions in-between, in which a communication infrastructure is required to link decision making units, installed at different locations in the grid, with plant components.

The system level remedies with the high effectiveness in the LV grids are [2]

- **Grid Reinforcement** [2, 9] in which the capacity of transformers and the cross-sectional area of conductors can be augmented by adding new transformers and lines. Though this solution is effective and simple for supporting the voltage profile, it is first costly, especially in the case of underground cables, and second quite cumbersome in terms of making an efficient planning to address further developments of loads and generation.

- **On Load Tap Changer (MV/LV transformer)** [9, 20–22] can control the low voltage side of the transformer to suppress the overvoltage. On the contrary, since the MV/LV transformers usually feed several feeders, lowering voltage to mitigate overvoltage on one feeder may lead to undervoltage in a neighboring feeder with less or no PV power surplus. It is also worth mentioning that MV/LV transformers in

the current distribution grids are not equipped with on load tab changer capability; therefore, adding this function will increase the cost of MV/LV stations.

The plant level remedies with the high effectiveness in the LV grids are [2]

- **Plant Level Storage** [22, 23] can be deployed to save the surplus of the PV power for the later use especially in peak demand. The large cost of storage systems is the main disadvantage.

- **Active Power Curtailment** [9, 12, 16, 24] can be used to reduce feed-in peaks of PV systems and in turn reduce the surplus of the PV power generation. The loss of income followed by the loss of energy is the main disadvantage of this approach. It is also important to state that this remedy is in contrary with the spirit of the European Directive rules on privileged integration and priority access for renewable energy sources [2]. Therefore, this remedy should be the last applicable option, when all other inexpensive remedies cannot solve the problem [2].

- **Reactive Power Control** [9,13,25–28] through PV systems can mitigate the voltage violation caused by PV active power generation. The effectiveness of voltage control via reactive power regulation depends on the R/X ratio of the feeder; the lower the R/X ratio the better the efficiency. Therefore, reactive power supports are relatively more effective in the MV grids than the LV grids due to the inherited lower R/X ratios.

- **Static var compensator (SVC)** [2] can be installed in LV grids to suppress the voltage rise caused by PV systems generation. This approach is relatively expensive and it is often necessary to install SVC outside of substations in order to reach a high efficiency in voltage mitigation. Moreover, as mentioned earlier, voltage compensation via reactive power in LV grids might be less effective than MV grids.

The interactive level remedies such as demand side management and supervisory control systems rely on a communication infrastructure. Moreover, the effectiveness of these methods in the LV grids, in contrast to the aforementioned methods on the system level and the plant level, are considered less [2].

With that being said, each remedy has its own pros and cons. However, from an economic point of view, the voltage profile regulation via reactive power contribution of PV systems is to be preferred over other remedies [9]. Moreover, there is no technological barrier because PV systems can simply modulate reactive power similar to producing active power; therefore, reactive power regulation does not require any new physical component except oversizing the PV inverter to accommodate the reactive power contribution. Since the cost of a residential PV inverter is less than 9% of the installed PV system cost [1], oversizing the PV inverter by 12% for accommodating a power factor of 0.9 would not be costly. From the regulations perspective, the regulatory barriers have been resolved in some countries like Germany and the German Grid Codes (GGC) allow reactive power contribution in the LV grids [29].

Therefore, the main focus of the research presented in this thesis is on using reactive power capability of PV systems at the plant level to regulate voltage.

Considering large numbers of PV systems in grids, unnecessary reactive power consumption by PV systems firstly increases the total line losses, and secondly it may also jeopardize the stability of the network in the case of contingencies in conventional power plants, which supply reactive power [30]. Therefore, it is of great importance to figure out mechanisms that can keep the voltage within the designated boundaries with the minimum reactive power consumptions. Furthermore, since the communication infrastructure does not normally exist in the distribution grids, it is crucial to develop offline coordination mechanisms between adjacent PV systems. Hence, this thesis, as compared to the current available methods, investigates and proposes voltage support schemes that are able to coordinate PV systems to reduce reactive power consumption without the aid of communication systems.

Due to the high-density interconnection of PV systems in the contemporary power systems, the power flow is not unidirectional anymore. This phenomenon, apart from the local challenges, may change active and reactive power responses of distribution grids (lower level grids) to voltage variations in power transmission grids (higher level grids). The change in the voltage-power characteristic at the lower level grids may affect the behavior of the higher level grids. Accordingly, it is a matter of importance to address how to model new distributions grids for the higher level studies.

Normally, the dimension of distribution grids is high due to large number of sections, branches and load points necessary in routing feeders through public districts [31]. Besides, the real size of power transmission grids can basically be quite big and, therefore, considering a detailed distribution grid to study power transmission systems is neither practical nor necessary. Consequently, distribution grids are generally considered as an aggregated load model in studies of the higher level grides. The aggregated load model of a distribution grid is normally represented by the constant voltage, constant current and constant power load model (ZIP load model) [32–37]. With emerging PV systems, they have normally been considered as a negative load due to their scarcity [38–41]. Nevertheless, as stated earlier, the growing PV penetrations can change the voltage-power characteristic of the distribution grids. Furthermore, equipping PV systems with voltage support schemes may even cause more changes in the behavior of the distribution grids. Consequently, it is necessary to find new equivalent models that can capture the dominant behavior of the distribution grids with the high density of PV systems embedded with voltage support schemes.

To summarise what said above, this thesis addresses the following questions

1. How does an individual PV model with the reactive power regulation ability behave?

2. Is it possible to obtain a certain voltage profile via PV systems considering controller reactions?

3. Are the proposed reactive power regulations in the standards efficient? If not, how can they be improved?

4. Is there a need for a new reactive power characteristic than the proposed ones by standards? If yes, how should they be designed?

5. How to make a proper equivalent of distribution grids with high PV penetration?

1.3 Scope and objective

The work presented in this thesis was performed within Sustainable Energy Technologies and Strategies (SETS) Erasmus Mundus Joint Doctorate Program supported by the European Commission. The overall aim of this thesis is to investigate and develop proper voltage support schemes via reactive power regulation of PV systems, and further to develop an equivalent model of distribution grids with the high density of PV systems embedded with voltage support schemes. To do this, one first needs to get a proper insight into operation of one individual PV system. Thus, at the first stage of the doctoral project, the work focus was mainly on the instantaneous modelling of a PV system to study its behavior.

Since voltage regulation through PV systems must operate within one to a few seconds, a quasi-static analysis is assumed to be appropriate. Therefore, quasi steady-state power flow calculation is considered for designing voltage support schemes, which basically means the system dynamics and transient disturbances are not considered. Features of the voltage sensitivity matrix are deployed for designing different voltage support schemes.

This thesis only addresses technical aspects of possible solutions for keeping voltage profile under the steady-state voltage limit while reducing PV reactive power consumption, and so, the financial consequences of different policies are not analysed here.

It is worth mentioning that the focus in this thesis is to propose and develop methods that can address overvoltage associated with high PV penetration. Nevertheless, the proposed methods can be extended to address under voltage situations in case of weak grids when load demand is much higher than the production of PV systems. However, this is not studied in this thesis.

The applications of load modelling can basically be divided in two categories: 1) static applications and 2) dynamic applications. In this thesis only the static applications, which incorporate only the voltage-dependant characteristics, are considered for equivalencing distribution grids with high PV penetrations.

1.4 Scientific contribution

The contributions of this thesis lie in three areas: first in modelling and studying behavior of an individual PV system; second, in evaluating voltage profile support schemes through different reactive power strategies embedded in PV systems; third, developing a static equivalent model of distribution grids with a high density of PV systems. The contributions of the thesis are summarized as follows:

1. Modelling

- Developing a non-proprietary PV model of a three-phase, single stage PV system incorporated with three different reactive power regulation strategies in PSCAD/EMTDC simulation platform [P-I];
- Comparing the developed model based on the time domain instantaneous values, PSCAD/EMTDC platform, with a similarly developed model based on the rms values in PowerFactory platform [P-II];

2. Voltage Control/Support

   - Using the voltage sensitivity matrix along with control theories, namely Relative Gain Array and Condition Number, to evaluate the possibility of controllability among PV systems for controlling voltage profile to predefined setpoints, [P-III];
   - Developing a novel coordinated active power dependent voltage regulation method Q(P), which utilizes the voltage sensitivity matrix of one operating point to determine individual Q(P) characteristics that use local information but provides a coordinated response without the aid of communication systems. [P-IV].
   - Optimizing the proposed method in paper IV using an optimization formulation to optimally coordinate the parameters of individual Q(P) characteristics while still local measurements are employed [P-V];
   - Developing a multi-objective coordinated droop-based voltage regulation method Q(V) in which a multi-objective design is used to adjust the parameters of the Q(V) characteristic without the aid of communication systems [P-VI];

3. Equivalencing

   - Using gray-box modelling concept to develop a static equivalent model of distribution grids with large number of PV systems embedded with voltage support schemes [P-VII].

Table 1.1 illustrates the correspondence between the publications and the concepts used in the contributions.

1.5 List of publications

Publication I (P-I)

A. Samadi, M. Ghandhari and L. Söder, "Reactive Power Dynamic Assessment of a PV System in a Distribution Grid," *Energy Procedia*, vol. 20, pp. 98-107, 2012.

Publication II (P-II)

A. Samadi, R. Eriksson, D. Jose, F. Mahmood, M. Ghandhari and L. Söder, "Comparison of a Three-Phase Single-Stage PV System in PSCAD and PowerFactory," *Proc. 2nd International Workshop on Integration of Solar Power into Power Systems*, Lisbon, Portugal, pp. 237-244.

Table 1.1: Items considered in the various publications.

	Publication						
	I	II	III	IV	V	VI	VII
PV modelling	✓	✓					
Dynamic studies	✓	✓					
Quasi steady-state			✓	✓	✓	✓	✓
Evaluation of voltage controllability via PVs			✓				
Active power dependent power factor $Cos\phi(P)$	✓	✓		✓	✓	✓	✓
Active power dependent reactive power characteristic Q(P)				✓	✓		
Droop-based voltage regulation Q(V)	✓	✓				✓	
Aggregation							✓
Optimization					✓	✓	✓

Publication III (P-III)

A. Samadi, R. Eriksson and L. Söder, "Evaluation of Reactive Power Support Interactions Among PV Systems Using Sensitivity Analysis," *Proc. 2nd International Workshop on Integration of Solar Power into Power Systems*, Lisbon, Portugal, pp. 245-252.

Publication IV (P-IV)

A. Samadi, R. Eriksson, L. Söder, B. Rawn and J.C. Boemer "Coordinated Active Power Dependent Voltage Regulation in Distribution Grids with PV Systems," *IEEE Transaction on Power Delivery*, vol. 29, pp. 1454-1464, June 2014.

Publication V (P-V)

A. Samadi, E. Shayesteh and L. Söder "Optimal Coordination of Q(P) Characteristics for PV Systems in Distribution Grids for Minimizing Reactive Power Consumption" *CIGRE, AORC Technical meeting* , May 2014, Japan.

Publication VI (P-VI)

A. Samadi, E. Shayesteh, R. Eriksson, B. Rawn and L. Söder "Multi-Objective Coordinated Droop-Based Voltage Regulation in Distribution Grids with PV Systems" *Renewable Energy*,vol. 71, pp. 315-323, Nov. 2014.

Publication VII (P-VII)

A. Samadi, L. Söder, E. Shayesteh and R. Eriksson "Static Equivalent of Distribution Grids with High Penetration of PV Systems Embedded with Voltage Support Scheme" *Provisionally accepted to IEEE Transaction on Smart Grid*.

1.6 Division of work between authors

Publication I, III, IV

A. Samadi made the outline, work and wrote these papers under the supervision of L.Söder, R. Eriksson, M. Ghandadhari and B. Rawn.

Publication II

A. Samadi made the outline, wrote the paper and performed the work except the model in PowerFactory which was developed by D. Jose and F. Mahmood with the help of **A. Samadi**. This work was performed under the supervision of R. Eriksson, M. Ghandhari and L. Söder.

Publication VI

A. Samadi made the outline and wrote the paper. **A. Samadi** performed the simulation, modeling and analysis except the optimization in GAMS which was contributed by E. Shayesteh. This work was performed under the supervision of B. Rawn, R. Eriksson, and L. Söder.

Publication V and VII

A. Samadi made the outline, work and wrote the paper. E. Shayesteh contributed his knowledge in optimization and equivalencing. These studies were performed under the supervision of L. Söder and R. Eriksson.

1.7 Thesis outline

The rest of this thesis is organised as follows:

Chapter 2 briefly describes the evolution history of PV systems, defines various components involved in a PV system, presents a three-phase single-stage PV model, and further discusses different strategies for regulating reactive power of PV systems presented in Papers I and II.

Chapter 3 provides a brief background on load flow and sensitivity analysis. It also describes how features of voltage sensitivity matrix in conjunction with the relative gain array and the singular value decomposition can be used to quantify the level of interaction among PV systems in case of using direct AC-bus voltage control strategy, and along with evaluation of the voltage controllability.

Chapter 4 demonstrates how the features of the voltage sensitivity matrix allow systematic coordination of Q(P) characteristics among PV inverters while still using local measurements as presented in Papers IV and V.

Chapter 5 depicts how the features of the voltage sensitivity matrix in association with droop control concept can be used through a multi-objective design to optimally coordinate characteristics of the droop-based voltage reactive power among PV systems in radial distribution feeders. Along with Paper VI is introduced.

Chapter 6 describes the use of gray-box modeling concept in system identification to develop a static equivalent model of distribution grids with high level penetrations of PV systems embedded with the GGC standard characteristic $Cos\phi(P)$. This chapter also introduces Paper VII.

Chapter 7 highlights the key conclusions of the thesis and summarizes ideas for future research work.

Chapter 2

Grid-connected PV systems

This chapter briefly describes the evolution history of PV systems, defines various components involved in a PV system, presents a three-phase single-stage PV model, and further discusses different strategies for regulating reactive power of PV systems presented in Papers I and II.

2.1 Background

The fundamental element of PV systems is solar cells, which are made of semiconductor materials to convert sunlight to the electricity. The very first practical application of PV systems was providing electricity for the orbiting satellite Vagnuard I in 1958 [42]. The material of the first generation solar cells was single crystal silicon wafers. The huge cost of solar cells as well as the low efficiency limited the use of photovoltaic systems to only space applications for many years. Nevertheless, the need for alternative energy resources directed much attention towards terrestrial applications of PV systems. Therefore, solar cells were gradually used in terrestrial applications such as grid connected PV systems. During the last decade, long term supporting schemes have provided big markets for grid-connected applications that in turn channelled more researches and investments in solar cells technologies. Consequently, the price and the efficiency of solar cells have dramatically improved to the extent that new generations of solar cells have been introduced and, moreover, grid-parity (defined as the moment when the cost of electricity generated by a grid-connected PV is competitive with the retail price) has already been met in some residential regions [1, 5, 6]. PV systems hereafter refer to grid-connected PV systems.

2.2 Components of PV systems

The building blocks of a typical PV system is illustrated in Fig. 2.1. The system is composed of two main components: 1) solar arrays, and 2) a power conditioning unit (PCU). The sunlight is converted to DC power electricity via solar arrays and the generated DC power is in turn converted to AC power through the PCU. Some part of the generated AC

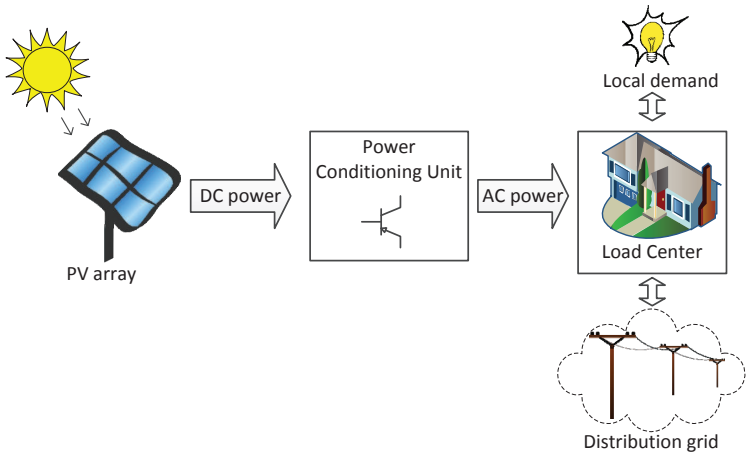

Figure 2.1: Schematic of the building blocks of a typical grid-connected PV system.

electricity power is consumed by local loads and the surplus of the AC power is pumped into the distribution grid. In the following, elements involved in PV system operation are briefly discussed.

2.2.1 Sunlight

The solar radiation incident on a particular earth's surface drastically varies due to different reasons such as atmospheric effects, clouds, water vapors, pollution, latitude of the location, the time of the day, and the season of the year. Therefore, the instantaneous received power of solar radiation on the earth's surface significantly varies. The instantaneous power of radiation incident per unit area is called irradiance and expressed in [W/m^2]. The global solar irradiance on a horizontal surface on the earth is composed of two components, namely direct and diffuse [43, 44]. The direct component is the part of global irradiance that directly reaches on the horizontal surface. The diffuse component is the part of the global irradiance that scattered by passing through the atmosphere. For tilted surfaces, there is another component called Albedo, which is the part of solar irradiance that is reflected by the earth's surface [43, 44]. The irradiance is normally used to evaluate the performance of a PV system at each point of a day. In design of a PV system, however, the average of the solar irradiance over a time period is deployed. The integration of solar irradiance at a particular location over a time period is called solar irradiation or insolation expressed in [kWh/m^2]. The yearly solar irradiation is normally used as a measure to assess the potential of solar electricity generation as well as economic aspects at different regions. For a typical crystal silicon PV system with horizontally mounted solar panels, for instance, yearly solar electricity generation at residential areas in Northern European countries (e.g. Denmark, South Sweden, Baltic countries, North Germany and France)

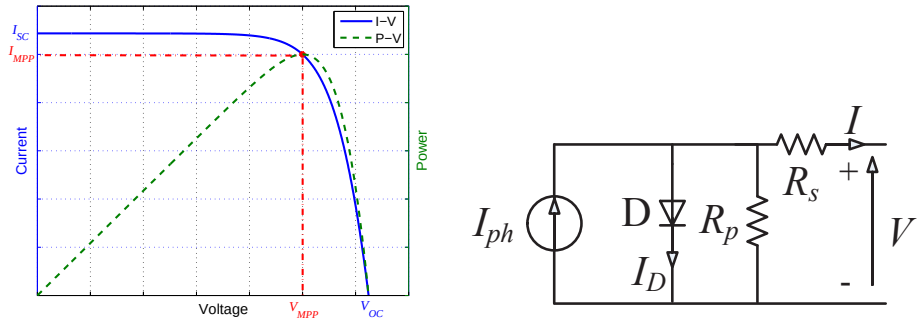

(a) (b)

Figure 2.2: Solar cell: (a) I-V and P-V characteristics; (b) Electrical equivalent model.

mainly falls in the range of 700-800 kWh per kWp; the diffuse radiation has the highest share in these regions [45]. The highest potential for solar electricity generation is located at Southern European countries (e.g. Portugal, Spain and Italy) with yearly production in the range of 1100-1350 kWh per kWp [45]. The poorest solar electricity generation is in Northern Sweden and Finland that falls bellow 700 kWh/kWp [45]. Installing solar panels in an optimum inclination angle and orientation can boost yearly solar electricity production by 9-26%; increments higher than 16% can be attained in Scandinavian and Baltic countries [45].

2.2.2 Solar cells

Solar cells are generally a semiconductor-based electronic device that converts sunlight to electricity power composed of voltage and current. Normally, the output of a solar cell is characterized by current-voltage curve and power-voltage curve. Fig. 2.2a shows the typical I-V characteristic curve of a solar cell for a certain irradiance assigned to the left hand side *y*-axis. Two main parameters of each I-V characteristic are open circuit voltage V_{OC} and short circuit current I_{SC}. These two parameters heavily depend on the irradiance level and the cell temperature. Irradiance variations mainly affect the short circuit current of solar cells while temperature variations mainly affect the open circuit voltage. Fig. 2.2a shows a typical P-V characteristic of a solar cell for a certain irradiance assigned to the right hand side *y*-axis. Two main parameters of the P-V curve are voltage V_{MPP} and current I_{MPP} at maximum power point.

An ideal electrical equivalent of a solar cell is modeled by a current source in parallel with a diode. Nevertheless, since losses are inherited part of any physical component in the real world, a series resistance and a shunt resistance may be added to make a more realistic equivalent. The schematic of a single-diode electrical equivalent of a solar cell is shown in Fig. 2.2b.

The I-V characteristic of the single-diode model is mathematically represented as follows [46, 47]:

$$I = I_{ph} - I_o \left(e^{\frac{V+R_s I}{AV_t}} - 1 \right) - \frac{V + R_s I}{R_p} \tag{2.1}$$

where I_o is the dark saturation current, R_s is the cell series resistance, R_p is the cell parallel resistance, A is the diode quality factor, I_{ph} is the photo-generated current and V_t is the junction thermal voltage, which is described by

$$V_t = \frac{kT_{STC}}{q} \tag{2.2}$$

where k is the Boltzmann's constant, q is the charge of the electron and T_{STC} is the temperature at standard test condition (STC), when the solar irradiance on the surface of the cell is 1000 [kW/m^2] and the temperature of the cell are 25^{o}C. Different approaches have been proposed to identify the parameters of the solar cell equivalent [46–48].

A solar cell delivers a certain power according to its I-V characteristic. Therefore, solar cells must be connected together to provide adequate voltage and current for practical applications. In this regard, solar cells are connected in series to form solar modules; solar modules in turn are connected in series or in parallel and mounted on a supporting frame to form solar panels. Solar panels are also connected in series and in parallel to form solar array in order to provide adequate power and voltage for being connected to grid.

The equivalent model of a solar array is represented analogous to the solar cell equivalent in 2.1 by incorporating the number of parallel and series cells of the solar array.

The size of PV systems is typically expressed in watt-peak (Wp) and this basically represents the output power of PV array at the STC [45].

2.2.3 Power conditioning units

Solar arrays produce uncontrolled DC power; therefore, PCUs are employed to first control the arrays DC output power and second convert the DC power to the high quality AC power. From power processing perspective, the PCU of PV systems can be either single-stage or double-stage systems. In a single-stage PV system, the DC power of solar arrays is directly converted to the AC power via an inverter, while a DC-DC converter prior to the PV inverter is incorporated into a double-stage PV system. In contrast to single-stage PV systems, double-stage PV systems provide higher flexibility in power control, but at the expense of extra cost and lower reliability [49].

At a specific irradiance, the power operating point of solar cells and similarly solar arrays is not necessarily located at the corresponding maximum power point. Therefore, one of the main tasks of PCUs is to regulate the voltage and the current of a PV array such that the PV array can deliver its corresponding maximum power at that certain irradiance. This task is called maximum power point tracking (MPPT). Different MPPT algorithms have been proposed and implemented in PV systems to the extent that there are at least nineteen distinct algorithms in the literature [50].

The other main task of PCUs is controlling injected AC current such that the injected AC current first attains the same frequency as the grid, and second, depending on size of PV active and reactive power, yields a proper phase-shift with respect to the voltage at the point of connection.

PCUs must also be able to perform other tasks such as islanding detection, protection, voltage amplification, and filtering harmonics [51, 52].

2.3 Single-stage PV model

One of the main challenges associated with studying PV system behaviors has been the availability/lack of non-proprietary PV models. Though companies may have their own proprietary detailed-model information, it is hard to get the information of such models. Hence, there has been a need to develop a non-proprietary model that can capture the dominant behaviour of PV systems embedded with reactive power regulation functions in order to examine the behavior of PV systems in a distribution grid. Moreover, it is worth mentioning that implementation of reactive power control strategies is a challenge, because some criteria, according to standards, must be fulfilled, but it has not explicitly been mentioned which procedure and how.

There were some PV models in the literature [28, 53–55], these models mostly assumed unity power factor operation for PV systems [53–55] or just considered reactive power support for medium voltage connected PV systems [28]. However, a detailed residential PV model in LV grids that can represent different reactive power regulation strategies had not been addressed in the literature.

In the first stage of the PhD project, therefore, a non-proprietary PV model of a three-phase, single-stage PV system is developed in Paper I, which describes controller design procedure and introduces a novel investigation on the important aspects of three different reactive power regulation strategies. The model first implemented in the PSCAD simulation platform based on the instantaneous values, and further developed in the PowerFactory simulation platform based on the rms values to also evaluate differences and similarities between these two domains.

Fig. 2.3 illustrates the main schematic of the developed, three-phase, single-stage PV system model connected through a transformer to a distribution grid. The PV system model consists of solar array, dc-link capacitor, voltage source converter (VSC) and peripheral control systems. The output power of the solar array feeds in the dc-link capacitor and is converted through the parallel connected VSC to AC power. Terminals of the VSC are connected to the PCC via an interface reactor, which shown by L and R, where R represents the resistance of both the reactor and VSC's valves. C_f is a low-pass filter to eliminate high order current harmonics generated by VSC switching. The PV system is interfaced with the grid through a transformer, which makes an isolated ground and also amplifies the output voltage of the PV system to match with the grid voltage level. The distribution grid is modeled by the Thevenin equivalent, where R_g and L_g are equivalent grid resistance and inductance, respectively.

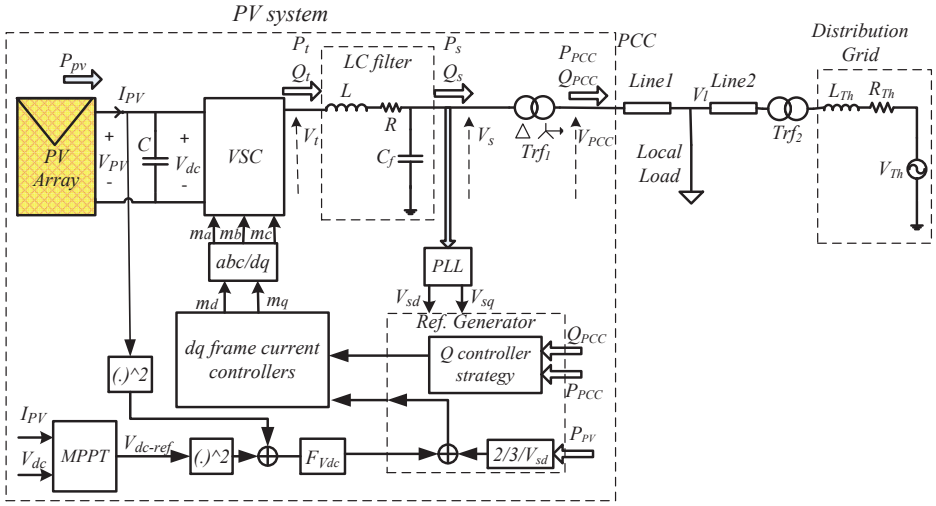

Figure 2.3: Schematic of a three-phase, single-stage PV system structure connected to a distribution grid.

Phase Lock Loop (PLL) is used to convert ac signals in the abc-frame to corresponding dc quantities in a proper dq-frame. Using dc control signals instead of sinusoidal-varying signals, which are synchronized with the grid frequency, streamlines control process. Active and reactive powers of the PV system are controlled via the d and q axes, respectively. Active power is controlled through regulating dc-link voltage. Reactive power control will be explained in the next subsection. Control process comprises three control loops: inner, middle and outer loops. The inner one is current control loop; the middle one is dc-link voltage regulator loop as well as reactive power control loop; and outer loop is the MPPT loop. As can be seen, the MPPT determines dc-link voltage reference. The error between dc-link voltage and its corresponding reference voltage compensated by $F_{vdc}(s)$ compensator to provide the reference active power, which in turn creates i_{dref}. In order to augment the performance of the dc-link voltage regulator, output power of PV is deployed as a feed-forward to eliminate the nonlinearity and destabilizing impact of the PV array output power [53]. Depending on reactive power regulation strategy i_{qref} reference command is generated. i_{dref} and i_{qref} are passed through current controllers to produce modulating signals for valves of the VSC.

2.3.1 Reactive power regulation

Generally speaking, reactive power of the PV system at the PCC can be regulated in two main approaches:

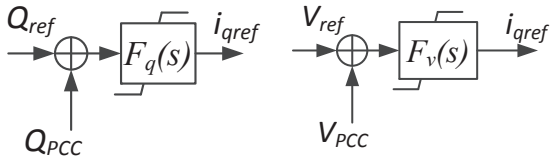

(a) (b)

Figure 2.4: Controller block diagrams for reactive power regulation: (a) direct regulation; (b) indirect regulation.

1. ***Direct regulation*** in which reactive power is directly regulated to a preset value as shown in Fig.2.4a

2. ***Indirect regulation or direct AC-bus voltage control*** in which AC voltage at the point of PV connection to the grid is directly controlled to a preset value as shown in Fig. 2.4b, and by doing so, reactive power is indirectly regulated.

However, one should keep in mind that the reactive power contribution of PV systems is limited due to the certain size of the VSC (for instance, in order to accommodate reactive power to achieve a power factor of 0.9 at the maximum PV active power without any active power curtailing, the VSC must be oversized by 11%) as well as regulation barriers specified by standards such as the German Grid Codes, which will be discussed in Chapter 4. In other words, active and reactive power of a PV system must be limited to the nominal apparent power of its VSC, $\sqrt{P^2+Q^2} \leq S$.

The reactive power preset in the direct regulation mode can be attained via different characteristics such as:

Constant power factor characteristic: in which PV systems regardless of the feed-in active power levels, contribute a constant fraction of feed-in active power as reactive power. It is worth mentioning that unity power factor is not considered in this category. In this approach, hence, when there is no voltage violation, PV systems still may contribute reactive power (unnecessary reactive power).

Dynamic power factor characteristic *Cosϕ(P)*: this method was originally proposed by the GGC to reduce reactive power consumption as compared to the constant power factor approach [29]. Fig. 2.5a depicts a more general characteristic curve of this method in both inductive and capacitive modes. Depending on the feed-in active power level of the PV system, the power factor level as well as the type of generated reactive power varies. This method, in contrast to its predecessor, can reduce the unnecessary reactive power contribution of PV systems.

Active power dependent reactive power characteristic Q(P): the main concept of Q(P) characteristic shown in 2.5b and the *Cosϕ(P)* characteristic is the same. In other

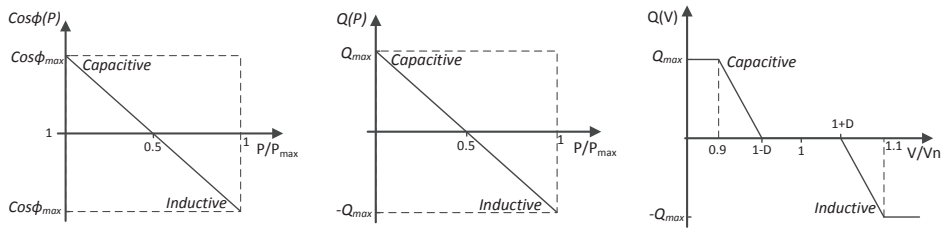

(a) (b) (c)

Figure 2.5: (a) Dynamic power factor characteristic $Cos\phi(P)$; (b) Active power dependent reactive power characteristic Q(P); (c) Droop-based voltage regulation characteristic Q(V).

words, both of them are an active power dependent characteristic, in which the feed-in active power of the PV system is used as a feedforward signal to calculate the required reactive power.

Droop-based voltage regulation characteristic Q(V): voltage at the PCC is employed as a feedforward signal to calculate the required reactive power according to the droop characteristic as shown in 2.5c.

The $Cos\phi(P)$, Q(V) and direct AC-bus voltage control strategies were incorporated into the developed model. Detailed design procedure of developed PV model controllers including parameters tuning is presented in Paper I.

2.3.2 Results and discussion

The developed model in Fig. 2.3 is implemented in PSCAD simulation platform to evaluate and compare the performance of three reactive power regulation strategies, namely *Cosϕ(P)*, Q(V), and direct AC-bus voltage control. Simulation results show that the model works as expected based on the given design procedure in Paper I. It is also noticed that the dynamic of the PV system in terms of reactive power provision can be quite fast (in order of tens of milliseconds). Furthermore, based on this configuration, two identical PV systems are integrated into a quite small distribution grid to investigate the interactive impact of the controllers and reactive power strategies. It is demonstrated that a lack of coordination between set-points of PV systems in the direct AC-bus voltage control strategy brings about negative interaction among installed PV systems in the same vicinity. This is presented in Paper I.

The implemented model in PSCAD simulation platform was further developed in PowerFactory simulation platform in the rms domain. The results demonstrate that the rms domain model in PowerFactory can provide quite similar results as time domain instantaneous values model in PSCAD and with advantage of lower simulation time. Therefore, the performance of large number of PV systems can be easily studied using rms simulations.

At this stage of doctoral project, two questions were raised:

1. How can one quantify the interaction level of voltage control among PV systems?;
2. Is there the possibility of decoupling interactions in case of using direct AC-bus voltage control method?

PSCAD and PowerFactory simulations are not efficient in providing analytical insight into controllability and quantification of voltage control interactions. Therefore, the features of voltage sensitivity matrix, which indicates how voltage at one node varies with regard to active and reactive power variations at any node, along with some control theory concepts are employed to address the raised questions.

Chapter 3

Direct AC-bus voltage control via PV systems and associated interactions

This chapter provides a brief background on load flow and sensitivity analysis. It also describes how features of voltage sensitivity matrix in conjunction with the relative gain array and the singular value decomposition can be used to quantify the level of interaction among PV systems in case of using direct AC-bus voltage control strategy, and along with evaluate the possibility of the controllability.

3.1 Introduction

Prior to design of a control scheme for a process one should investigate the input-output controllability of that control scheme defined as the ability to achieve acceptable control performance, i.e. keeping outputs within designated references despite small bounded disturbances and uncertainties [56]. The main aim of this chapter is to measure controllability among the PV systems in a distribution grid for direct AC-bus voltage control by use of voltage sensitivity features as well as concepts of the *relative gain array* (RGA) and the *singular value decomposition* (SVD). For this purpose, the voltage sensitivity matrix is used as the steady-state gain of the multi-variable system. In the first method, the RGA of the voltage sensitivity matrix is utilized as a quantitative measure to address controllability and the level of voltage control interaction among PV systems. The second method is *condition number* (CN), in which the SVD of the voltage sensitivity matrix is used as a mathematical measure to indicate the voltage control directionality among PV systems. In the direct AC-bus voltage control process, reactive power of PV systems indicates manipulated variables, which are fed to the plant system, while AC-bus voltages indicate controlled variables (the plant outputs). Operating modes of PV systems reactive power (inductive and capacitive modes) determine the input direction to the plant system. Different input directions can cause different impacts on voltage variations; strong directionality indicates a large range of variations in the plant gain for various input directions, i.e. the plant gain is strongly dependent on the input direction.

Sub-matrices of the voltage sensitivity matrix indicate the sensitivity of the bus voltages and angels to the variation of active and reactive power injections at all buses. The voltage sensitivity matrix of a power grid, therefore, provides analytical insight into power grid behavior. The voltage sensitivity matrix has widely been employed in quite different studies [12, 24, 57, 58]. However, the application of the RGA and CN in the voltage sensitivity analysis to indicate the degree of the voltage control interaction among PV systems was not addressed in the literature.

This chapter, therefore, takes advantage of the voltage sensitivity matrix in conjunction with the RGA and CN concepts to analytically investigate the direct voltage controllability via PV systems in a distribution grid and associated interactions. Moreover, impacts of feeder R/X ratio and distance between buses on the direct voltage control are also of concern. Applying the aforementioned methods provides an analytical view that how the voltage control interaction and directionality among PV systems in a distribution grid would be affected by the distance and R/X variations.

3.2 Load flow and sensitivity analyses

In power systems, where power values are known rather than currents, set of power system algebraic nonlinear equations are expressed in terms of power known as power flow equations. Power system analysis via power flow equations, commonly known as load flow analysis, form the core of power system studies. They are essential for many static analyses such as planning, economic assessments, reliability studies, and sensitivity analysis, as well as being used as the starting point for dynamic analyses such as transient stability and contingency studies.

The π-model equivalent of a line between two nodes of a power system is shown in Fig. 3.1. Node-voltage-based power equations are formulated as follows:

$$\begin{aligned} S_{ik} &= V_{ik} I_{ik}^{*} \\ &= P_{ik} + jQ_{ik} \qquad (3.1) \\ P_{ik} &= V_i \left(g_{ik} V_i - \left(g_{ik} cos(\delta_{ik}) + b_{ik} sin(\delta_{ik}) \right) V_k \right) \qquad (3.2) \\ Q_{ik} &= V_i \left((-b_{i0} - b_{ik}) V_i - \left(g_{ik} sin(\delta_{ik}) - b_{ik} cos(\delta_{ik}) \right) V_k \right) \qquad (3.3) \end{aligned}$$

where S_{ik} is the transmitted apparent power from node i to node k; P_{ik} and Q_{ik} are active and reactive part of S_{ik}, respectively; g_{ik} and b_{ik} are the conductance and the susceptance of the line between node i and k; b_{i0} is half of the shunt capacitance of the line; V_i and δ_i are the magnitude and the angle of the voltage at node i.

Power balance equations at node i of a power system with several interconnected nodes can in general be expressed as follows:

$$\begin{aligned} P_i &= V_i \sum_{k=1}^{N} V_k \left(G_{ik} cos(\delta_{ik}) + B_{ik} sin(\delta_{ik}) \right) \\ Q_i &= V_i \sum_{k=1}^{N} V_k \left(G_{ik} sin(\delta_{ik}) - B_{ik} cos(\delta_{ik}) \right) \qquad (3.4) \end{aligned}$$

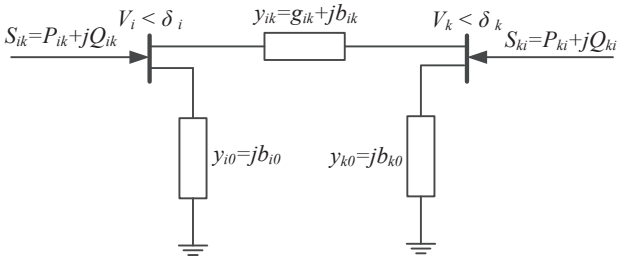

Figure 3.1: π-model of a line.

where G_{ii} is equal to the sum of all conductances connected to node i, G_{ik} is equal to the conductance between node i and k with the negative sign, B_{ii} is equal to the sum of all susceptances connected to node i, B_{ik} is equal to the susceptance between node i and k with the negative sign.

Therefore, the power flow equations are functions of the magnitude and the angle of voltages.

$$\begin{aligned} P_i &= g_P(V,\delta) \\ Q_i &= g_Q(V,\delta) \end{aligned} \tag{3.5}$$

The aim of the load flow analysis is to use iterative methods to solve the compact form of power flow equations in (3.6) to find the voltages at all buses and, consequently, determine the state of the power system.

$$0 = g(V,\delta) \tag{3.6}$$

Once the power flows are known, the active power losses can be computed as well. The total active power losses on the line between node i and k in Fig. 3.1 is derived as follows:

$$\begin{aligned} P_{Lik} &= P_{ik} + P_{ki} \\ &= \left(V_i^2 + V_k^2\right) g_{ik} - 2V_iV_k g_{ik} cos(\delta_{ik}) \end{aligned} \tag{3.7}$$

The P_{Lik} can be split up between two corresponding nodes as follows:

$$\begin{aligned} P_{Lik,i} &= V_i^2 g_{ik} - V_iV_k g_{ik} cos(\delta_{ik}) \\ P_{Lik,k} &= V_k^2 g_{ki} - V_kV_i g_{ki} cos(\delta_{ki}) \end{aligned} \tag{3.8}$$

where $P_{Lik,i}$ and $P_{Lik,k}$ correspond to node i and k, respectively.

Considering all connected nodes to i, the total active power losses associated with node i becomes

$$P_{L,i} = \sum_{\substack{k=1 \\ k\neq i}}^{N} \left(V_i^2 g_{ik} - V_iV_k g_{ik} cos(\delta_{ik})\right) \tag{3.9}$$

and, consequently, the total line losses can be determined as

$$P_L = \sum_{i=1}^{n} V_i \sum_{\substack{k=1 \\ k\neq i}}^{n} g_{ik} \left[V_i - V_k cos\left(\delta_{ik}\right) \right] \tag{3.10}$$

3.2.1 Voltage sensitivity matrix

The voltage sensitivity matrix is a measure to quantify the sensitivity of voltage magnitudes (V) and angles (δ) with respect to injected active and reactive power. The sensitivity matrix is obtained through partial derivatives of power flow equations in (3.5) as follows [59]:

$$\begin{aligned} \begin{bmatrix} \Delta\delta \\ \Delta V \end{bmatrix} &= \begin{bmatrix} \frac{\partial g_P(\delta,V)}{\partial \delta} & \frac{\partial g_P(\delta,V)}{\partial V} \\ \frac{\partial g_Q(\delta,V)}{\partial \delta} & \frac{\partial g_Q(\delta,V)}{\partial V} \end{bmatrix}^{-1} \begin{bmatrix} \Delta P \\ \Delta Q \end{bmatrix} \\ &= \underbrace{\begin{bmatrix} S_P^{\delta} & S_Q^{\delta} \\ S_P^{V} & S_Q^{V} \end{bmatrix}}_{S_V} \begin{bmatrix} \Delta P \\ \Delta Q \end{bmatrix} \end{aligned} \tag{3.11}$$

The voltage sensitivity matrix S_V consists of four sub-matrices that denote the partial derivatives of bus voltage magnitude and angle with respect to active and reactive power. Due to the importance of the voltage magnitude regulation by variation of active and reactive power, sub-matrices that are related to variation of voltage magnitude, S_P^V and S_Q^V, are of more interest and concern in this study. Each element of these sub-matrices is interpreted as the variation that may happen in voltage at bus i if active power (or reactive power) at bus j changed 1 p.u.

3.2.2 Loss sensitivity analysis

Total line losses in (3.10) and power flow equations in (3.5) are functions of voltage magnitude and angle. Therefore, sensitivity coefficients of total line losses with respect to active and reactive power variations at bus i can be derived as follows:

$$\begin{aligned} \frac{dP_L}{dP_i} &= \sum_{j=1}^{n} \frac{\partial P_L}{\partial \delta_j} \frac{\partial \delta_j}{\partial P_i} + \sum_{j=1}^{n} \frac{\partial P_L}{\partial V_j} \frac{\partial V_j}{\partial P_i} \\ \frac{dP_L}{dQ_i} &= \sum_{j=1}^{n} \frac{\partial P_L}{\partial \delta_j} \frac{\partial \delta_j}{\partial Q_i} + \sum_{j=1}^{n} \frac{\partial P_L}{\partial V_j} \frac{\partial V_j}{\partial Q_i} \end{aligned} \tag{3.12}$$

Eq. (3.12) can be rearranged in a matrix form with the help of the voltage sensitivity matrix S_V as follows:

$$\begin{bmatrix} \frac{dP_L}{dP} \\ \frac{dP_L}{dQ} \end{bmatrix} = S_V^T \begin{bmatrix} \frac{\partial P_L}{\partial \delta} \\ \frac{\partial P_L}{\partial V} \end{bmatrix} \tag{3.13}$$

where $\partial P_L/\partial \delta$ and $\partial P_L/\partial V$ can also be derived from (3.10).

3.3 Control concepts and applications

Before designing a particular control strategy for a system, it is essential to investigate the input-output controllability of the system defined as the ability to achieve acceptable control performance via the control strategy. Direct AC-bus voltage control via PV systems can generally be considered as a multiple-input multiple-output (MIMO) control process in which voltages are controlled variables and reactive power values of PV systems are the manipulated variables. The presence of directions in MIMO systems characterizes their main difference with scalar single-input single-output (SISO) systems [56]. Unlike scalars, matrices and vectors include directions. The gain of MIMO systems may dramatically vary with the input direction. Two methods to quantify the degree of directionality and interactions in MIMO systems are the relative gain array and the condition number, respectively [56].

As mentioned earlier, the main contribution of this chapter, as also presented in Paper III, is applying the aforementioned control concepts to the voltage sensitivity matrix derived from load flow analysis in order to analytically investigate the direct voltage controllability via PV systems and quantify associated interactions.

3.3.1 RGA method

Although the RGA was basically introduced by Britsol [60] for pairing the input and output variables in a MIMO system, it has also been exploited as a general measure of controllability [56, 61]. The relative gain array has been addressed in many literatures and is frequently employed as a quantitative measure of controllability and control loop interaction in a MIMO control design. The RGA is originally formulated for steady-state analysis and it was later extended to include the dynamics [56]. In this study, the RGA concept is used to analyze the voltage sensitivity matrix, which is calculated from system algebraic equations and therefore does not comprise dynamic.

The proposed interaction measure through the RGA indicates how the apparent transfer function between manipulated or input variable (u_i) and controlled or output variable (y_j) is affected by control of other controlled variables. This measure is shown by λ_{ij} and is described by the ratio of the transfer function between a given manipulated variable and controlled variable while all other loops are open, and the transfer function between the same variables while all other outputs are closed as follows:

$$\lambda_{ij} = \frac{\left(\frac{\partial y_i}{\partial u_j}\right) \mid u_{k\neq j} constant}{\left(\frac{\partial y_i}{\partial u_j}\right) \mid y_{k\neq j} constant} \tag{3.14}$$

In other words, the RGA is the ratio of the open loop gain between two variables to the closed loop gain of the same variables while other outputs are perfectly controlled. For a MIMO system with *G(0)* as the steady-state transfer function, the RGA is defined as follows:

$$\Lambda(G(0)) = G(0) \otimes \left(G(0)^{-1}\right)^T \tag{3.15}$$

Where $\otimes$ denotes element-by-element multiplication.

Equation (3.14) demonstrates that the open loop gain between y_j and u_i changes by the factor λ_{ij}^{-1} while the rest of loops are closed by integral feedback control. This implies that the pairing should be preferred for RGAs that are as close to unity as possible. λ_{ij}=1 implies that there is no interaction with other control loops. A decentralized control system, intuitively, requires the RGA becomes close to the identity matrix [56]. A MIMO process with a decentralized control system works as several independent SISO sub-plants. If RGA elements are greater than one, the decoupling or inverse-based controllers can be used to decouple interactions. However, systems with large RGA elements are basically hard to control owing to high interactions and input uncertainties, and hence inverse-based controllers should be prevented, because they are not robust. Besides, pairing with negative RGA elements must be avoided due to the integral instability [56].

Application of the RGA in the voltage sensitivity matrix

Sub-matrices of the voltage sensitivity matrix in (3.11) represent steady-state gain of the system, and so, the RGA of S_Q^V, which describes the voltage sensitivity with respect to reactive power variations, is given as follows:

$$\Lambda(S_Q^V) = S_Q^V \times \left(\left(S_Q^V\right)^{-1} \right)^T \tag{3.16}$$

The RGA of S_Q^V in (3.16) is used to investigate the possibility of controllability and interaction among voltage controllers of PV systems to control voltage of buses to pre-defined set-points via regulating reactive power.

To sum up, in the RGA method, first the voltage sensitivity matrix is derived; then, the RGA of S_Q^V is calculated; and in the final step, RGA values are evaluated. RGA values close to one demonstrate a decentralized system. If the RGA values are large but less than 5, the decoupling compensators can be used. However, large RGA values, more than 5, correspond to controllability problems because of high interactions and input uncertainties [56].

3.3.2 CN method

The CN method is a useful way to quantify how the range of possible gains of a MIMO process varies for an input direction [56, 61]. Wide (or narrow) range of possible gains for a process implies high (or low) directionality. Therefore, another measure to quantify the level of interaction in a MIMO system is the CN defined as the ratio between maximum and minimum singular values of the system with $G(0)$ as its steady-state gain [56, 61]:

$$\gamma(G(0)) = \frac{\overline{\sigma}(G(0))}{\underline{\sigma}(G(0))} \tag{3.17}$$

A process with a large CN implies high directionality and is called to be ill-conditioned [56]. The steady-state gain of MIMO process varies between $\underline{\sigma}(G(0))$ and $\overline{\sigma}(G(0))$. Wide

range of possible gains for a MIMO system indicates large directionality. Such a plant is often considered sensitive to uncertainty that, in turn, may lead to a poor control performance [56]. A large CN may be brought about by a small singular value that is generally undesirable.

Application of the CN in the voltage sensitivity matrix

Similar to the RGA method, in the CN method, the voltage sensitivity matrix must first be derived. Then, SVD of S_Q^V is computed and, consequently, the CN is calculated. CN larger than 10 demonstrates controllability problems [56].

3.4 Results and discussion

The RGA and CN methods are applied to a test radial grid with five PV-equipped houses connected through a step-down transformer to a medium voltage grid. To address the effect of R/X ratio, both overhead lines and underground cables are considered. The results demonstrate that the RGA increases for larger R/X ratios. Therefore, the larger the R/X ratio the higher the interaction level among AC-bus voltage controllers of PV systems. It is shown in the test system that the positive elements of the RGA, for the all case studies, are larger than one, irrespective of the R/X ratio, the total net load/generation, node distances (tested up to 500 m) and power factor. Hence, decentralized AC-bus voltage control (controlling voltages to predefined set-points) without decoupling is impossible. Moreover, since the positive numbers of RGA are large, more than 5, using decoupling controllers is not recommended due to sensitivity to input uncertainty [56]. The CN results are also along with the RGA results. More details can be found in paper III. The results indicates that the AC-bus voltage control to the predefined set-points will not work in larger radial LV grids either.

To sum up, the direct AC-bus voltage control is not a proper control strategy for LV radial distribution grids; therefore, it is more practical to support the voltage instead of directly controlling it. Accordingly, the doctoral project mainly focused on direct reactive power regulation strategies to support the voltage such as Q(P) and Q(V) methods, which will be discussed in the next two chapters.

Chapter 4

Active power dependent reactive power characteristic Q(P)

This chapter demonstrates how the features of the voltage sensitivity matrix allow systematic coordination of Q(P) characteristics among PV inverters while still using local measurements as presented in Papers IV and V.

4.1 Introduction

The GGC proposes a $cos\phi(P)$ characteristic curve to support the voltage profile via a PV system's reactive power [29]. In such an active power dependent (APD) power factor characteristic, the required reactive power is determined according to an identical $cos\phi(P)$ characteristic for each PV system, independent of its location in the grid. Though the GGC states the distribution system operators (DSO) can use a characteristic differing from the standard characteristic depending upon the grid configuration, the specification of such a characteristic is left with the DSO. Moreover, since the standard characteristic does not consider the voltage profile, its employment can cause unnecessary reactive power consumption. Considering large numbers of PV systems in grids, unnecessary reactive power consumption by PV systems firstly increases the total line losses, and secondly it may also jeopardize the stability of the network in the case of contingencies in conventional power plants, which supply reactive power [30].

A method that can provide a coordinated, systematic characteristic for each PV system along a feeder is, therefore, needed. This chapter provides such a method. This method utilizes the voltage sensitivity matrix of one operating point to determine individual Q(P) characteristics that use local information but provides a coordinated response without the aid of communication systems. As mentioned in Chapter 2, since the concept of Q(P) and $cos\phi(P)$ characteristics is the same, the proposed method in fact is a systematic approach of adjusting setting parameters of the GGC standard characteristic. Since the grid configuration is addressed in the voltage sensitivity matrix, the proposed method basically introduces a specific characteristic based on the grid configuration for each PV system.

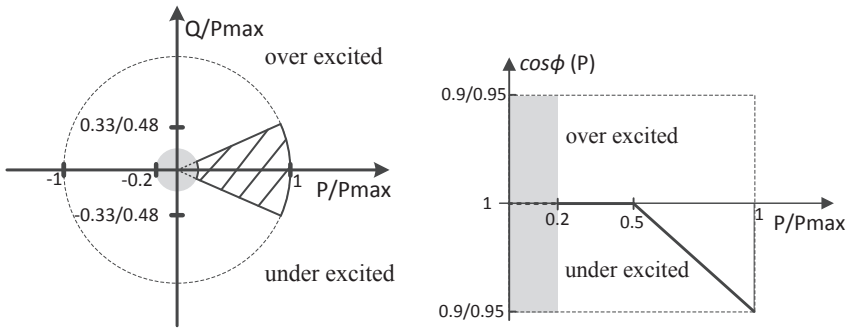

(a) (b)

Figure 4.1: (a) Reactive power operation area for a generation unit connected to LV grids; (b) Standard characteristic curve for $cos\varphi$ (P).

The voltage sensitivity matrix has been widely used to compare impacts of active power curtailment and reactive power support through PV systems on the voltage profile in low voltage grids [24], to define coordinated droop factors in the active power curtailment of PV systems [12], to demonstrate the voltage control interaction among PV systems using control theory [62], and to eliminate the voltage variation at a target node due to the operation of a wind turbine in a microgrid via reactive power support [58]. However, locally coordinated Q(P) characteristics for several PV systems in distribution grids have not yet been addressed.

4.2 German Grid Codes

The GGCs comply with the limit values of voltage quality specified by EN 50160 [63]. According to the EN 50160, the allowable voltage range in LV grids is between 90% to 110% of the nominal voltage. Within this voltage tolerance band, the GGC states DG units that deliver at least 20% of their rated power are permitted to freely change their power factor within the hatched sector represented in Fig. 4.1a. The power factor range for units larger than 13.8 kVA is between 0.9 under-excited and over-excited while for units between 3.68 kVA and 13.8 kVA it is 0.95 [29]. Reactive power contribution augments the integration of DG units into LV grids.

The reactive power control comes along with a considerable power loss in LV grids. Hence, in order to reduce the power loss, the GGC proposes the $cos\varphi(P)$ standard characteristic curve in Fig. 4.1b, where P and P_{max} represent the feed-in and the maximum active power of the generator unit, respectively [29]. The objective of the standard $cos\varphi(P)$ characteristic is requiring the generation unit to operate in an under-excited mode when the feed-in active power passes over a threshold of 50% of P_{max} in order to mitigate the related voltage rise. Therefore, the GGC standard setting for PV systems can be illustrated

according to Fig. 4.1b. The proposed $cos\varphi(P)$ characteristic requires inverter-based variable generation units such as PV systems. Upon a change in active power, the generation unit should provide the required reactive power based on the set-point on the characteristic curve within 10 seconds [29], which can be fulfilled by adjusting the band-width of the reactive power controller. The GGC mentions that depending upon different aspects, i.e. grid configuration, load and feed-in power, the DSO may need a characteristic different from the standard $cos\varphi(P)$ curve shown in Fig. 4.1b. Nevertheless, the GGC does not address how to specify the setting parameters.

The $cos\varphi(P)$ method can not explicitly consider grid voltage stability because the curve used is not a function of voltage. Furthermore, local demand is not also addressed in the $cos\varphi(P)$ characteristic. The local active power demand can affect the local voltage and in turn the overall voltage profile; the higher the active demand the lower the voltage. Besides, inductive demand, e.g induction motors and lighting ballast that are frequently used, can also lower voltage. Therefore, since the $cos\varphi(P)$ characteristic does not take into account either voltage or demand, unnecessary reactive power consumption can be expected in the case of high or medium demand, when the overvoltage is less likely. This can be considered as the main drawback of the $cos\varphi(P)$ characteristic or in general any $Q(P)$ characteristic. Nevertheless, one can use the net load/generation, i.e. generation minus load, at the connection point of load demand and PV system to a grid in the $Q(P_{net})$ characteristic instead of using only the feed-in power of the PV system in order to consider the effect of local demand. This though is not investigated in this thesis, it can be considered as a further investigation in the future works, which will also be worthwhile to compare it against voltage dependant characteristics Q(V).

4.3 Coordination and design of Q(P) characteristics

In the APD reactive power characteristic shown in Fig. 4.2a, the general relationship between active and reactive power of a PV system is defined as follows:

$$Q = \begin{cases} m(P - P_{th}) & P > P_{th} \\ 0 & P < P_{th} \end{cases} \tag{4.1}$$

where m is a slope factor and P_{th} is an active power threshold above which the PV system commences consuming reactive power to regulate the voltage. Therefore, in the APD method two parameters must be defined for each PV system.

Figs. 4.2b and 4.2c provides a comprehensive picture of characteristics of the proposed APD method that will be discussed in detail. In this method, a unique slope is designated to each PV system while active power thresholds can be either identical or non-identical. Once the feed-in power passes the power threshold, reactive power compensation unit kicks in to regulate the voltage to the steady-state limit based on its designated slope factor. In the proposed APD method, the voltage sensitivity matrix is employed to coordinate these two parameters among PV systems along a radial feeder by regulating either the target-bus (TB) voltage or the voltage profile (VP).

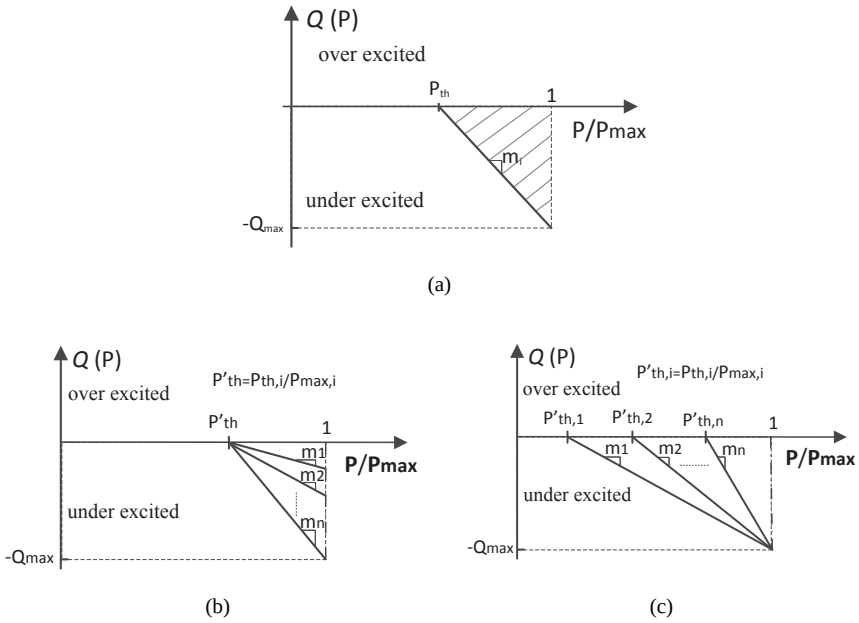

Figure 4.2: (a) General characteristic of APD reactive power Q(P);(b) characteristic curves of the proposed APD method at the presence of identical threshold; (c) characteristic curves of the proposed APD method at the presence of non-identical thresholds.

The voltage sensitivity matrix is calculated for the maximum net load/generation, i.e. generation minus load, without voltage support scheme. This point is called critical operating point. For the defined critical operating point an adequate amount of reactive power is calculated that can cancel out the associated maximum overvoltage. If the calculated reactive power eliminates the maximum overvoltage, one can also intuitively assume over-voltage cancelation for all other less severe cases compared to the critical operating point. In other words, the critical operating point is the worst case scenario, which is considered as a designing criterion to ensure over-voltage cancelation for any other cases. The voltage deviation required to remain under the steady-state voltage limit is considered as a measure to find the active power thresholds. The threshold levels are adjusted in such a way to keep the target-bus voltage (the most critical voltage) under the steady-state voltage limit. Information from the voltage magnitude sensitivity sub-matrices are used to derive the slope factors to regulate the target-bus or the whole voltage profile, whichever case is chosen. In the following subsections, it is first discussed how to derive the slope factors and later explained how to adjust the active power thresholds.

4.3.1 Computing the slope factors

The proposed APD method uses the voltage sensitivity matrix to locally regulate either the TB voltage in a radial feeder or the VP of a radial feeder with several PV systems.

Target-bus voltage regulation

Concerning the ideal voltage regulation, based on (3.11) it is possible to regulate reactive power of each PV system at each node in such a way to make the target-bus voltage deviation zero as follows:

$$\Delta V_{TB} = 0 = \sum_{i=1}^{n} \left(S^{V}_{P\ i,TB} \Delta P_i + S^{V}_{Q\ i,TB} \Delta Q_i \right) \tag{4.2}$$

where n is the number of PV systems, ΔV_{TB} is the voltage deviation at the target-bus, $S^{V}_{Pi,TB}$ and $S^{V}_{Qi,TB}$ are respectively voltage magnitude sensitivity indices at the target-bus with respect to active and reactive power corresponding to the bus i. The controlled relation between active and reactive power variations of each PV system can be expressed as follows:

$$\begin{aligned} \Delta Q_i &= m_i \Delta P_i \\ (Q_i - Q_{th,i}) &= m_i (P_i - P_{th,i}) \end{aligned} \tag{4.3}$$

where m_i, the slope factor at the bus i, is assigned to be the value obtained by substituting (4.3) into (4.2):

$$m_i = -\frac{S^{V}_{P\ i,TB}}{S^{V}_{Q\ i,TB}} \tag{4.4}$$

$P_{th,i}$ and $Q_{th,i}$ are active and reactive power thresholds of the PV system at the bus i. The threshold $P_{th,i}$ is specified as described in the next section. Since the APD voltage regulation should kick in above $P_{th,i}$, $Q_{th,i}$ is, therefore, assumed zero. The choice of (4.4) ensures voltage regulation by setting ΔQ to cancel the left term of (4.2). By doing so, analogous to (4.1), the required reactive power injections at each bus can be derived as follows:

$$Q_i = \begin{cases} m_i (P_i - P_{th,i}) & P_i > P_{th,i} \\ 0 & P_i < P_{th,i} \end{cases} \qquad \forall i \tag{4.5}$$

Eq. (4.5) can be rearranged to express the active power threshold level as a fraction of its maximum power, $P^{'}_{thi} = P_{th,i}/P_{max,i}$ which is hereafter called simply threshold, as follows:

$$Q_i = \begin{cases} m_i P_{max,i} (\frac{P_i}{P_{max,i}} - P^{'}_{th,i}) & \frac{P_i}{P_{max,i}} > P^{'}_{th,i} \\ 0 & \frac{P_i}{P_{max,i}} < P^{'}_{th,i} \end{cases} \qquad \forall i \tag{4.6}$$

where $P_{max,i}$ is the maximum power of the i-th PV system.

Voltage profile regulation

In the previous subsection, the voltage at the target-bus is regulated and the main reactive power pressure is imposed on the PV system at the target-bus in the case of thresholds with equal values. It is, however, possible to regulate the voltage along the feeder by keeping the voltage profile deviations at all nodes as close as possible to zero using the following objective function:

$$min_{(m_j)} \left(\sum_{i=1}^{n} W_i \sum_{j=1}^{n} (S^V_{P,ij} + S^V_{Q,ij} m_j)^2 \right) \tag{4.7}$$

where m_j is the optimization variable and represents the relation between reactive and active power variation at bus j (similar to Eq. (4.3)), $S^V_{P,ij}$ and $S^V_{Q,ij}$ are given parameters from load-flow analysis at the critical operating point, and W_i is a weighting factor parameter, which determines the importance of the voltage regulation at bus i with respect to other buses. The W_i could be set equal to each other, which in turn implies no priority concerning voltage regulation. However, the target-bus voltage regulation is normally more of concern, and so, one can attribute a larger wight factor to the target-bus. For instance, the characteristic of S^V_Q can be employed to find a weight vector. The diagonal entries of S^V_Q depict the influence of the reactive power variation at one bus on the voltage at the same bus. Therefore, normalized diagonal entries of S^V_Q can be used as a measure to determine weighting parameters in order to indicate the importance of voltage regulation at each bus:

$$W_i = \frac{S^V_{Q,ii}}{\frac{1}{n} tr(S^V_Q)}. \tag{4.8}$$

Computing the slope factors to minimize (4.7) uses the whole information of the voltage sensitivity matrix. In other words, minimization of all voltage deviations at all nodes are addressed in (4.7) as compared to (4.2) where only considers the voltage deviation at the target-bus and merely employs sensitivity entries corresponded to the target-bus. Once the slope factors are computed, the required reactive power at each bus can be derived similar to (4.5).

4.3.2 Computing the thresholds

As discussed earlier, thresholds, P'_{th}, are adjusted in a way to regulate the TB voltage to steady-state voltage limit. The maximum deviation at the TB is

$$\Delta V_{max,TB} = \left(V_{max,TB} - \overline{V} \right) \tag{4.9}$$

where $V_{max,TB}$ is the maximum target-bus voltage that occurs at the critical operating point and $\overline{V}$ is the steady-state upper voltage limit in LV grids.

The overvoltage $\Delta V_{max,TB}$ is due to the active power injections corresponding to the left term within brackets of (3.11). The required under-excited reactive power to cancel the

overvoltage is given by the equality

$$\Delta V_{max,TB} = -\sum_{i=1}^{n} \left(S^{V}_{Q\ i,TB} \Delta Q_i \right). \tag{4.10}$$

The negative sign in (4.10) is due to under-excited nature of the required reactive power that is basically negative in the defined Q(P) plane. Thus, the negative sign is used to match both sides of the equivalence in (4.10).

In order to calculate the thresholds, ΔQ_i in (4.10) must be substituted by (4.3). In this regard, there are two possible options. If thresholds are assumed to be identical, this leads to unequal reactive power sharing among PV systems according to (4.6) and as shown in Fig. 4.2b. If equal reactive power sharing among PV systems is desired, this at the critical operating point means unequal thresholds as shown in Fig. 4.2c. Identical thresholds force PV systems close the target-bus to contribute more reactive power. By doing so, those PV systems are more prone to excessive reactive power loading in their inverters. However, it is possible to equally share reactive power among PV systems at the critical operating point using non-identical ratio values of active power thresholds. Equally distributing reactive power among PV systems can prevent excessive reactive power loading on PV inverters, but it also results in higher total reactive power consumption.

Thus, the threshold can, generally, be derived in two ways as explained below:

Identical thresholds, $P^{'}_{th}$ iden

By substituting (4.3) in (4.10) and assuming identical thresholds, one deduces:

$$P^{'}_{th} = 1 + \frac{\Delta V_{max,TB}}{\sum_{i=1}^{n} m_i P_{max,i} S^{V}_{Q,\ TBi}}. \tag{4.11}$$

Non-identical thresholds, $P^{'}_{th}$ non-iden

Considering the equal share of reactive power for each PV system at the critical operating point, $\Delta Q_i = -Q_{max}$, according to (4.10) the required under-excited reactive power for each PV system is calculated as follows:

$$Q_{max} = \frac{\Delta V_{max,TB}}{\sum_{i=1}^{n} S^{V}_{Q,TBi}}. \tag{4.12}$$

Then, based on (4.3), the thresholds for each bus are calculated as follows:

$$P^{'}_{th,i} = 1 + \frac{Q_{max}}{m_i P_{max,i}} \qquad i = 1, ..., n. \tag{4.13}$$

4.4 Optimal coordination and design of Q(P) characteristics

The developed APD approach in the previous section comprises four different variants for designing parameters of the APD reactive power characteristic, namely 1) target-bus

voltage regulation with identical thresholds (APD TB iden), 2) target-bus voltage regulation with non-identical thresholds (APD TB non-iden), 3) voltage profile regulation with identical thresholds (APD VP iden), and 4) voltage profile regulation with non-identical thresholds (APD VP non-iden). Though Paper IV provides a detailed discussion regarding the advantages and disadvantages of each variant, the final optimal choice of the variant is left to users. The APD Q(P) characteristic design methods presented in Section 4.3 are further developed in Paper V, and the fundamental concept of this alternative approach is discussed in this section. The main aim of the new approach is developing an optimization formulation that can streamline deployment of the APD design concept presented in Section 4.3 to optimally coordinate the APD Q(P) parameters among PV systems within the grid.

4.4.1 Optimization formulation

The objective of the new proposed method is to design the slope and the threshold of Q(P) characteristics in such a way to minimize the sum of the hatched areas in Fig. 4.2a. The total area is related to the total reactive power consumption, but not exactly since the probability of different consumption levels is not constant. In this regard, the following objective function is proposed

$$min_{\left(Q_{max,i}\ ,\ P_{th,i}\right)} \quad \sum_{i=1}^{n} \left(\left(P_{max,i} - P_{th,i} \right) Q_{max,i} \right) \tag{4.14}$$

where $P_{th,i}$ and $Q_{max,i}$ are optimization variables, and, respectively, are the active power threshold and the maximum required reactive power of the Q(P) characteristic for the $i-th$ PV system. As illustrated in Fig. 4.2a, the slope m_i is a dependant variable, which is a by-product of the optimization variables.

4.4.2 Constraints

The theoretical concept behind the APD method in addition to some new concepts is employed to figure out the constraints of the proposed objective function. Accordingly, the proposed objective function must be subjected to the following constraints:

I. Voltage regulation

The main goal of using Q(P) characteristics is to eliminate the TB overvoltage at the critical operating point by generating a proper set of reactive power candidates that satisfies the defined equality in (4.10).

II. Maximum reactive power contribution

The reactive power contribution of PV systems is limited according to the GGC regulation; thus, to comply with the GGC standard, the $Q_{max,i}$ is subjected to

$$0 \leq Q_{max,i} \leq P_{max,i}\sqrt{\frac{1}{cos^2\varphi_{max,i}} - 1} \tag{4.15}$$

III. The slope limit

The rate of reactive power changes versus active power variations depends on the slope, and in order to limit rapid changes of reactive power, the slope factor of the Q(P) characteristic has to be limited. This limit is defined using the sensitivities. Based on sensitivities in (3.11), the voltage deviations of buses within the grid can be represented by

$$\begin{bmatrix} \Delta V_1 \\ \vdots \\ \Delta V_{TB} \\ \vdots \\ \Delta V_n \end{bmatrix} = \begin{bmatrix} S^V_{P\ 1,1} & \cdots & S^V_{P\ 1,n} & S^V_{Q\ 1,1} & \cdots & S^V_{Q\ 1,n} \\ \vdots & \ddots & \vdots & \vdots & \ddots & \vdots \\ S^V_{P\ TB,1} & \cdots & S^V_{P\ TB,n} & S^V_{Q\ TB,1} & \cdots & S^V_{Q\ TB,n} \\ \vdots & \ddots & \vdots & \vdots & & \vdots \\ S^V_{P\ n,1} & \cdots & S^V_{P\ n,n} & S^V_{Q\ n,1} & \cdots & S^V_{Q\ n,n} \end{bmatrix} \begin{bmatrix} \Delta_{P1} \\ \vdots \\ \Delta_{Pn} \\ \Delta_{Q1} \\ \vdots \\ \Delta_{Qn} \end{bmatrix} \tag{4.16}$$

Substituting ΔQ_i in (4.16) by (4.3), according to the controlled relation between active and reactive power variations of each PV system, gives

$$\begin{bmatrix} \Delta V_1 \\ \vdots \\ \Delta V_n \end{bmatrix} = \begin{bmatrix} \alpha_{1,1} & \cdots & \alpha_{1,n} \\ \vdots & \ddots & \vdots \\ \alpha_{n,1} & \cdots & \alpha_{n,n} \end{bmatrix} \begin{bmatrix} \Delta_{P1} \\ \vdots \\ \Delta_{Pn} \end{bmatrix} \tag{4.17}$$

where α_{ji} is defined as follows:

$$\alpha_{ji} = S^V_{Pj,i} + m_i S^V_{Qj,i} \tag{4.18}$$

If all αs become non-positive, voltage variations ΔV will be suppressed for any increase in production of PV systems. Accordingly, m_i is limited as follows

$$m_i \leq -\frac{S^V_{Pj,i}}{S^V_{Qj,i}} \quad \forall j \tag{4.19}$$

So, the maximum value of m_i that satisfies (4.19) for all cases is selected as the slope of the $i-th$ PV system.

Table 4.1: Qualitative Comparison.

Method	Voltage Regulation[1]	Reactive Power[2]	Inverter Loading[3]	Total Loss[4]
APD TB iden	+++	++	o	++
APD TB non-iden	+++	o	+++	+
APD VP iden	+++	+	+++	++
APD VP non-iden	+++	+	+++	++
Optimal APD	+++	+++	+++	+++
GGC	- -	- -	++	- -

*+++ superior, ++ very good, + good, o average, - poor, - - inferior

[1] Regulate the voltage to steady-state limit
[2] Causing less reactive power consumption
[3] Decreasing reactive power loading in PV inverters
[4] Causing less active power loss by reactive power

4.5 Results and discussion

The proposed methods are applied to a utility LV grid located at Northern Jutland in Denmark, consisted of eight feeders and thirty five buses. The results demonstrate that the proposed methods considerably reduce reactive power usage as well as active power losses caused by reactive power injections as compared to the GGC standard characteristic. Moreover, the results show the advantage of optimization formulation in the optimal APD method. A qualitative comparison of the proposed methods with the state of the art, which is the GGC method, is provided in Table 4.1. More detailed can be found in Papers IV and V.

Chapter 5

Voltage dependent reactive power characteristics Q(V)

This chapter depicts how the features of the voltage sensitivity matrix in association with droop control concept can be used through a multi-objective design to optimally coordinate characteristics of the droop-based voltage reactive power among PV systems in radial distribution feeders. Along with Paper VI is introduced.

5.1 Introduction

The APD reactive power characteristic Q(P) cannot explicitly address voltage limits; this is considered as a shortcoming of the APD method. The GGC also admits this lack and thereby recommends network voltage dependent reactive power regulation methods, Q(V), in the near future. Nevertheless, the GGC does not propose any specific Q(V) characteristic. A grid impedance-adaptive Q(V) approach has been proposed in [64] that requires the PV inverter to measure the grid impedance. In the case of multiple PV systems, the lack of a synchronized injection signal contributes to a low accuracy of impedance measuring [52, 65] and the performance of the Q(V) can negatively be affected. It was shown in [66] that for different LV grid classes a set of static parameters can be found by trial and error for grid impedance based Q(V) characteristic to get sub-optimal but still acceptable performance. An improved Q(V) algorithm is proposed in [15, 67]; however, it needs a communication infrastructure to transmit all nodal information to a centralized controller in order to dispatch the minimum reactive power among PV systems. Investing for a communication infrastructure may be costly and there may be reliability challenges, so there is a need of an alternative approach.

There is a need to develop Q(V) characteristics that are based on local information, but still take account of the system's structure and dependencies, and minimize reactive power consumption and total line losses caused by reactive power. Information about the effects of a local injection on power flow are described by the voltage sensitivity matrix. The voltage sensitivity matrix, as discussed in the previous chapter, has been widely employed.

The droop control concept has been primarily utilized in power systems with multiple generators and converters to droop frequency of each source with its delivered active power in order to share the load among them [68, 69]. However, it can also be employed to share the reactive power by drooping the voltage.

The main contribution of this chapter is utilizing the voltage sensitivity matrix and the droop control concept to systematically coordinate and optimize the Q(V) characteristic of each PV system in a radial grid using only local measurements in order to regulate the voltage profile under the upper steady-state voltage limit. A multi-objective design is taken into consideration to optimally adjust the settings of individual droop-based Q(V) characteristics of PV systems such that the reactive power consumption profile and total line losses profile are minimized.

5.1.1 Drooping technique background

Droop control is a well-known concept in conventional power systems used primarily for the load sharing among multiple generation units [68, 69]. In this method, the frequency of each generation unit is allowed to droop in accordance with its delivered active power in order to share the system load. Analogous with the frequency droop control, drooping voltage magnitude via reactive power can provide the possibility of sharing reactive power among generation units. Power flow concept between two generation sources can basically demonstrate the theory of load and reactive power sharing methods. For instance, active and reactive power flow between two voltage sources, V_1 and V_2, can be derived as follows:

$$P = V_1 \frac{R\,(V_1 - V_2 cos(\delta_1 - \delta_2)) + XV_2 sin(\delta_1 - \delta_2)}{R^2 + X^2} \tag{5.1}$$

$$Q = V_1 \frac{X\,(V_1 - V_2 cos(\delta_1 - \delta_2)) - RV_2 sin(\delta_1 - \delta_2)}{R^2 + X^2} \tag{5.2}$$

Assuming that the resistance is negligible, which is the case in HV grids, and the difference between δ_1 and δ_2 is small, one can easily see that active and reactive power are predominately controlled by power angle, which in turn related to the frequency, and voltage magnitude, respectively. In LV feeders, however, the R/X ratios are generally large and thus the reactance term (X) becomes much smaller than resistance. By doing so, the voltage magnitude and angle in LV grids are mainly affected by active power and reactive power, respectively. Nevertheless, [25] shows that the conventional droop approaches in interconnected HV systems can be applied in the same manner in LV grids. However, with regard to the line losses and the inverter loading, voltage regulation through reactive power in LV grids may be less effective for feeders with high R/X ratios. Therefore, it is necessary to develop a method to be able to minimize the reactive power consumption required for voltage support.

5.2 Formulation of DBV regulation

In the DBV regulation method, the local voltage of the connection point of a PV system is directly employed as an input to calculate the required local reactive power to regu-

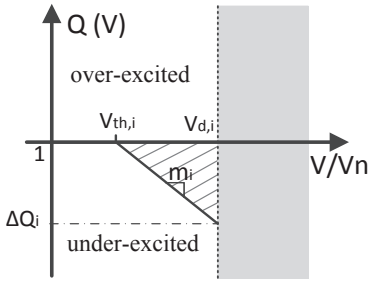

Figure 5.1: Characteristic curve of reactive power droop with voltage level.

late the voltage. Therefore, the consumption of reactive power can be explicitly managed by severity of the voltage violation. Consequently, using the Q(V) method can prevent unnecessary reactive power consumption in contrast to Q(P) method, which employs the delivered power of the generation unit as an input.

In the DBV method, the general relation between reactive power of a PV system and the local grid voltage is defined as follows:

$$Q = \begin{cases} m(V - V_{th}) & V > V_{th} \\ 0 & V < V_{th} \end{cases} \tag{5.3}$$

where m is the slope factor ($kVar/V$) and V_{th} is the voltage threshold above which the PV system must absorb reactive power to mitigate the voltage. Therefore, the DBV characteristic has two parameters that must be defined for each PV system.

Fig. 5.1 provides a general picture of the DBV characteristic. V_d is the drooped voltage at the critical operating point, which occurs for maximum net load/generation, and ΔQ is the required reactive power to push the critical voltage value back under the steady-state voltage limit. Thus, m can be calculated as follows:

$$m = \frac{\Delta Q}{V_d - V_{th}} \tag{5.4}$$

In the proposed DBV method, the voltage sensitivity matrix is employed to coordinate the slope factor and the voltage threshold of each PV system along a radial feeder by considering overvoltage at the target-bus on the feeder, where the maximum critical voltage deviation occurs. This worst case deviation occurs for the maximum net load/generation point. The maximum voltage deviation with respect to the upper steady-state voltage limit has to be canceled, hence, the ΔQ required in (5.4) is computed using the voltage sensitivity matrix computed at the maximum net load/generation operating point.

5.2.1 Computing the parameters of Q(V) characteristic

The maximum voltage deviation from the upper steady-state voltage limit in (4.9) occurs at the target-bus and at the presence of the critical operating point. It was shown in (4.10)

that it is possible to regulate reactive power of each PV system at each node in such a way to compensate the last-bus voltage deviation. However, the challenge is how to associate the ΔQ in (4.10) with individual PV systems in order to properly distribute the required reactive power of each PV system along the feeder.

Obviously, the drooped voltage of the target-bus, $V_{d,TB}$, must be equal to $\overline{V}$; once the required reactive power of each PV is known, the drooped voltage for the rest of buses can be calculated by the following equation

$$V_{d,i} = V_{cri,i} - \sum_{j=1}^{n} \left(S^{V}_{Q,ij} \Delta Q_j \right) \tag{5.5}$$

where $V_{cri,i}$ is the critical voltage at the bus i at the presence of the critical operating point. As can be seen in Fig. 5.1, the $V_{d,i}$ should be higher than the corresponding $V_{th,i}$. Thus, if the calculated $V_{d,i}$ is lower, the corresponding ΔQ_i in (4.10) must be set to zero because the corresponding PV should not contribute reactive power according to (5.3) and the other injections (ΔQ_j, $i \neq j$) must be recalculated.

By having the value of the voltage threshold and the required reactive power of each PV system, the corresponding slope factor is calculated based on (5.4).

In the DBV method, the voltage threshold and ΔQ of each PV system can be determined through two approaches, namely multi-objective DBV design and equal reactive power sharing, that will be explained in the following subsections.

5.2.2 Approach I: Multi-objective DBV design

The slope factor and the voltage threshold of the DBV characteristic for each PV system can be determined through an optimization that will be explained in the following subsections.

Objective Function

In the proposed multi-objective approach, three different target objectives are minimized, namely maximum reactive power consumption, maximum line losses caused by reactive power, and overall profile of reactive power consumption. The general form of the proposed objective function is:

$$max_{(\Delta Q, V_{th})} \quad \begin{pmatrix} w_1 \times f_1(\Delta Q) + \\ w_2 \times f_2(\Delta Q, V_{th}) - \\ w_3 \times f_3(\Delta Q) \end{pmatrix} \tag{5.6}$$

where target objectives are weighted by factors $w_1 - w_3$. How to set the weighting factors depends on the DSO's choice of what is the main concern. In Paper VI, these factors were chosen to weight in a similar manner the three target objectives included in the objective function, w1=w2=w3. This value selection implies an equal optimization priority among the three target objectives.

- Target Objective 1:
  The required reactive power for PV systems can be chosen in such a way to minimize the sum of individual reactive power consumption of each PV system at the critical operating point in (4.10). Thus, the first objective target is formulated as follows:

$$f_1 = \sum_{i=1}^{n} \Delta Q_i \tag{5.7}$$

  Since the nature of under-excited reactive power is assumed to be negative, the objective target is considered by positive sign in the objective function (5.6).

- Target Objective 2:
  The first objective target only minimizes the total reactive power consumption at the critical operating point. However, since the system's operating points vary, it is required to minimize the reactive power usage over the range of voltages experienced, represented by the hatched triangle in Fig. 5.1. The hatched area is related to the reactive power consumption, but not exactly since the probability of different voltage levels is not constant. Nevertheless, minimizing the sum of hatched areas of all Q(V) characteristics can reduce the total reactive power consumption. Therefore, the voltage threshold in the DBV characteristic can be adjusted in such a way to minimize the reactive power profile over the voltage profile through the following objective target:

$$f_2 = \sum_{i=1}^{n} \Delta Q_i \left(V_{d,i} - V_{th,i}\right) \tag{5.8}$$

  Similar to the previous objective target, due to the negative nature of under-excited reactive power, this objective target is also considered with positive sign in (5.6).

- Target Objective 3:
  Since consumption profile of reactive power is minimized in (5.8), the profile of line losses is, in turn, supposed to be minimized. Nevertheless, the active power loss caused by reactive power at the critical point can also be minimized. According to (3.12), the variation of total line losses caused by reactive power variation is:

$$\Delta P_L = \sum_{i=1}^{n} S_{Qi}^{L} \Delta Q_i \tag{5.9}$$

  Therefore, in order to minimize the line losses one should minimize the right hand side of (5.9)

$$f_3 = \sum_{i=1}^{n} S_{Qi}^{L} \Delta Q_i \tag{5.10}$$

  Since both multiplying terms in (5.10) are negative, this objective target must be considered with negative sign in (5.6).

Optimization variables

In the proposed optimization, the decision variables are reactive power consumption, ΔQ, and threshold voltage, V_{th}, at the critical operating point.

Constraints

In order to find a proper, feasible set of candidate solutions following constraints must be fulfilled:

- Constraint 1:
  The main goal of the DBV method is to eliminate the maximum overvoltage at the worst case operating point; hence, the set of candidate reactive power values has to fulfill this criterion by satisfying the equality in (4.10).

- Constraint 2:
  Reactive power consumption imposes extra loading on PV inverters as well as the grid transformers. In this regard, as also mentioned earlier, the GGC limit the amount of reactive power to a specific value based on the size of PV systems. Therefore, reactive power of each PV system should stay within the following band

$$-P_{max,i}\sqrt{\left(\frac{1}{cos^2\phi_{max,i}}-1\right)} \leq \Delta Q_i \leq 0 \tag{5.11}$$

  where $P_{max,i}$ and $cos\phi_{max,i}$ are the maximum generation power and the minimum allowable power factor of the PV system at the bus i.

- Constraint 3:
  The analysis of unit characteristics is based on the assumption that they contribute appropriately to limit the voltage of the target bus, which in a radial feeder, normally, happens to be the last bus downstream on the feeder. This need not in general to be true but normally occurs in the worst case of light load and full PV production conditions without any voltage support. In this case voltages will increase monotonically along a radial feeder. Hence to preserve the analysis intended in (4.10), the voltage thresholds

$$1 < V_{th,1} < V_{th,2} < \ldots < V_{th,n} < V_{d,n} = \overline{V} \tag{5.12}$$

- Constraint 4:
  Each PV system on the feeder can contribute reactive power if and only if its corresponding drooped voltage in (5.5) drops below its corresponding voltage threshold. Therefore, according to the negative nature of under-excited reactive power, $\Delta Q_i \leq 0$, the following constraint must be satisfied for all PV systems:

$$\Delta Q_i \left(V_{d,i} - V_{th,i}\right) \leq 0 \tag{5.13}$$

which is met when first there is a need for under-exited reactive power contribution (non-positive ΔQ_i) at the $i-th$ PV system, and second the drooped voltage of the same PV system is greater than the corresponding voltage threshold.

- Constraint 5:
  The slope factor in the Q(V) characteristic shown in Fig. 5.1 is a dependent variable, which is a byproduct of the decision variables and the drooped voltage derived in (5.4). Since one does not want to have rapid changes in reactive power support just because of a small change in load and/or solar irradiance, the slope factor has to be limited. This limit is defined by use of the sensitivities. According to Fig. 5.1, for a voltage variation at the bus i above the voltage threshold, the required reactive power variation at the same bus is given by

$$\Delta Q_i = m_i \Delta V_i \tag{5.14}$$

  According to (3.11), the relation between the voltage variation at the bus i and the reactive power variation at the same bus can be related by

$$\Delta V_i \geq -S^V_{Qi,i} \Delta Q_i \tag{5.15}$$

  By substituting (5.14) in (5.15), one can get

$$m_i \geq -\frac{1}{S^V_{Qi,i}} \tag{5.16}$$

5.2.3 Approach II: Equal reactive power sharing

The general tendency in the approach I of DBV method is that PV systems at the beginning of the feeder contribute less or no reactive power for the voltage regulation compared to PV systems at the end, and so, the main reactive power pressure would be imposed on PV systems located downstream on the feeder. This in turn, depending upon the maximum overvoltage level, may result in overloading at the corresponding PV inverters. Therefore, one possible option is to set ΔQ_i in (4.10) equal to each other in order to take the advantage of all PV systems in the grid and, moreover, to prevent disparity between PV owners. Then, the equal required reactive power, $\Delta Q_i = q$, can be easily calculated from (4.10). Nevertheless, as it is demonstrated in Paper VI, this causes more overall reactive power consumption and line losses.

Apart from the ΔQ setting in the DBV characteristics, the voltage thresholds must also be adjusted to provide the possibility of equal reactive power sharing among all PV systems. Therefore, it is important to find a set of voltage thresholds that can guarantee the participation of the nearer upstream PV systems on the feeder. Hence, since the first PV system on the feeder has the least participation tendency, the maximum possible voltage threshold of the first PV system that allows its participation is considered as a criterion to find the rest of voltage thresholds. The maximum voltage threshold of the first PV system

coincides with its corresponding minimum slope factor. Therefore, the maximum voltage threshold of the first PV system on the feeder can easily be calculated as follows

$$V_{th,1} = V_{d,1} - \frac{q}{m_{min1}} \tag{5.17}$$

In order to determine the rest of voltage thresholds, the net load/generation of all PV systems is monotonically and simultaneously increased and in the mean time the first-bus voltage is tracked; once the maximum voltage threshold appears at the first bus, the voltages of other buses represent the rest of voltage thresholds.

5.3 Results and discussion

The DBV method are applied to a LV radial test grid consisted of five PV-equipped houses, connected via a step-down transformer to a medium voltage grid, presented in Paper VI. However, the DBV method further developed and applied to a larger system presented in Paper VII. The result demonstrate that the features of the voltage sensitivity matrix in association with a multi-objective design can be used to optimally coordinate characteristics of the droop-based voltage regulation among PV systems in the radial feeders. It is shown that the total reactive power consumption and associated losses are lower in the multi-objective approach, which also finds better combinations of V_{th} and ΔQ that not only reduce maximum reactive power consumption and line losses at the critical operating point but also decline the reactive power consumption profile, as compared to the equal reactive power. It is also shown in the test case that a characteristic minimizing of reactive power consumption and line losses has higher and narrower ranges of activation for each PV, and a large slope, with the effect that voltage deviations are compensated only when they approach the highest allowable value. At the other extreme, a characteristic that instead results in equal sharing by PVs is shown to require wider activation ranges and lower gains, but to also incur the penalty of higher losses and reactive power consumption. If the narrow activation range is considered as a problem then possible extension is adding additional constraints on activation range and other parameters to accommodate practical issues. Moreover, in the future scenarios if consuming reactive power by household PV systems come along with the cost penalties, finding a mechanism to equally share the penalty of reactive power may be more efficient than equally distributing reactive power among household PV systems.

Chapter 6

Static equivalent model

This chapter describes the use of gray-box modeling concept in system identification to develop a static equivalent model of distribution grids with high level penetrations of PV systems embedded with voltage support schemes. This chapter also introduces Paper VII.

6.1 Introduction

Generally speaking, traditional power systems feed power via transmission lines to distribution grids, where the majority of power system loads are installed. In contemporary power systems, this, however, may not be the case because the integration of distributed generation units such as PV systems into distribution grids has resulted in pumping power to transmission lines in light load conditions. Therefore, a different response behavior of distribution grids in terms of active and reactive power variations versus voltage variations on the transmission side can be expected. Moreover, as mentioned earlier, high penetration of PV systems into distribution grids can cause local problems such as overvoltage [2, 9, 11–19]; using reactive power based schemes to support voltage may even change more the power-voltage characteristics of distribution grids. Hence, with a rapid transformation of pure consumers to prosumers, modelling of active distribution grids is important for studying future smart grids.

Normally, the dimension of distribution grids is high due to large number of sections, branches and load points as compared to a power transmission system with generation and transmission [31]. On the other hand, the real size of a power system can basically be quite big and, therefore, considering a detailed distribution grid to study the power system is neither practical nor necessary. Running a power system simulation including a complex, detailed distribution grid is cumbersome and, hence, it is important to have a simple model that can encapsulate the general behavior of the complex distribution grid in order to facilitate the investigation of power systems. In other words, if the area of investigation is the transmission system, considering the distribution grid with its all dimension is inefficient. Besides, even considering the whole dimension of the distribution grid to only study

one part of it, is not appropriate. Hence, there is a need to find a simple equivalent of the distribution grid that still can provide reasonable precision.

The aggregated static model of traditional distribution grids is normally represented by the constant impedance, constant current and constant power load model (ZIP load model) [32–37]. Distributed renewable energy sources such as PV systems are traditionally addressed as a negative load in the aggregation of loads and PV systems [38–41]. Nevertheless, as mentioned earlier, high penetrations of PV systems in contemporary distribution grids can change the behaviour of distribution grids. Equipping PV systems with voltage support schemes such as the standard $Cos\phi(P)$ characteristic required by German Grid Codes (GGC) [29] may even cause more changes in the power-voltage behavior of distribution grids. For instance, the feed-in power of PV systems in the $Cos\phi(P)$ characteristic is directly imported as a feedforward signal to estimate the required reactive power. Therefore, PV systems not only change the behaviour of the grid in terms of active power but also in terms of reactive power. However, these issues have not been addressed in static aggregation of contemporary distribution grids in the literature. Accordingly, it is needed to develop a new equivalent model of contemporary distribution grids that can capture the dominant behavior of PV systems embedded with voltage support schemes.

The main contribution of this chapter is developing a static equivalent of the distribution grid consisting of large number of PV systems equipped with voltage support schemes by the use of the gray-box modelling concept in system identification. In the proposed model, distributed PV systems within the grid are represented as a separate entity in the aggregation, and loads are also aggregated as a separate ZIP equivalent. In the proposed procedure, all inputs and outputs are measured at the feeding point, which is the boundary point between the part of the distribution grid that is of concern to be aggregated (lower-level grid) and the rest of the grid (higher-level grid). The voltage at the feeding point serves as the input, while the outputs are the net generation/consumption active and reactive power of the ZIP/PV equivalent. The proposed static equivalent model of the distribution grid is formulated for load-flow studies that can simply be integrated into load-flow programs and replace the true distribution grid, while still can keep the overall accuracy high.

6.2 Backbone of equivalencing procedure

Developing an equivalent model is mathematically an identification problem. Depending upon the available physical information and insight of the true system, there are three choices for the model structure, namely black box, gray box and white box [70]. In the black-box model, the topology of the true system is not known and merely the input and output data of the true system are available, which the aim is to map the input data set to the output data set by adjusting free parameters such that the output of the equivalent model becomes as similar as possible to the true system. In the white-box model, as the other extreme case, not only the topology of the true system is known, but also the physical components and their associated composition rates are also available. Thus, the task in the white-box model is to find an exact mathematical model of the true system. In many cases

developing such a model can be complex and may deviate from the purpose of developing a simple equivalent model. The gray-box modeling is something in between, in which the topology of the true system is available but not the exact components and their composition rate. Hence, there are still number of free parameters that must be estimated via the system identification and, in this regard, the aim in the gray-box model is to identify the free parameters based on the observed data behavior similar to the black-box model.

The physical structure of distribution grids is known; however, physical components of demand and their composition rates are not available. Therefore, one can select a gray-box model to develop a load equivalent. The dominant physical behavior of the true grid is represented via a set of equations in the described gray-box model, and the mismatch between the model and the true grid is left to an optimization process to estimate the free parameters of the gray-box model.

The gray-box load modeling has been addressed in the previous literature [35–37, 71]. A dynamic equivalent of a MicroGrid, which consists of only solid oxide fuel cells and high speed single shaft microturbines, was developed using the gray-box model along with evolutionary particle swarm optimization algorithm for identifying equivalent parameters in [71]. The dynamic equivalent of an active distributed network was developed using gray-box model and MATLAB System Identification Toolbox for parameter estimation purpose [35–37]. However, equivalents of distribution grids comprising large amount of PV systems embedded with voltage control scheme have not been addressed in the literature yet.

6.3 Set-up

In order to develop an equivalent model of a target distribution grid as a true system via the gray-box model, the following steps must be carried out:

- selecting a proper equivalent topology that could capture the dominant behavior of the true system;
- formulating the corresponding equations of the selected topology;
- determining the inputs and outputs;
- estimating free parameters through the identification process;
- validating the performance of the identified free parameters of the equivalent model.

6.3.1 True system

The main objective of this study is to develop a static equivalent model of a true distribution grid with a high penetration of PV systems embedded with $Cos\phi(P)$ characteristic that can be integrated into load-flow programs. Therefore, the true system, in this study, is a distribution grid that consists of one feeding point; distribution transformers and lines; individual loads at different nodes within the grid; and individual PV systems. The feeding

point is the boundary point between the distribution level and a higher level grid, where the equivalent of the distribution grid is to be obtained.

Active and reactive power of loads in the true grid are represented by constant impedance, constant current, and constant power load model (ZIP model)

$$P_L = P_{L0}\left(\alpha_z V^2 + \alpha_i V + \alpha_p\right) \tag{6.1}$$

$$Q_L = Q_{L0}\left(\beta_z V^2 + \beta_i V + \beta_p\right) \tag{6.2}$$

where P_{L0} and Q_{L0} are the load active and reactive power at the base voltage. α_z, α_i and α_p are the ZIP coefficient for active power that their sum must be equal to one. Besides, β_z, β_i and β_p are the ZIP coefficients for reactive power that also must have a sum equal to one. Though simulated results using ZIP load model may deviate from the actual field test results, the ZIP load model has been widely recommended and utilized in majority of system studies [32–37]. Therefore, in this study the ZIP load model is employed to represent the behavior of the actual load model in the true system.

Furthermore, PV systems are assumed embedded with either the required GGC standard characteristic $cos\phi(P)$ represented in Fig. 4.1b or the DBV characteristic represented in Fig. 5.1.

In order to roughly simulate field test results, quasi-static analysis of the true grid is deployed to provide the simulated data of active power and reactive power versus the voltage variation at the feeding-point of the grid.

In order to consider variations of solar and demand, different scenarios are investigated for developing the equivalent load model. In each scenario, the state parameters of the grid that represent the status of the grid are assumed known. The state parameters of the grid are

1. the total load active power consumption within the grid at the base voltage $P_{L0,t}$, which is the sum of all individual loads at the base voltage

$$P_{L0,tot} = \sum_{i=1}^{L} P_{L0,i} \tag{6.3}$$

   where L is the number of loads within the grid;

2. power factor of individual loads $cos\phi_{L0,i}$ that in turn yields the total load reactive power;

3. the total PV production $P_{pv,tot}$, which is the sum of all individual PV systems.

6.3.2 General layout of the equivalent

The general layout of the equivalent is depicted in Fig. 6.1. The topology of equivalent model and formulating its corresponding equations are discussed in Section 6.4. As can be seen in Fig. 6.1, the input of the equivalent model is the bus voltage at the feeding point (V). State parameters of the grid are also imported to the equivalent model to determine

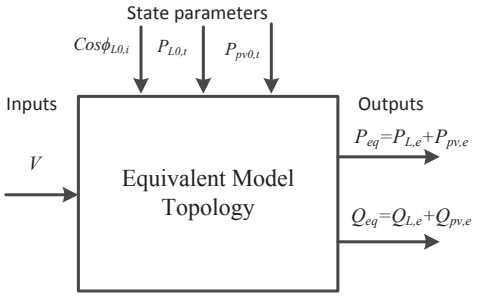

Figure 6.1: Schematic of the equivalent model set-up.

the status of the equivalent model. The values of state parameters and the voltage can vary within specific ranges. Thus, the free parameters of the equivalent model must be estimated such that the output of the equivalent model can demonstrate similar behavior as the output of the true system within the same ranges of variations in the state parameters and the voltage. The outputs of the proposed equivalent model are the net active and reactive power of the equivalent PV model and the equivalent load model.

6.3.3 Estimating free parameters

The flowchart of free parameters estimation process is illustrated in Fig. 6.2, where the bus voltage at the feeding point serves as the input. The variation of V triggers the corresponding variations in the load characteristics at each node in the true system. The larger variation of the V provides a better insight into the load characteristic. Generally, voltage variations bigger than 0.1 p.u. can demonstrate the voltage dependency behavior of the load [33]. Under the V variations and grid state variables, the noise-free outputs of the true system P_u and Q_u are obtained. In real case applications, however, there are always some noise and disturbance associated with measurements as well as uncertainty at the load level and its composition rate at each node. In other words, the noise is an inherited part of any measurement based load modelling approach. Therefore, in this study, the noise-free simulated results are polluted with a Gaussian noise to resemble P and Q characteristics as a real case application.

The V variations along with corresponding grid state parameters are also imported to the gray-box model to estimate $\hat{P}$ and $\hat{Q}$. The difference between output of the true system and the gray-box model e is fed back to the parameters tuning algorithm to estimate the free parameters by minimizing the sum of squared errors ($\sum e^2$), which represents the model error at the end.

In a nutshell, the procedure of estimating free parameters is summerized as follows:

- selecting N different feeding voltages;
- selecting M different scenarios for state parameters of the grid;

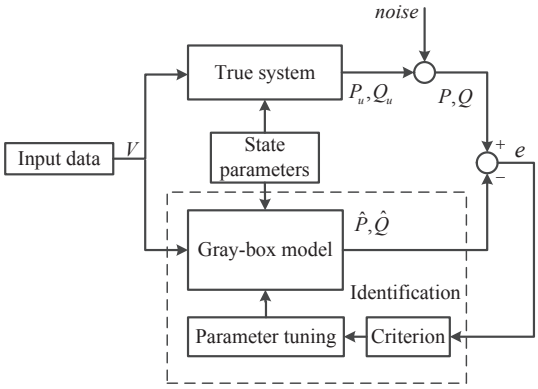

Figure 6.2: Free parameter estimation process in the gray-box model.

- analysing the reaction of the true system for each case via load-flow analysis;
- estimating free parameters such that the equivalent provides a reaction which is as close as possible to the one in the true system for all cases.

6.3.4 Model error

Any model identification method introduces a model error composed of two components, namely bias error and the variance error [70]:

$$(Model\ error)^2 = (Bias\ error)^2 + Variance\ error \tag{6.4}$$

The bias error has to do with the model structure and basically demonstrates the systematic deviation between the true system and the model structure. Normally, modelling a non-linear process leaves a bias error. Bias error in aggregation of a distribution grid consisting of various load components is unavoidable. Generally, increasing the flexibility of the model by increasing the number of parameters will lead to lower bias error. Nevertheless, the bias error and the variance error are in conflict and choosing a complex model results in a larger variance error. It is shown in [70] that the variance error increases by number of the parameters. The variance error depicts the deviation between estimated parameters and their optimal value that happens due to using a finite and noisy data set. Moreover, it can be shown that regardless of the model, for a large training data set (data set that is employed to estimate the parameters) the variance error approximately has a linear relation with the number of free parameters n as follows:

$$variance\ error \sim \sigma \frac{n}{N} \tag{6.5}$$

where σ is the noise variance and N is the number of training data samples [70]. Therefore, the fewer the parameters, the more accurate the estimation is. In regard to this fact, it can be shown that among all models that describe a process accurately, the simplest one causes lowest error [70]. Moreover, it is obvious that the larger training data sets can cancel out the noise impact and lower the variance error.

With that being said, due to the bias/variance error dilemma, the model should be neither too simple nor too complex and instead somewhere in between.

6.3.5 Optimization problem

Identification task is an optimization problem and so an objective function must be formulated. The root mean square error (RMSE) is a frequently used measure to evaluate residuals between the predicted model values and actual values observed from the true system. As discussed earlier, the number of training data sets plays a key role in the accuracy of the model identification. Thus, assuming M as the number of the data sets, the RMSEs of active and reactive power associated with *i*th data set are represented as follows:

$$E_{pi} = \sqrt{\frac{\sum_{i=1}^{N}\left(P_i-\hat{P}_i\right)^2}{N}} \tag{6.6}$$

$$E_{qi} = \sqrt{\frac{\sum_{i=1}^{N}\left(Q_i-\hat{Q}_i\right)^2}{N}} \tag{6.7}$$

since the value of P and Q can vary significantly in different data sets, the relative RMSEs of E_{pi} and E_{qi} are employed

$$e_{pi} = \frac{E_{pi}}{\overline{P}_i} \tag{6.8}$$

$$e_{qi} = \frac{E_{qi}}{\overline{Q}_i} \tag{6.9}$$

where $\overline{P}_i$ and $\overline{Q}_i$ are the average active and reactive power of the *i*th data set, respectively. Therefore, the proposed objective function for the model identification is

$$min\left(\sum_{i=1}^{M}\left(e_{pi}^2+e_{qi}^2\right)\right) \tag{6.10}$$

Here, it is assumed that the relative RMSEs of P and Q are of equal importance. However, if the DSO has other priorities, then one can add different weighting factors.

It will be shown in the next section that the formulated optimization problem in this study is non-linear. Generally, there are two types of non-linear optimization techniques, namely local optimization techniques and global optimization techniques. As it stems from the name of non-linear local optimization techniques, the found optimum via these techniques is a local optimum located in the vicinity of the initial guess without searching

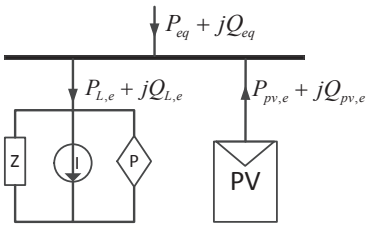

Figure 6.3: Equivalent ZIP/PV model.

other parameter space and, therefore, the performance of them heavily depends upon the starting point guess. Nevertheless, the convergence speed in local optimization techniques are relatively higher than global techniques. Global techniques, on the one hand, try to escape from being trapped in a local optimum by searching through the entire parameter space, but on the other hand the convergence speed to any optimum is likely slow. Thus, it is a good idea to employ a hybrid procedure using a global optimization technique to get near the region of parameter space that the optimum may lie and then feeding the estimated free parameter to a local optimization technique to find the optimum [70]. In this study, the genetic algorithm is employed to find the region and sequential quadratic programming is used to find the optimum.

6.4 Model structure

According to what discussed, in order to reduce the model error, there has to be a compromise with the flexibility of equivalent topology. Therefore, the proposed equivalent topology (Model I) consists of only a ZIP equivalent of load next to an equivalent of PV systems, which will be discussed in the following. The quality of proposed model is examined against the traditional way of addressing PV systems as the negative load (Model II).

6.4.1 Model I: ZIP/PV equivalent

The schematic of the proposed equivalent ZIP/PV model is shown in Fig. 6.3. The equivalent model consists of 1) a ZIP equivalent load model; 2) a PV equivalent associated with an equivalent $cos\phi(P)$ characteristic.

The ZIP load model is described by the following set of equations

$$P_{L,eq} = P_{L0,tot}\left(\alpha_Z V^2 + \alpha_I V + \alpha_P\right) \quad (6.11)$$

$$Q_{L,eq} = Q_{L0,tot}\left(\beta_Z V^2 + \beta_I V + \beta_P\right) \quad (6.12)$$

where $P_{L,eq}$ and $Q_{L,eq}$ are the active and reactive power of the equivalent ZIP load, respectively. $P_{L0,tot}$ and $Q_{L0,tot}$ are total active and reactive power at the base voltage. α_Z, α_I and

α_P are, respectively, constant impedance part, constant current part and constant power part of active power of the equivalent ZIP load that must satisfy the constraint in (6.13). In the same way, β_Z, β_I and β_P are, respectively, constant impedance part, constant current part and constant power part of reactive power of the equivalent ZIP load that are subjected to the constraint in (6.14).

$$\alpha_Z + \alpha_I + \alpha_P = 1 \quad (6.13)$$
$$\beta_Z + \beta_I + \beta_P = 1 \quad (6.14)$$

Depending upon the employed voltage support scheme in the true system, the equivalent PV in the proposed gray-box model is represented in either of the following two ways:

1) GGC characteristic

If the PV systems in the true system are equipped with the GGC standard characteristic, the equivalent of PV systems is depicted by the following set of equations:

$$P_{pv,eq} = \alpha_{pv} P_{pv,tot} \quad (6.15)$$
$$cos\phi_{pv,eq} = m_{pv,eq}\left(P_{pv,eq} - P_{th,eq}\right) \quad (6.16)$$
$$Q_{pv,eq} = P_{pv,eq}\sqrt{\frac{1}{(cos\phi_{pv,eq})^2} - 1} \quad (6.17)$$

where $P_{pv,eq}$ and $Q_{pv,eq}$ are active and reactive power of the equivalent PV model. $P_{pv,tot}$ is the total generated active power by PV units in the true system. α_{pv} represents the mismatch of losses via lines. The voltage support characteristic of the equal PV system shown in Fig. 6.4 is assumed to be similar to the standard characteristic of the GGC. Nevertheless, in the proposed ZIP/PV equivalent model, the slope and the threshold power of the $cos\phi(P)$ characteristic for the equivalent PV model are free parameters and their tuning is left to the identification process. In this regard, $m_{pv,eq}$ and $P_{th,eq}$ are the slope and the threshold power of the equivalent $cos\phi(P)$ characteristic. The motivation to have different P and Q modelling in the equivalent PV model are owing to the following reasons:

- it is assumed that the total generated active power by PV units in the true system is available and not the individual PV production;
- reactive power of PV systems is functioning via a piecewise characteristic with respect to the feed-in power of PV systems.

It is also worth mentioning that the loss for reactive power is accommodated via the free parameters assigned to model the equivalent reactive power of PV systems.

Based on (6.11), (6.12), (6.15) and (6.17), the equivalent active and reactive power at the feeding point can be stated as follows:

$$P_{eq} = P_{L,eq} - P_{pv,eq} \quad (6.18)$$
$$Q_{eq} = Q_{L,eq} - Q_{pv,eq} \quad (6.19)$$

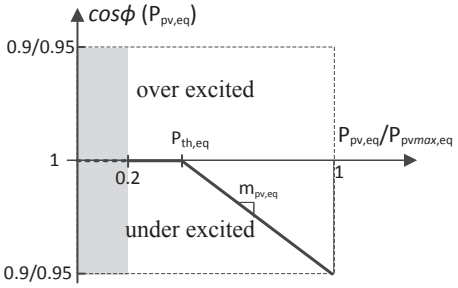

Figure 6.4: *cosφ* (P) characteristic curve of the equivalent PV model.

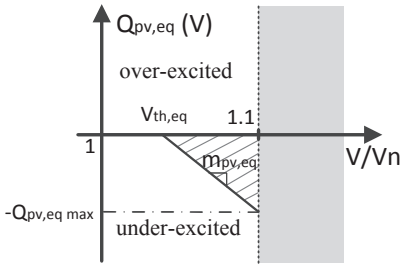

Figure 6.5: DBV characteristic curve of the equivalent PV model.

Therefore, there exists, as demonstrated in the following vector, nine free parameters in the proposed ZIP/PV model that must be estimated via the proposed optimization process.

$$\begin{bmatrix} \alpha_Z & \alpha_I & \alpha_P & \beta_Z & \beta_I & \beta_P & \alpha_{pv} & m_{pv,eq} & P_{th,eq} \end{bmatrix} \tag{6.20}$$

2) DBV characteristic

If the PV systems in the true system are equipped with DBV characteristics, the equivalent reactive power must be modelled in a different way in comparison with the GGC characteristic. In this regard, equations corresponding to reactive power of the equivalent PV system (6.16) and (6.17) in the previous subsection must be replaced by the following equation

$$Q_{pv,eq} = m_{pv,eq}\left(V - V_{th,eq}\right) \tag{6.21}$$

where $m_{pv,eq}$ and $V_{th,eq}$ are respectively the slope and the voltage threshold of the equivalent Q(V) characteristic represented in Fig. 6.5.

Therefore, the free parameters in the proposed ZIP/PV model with the DBV equivalent characteristic are as follows

$$\begin{bmatrix} \alpha_Z & \alpha_I & \alpha_P & \beta_Z & \beta_I & \beta_P & \alpha_{pv} & m_{pv,eq} & V_{th,eq} \end{bmatrix} \tag{6.22}$$

It is worth mentioning that parameters of the Q(V) characteristic (slope and voltage threshold) of PV systems in the true system are set according to the proposed multi-objective coordinated DBV approach in Chapter 5 to minimize reactive power consumption. So, with the use of the Q(V) characteristic, one can expect a lower share of reactive power as compared to the GGC standard characteristic employed in the previous subsection.

6.4.2 Model II: PV system as the negative load

Non-dispatchable renewable generation units such as solar power productions are often addressed as negative loads [38–41]. Hence, PV systems are not considered as a separate entity. The following set of equations represent PV systems as a negative load within the ZIP load equivalent model:

$$P_{eq} = (P_{L0,tot} - P_{pv,tot})\left(\alpha_Z V^2 + \alpha_I V + \alpha_P\right) \tag{6.23}$$

$$Q_{eq} = (Q_{L0,tot} - Q_{pv,tot})\left(\beta_Z V^2 + \beta_I V + \beta_P\right) \tag{6.24}$$

where $Q_{pv,tot}$ is the total reactive power consumptions by PV systems and in the case of using GGC characteristics derived based on the GGC characteristic in Fig 4.1b and total active power production of PV systems. In the case of DBV method, $Q_{pv,tot}$ is the total reactive power consumptions by PV systems at the base voltage.

As depicted in the following vector, there are therefore only six free parameters in this equivalent model:

$$\begin{bmatrix}\alpha_Z & \alpha_I & \alpha_P & \beta_Z & \beta_I & \beta_P\end{bmatrix} \tag{6.25}$$

6.5 Results and discussion

A utility distribution grid with eight feeders and thirty five buses is used as the test true system to implement proposed equivalencing procedure. In this system with maximum active and reactive demand of 515 kW and 170 kVar, the average active and reactive power errors of the proposed ZIP/PV equivalent in the presence of the GGC characteristic were in the range of $2.44\,kW$ (0.5%) and $3.84\,kvar$ (2.2%), respectively; and in the presence of the DBV characteristics were in the range of $2.6\,kW$ (0.5%) and $8.3\,kvar$ (4.9%), respectively. However, the average active and reactive power errors of the traditional way in the presence of the GGC characteristic were in the range of 8.61 kW (1.7%) and 6.55 kVar (3.8%), respectively; and in the presence of the DBV characteristics were in the range of 9 kW (1.75%) and 21.2 kVar (12.5%). The results demonstrate that the proposed equivalent model not only reduces active and reactive errors as compared to the traditional way but also represents a similar trajectory behavior in $P_{eq}(V)$ and $Q_{eq}(V)$ at the feeding point as the true distribution grid does. Furthermore, it is shown that the active power-voltage behavior of the traditional model cannot be a proper representative of the true system for different possible scenarios of consumption and production levels (e.g. in this case study when the total production of PV systems goes beyond the total load consumption level) due

to inflexibility of the model that causes a bad parameter setting. It is also demonstrated that in the case of PV systems equipped with DBV characteristics, the reactive power-voltage characteristic of the traditional model cannot capture the piecewise functioning behavior of DBV characteristics embedded in PV systems. Besides, the trajectory behavior of the traditional way tangibly differs from the true grid even when the total load consumption level is higher than the PV production level. Further details can be found in Paper VII.

Thus, in the current and future distribution grids with high level PV penetrations, it is beneficial to address PV systems as a separate entity in the aggregation as demonstrated in the proposed ZIP/PV equivalent.

Chapter 7

Conclusions and future work

This chapter highlights the key conclusions of the thesis and summarizes ideas for future research work.

7.1 Conclusions

Voltage profile control via reactive power contribution of PV systems can generally be done in two ways: 1) directly controlling voltage at each bus to obtain a certain voltage profile in which reactive power is indirectly regulated; 2) indirect control of voltage via reactive power to support voltage profile in order to keep it within designated limits. In the latter, reactive power is directly controlled. This thesis demonstrates that direct voltage control in radial distribution grids to obtain a certain profile can cause interactions among PV systems. In this regard, the features of voltage sensitivity matrix and concepts of relative gain array as well as singular value decomposition in control science are employed to first quantify interactions, and second, assess the possibility of decoupling interactions among voltage controllers. The results demonstrate that the direct voltage control strategy via PV systems for obtaining a certain voltage profile is not a proper solution. In other words, it is beneficial to use reactive power to support voltage instead of directly controlling it. In this regard, two main reactive power regulation strategies are developed, namely coordinated active power dependent reactive power characteristic Q(P), and coordinated droop-based voltage regulation characteristic Q(V). In these methods, voltage profile is indirectly regulated via reactive power to remain within the designated limits instead of deriving a certain profile.

This thesis accordingly demonstrates how advantages of the voltage sensitivity matrix allow systematic coordination of Q(P) characteristics among PV inverters while still using local measurements. Two main parameters of the Q(P) characteristic for each PV system in a distribution grid, namely the slope factor and the threshold, are specified based on analysis of the voltage sensitivity matrix. The proposed approach regulates either the target-bus voltage or the voltage profile for several nodes under the steady-state voltage limit. Therefore, the slope factors are derived in two different ways. Moreover, the thresholds are also

calculated via two different ways, namely identical threshold and equal reactive power sharing. The results demonstrate that the proposed methods are able to regulate the voltage to the steady-state voltage limit, while the voltage regulation in the German Grid Codes (GGC) method is not addressed. Since the four variants of the proposed method explicitly include voltage limits, they can decrease the total required reactive power as well as active power loss caused by reactive power in comparison with the GGC. The proposed method is further developed by accommodating an optimization formulation to optimally coordinate the Q(P) parameters among PV systems.

Further, this thesis demonstrates that the features of the voltage sensitivity matrix in association with a multi-objective design can be used to optimally coordinate characteristics of the droop-based voltage regulation among PV systems in radial feeders. Each characteristic is specified by two main parameters, namely the voltage threshold and the slope factor, which are determined based on the voltage sensitivity analysis and the multi-objective approach in order to balance the individual reactive power distribution against total reactive power consumption and line losses. It is shown in the test case that a characteristic minimizing of reactive power consumption and line losses has higher and narrower ranges of activation for each PV, and a large slope, with the effect that voltage deviations are compensated only when they approach the highest allowable value. At the other extreme, a characteristic that instead results in equal sharing by PVs was shown to require wider activation ranges and lower gains, but to also incur the penalty of higher losses and reactive power consumption. If the narrow activation range is considered as a problem then possible extension is adding additional constraints on activation range and other parameters to accommodate practical issues. Moreover, in the future scenarios if consuming reactive power by household PV systems come along with the cost penalties, finding a mechanism to equally share the penalty of reactive power may be more efficient than equally distributing reactive power among household PV systems.

The application of proposed coordinated Q(P) and Q(V) methods may be regarded as cumbersome since an adjustment of parameters, following the connection of any additional PV system to the feeder, would be required by the DSO in order to use the proposed methods to their full capability. A more practical approach, however, is an implementation of the proposed methods in the DSO's long-term (strategic, i.e., 10-year ahead) network planning process. The DSO would pre-define the threshold and slope values for PV systems in certain grid locations based on an expected future PV integration level and distribution in the grid. While this may result in sub-optimal performance in the transitional period, an optimal choice of parameters with regard to the finally expected grid stage would be achieved.

Moreover, this thesis demonstrates that in the aggregation of modern distribution grids with high level PV penetrations, it is beneficial to address PV systems as a separate entity. In this regard, this thesis deploys the gray-box modelling concept to propose a new static equivalent model of distribution grids with a high level penetration of PV systems embedded with voltage support schemes. In the proposed model, PV systems within the grid are aggregated as a separate entity in addition to the ZIP equivalent load. So, the proposed structure of the equivalent consists of a ZIP equivalent load and a PV equivalent embedded with an equivalent of the corresponding voltage support scheme utilized in the

grid. The quality performance of the proposed method is compared against traditional way of modelling PV systems as the negative load in the grid. It is shown that in a utility test case with maximum active and reactive demand of 515 kW and 170 kVar, the average active and reactive power errors of the proposed ZIP/PV equivalent in the presence of the GGC characteristic are in the range of 2.44 kW (0.5%) and 3.84 kVar (2.2%), respectively; while in the traditional model are in the range of 8.61 kW (1.7%) and 6.55 kVar (3.8%), respectively. It is also shown that in the presence of the DBV characteristics the average active and reactive power errors of the proposed ZIP/PV equivalent are in the range of 2.6 kW (0.5%) and 8.3 $kvar$ (4.9%), respectively; while in the traditional model are in the range of 9 kW (1.75%) and 21.2 kVar (12.5%). The proposed equivalent model not only reduces active and reactive errors compared to the traditional way but also represents a similar trajectory behavior in $P_{eq}(V)$ and $Q_{eq}(V)$ at the feeding point as the true distribution grid does. Furthermore, it is shown that the traditional way leads to a larger error especially when the total production of PV systems goes beyond the total load consumption level. Besides, the trajectory behavior of the traditional way tangibly differs from the true grid even when the total load consumption level is higher than the PV production level. It is also demonstrated that in the case of PV systems equipped with DBV characteristics, the reactive power-voltage characteristic of the traditional model cannot capture the piecewise functioning behavior of DBV characteristics embedded in PV systems.

7.2 Future work

Challenges and studies associated with large numbers of PV systems integration are quite new in power systems, and comparatively little research has been done in this area. Consequently, the list of future work can be long. The presented future ideas here are in conjunction with the work carried out in this thesis.

In general, other simulation platforms and test systems can be used for the proposed coordinated Q(P) and Q(V) characteristics. These methods can be integrated into the developed PV model in PowerFactory to evaluate their effectiveness.

Optimization

Though the optimization formulations for the both Q(P) and Q(V) methods in this thesis are fundamentally non-linear, linearized load flow equations in the form of the voltage sensitivity matrix are employed in these formulations to streamline calculations and challenges associated with non-linearities. Nevertheless, optimal power flow (OPF) formulation can be used as an alternative solution at the expense of additional non-linearities. Hence, there is a possible research room to formulate OPF to optimally coordinate Q(P) and Q(V) characteristics and compare the upshot with the proposed APD and DBV methods in this thesis.

Weighting factors

In the proposed multi-objective method, equal weighting factors were considered for the three different target objectives in the objective function. However, one may use multi-

criteria decision analysis (MCDA) to find a different order of priorities or importance according to concerns of DSOs.

Target bus and design operating point

Normally speaking, overvoltage occurs during high PV production and low demand. Along with, in this thesis, the minimum demand (almost no demand) is roughly correlated to the maximum PV production to define the critical operating point for design. However, if daily demand profiles and daily irradiation profiles (or PV production profiles) within the grid are available, one can correlate the minimum demand with the maximum solar electricity production. This would indicate a more realistic critical operating point and can be used in the proposed design procedures, though this was not studied in this thesis. Moreover, the bus with the most violated voltage in the critical operating point is selected as the target bus; however, it may be needed to consider more than one target bus depending on specifications of grids to properly address overvoltage at all buses. This needs to be studied further. Overvoltage in this thesis is calculated based on EN 50160, however DSOs may need to fulfill different requirements. This can also be considered in the design procedure of the proposed voltage support schemes.

Comparison of Q(P) and Q(V)

The performance of Q(V) can be compared and evaluated against Q(P). As a future work, it can also be interesting to deploy the net generation/load as the input signal in the Q(P) characteristic instead of only PV feed-in power, i.e. $Q(P_{net})$. Accordingly, one can compare $Q(P_{net})$ method against Q(V)method.

Under voltage situations

If under voltage is a case in some weak distribution grids during high demand and low PV production periods, the proposed Q(P) and Q(V) methods can further be extended to evaluate their performance in addressing under voltage.

Economic aspects

This thesis neither assesses the economical pros and cons of proposed reactive power regulation strategies against each other and nor compares them against other overvoltage remedies. Therefore, it would be interesting to evaluate these methods from an economic point of view using yearly basis load and solar profiles.

Dynamic aspects

Unlike coordinated Q(P) characteristics, coordinated Q(V) characteristics use voltage as the input to calculate the required reactive power for each PV systems. Since voltage is influenced by many factors such as load consumption and PV productions, dynamic interactions among PV systems operating in tandem is likely. Therefore, it is important

to do more research to address how possible interactions can be canceled out in order to eliminate oscillatory behavior in controllers. In this thesis, a rate limiter was employed in quasi steady-state analysis to limit the sudden changes in reactive power due to changes in voltage in order to damp oscillations. The settings of rate limiters may also be considered in the design procedure of Q(V) parameters. Other delay functions may also be utilized to damp the possible oscillation. Therefore, it would be interesting to do more studies on these issues.

Equivalencing

It is important to examine the influence of different reactive power regulation strategies (e.g. Q(P) and Q(V) characteristics) and/or a combination of different regulation strategies for different PV systems on the equivalencing to further evaluate the quality of the proposed ZIP/PV equivalent. Besides, voltage control via transformers at the feeding point may have an impact on the equivalent, and so, requires coordination with PV system control. Furthermore, it is crucial to consider load and PV system dynamics in aggregation to develop a dynamic equivalent of distribution grids with high penetration of PV systems.

Bibliography

[1] A. Jaeger-Waldau, "PV status report 2013," tech. rep., European Commission, DG Joint Research Center, Institute for Energy and Transport, Renewable Energy Unit, Sept. 2013.

[2] M. Vandenbergh, D. Craciun, V. Helmbrecht, R. Hermes, R. Lama, P. Michele Sonvilla, M. Rekinger, and G. Concas, "Prioritisation of technical solutions available for the integration of pv into the distribution grid," tech. rep., DERlab, European Distributed Energy Resources Laboratories e. V., June 2013.

[3] D. Verma, O. Midtgard, and T. Satre, "Review of photovoltaic status in a european (EU) perspective," in *2011 37th IEEE Photovoltaic Specialists Conference (PVSC)*, pp. 003292 –003297, June 2011.

[4] U. Schwabe and P. Jansson, "Utility-interconnected photovoltaic systems reaching grid parity in new jersey," in *2010 IEEE Power and Energy Society General Meeting*, pp. 1 –5, July 2010.

[5] D. Pérez, V. Cervantes, M. J. Báez, and J. González-Puelles, "PV grid parity monitor," tech. rep., ECLAREON, Oct. 2012.

[6] M. Bazilian, I. Onyeji, M. Liebreich, I. MacGill, J. Chase, J. Shah, D. Gielen, D. Arent, D. Landfear, and S. Zhengrong, "Re-considering the economics of photovoltaic power," *Renewable Energy*, vol. 53, pp. 329–338, May 2013.

[7] G. Masson, M. Latour, M. Rekinger, I.-T. Theologitis, and M. Papoutsi, "GLOBAL MARKET OUTLOOK for photovoltaics 2013-2017," tech. rep., EPIA European Photovoltaic Industry Association, 2013.

[8] "Photovoltaic power systems programme anuual report 2013," tech. rep., IEA International Energy Agency, 2013.

[9] T. Stetz, F. Marten, and M. Braun, "Improved low voltage grid-integration of photovoltaic systems in Germany," *IEEE Transactions on Sustainable Energy*, vol. PP, no. 99, pp. 1 –9, 2012.

[10] Yves-Marie Saint-Drenan, S. Bofinger, B. Ernst, T. Landgraf, and K. Rohrig, "Regional nowcasting of the solar power production with pv-plant measurements and satellite images," in *ISES SolarWorld Congress*, 2011.

[11] R. Shayani and M. de Oliveira, "Photovoltaic generation penetration limits in radial distribution systems," *IEEE Transactions on Power Systems*, vol. 26, pp. 1625 –1631, Aug. 2011.

[12] R. Tonkoski, L. Lopes, and T. El-Fouly, "Coordinated active power curtailment of grid connected PV inverters for overvoltage prevention," *IEEE Transactions on Sustainable Energy*, vol. 2, pp. 139 –147, Apr. 2011.

[13] E. Demirok, P. Casado Gonzalez, K. Frederiksen, D. Sera, P. Rodriguez, and R. Teodorescu, "Local reactive power control methods for overvoltage prevention of distributed solar inverters in low-voltage grids," *IEEE Journal of Photovoltaics*, vol. 1, pp. 174 –182, Oct. 2011.

[14] A. Pinto and R. Zilles, "Reactive power excess charging in grid-connected PV systems in brazil," *Renewable Energy*, vol. 62, pp. 47–52, Feb. 2014.

[15] A. Cagnano, F. Torelli, F. Alfonzetti, and E. De Tuglie, "Can PV plants provide a reactive power ancillary service? a treat offered by an on-line controller," *Renewable Energy*, vol. 36, pp. 1047–1052, Mar. 2011.

[16] R. Tonkoski and L. A. Lopes, "Impact of active power curtailment on overvoltage prevention and energy production of PV inverters connected to low voltage residential feeders," *Renewable Energy*, vol. 36, pp. 3566–3574, Dec. 2011.

[17] N. El Halabi, M. Garcia-Gracia, J. Borroy, and J. Villa, "Current phase comparison pilot scheme for distributed generation networks protection," *Applied Energy*, vol. 88, pp. 4563–4569, Dec. 2011.

[18] M. Baran, H. Hooshyar, Z. Shen, and A. Huang, "Accommodating high PV penetration on distribution feeders," *IEEE Transactions on Smart Grid*, vol. 3, pp. 1039–1046, June 2012.

[19] S. Steffel, P. R. Caroselli, A. M. Dinkel, J. Q. Liu, R. N. Sackey, and N. R. Vadhar, "Integrating solar generation on the electric distribution grid," *IEEE Transactions on Smart Grid*, vol. 3, pp. 878–886, June 2012.

[20] Y. Liu, J. Bebic, B. Kroposki, J. De Bedout, and W. Ren, "Distribution system voltage performance analysis for high-penetration PV," in *IEEE Energy 2030 Conference, 2008. ENERGY 2008*, pp. 1–8, Nov. 2008.

[21] D. Geibel, T. Degner, T. Reimann, B. Engel, T. Bülo, J. Da Costa, W. Kruschel, B. Sahan, and P. Zacharias, "Active intelligent distribution networks - coordinated voltage regulation methods for networks with high share of decentralised generation," in *Integration of Renewables into the Distribution Grid, CIRED 2012 Workshop*, pp. 1–4, May 2012.

[22] X. Liu, A. Aichhorn, L. Liu, and H. Li, "Coordinated control of distributed energy storage system with tap changer transformers for voltage rise mitigation under high photovoltaic penetration," *IEEE Transactions on Smart Grid*, vol. 3, pp. 897 –906, June 2012.

[23] G. Mulder, D. Six, B. Claessens, T. Broes, N. Omar, and J. V. Mierlo, "The dimensioning of PV-battery systems depending on the incentive and selling price conditions," *Applied Energy*, 2013.

[24] R. Tonkoski and L. Lopes, "Voltage regulation in radial distribution feeders with high penetration of photovoltaic," in *IEEE Energy 2030 Conference, 2008. ENERGY 2008*, pp. 1 –7, Nov. 2008.

[25] A. Engler and N. Soultanis, "Droop control in LV-grids," in *2005 International Conference on Future Power Systems*, pp. 1–6, Nov. 2005.

[26] M. Braun, "Reactive power supply by distributed generators," in *2008 IEEE Power and Energy Society General Meeting - Conversion and Delivery of Electrical Energy in the 21st Century*, pp. 1 –8, July 2008.

[27] K. Turitsyn, P. Sulc, S. Backhaus, and M. Chertkov, "Options for control of reactive power by distributed photovoltaic generators," *Proceedings of the IEEE*, vol. 99, pp. 1063–1073, June 2011.

[28] A. Yazdani, A. Di Fazio, H. Ghoddami, M. Russo, M. Kazerani, J. Jatskevich, K. Strunz, S. Leva, and J. Martinez, "Modeling guidelines and a benchmark for power system simulation studies of three-phase single-stage photovoltaic systems," *IEEE Transactions on Power Delivery*, vol. 26, pp. 1247 –1264, Apr. 2011.

[29] "Power generation systems connected to the low/voltage distribution network," in *VDE application rule VDE-AR-N 4105:2011-08*, 2011.

[30] "Studie zur Ermittlung der technischen Mindesterzeugung des konventionellen Kraftwerksparks zur Gewährleistung der Systemstabilität in den deutschen Übertragungsnetzen bei hoher Einspeisung aus erneuerbaren Energien," tech. rep., Studie im Auftrag der deutschen Übertragungsnetzbetreiber, Jan. 2012.

[31] A. Neto, A. Rodrigues, R. Prada, and M. Da Guia da Silva, "External equivalent for electric power distribution networks with radial topology," *IEEE Transactions on Power Systems*, vol. 23, no. 3, pp. 889–895, 2008.

[32] "Standard load models for power flow and dynamic performance simulation," vol. 10, no. 3, pp. 1302–1313.

[33] H. Renmu, M. Jin, and D. Hill, "Composite load modeling via measurement approach," vol. 21, no. 2, pp. 663–672.

[34] A. Bokhari, A. Alkan, R. Dogan, M. Diaz-Aguilo, F. de Leon, D. Czarkowski, Z. Zabar, L. Birenbaum, A. Noel, and R. Uosef, "Experimental determination of the ZIP coefficients for modern residential, commercial, and industrial loads," *IEEE Transactions on Power Delivery*, vol. 29, pp. 1372–1381, June 2014.

[35] S. M. Zali and J. Milanovic, "Modelling of distribution network cell based on grey-box approach," in *7th Mediterranean Conference and Exhibition on Power Generation, Transmission, Distribution and Energy Conversion (MedPower 2010)*, pp. 1–6.

[36] S. Zali and J. Milanovic, "Generic model of active distribution network for large power system stability studies," vol. 28, no. 3, pp. 3126–3133.

[37] J. Milanovic and S. Mat Zali, "Validation of equivalent dynamic model of active distribution network cell," vol. 28, no. 3, pp. 2101–2110.

[38] T. Kato, T. Inoue, and Y. Suzuoki, "Impact of large-scale penetration of photovoltaic power generation systems on fluctuation property of electricity load," in *Transmission and Distribution Conference and Exposition, 2010 IEEE PES*, pp. 1–6.

[39] D. Halamay, T. Brekken, A. Simmons, and S. McArthur, "Reserve requirement impacts of large-scale integration of wind, solar, and ocean wave power generation," in *2010 IEEE Power and Energy Society General Meeting*, pp. 1–7.

[40] Warsono, D. King, C. Ozveren, and D. Bradley, "Economic load dispatch optimization of renewable energy in power system using genetic algorithm," in *Power Tech, 2007 IEEE Lausanne*, pp. 2174–2179.

[41] B. Tamimi, C. Canizares, and K. Bhattacharya, "System stability impact of large-scale and distributed solar photovoltaic generation: The case of ontario, canada," *IEEE Transactions on Sustainable Energy*, vol. 4, no. 3, pp. 680–688.

[42] D. Flood, "Satellite solar energy systems," in *Telecommunications Energy Conference, 1997. INTELEC 97., 19th International*, pp. 12–12, Oct. 1997.

[43] R. Burlon, S. Bivona, and C. Leone, "Instantaneous hourly and daily radiation on tilted surfaces," *Solar Energy*, vol. 47, no. 2, pp. 83–89, 1991.

[44] R. Chenni, "Study of solar radiation in view of photovoltaic systems optimization," *Smart Grid and Renewable Energy*, vol. 02, no. 04, pp. 367–374, 2011.

[45] M. Suri, T. A. Huld, E. D. Dunlop, and H. A. Ossenbrink, "Potential of solar electricity generation in the european union member states and candidate countries," *Solar Energy*, vol. 81, pp. 1295–1305, Oct. 2007.

[46] W. De Soto, S. A. Klein, and W. A. Beckman, "Improvement and validation of a model for photovoltaic array performance," *Solar Energy*, vol. 80, pp. 78–88, Jan. 2006.

[47] D. Sera, R. Teodorescu, and P. Rodriguez, "PV panel model based on datasheet values," in *IEEE International Symposium on Industrial Electronics, 2007. ISIE 2007*, pp. 2392 –2396, June 2007.

[48] M. Hejri, H. Mokhtari, M. Azizian, M. Ghandhari, and L. Söder, "On the parameter extraction of a five-parameter double-diode model of photovoltaic cells and modules," *IEEE Journal of Photovoltaics*, vol. 4, pp. 915–923, May 2014.

[49] S. Kjaer, J. Pedersen, and F. Blaabjerg, "A review of single-phase grid-connected inverters for photovoltaic modules," *IEEE Transactions on Industry Applications*, vol. 41, pp. 1292–1306, Sept. 2005.

[50] T. Esram and P. Chapman, "Comparison of photovoltaic array maximum power point tracking techniques," *IEEE Transactions on Energy Conversion*, vol. 22, pp. 439–449, June 2007.

[51] Y. Huang, F. Peng, J. Wang, and D.-W. Yoo, "Survey of the power conditioning system for PV power generation," in *37th IEEE Power Electronics Specialists Conference, 2006. PESC '06*, pp. 1–6, June 2006.

[52] I. Balaguer, H.-G. Kim, F. Peng, and E. Ortiz, "Survey of photovoltaic power systems islanding detection methods," in *34th Annual Conference of IEEE Industrial Electronics, 2008. IECON 2008*, pp. 2247–2252, Nov. 2008.

[53] A. Yazdani and P. Dash, "A control methodology and characterization of dynamics for a photovoltaic (PV) system interfaced with a distribution network," *IEEE Transactions on Power Delivery*, vol. 24, pp. 1538 –1551, July 2009.

[54] S.-K. Kim, J.-H. Jeon, C.-H. Cho, E.-S. Kim, and J.-B. Ahn, "Modeling and simulation of a grid-connected PV generation system for electromagnetic transient analysis," *Solar Energy*, vol. 83, pp. 664–678, May 2009.

[55] Y. T. Tan, D. Kirschen, and N. Jenkins, "A model of PV generation suitable for stability analysis," *IEEE Transactions on Energy Conversion*, vol. 19, pp. 748 – 755, Dec. 2004.

[56] S. Skogestad and I. Postlethwaite, *Multivariable Feedback Control: Analysis and Design*. Wiley-Interscience, 2 ed., Nov. 2005.

[57] E. Demirok, D. Sera, R. Teodorescu, P. Rodriguez, and U. Borup, "Evaluation of the voltage support strategies for the low voltage grid connected PV generators," in *2010 IEEE Energy Conversion Congress and Exposition (ECCE)*, pp. 710 –717, Sept. 2010.

[58] R. Aghatehrani and R. Kavasseri, "Reactive power management of a DFIG wind system in microgrids based on voltage sensitivity analysis," *IEEE Transactions on Sustainable Energy*, vol. 2, pp. 451 –458, Oct. 2011.

[59] H. Saadat, *Power System Analysis Third Edition*. PSA Publishing, THIRD EDITION ed., June 2010.

[60] E. Bristol, "On a new measure of interaction for multivariable process control," *IEEE Transactions on Automatic Control*, vol. 11, pp. 133 – 134, Jan. 1966.

[61] S. Skogestad and K. Havre, "The use of RGA and condition number as robustness measures," *Computers & Chemical Engineering*, vol. 20, Supplement 2, no. 0, pp. S1005–S1010, 1996.

[62] A. Samadi, R. Eriksson, and L. Söder, "Evaluation of reactive power support interactions among PV systems using sensitivity analysis," in *2nd International Workshop on Integration of Solar Power into Power Systems*, (Lisbon, Portugal), pp. 245–252.

[63] "Voltage characteristics of electricity supplied by public distribution systems," in *DIN EN 50160*.

[64] Kerber,Georg, "Konzept für eine autonome blindleistungsregelung von umrichteranlagen," Feb. 2008.

[65] A. Timbus, R. Teodorescu, F. Blaabjerg, and U. Borup, "Online grid impedance measurement suitable for multiple PV inverters running in parallel," in *Twenty-First Annual IEEE Applied Power Electronics Conference and Exposition, 2006. APEC '06*, pp. 907–911, 2006.

[66] G. Kerber, R. Witzmann, and H. Sappl, "Voltage limitation by autonomous reactive power control of grid connected photovoltaic inverters," in *Compatibility and Power Electronics, 2009. CPE '09.*, pp. 129 –133, May 2009.

[67] B.-I. Craciun, E. Man, V. Muresan, D. Sera, T. Kerekes, and R. Teodorescu, "Improved voltage regulation strategies by PV inverters in LV rural networks," in *2012 3rd IEEE International Symposium on Power Electronics for Distributed Generation Systems (PEDG)*, pp. 775 –781, June 2012.

[68] M. Chandorkar, D. Divan, and R. Adapa, "Control of parallel connected inverters in standalone AC supply systems," *IEEE Transactions on Industry Applications*, vol. 29, no. 1, pp. 136–143, 1993.

[69] M. Marwali, J.-W. Jung, and A. Keyhani, "Control of distributed generation systems - part II: load sharing control," *IEEE Transactions on Power Electronics*, vol. 19, pp. 1551 – 1561, Nov. 2004.

[70] O. Nelles, *Nonlinear System Identification: From Classical Approaches to Neural Networks and Fuzzy Models*. Springer, 2001.

[71] F. O. Resende and J. Peas Lopes, "Development of dynamic equivalents for MicroGrids using system identification theory," in *Power Tech, 2007 IEEE Lausanne*, pp. 1033–1038.

P-I

Reactive Power Dynamic Assessment of a PV System in a Distribution Grid

Available online at www.sciencedirect.com

SciVerse ScienceDirect

Energy Procedia 20 (2012) 98 – 107

Energy Procedia

Technoport RERC Research 2012

Reactive Power Dynamic Assessment of a PV System in a Distribution Grid

Afshin Samadi[a*], Mehrdad Ghandhari[a], Lennart Söder[a]

[a]*Royal Institute of Technology, KTH, Stockholm 100 44, Sweden*

Abstract

Accommodating more and more PV systems in grids has raised new challenges that formerly had not been considered and addressed in standards. According to recently under-discussed standards, each PV unit is allowed to participate in reactive power contributions to the grid to assist voltage control. There are some PV models in the literature however those models mostly assumed unity power factor operation for PV systems owing to the contemporary standards. Therefore, there is a need to develop a PV model considering the reactive power contribution and its dynamic influence on power system. This paper describes non-proprietary modeling of a three-phase, single stage PV system consisting of controller scheme design procedure and coping with the important aspects of three different reactive power regulation strategies and their impact assessment studies. The model is implemented in PSCAD to examine the behavior of the proposed model for recently codified reactive power strategies. Furthermore, this model is integrated in a distribution grid with two PV systems in order to effectively investigate consequences of the different reactive power control strategies on the distribution network.

Keywords: PV system modelling; instantaneous model; reactive power control.

1. Introduction

The growing trend in photovoltaic system installations due to encouraging feed-in-tariffs via long-term incentives has led to high penetration of PV systems in distribution grids which has brought about new issues that initially had not been addressed. In Germany, for instance, there are currently 18 GWp installed PV systems [1]. According to recent drop in costs of PV systems, especially PV panel

* Corresponding author. *E-mail address*: afshins@kth.se

1876-6102 © 2011 Published by Elsevier Ltd. Selection and/or peer-review under responsibility of the Centre for Renewable Energy.
doi:10.1016/j.egypro.2012.03.012

technologies, which has occurred during recent years, grid-parity is not anymore unimaginable and in near future will come close to reality [2]. Thus, PV systems without incentives are more likely to be interesting in many different countries. So studying the technical aspects of integrating large amount of PV systems into grid will be an inevitable essential to keep the system on an even keel.

According to the new German grid codes [3], each PV unit is allowed to participate in reactive power contributions to the grid to assist voltage control. The reactive power regulation, in LV grid, should fulfill 0.9 under-exited to 0.9 over-exited by means of the following strategies; either fixed power factor or power factor as a function of feed-in power (*PF(P)*). Although depending on the size of PV system other methodologies such as reactive power depending the voltage (*Q(V)* droop) would be imposed by system operators. Implementation of the reactive power control is a challenge since according to standards, some criteria must be fulfilled but it has not been explicitly mentioned that which procedure and how. Another challenge associated with PV systems is that companies have their own proprietary detailed-model information which is hard to get that information. By doing so, there is a need to have some model that could capture all the fundamental characteristics of a PV system and in the meantime, being non-proprietary in order to examine the impact of PV system on distribution grid.

There are some PV models in the literature [4-7], however those models mostly assumed unity power factor operation for PV systems [4-6] or just considering reactive power support for medium voltage connected PV system [7].

Therefore, there is a need to develop PV model considering the reactive power contribution and its dynamic influence on distribution power system. In this paper a non-proprietary PV model of a three-phase, single stage PV system is proposed which consists of design procedure of two reactive power controller schemes and deals with the important aspects of three different reactive power regulation strategies. PSCAD/EMTDC is used as a platform to study widely the behavior of the proposed model along with comparing three reactive power regulation strategies. Furthermore, this model is integrated in a distribution system with two PV systems in order to effectively investigate consequences of the dynamic characteristics of the proposed model on a distribution network. Simulation results demonstrate the credibility of the designed model as well as the interaction of the three different PV reactive power regulation strategies on the bus voltages profile and on next-door PVs.

In the following, a general perspective of a PV system will be given in section 2, dynamic equations of a PV system are presented in section 3, section 4 deals with controller design procedure, reactive power control strategies are discussed in section 5 and simulations results and conclusion are presented in sections 6 and 7, respectively.

2. Structure of PV system

Fig.1 illustrates the main schematic of a single stage PV system connected through a transformer to a distribution grid. PV systems consist of PV array, dc-bus capacitor, voltage source converter and peripheral control systems. Solar cells are connected in series to form PV modules and PV modules in turn are connected in series or in parallel to form PV panels. PV panels are connected in series and in parallel to form solar array in order to provide adequate power and voltage for being connected to grid. The output power of PV array feeds in capacitor link which is connected in parallel and is transformed through parallel connected voltage source converter to AC power. The VSC terminals are connected to the point of common coupling via the interface reactor which shown by L and R, where R represents the resistance of both reactor and VSC valves. C_f is the shunt capacitor filter that absorbs undesirable low-frequency current harmonics generated by PV system. PV system is interfaced with grid through a transformer which makes an isolated ground for PV system as well as boosting the level of output voltage

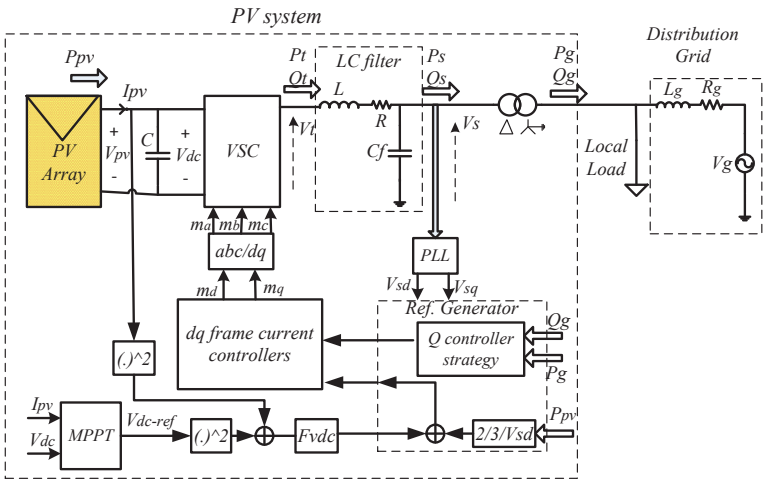

Fig. 1. Schematic of a PV system structure connected to a distribution grid.

of PV system to the grid voltage level. Distribution grid is assumed by Thevenin model where R_g and L_g are equivalent grid resistance and inductance, respectively.

Employing Phase Lock Loop (PLL) helps to move from *abc*–frame to a proper *dq*-frame and in the meantime streamlines control process by having access to dc control signals instead of sinusoidal-varying signals which are synchronized with grid frequency. Active and reactive powers of PV system are controlled via the d and q axis, respectively. Active power is controlled through regulating DC-bus voltage. Reactive power control will be explained later. Control systems comprise three control loops, inner loop is current control, middle loop is DC-bus voltage regulator as well as reactive power control loop and outer loop is maximum power point tracking (MPPT). PV system always needs additional function to exploit maximum power of PV array which is named MPPT in literature. As can be seen in Fig. 1, MPPT determines DC-bus voltage reference. The error between DC-bus voltage and its corresponding reference voltage compensated by $F_{vdc}(s)$ to provide reference active power and in turn creates i_{dref}. In order to augment the performance of DC-bus voltage regulator, output power of PV is deployed as a feed-forward to eliminate the nonlinearity and destabilizing impact of PV array output power [4,9]. I_q reference command, depending on reactive power control strategy is issued. I_{dref} and I_{qref} are passed through current controllers to produce modulating signals for SPWM that in turn provides gate signals for VSC valves.

3. Dynamic of PV system and distribution grid

Dynamic of the DC-link is depicted by

$$\frac{d}{dt}[\frac{1}{2}CV_{dc}^2] = P_{pv}(V_{dc},G,T) - P_{loss} - P_t \tag{1}$$

$P_{pv}(V_{dc},G,T)$ is output power of PV array that is function of irradiance (G) and temperature (T); Sera [8] describes how to calculate solar panel parameters via datasheet in order to model PV array which is also employed in this paper. P_{loss} is VSC switching power loss and P_t is the delivered active power by VSC. P_t can also be described by delivered active power at PCC, $P_s = 3/2\,\mathrm{Re}(\vec{V}_s \vec{i}^{\,*})$ where $\vec{x}$ denotes phasor representation [9], and instantaneous active power consumed by interface reactor as follows:

$$P_t = P_s + \frac{3}{2}\mathrm{Re}(L\frac{d\vec{i}}{dt}\vec{i}^{\,*}) + \frac{3}{2}\mathrm{Re}(R\vec{i}\,\vec{i}^{\,*}) \tag{2}$$

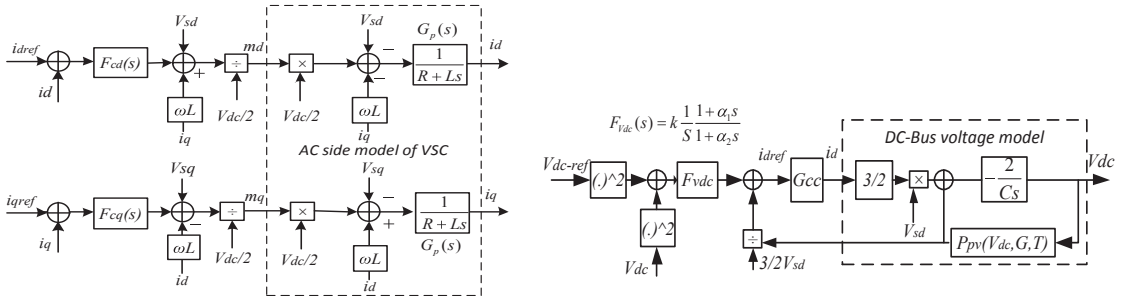

Fig. 2. (a) Schematic of current control block diagram; (b) Block diagram of DC-bus voltage control loop

Following equation describes the dynamic of AC side of VSC in space-phasor domain.

$$\vec{v}_t + L\frac{d\vec{i}}{dt} + R\vec{i} + \vec{v}_s = 0 \tag{3}$$

Terminal voltage of VSC is a controllable variable that corresponds to PWM modulation index $\vec{v}_t = \vec{m}V_{dc}/2$ where $\vec{m}$ is the normalized, phasor modulating signal.

Dynamic of the distribution network can be shown as follows:

$$\vec{v}_s = L_g\frac{d\vec{i}_g}{dt} + R_g\vec{i}_g + \vec{v}_g \tag{4}$$

4. PV system control

Projection of space-phasor variables on rotating *dq*-frame gives two components in *d* and *q* axes. PLL regulates V_{sq} to zero and subsequently determines the speed of rotating *dq*-frame which is synchronized to V_s [9]. By doing so, PV system output active and reactive powers are expressed as follows:

$$P_s = 3/2 v_{sd} i_d \quad \& \quad Q_s = -3/2 v_{sd} i_q \tag{5}$$

So, P_s is proportional to i_d and can be regulated by that. As mentioned beforehand, active power is controlled to regulate dc-bus voltage in such a way that could extract maximum power from PV arrays with the help of MPPT. Analogous with P_s, Q_s is also proportional to i_q and therefore can be controlled through it which will be explained later on.

4.1. Current control loop

According to (3), the dynamics of VSC AC-side in *dq*-frame are expressed as follows:

$$\begin{cases} -v_{td} + L\omega i_q + L\dfrac{di_d}{dt} + Ri_d + v_{sd} = 0 \\ -v_{tq} - L\omega i_d + L\dfrac{di_q}{dt} + Ri_q + v_{sq} = 0 \end{cases} \tag{6}$$

These equations are deployed to design current controllers and as can be seen, those are nonlinear, cross-coupled equations. Therefore, following equations are employed to decouple and linearize them:

$$\begin{cases} v_{td} = \left(L\omega i_q + v_{sd} + U_d\right) \\ v_{tq} = \left(-L\omega i_d + v_{sq} + U_q\right) \end{cases} \tag{7}$$

Where U_d and U_q are new control inputs. By substituting (7) in (6), the corresponding control scheme can be represented in Fig. 2(a). The plant transfer function of current loop is $G_p(s) = 1/(R + Ls)$. Since the resultant dynamics of *d* and *q* axis are identical, compensators could also be identical. Direct synthesis method can be employed to shape current closed-loop transfer function as a first order system like $G_{cc}(s) = \alpha_c / (\alpha_c + s)$. To achieve it, the controller should be as follows:

$$F_c(s) = \frac{\alpha_c}{s} G_p^{-1}(s) = \alpha_c L + \frac{\alpha_c R}{s} \tag{8}$$

$F_c(s)$ resembles a proportional-integral controller. α_c is the current closed-loop band-width which on one hand should be large to give fast current control response and on the other hand should be small enough to become considerably smaller than switching frequency(in *rad/s*) for instance 10 times. α_c relation with the rise time (t_{rc}) is $\alpha_c t_{rc} = \ln 9$.

4.2. DC-Bus voltage regulator

The instantaneous active power of interface reactor and VSC switching loss, which are relatively much smaller than PV arrays output power and delivered power at PCC (P_s), can be ignored. Therefore, based on (1) and substituting (2) and (5) in it, the dynamic of DC-bus voltage in *dq*-frame would be as follows:

$$\frac{d}{dt}[\frac{1}{2} C V_{dc}^2] \cong P_{pv}(P_s, G, T) - \frac{3}{2} v_{sd} i_d \simeq P_{pv}(P_s, G, T) - \frac{3}{2} v_{sd} i_{dref} \tag{9}$$

Fig. 2(b) illustrates DC-bus voltage regulator model which the feed-forward helps to eliminate the effect of the P_{pv} on the dynamic of DC-bus [4,9]. F_{Vdc} consists of an integrator and a lead compensator.

4.3. MPPT function

Actually MPPT is the third control loop or in other words the outer control loop of the PV system which has a memory to provide DC-bus voltage reference by measuring the output voltage and current of PV arrays and comparing them with previous states through a processing algorithm. Here in this paper, incremental conductance [10] algorithm is employed.

4.4. Reactive power controller

Reactive power control can be done either by regulating reactive power at the reference value or controlling the voltage at the connection point, although it must be considered that the reactive power contribution of PV system is limited according to the current standards and moreover the set-point is dependent on the voltage magnitude at the connection point. Nevertheless, in this section mainly controller design procedure will be discussed. According to (5) reactive power can be regulated via i_q by doing so, one simple way is to calculate required reference reactive power and then translating it into reference current in *q* axis through a straightforward calculation. Although the reactive power seen by grid is not equal to the generated reactive power by VSC due to presence of the reactor, filter capacitor and the leakage inductance of the transformer. Therefore, in order to augment the performance of reactive power regulation, reactive power can be controlled through an extra control loop (Fig. 3(a)). The difference between measured reactive power and reference reactive power passes through a controller to provide i_{qref}. Similar to $F_c(s)$ design procedure, direct synthesis method is employed to derive reactive power controller in such a fashion that leads to first order closed-loop transfer function.

$$F_q(s) = -\frac{2}{3V_{sd}} \frac{\alpha_q}{s} G_{cc}^{-1}(s) = \frac{-2\alpha_q}{3\alpha_c V_{sd}} + \frac{-2\alpha_q}{3V_{sd}} \frac{1}{s} \tag{10}$$

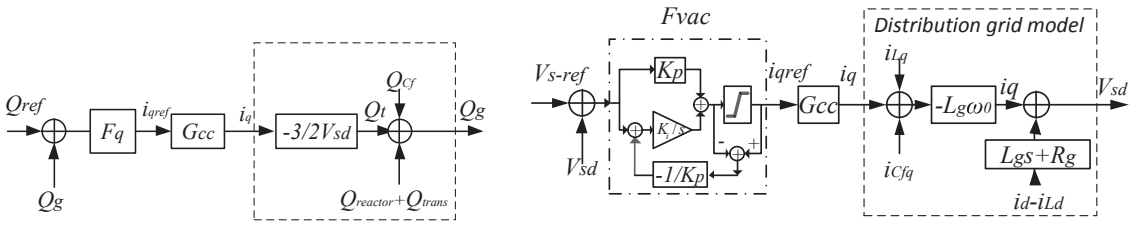

Fig. 3. (a) Block diagram of reactive power control loop; (b) Block diagram of AC bus voltage regulator

α_q is the closed-loop bandwidth of reactive power controller and must be much smaller than α_c . So through this scheme the contribution of other passive elements such as reactor and filter capacitor as well as the PV connecting transformer are considered as disturbances and therefore the desired reactive power can be achieved more precisely.

Another approach to control reactive power is through controlling the AC bus voltage. In this approach the difference between the AC-bus voltage and reference value passes through a controller to attain i_{qref}. A few assumptions are taken into account in order to design AC voltage controller. All the transient excursions in the frequency angle of PLL output are neglected even though v_s is not anymore a stiff grid. Moreover, it can also be expected that v_{sq}=0, therefore, only the dynamic of v_{sd} is required. By doing so the linearized *dq*-frame form of (6) can be shown as follows [9]:

$$\tilde{V}_{sd} = L_g \frac{di_{gd}}{dt} + R_g \tilde{i}_{gd} - L_g \omega_0 \tilde{i}_{gq} \tag{11}$$

Where ~ stands for linearized variables and $\tilde{i}_{gdq} = \tilde{i}_{dq} - \tilde{i}_{Ldq} - \tilde{i}_{C_f dq}$. Fig. 3(b) depicts the block diagram of AC voltage regulator for a PV system. So, due to the prior assumptions, the dynamic of distribution grid is purely seen as a gain equal to $-L_g\omega_0$. Closed-loop transfer function of AC-bus voltage regulator can be shaped to a first order function such as $\alpha_v / (\alpha_v + s)$ where α_v is the closed loop band-width and must be much smaller than α_c. According to Fig. 3(b) and similar to F_c, F_{vac} can be shaped as following, although the proportional and integral gain probably may be retuned to get maximum phase margin on the grounds that the grid inductance is subjected to change; moreover, due to the assumptions.

$$F_{vac}(s) = \left(\frac{1}{-L_g \omega_0}\right) \frac{\alpha_v}{s} G_{cc}^{-1}(s) = \frac{-\alpha_v}{\alpha_c L_g \omega_0} + \frac{-\alpha_v}{L_g \omega_0} \frac{1}{s} \tag{12}$$

Since the reactive power contribution of the system is limited then it is more likely that the controller hits the limits and integrators saturates, so anti wind-up, which is shown in Fig. 3(b), should be employed to prevent the saturation and its negative effect on the controller performance.

Since V_s and V_g are electrically close to each other and the difference is only voltage drop across transformer leakage reactance, then it would also be possible to regulate magnitude of V_g in Fig. 3(b).

5. Reactive power control strategies

Regarding reactive power contribution, a PV system could carry out this task through one of the following approaches.

5.1. Constant power factor operation

PV system could have no reactive power contribution by unity power factor operation and the whole capacity of the PV system inverter is assigned to deliver generated active power by solar cells to AC network. This approach had been implemented for all-currently installed PV systems, although reactive

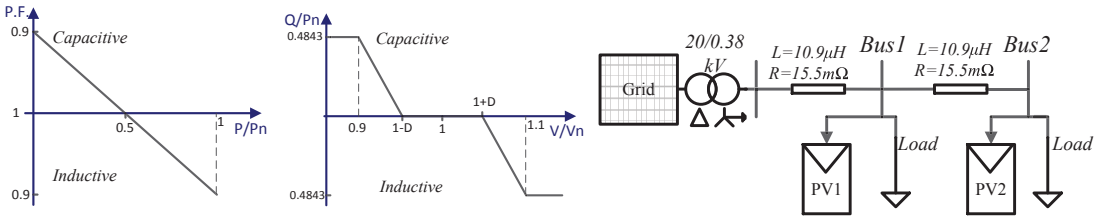

Fig. 4. (a) Dynamic power factor characteristic, *PF(P)*; (b) Droop control strategy, *Q(V)*; (c) Schematic of the studied network

power support has been considered by recently re-codified standards to work under non-unity power factor. In the constant power factor, PV system regardless of the AC bus voltage feeds reactive power into network. Reactive power contribution affects the sizing of PV inverter; for instance in order to accommodates reactive power to achieve PF=0.9 without any active power limitation, the inverter must be oversized by 11%.

5.2. Dynamic power factor operation, PF(P)

This method was proposed by German grid codes [3]. Fig. 4(a) could depict this approach more clearly. As can be seen, depending on the level of generated active power, the value of PF as well as the type of generated reactive power varies. This method also works regardless of the voltage profile of the line, however in contrast to previous approach reduces the unnecessary reactive power provision. To implement this scheme in the simulation, the active power is measured and normalized to the nominal power of the PV to get PF as well as command reactive power according to Fig. 4(a). In this paper the PF at the end of the PV connecting transformer is of a concern to be controlled.

5.3. Q(V)

This approach is a droop-based control strategy and Fig. 4(b) depicts a linear droop curve where the value of the dead band (D) depends on the network impedance [11]. In this method as far as the voltage is within the dead band region, unnecessary reactive power contribution is prevented.

5.4. AC-bus voltage regulation

The technical aspects of this approach were explained in section 4.4. The performance of this approach depends on the set points to the extent that neighborhood PVs might interact against each other. This issue would be shown in the following section.

6. Simulation results

In this part, based on the configuration of Fig. 4(c), two 10 kW PV systems are connected to a quite weak distribution grid to study the impact of the controllers and reactive power strategies. It is assumed that the distribution grid works on a light load condition, so the load value is *0.6 kW+j0.3 kVar*. Both PV systems are identical and are structured according to Fig.1 in PSCAD/EMTDC. Since the PV connecting transformer also contributes to the reactive power, output node of the PV connecting transformer is considered for reactive power regulation.

An identical simulation scenario is carried out in order to make a fair and comprehensive comparison between different strategies. Fig. 5(a) depicts irradiance variation during simulation which varies stepwise

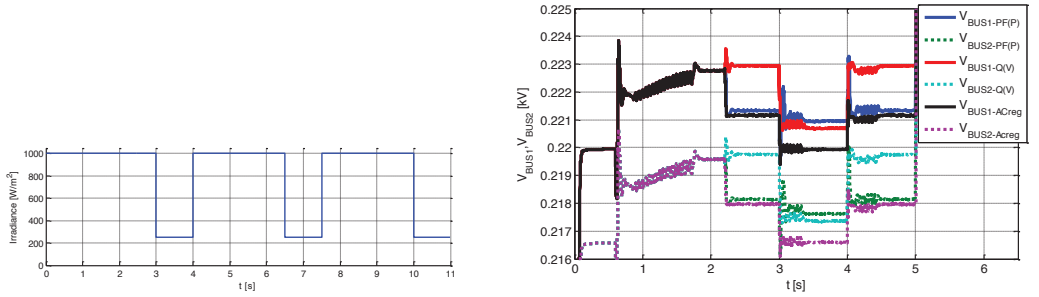

Fig. 5. (a) Irradiance step changes; (b) Bus voltages responses to PV connection and irradiance step changes at nominal voltage

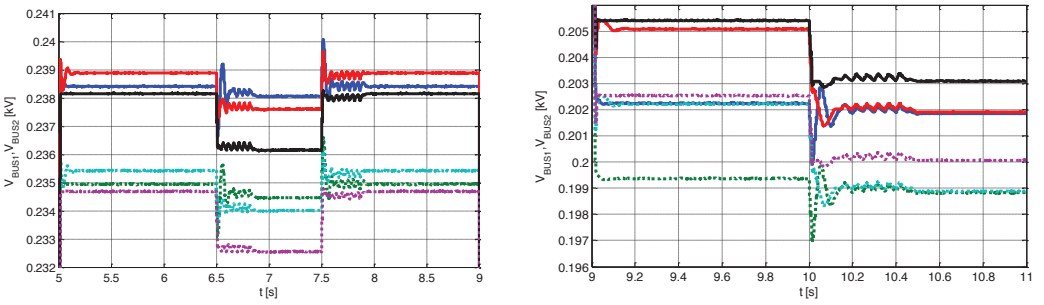

Fig. 6. (a) Bus voltages responses to irradiance step changes at high voltage limit; (b) Bus voltages responses to irradiance step changes at low voltage limit

to simplify investigations. PV systems at *t=0.6 sec* is connected to grid while irradiance is 1000 W/m^2, grid voltage is set to a value to get nominal voltage (0.22 kV) at bus 1 and reactive power regulator is inactivated. Once the PV systems stabilize at MPP by the assistance of the MPPT, at *t=2.2 sec* the reactive power regulator is activated to study its role on the voltage profile. At *t=3* and *4 sec* irradiance level is changed to 250 W/m^2 and again 1000 W/m^2 to explore the behavior of the PV system controllers at low and high power production. Furthermore, in order to investigate the performance of the three different reactive power control strategies the grid voltage is also changed. By doing so, two voltage incidents take place at *t=5 and 9 sec* that the grid voltage is boosted by 8% and then lowered by 16% approximately. Moreover, irradiance level also is varied within each voltage step change. Dead-band (D) in *Q(V)* strategy, Fig. 4(b), is assumed to be 0.03. The set-point of AC voltage regulation strategy is adjusted to the value of the bus voltages prior to PVs connection.

Since the voltage variations corresponding to irradiance step changes at bus 1 and 2 (Fig. 4(c)) are relatively small compared to the grid voltage step changes, different time frames are employed to illustrate the bus voltages through Figs. 5(b), 6(a) and 6(b). Reactive powers at the PVs connection points are depicted at Fig. 7(a). As can be seen in Fig. 7(a), once the reactive power regulator is activated the bus voltages vary and reactive strategies behave as the following:

- *PF(P)* strategy consumes reactive power and lowers the voltage, Fig. 7(b) illustrates power factor at the connection point of the PV for the *PF(P)* strategy. Within *t=9 to 10 sec* while the grid voltage is at the lowest point and irradiance at the highest level, this approach pushes the bus voltages even more down in contrast to other methods due to unnecessary inductive reactive power consumption.
- The small step change at the bus voltages after activating *Q(V)* strategy is due to the presence of the filter and the transformer. The i_q command of the PV controller is set to zero before *t=2.2 sec.*

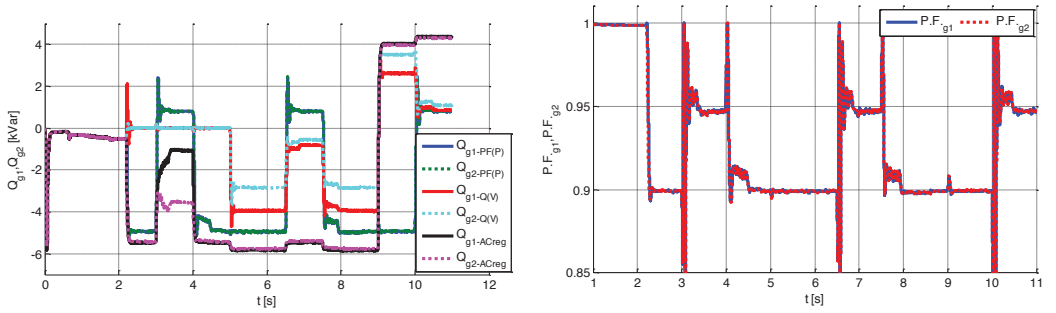

Fig. 7. (a) Reactive power at the output of PVs for three different strategies; (b) Power factor of PV systems in PF(P) strategy

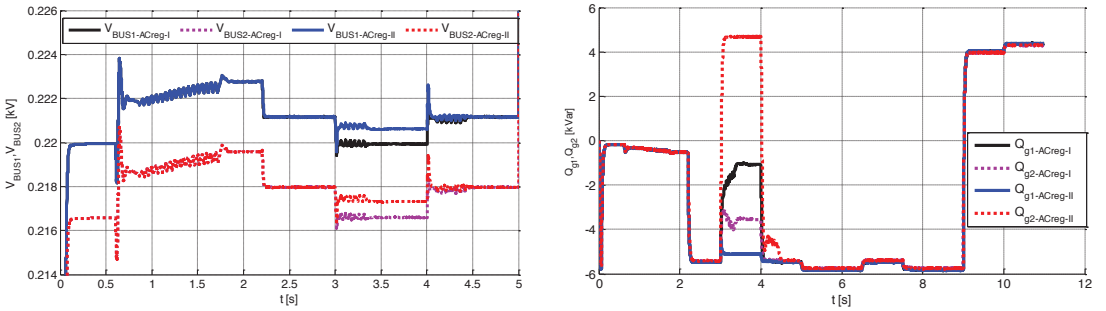

Fig. 8. (a) Bus voltages responses to different set-points corresponding to V_{AC} regulation strategy ; (b) Reactive power at the output of PVs corresponding to V_{AC} regulation strategy

Therefore the reactive power of the transformer and the filter affects the bus voltage, while after activating reactive power regulator, VSC works in a way to regulate reactive power to the command reactive power which should be zero as far as the voltage at the connection point is within the dead-band. In contrast to *PF(P)*, within *t=0 to 5 sec* interval, *Q(V)* strategy has no reactive power contribution because of operation within the dead-band region. Thus the bus voltages during this interval are effectively affected by PV active power variations. However, at higher or lower bus voltages *Q(V)* provides reactive power and in contrast to *PF(P)* the amount of generated reactive power depends on the voltage level.

- AC-bus voltage regulator strategy tries to consume reactive power as much as within the limits to return the voltage to its initial level prior to PV connection (case I). As can be seen in Fig. 5(b), this approach can only fulfill the set-points when the PVs are working at one fourth of the full power (G=250 W/m^2). Although changing the set-points would effectively influence the performance of the controller. For instance, in another case (case II), the set-point of PV 2 at bus 2 is increased by less than 0.7% and the results are in Fig. 8(a) and 8(b) which for the clarity only the time-interval before *t=5 sec* is demonstrated in Fig. 8(a), on the grounds that the rest has the same performance. As can be seen at low irradiance level (G=250 W/m^2), AC-voltage regulators are interacting against each other to the extent that PV 1 and PV 2 are operating in inductive and capacitive modes, respectively, and none of them can fulfill the desired set-points in contrast to case I. However in case II, at high irradiance, PV 2 can reach the desired set point in contrast to case I. Therefore, it is obvious that the lack of coordination between reactive power regulators leads to negative interaction among installed PV systems and their performance is affected.

7. Conclusion

In this paper a comprehensive model of a PV system was presented. Design procedure of PV model controllers including parameters tuning also were presented. Furthermore, two different reactive power controllers were developed for PV model. The model was developed in PSCAD software and integrated in a distribution grid with two PV systems. Simulation results shows the model works as expected. Three different reactive power regulation strategies were studied and the dynamic impact of them on the system and voltage profile was shown. It was also demonstrated that lack of coordination between PVs' set-point in AC-bus voltage regulator strategy brings about negative interaction among installed PV systems in the same vicinity.

References

[1] J. C. Boemer et al "Overview of German Grid Issues and Retrofit of Photovoltaic Power Plants in Germany for the Prevention of Frequency Stability Problems in Abnormal System Conditions of the ENTSO-E Region Continental Europe," 1th international workshop on integration of solar power into power systems, Denmark, October 2011.

[2] R. Brundlinger, C. Mayer, and H. Fechner, IEA-PVPS Task 14 – High Penetration of PV Systems in Electricity Grids Work-Plan 2010-2014.

[3] Verband der Elektrotechnik Elektronik Informationstechnike.V. (VDN) (2010). *Erzeugungsanlagen am Niederspannungsnetz Technische Mindestanforderungen für Anschluss und Parallelbetrieb von Erzeugungsanlagen am Niederspannungsnetz* – Draft of 07-08-2010. Berlin

[4] Yazdani and P. Dash, "A control methodology and characterization of dynamics for a photovoltaic (PV) system interfaced with a distribution network," *IEEE Trans*. Power Del., vol. 24, no. 3, pp. 1538–1555, Jul. 2009.

[5] Kim, S.K., J.H. Jeon, C.H. Cho, E.S. Kim and J.B. Ahn, 2009. "Modeling and simulation of a grid-connected PV generation system for electromagnetic transient analysis," Solar Energy, 83: 664-678. DOI: 10.1016/j.solener.2008.10.020

[6] Y. T. Tan, D. S. Kirschen, and N. Jenkins, "A model of PV generation suitable for stability analysis," *IEEE Trans. Energy Convers.*, vol. 19, no. 4, pp. 748–755, Dec. 2004.

[7] Yazdani et al "Modeling Guidelines and a Benchmark for Power System Simulation Studies of Three-Phase Single-Stage Photovoltaic Systems", IEEE Trans. Power Del., vol. 26, no. 2, pp. 1247–1264, April. 2011.

[8] Sera, R. Teodorescu, P. Rodriguez, "PV panel model based on datasheet values", IEEE International Symposium on Industrial Electronics ISIE 07, June 4-7, 2007, pp.2392-2396.

[9] A. Yazdani and R. Iravani, "Voltage-Sourced Converters in Power Systems" IEEE/John-Wiley, Feb. 2010.

[10] K. H. Hussein, I. Muta, T. Hoshino, and M. Osakada, "Maximum photovoltaic power tracking: An algorithm for rapidly changing atmospheric conditions," *Proc. Inst. Elect. Eng. Gen., Transm. Distrib.*, vol. 142, no. 1, pp. 59–64, Jan. 1995.

[11] Kerber G, Witzmann R: "Voltage Limitation by Autonomous Reactive Power Control of Grid Connected Photovoltaic Inverters". 2009 IEEE, CPE2009, 6th. International Conference Workshop, p. 129-133, 20 – 22 May 2009, Badajoz, Spain.

Appendix A. PV specifications

PV panel: $I_{mp}=3.56A$, $V_{mp}=33.7\ V$, $I_{sc}=3.87\ A$, $V_{oc}=42.1\ A$, $n_s=14$, $n_p=6$.
PV electrical circuit parameters: *DC link capacitor: C=10mF; LC filter: L =4mH, R =3mΩ (including switches on state resistance) and C=10μF; PV connecting transformer: ratio 0.18/0.38 kV, rating 15kVA, leakage inductance 5%.*
PV control circuit parameters: $\alpha_c=2000\ Hz$, $\alpha_1=0.02323$, $\alpha_2=0.001076$, $k=1.3e4$, $\alpha_q=100\ Hz$, $\alpha_V=100\ Hz$.

P-II

Comparison of a Three-Phase Single-Stage PV System in PSCAD and PowerFactory

Comparison of a Three-Phase Single-Stage PV System in PSCAD and PowerFactory

Afshin Samadi, Robert Eriksson, Della Jose, Farhan Mahmood, Mehrdad Ghandhari and Lennart Söder
Department of Electric Power Systems
KTH Royal Institute of Technology
Stockholm, Sweden 10044
Email: afshin.samadi@ee.kth.se, robert.eriksson@ee.kth.se, mehrdad.ghandhari@ee.kth.se, lennart.soder@ee.kth.se

***Abstract*—Accommodating more and more distributed PhotoVoltaic (PV) systems within load pockets has changed the shape of distribution grids. It is not, therefore, accurate anymore to address distribution grids just only as a lumped load. So it will be crucial in the near future to have an aggregate model of PV systems in distribution grids. By doing so, it is important to develop models for PV systems in different simulation platforms to study their behavior in order to derive an aggregate model of them. Although, there have been several detailed-switching model of a PV system in EMTDC/PSCAD simulation platform in literature, these non-proprietary switching models are slow in simulation, particularly when the number of the PV systems increases on the grounds that in PSCAD the simulation is based on time domain instantaneous values and requires more mathematical details of components. Therefore, in this paper a model of the PV system in DIgSILENT/PowerFactory is developed, which is a proper environment to run rms simulation and works based on the phasors and, moreover, from mathematical perspective is more simplified. The performance of the stemming model is compared with the switching model in PSCAD. Comparing the simulation results of the proposed model in PowerFactory with the model in PSCAD shows the credibility and accuracy of the proposed model.**

Keywords: Photovoltaic, PSCAD, PowerFactory, Reactive power support

I. Introduction

High penetration of solar PhotoVoltaic (PV) systems has shaped a new structure for distribution grid. Growing trends in generating power from distributed PV systems have accommodated more and more PV systems in distribution grids. In Germany, for instance, there are currently 20 GW installed PV systems, of which 80% have been connected in low voltage grids [1]. This high penetration of PV systems has also raised new challenges in distribution grids such as voltage profile. Violation of voltage profile in some regions in Germany has led to stopping PV installation by utilities. To contrive a way to solve the unwanted problems associated with high penetration, several approaches have been proposed in recent standards and literature, for instance the reactive power support and the active power curtailment [2]–[5].

In power system studies, distribution grids have mainly been modeled as a lumped load. However it is not anymore wise to just address distribution grids as a passive load [6], [7]. The aforementioned changes that gradually happen in distribution grids require deeming new models of distribution grids for static and dynamic studies of power systems. Therefore, it is crucial to find a proper aggregate model of distribution grids consisting of PV systems in order to properly study the behavior of distribution grids on power system stability and dynamics.

In order to find out a suitable aggregate model of distributed PV systems, it is required to study the behavior of an individual PV system to discover how it functions in the grid. A power test system including PV systems is simulated either as a transient simulation, which uses instantaneous values, or an rms simulation which is based on the phasor model. In the transient simulation, components are needed to be modeled in more mathematical details; however, it, in turn, takes more simulation time. Although rms simulation of the PV system using phasor model is run faster, it excludes some mathematical details. Nevertheless, it is important to find out differences and similarities between these two simulation platforms and models, and then if the dynamic behavior of both models are similar, using phasor model is more time efficient and convenient in order to investigate and attain an aggregated model of distributed PV systems.

Models of a PV system in PSCAD have been addressed in literature such as [8]–[11]. Due to the old standards in the past, those models did not consider different reactive power strategies; however contemporary standards, e.g. German Grid Codes [12], allow reactive power support by PV systems. For instance, [8] only considers unity power factor operation and does not address the reactive power support; Ref. [9] does not consider Maximum Power Point Tracking (MPPT) and reactive power support; proposed model in [10] has been mainly developed for utility application and does not address different reactive power support strategies in distribution grids. Ref. [11] developed a model of a PV system which comprises four different reactive power supports and this model was incorporated in a test distribution grid with two PV systems. In this research a model of the PV system based on the proposed model in [11] is developed in PowerFactory for the rms simulation. There is already one developed generic PV model in PowerFactory Library, however this model has a few differences with the developed PSCAD model, for instance the standard MPPT function is not included and dc-link capacitor has been modeled through power equation. Therefore, since the main aim is comparing two identical models in a similar way, a new model is needed to be developed in PowerFactory.

The objective of this paper is to validate two identical models of a three-phase single-stage PV system in two different simulation platforms, namely PSCAD and PowerFactory, which perform simulations based on time domain instan-

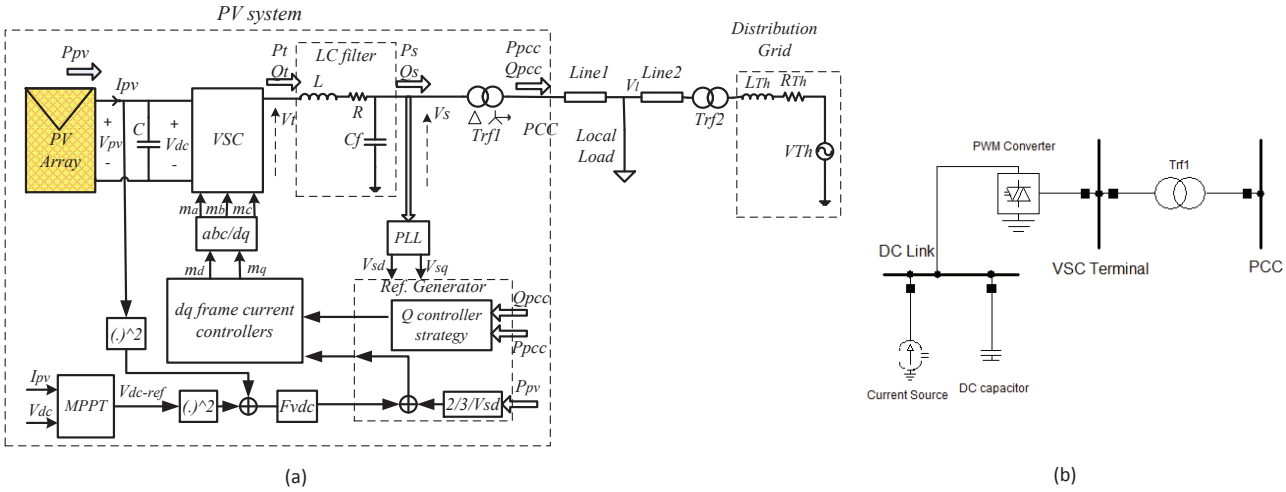

Figure 1. a) Schematic of a PV system structure connected to a distribution grid. b) Schematic of a PV system in PowerFactory.

taneous values and rms values, respectively. Four different reactive power support strategies have been incorporated into the models, i.e. fixed power factor, power factor as a function of feed-in power (hereinafter called dynamic power factor), reactive power depending the voltage Q(V), and AC-Bus voltage regulator. In conclusion, the both designed models are compared and simulation results demonstrate the credibility of those models; differences between them are shown and evaluated.

In the following, a general overview of PV systems structure will be given in section 2, differences and similarities between two models are presented in section 3, section 4 presents results of comparison of a single PV system connected to grid in the both simulation platforms and finally the conclusion comes at section 5.

II. PV SYSTEMS STRUCTURE

Fig. 1 illustrates the one-line diagram schematic of a three pahse single-stage PV system connected through a transformer to a distribution grid. The PV system consists of PV array, dc-link capacitor, Voltage Source Converter (VSC) and peripheral control systems.

Solar cells are connected in series to form PV modules and PV modules are, in turn, connected in series or in parallel to form PV panels. PV panels are connected in series and in parallel to form solar array in order to provide adequate power and voltage for being connected to a grid. The output power of PV array feeds in dc-capacitor link which is connected in parallel and is transformed through parallel connected VSC to AC power. The VSC terminals are connected to the Point of Common Coupling (PCC) via the interface reactor, shown by L and R, and a transformer. The transformer makes an isolated ground for PV system as well as boosting the level of output voltage of PV system to the grid voltage level. C_f is the shunt capacitor filter that absorbs undesirable low-frequency current harmonics generated by PV system. Distribution grid is assumed by Thevenin model where R_{Th} and L_{Th} are equivalent grid resistance and inductance, respectively.

Control system is performed in a dq-frame reference. Phase Locked Loop (PLL) is used to synchronize control system with the grid frequency by moving from the abc-frame reference to a proper dq-frame reference.

A. PV array model

Analogous with a diode, PV panel current-voltage characteristic is exponential and is depicted as follows:

$$I = I_{ph} - I_0 \left(exp\left(\frac{V - R_s I}{V_T} \right) - 1 \right) \tag{1}$$

In (1), I and V are output current and voltage of a PV panel respectively, I_o is the dark saturation current, R_s is the cell series resistance, I_{ph} is the photo-generated current and V_T is the junction thermal voltage. Ref. [13] shows how to calculate solar panel parameters R_s, I_o and I_{ph} by means of datasheet values in Standard Test Condition (STC). I_{ph}, short circuit current and open circuit voltage of the panel are linearly dependent on the irradiance and the temperature, while I_o is only the temperature-dependent [13].

As mentioned earlier solar panels are connected in series and parallel, so the (1) can be extended as follows:

$$I_{pv} = n_p I_{ph} - n_p I_0 \left(exp\left(\frac{V_{pv} - R_s I_{pv}}{n_s V_T} \right) - 1 \right) \tag{2}$$

where V_{pv} and I_{pv} are PV array output voltage and current, and n_s and n_p are number of series and parallel panels, respectively.

B. Controller model of PV system converter

Due to the different abc/dqo transformation, active power and reactive power are controlled on q and d axes in PSCAD, respectively, while it is the other way around in PowerFactory. Nevertheless, for integrity it is here assumed that active power is controlled on the d axis and reactive power on the q axis. Control system in a PV system on the each axis comprises two control loops where the inner loop is the current control (Fig. 2) and the outer loop is the dc-link voltage controller, which regulates active power, on the d axis and reactive power regulator on the q axis.

Active power control in PV systems is performed through regulating the dc-link voltage. The dc-link voltage regulator in the Laplace domain, $F_{vdc}(s)$, which in this study is an

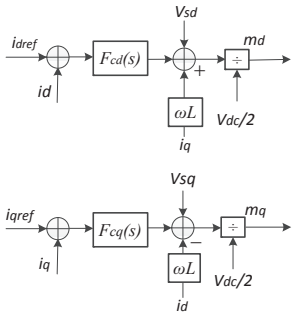

Figure 2. Schematic of current control block diagram.

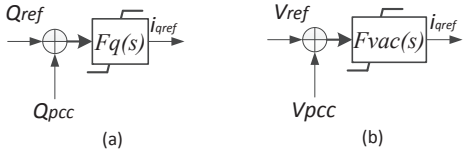

Figure 3. a) Block diagram of reactive power control loop. b) Block diagram of voltage control.

integrator and a lead compensator, adjusts i_{dref} through the dc-link voltage deviation signal (ΔV_{dc}). In order to augment the performance of the dc-link voltage regulator, output power of PV can also be deployed as a feed-forward to eliminate the nonlinearity and the destabilizing impact of the PV array output power [9], [14].

Reactive power control can be done by different strategies. Nevertheless, from regulator design perspective it can be done either by regulating reactive power at a reference value (Fig. 3(a)) or controlling the voltage at the connection point to a set-point value (Fig. 3(b)). It must, however, be considered that the reactive power contribution of the PV system is limited according to the current standards [12]. Reactive power regulators, $F_q(s)$ or $F_{vac}(s)$, which in general can be a PI controller, adjust i_{qref} using the reactive power deviation signal (ΔQ) or the AC-bus voltage deviation signal (ΔV_{AC}) depending on the reactive power control strategy. $\Delta i_d = i_{dref} - i_d$ and $\Delta i_q = i_{qref} - i_q$ are passed through current controllers to produce Sinusoidal Pulse Width Modulation (SPWM) signals for VSC in PSCAD.

Regarding reactive power contribution, a PV system could carry out this task through one of the following approaches:

I *Constant power factor operation*: PV system feeds reactive power into the grid irrespective of the voltage profile.

II *Dynamic power factor operation, PF(P)*: This method was proposed by German Grid Codes [12] (Fig. 4).

III *Droop-based control strategy, Q(V)*: This approach is a droop-based control strategy and Fig. 5 depicts a linear droop curve where the value of the dead-band (D) depends on the network impedance [15].

IV *Voltage control*: this approach is sensitive to the set-point adjustment to the extent that reactive power pumping interactions among PV systems in a distribution grid can occur [11].

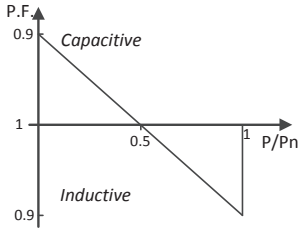

Figure 4. Dynamic power factor characteristic, PF(P).

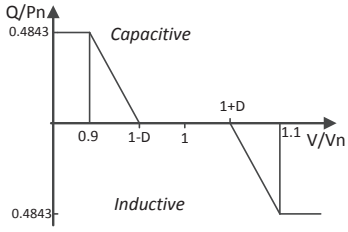

Figure 5. Droop control strategy, Q(V).

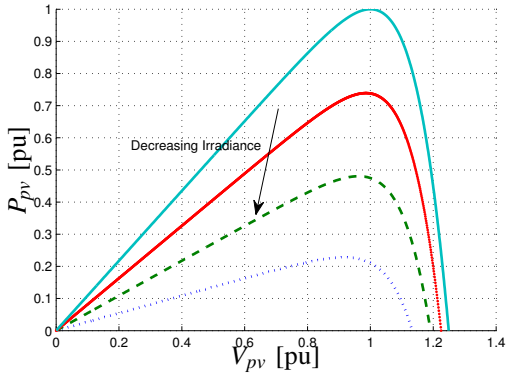

Figure 6. Voltage-Power characteristic of a PV array for different irradiance levels.

C. MPPT of PV system

The energy captured from PV array is not only proportional to irradiance, but also depends upon the location of the operating point, in Fig. 6 it can be noticed. Therefore, the output of PV array is not necessarily equal to its maximum and by doing so, PV system always needs additional function to exploit maximum power of PV array which is named Maximum Power Point Tracking in literature. As can be seen in Fig. 1, MPPT determines the dc-link voltage reference. MPPT is actually the most outer control loop of the PV system that has a memory to provide the dc-link voltage reference by measuring the output voltage and current of PV arrays and comparing them with previous states through a processing algorithm. Here in this paper, Incremental Conductance (INC) [16] algorithm is employed.

III. Differences and Similarities

In PSCAD, active power is controlled on the q axis and reactive power on the d axis due to abc/dq transformation characteristic. However, in PowerFactory the d axis represents the active power control and the q axis represents

Table I
SYSTEM PARAMETERS.

PV system parameter	Value
Vmp panel voltage at mpp	33.7 V
Imp panel current at mpp	3.56 A
Isc panel short circuit current	3.87 A
Voc panel open circuit voltage	42.1 V
Panel temperature coef. of Isc	0.065 $\%/^oC$
Panel temperature coef. of Voc	-160 mV/^oC
n_s num. of series panels	14
n_p num. of parallel panels	6
DC link capacitor C	10 mF
Interface reactor L	4 mH
Interface reactor R	3 mΩ
Trf1 rated power	15 kVA
Trf1 voltage ratio	0.38/0.18 kV
MPPT frequency	20 Hz
MPPT perturbation size	0.337 V
Line Parameter	**Value**
Line1 impedance	6 + 7.5j mΩ
Line2 impedance	15.5 + 3.4j mΩ
Grid Parameter	**Value**
Grid voltage	20 kV
Grid short circuit capacity	1.15 MVA
Grid R/X ratio	0.6
Trf2 rated power	250 kVA
Trf2 voltage ratio	0.38/0.18 kV
Load Parameter	**Value**
Rated active power	0.6 kW
Rated reactive power	0.3 kVar
Rated voltage	20 kV
Controller Parameter	**Value**
$F_{Vdc}=\frac{k}{s}\times\frac{1+sT_1}{1+sT_2}$	k=8.65e3 A/V/s T_1=0.0232 s^{-1} T_2=0.0011 s^{-1}
$F_{cc}=k_{pcc}+\frac{k_{icc}}{s}$	k_{pcc}=8Ω k_{icc}=2Ω/s
$F_q=k_{pq}+\frac{k_{iq}}{s}$	k_{pq}=-0.227 A/Var k_{iq}= -453.5 A/Var/s

reactive power. In PowerFactory, PWM converter block contains the current control block internally and it is possible to enable or disable it. The current control in PSCAD as can be seen in Fig. 2 comprises of decoupled terms while in PowerFactory the model of the current control is different. Therefore, the built-in current control is disabled by setting all the controller parameters to zero. Moreover, series reactor has been also located inside the PWM converter block in PowerFactory while in PSCAD the reactor is outside the converter. MPPT function uses same INC algorithm in both models.

IV. COMPARISON OF A SINGLE PV SYSTEM CONNECTED TO GRID IN THE BOTH SIMULATIONS PLATFORMS

Two models according to Fig. 1 are built in two simulation platforms, PSCAD and PowerFactory. The parameters of the system are presented in Table I.

An identical simulation scenario is carried out in order to make a fair and comprehensive comparison between two models. Fig. 7 depicts irradiance variations during simulation which varies stepwise for simplicity. Since PowerFactory starts simulation around one operating point while PSCAD simulates from scratch, the simulation are shown from the point that PSCAD has been settled down at the initial operating point for the both models, where irradiance is around 1000 W/m^2.

- *Case 1: Comparison without MPPT*

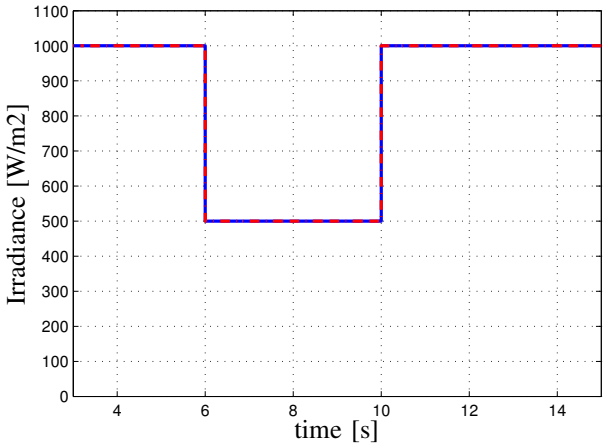

Figure 7. Irradiance variation

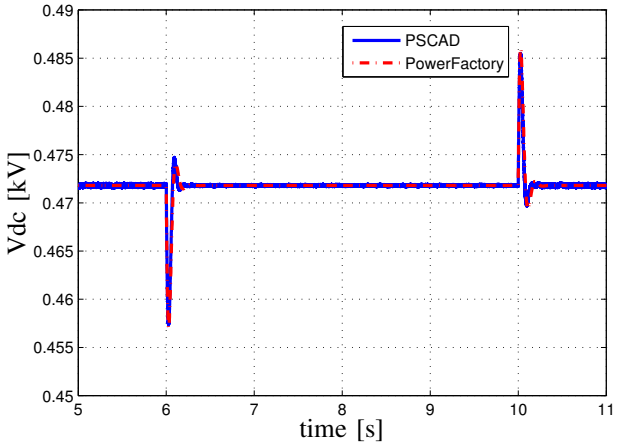

Figure 8. The dc-link voltage response to irradiance variations, without MPPT.

In this case study MPPT is disabled and dc-link voltage set-point v_{dc-ref} is imposed by a constant value equal to 471.8 V which is the voltage at the maximum power point for irradiance equal to 1000 W/m^2. The objective of this section is only to compare the performance of both models from numerical solving perspective not showing the necessity of MPPT, therefore the dc-link voltage is regulated at the STC value. Fig. 8 demonstrates the dc-link voltage for both models followed by irradiance variation according to Fig. 7, and as it shows the dynamic performance of the both models are quiet similar. Fig. 9 depicts the output power of PV system, as can be seen the general dynamic response structures of the both models are same, with the same numbers of overshoot and undershoot, although the only difference is that the size of overshoot in PowerFactory model is a bit higher than PSCAD that might be due to the converter model in PowerFactory.

- *Case 2: Comparison with MPPT*

This case study is similar to the prior case study, except that the MPPT is enabled in this case study. Fig. 10 shows the dc-link voltage in PowerFactory model has more oscillatory transients than PSCAD. Although the

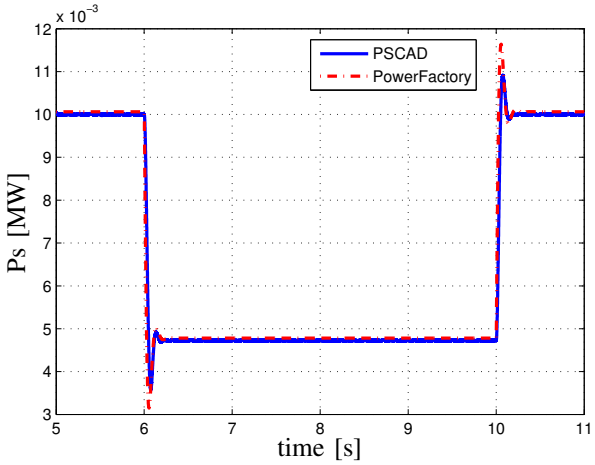

Figure 9. Active power response to irradiance variations, without MPPT.

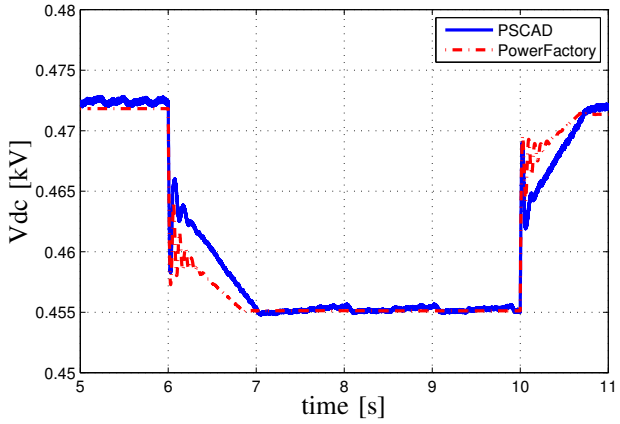

Figure 10. The dc-link voltage response to irradiance variations, with MPPT.

same algorithm for implementing MPPT has been taken into consideration for the both models, the difference in the transient response might be owing to different solvers of software. At the steady-state stage, PowerFactory model shows no distortion around the operating point which can be due to the switching in PSCAD that makes confusion for the perturbation orientation in MPPT algorithm and so it leads to oscillations around MPP for the PV system in PSCAD. Fig. 11 depicts the output active power of the PV system and as can be seen the PowerFactory model response has more oscillatory transient with higher overshoot that could be expected from the result of the previous case study.

Increasing the MPPT frequency decreases oscillations, as Fig. 12 shows increasing the MPPT frequency to 30 decreases considerably oscillations. Although the final values of V_{dc} in different frequencies are not the same, the difference is too small and it is due to the perturbation step and the design criterion in INC algorithm [16]. It boils down to this fact that once the PV system operating point goes close to MPP, the MPPT algorithm stops generating new perturbation as long as the absolute summation of the incremental conductance and the instantaneous conductance is smaller than a selective small value that is 0.001 in this study [16]. Furthermore, it is obvious that increasing the MPPT frequency increases noticeably the speed of the dc-link voltage response.

- *Case 3: Different specification for dc-link voltage controller*

This case study is analogous with the previous case study, the only exception is the dc-link controller that has been designed for another specifications. In case 2 the specifications are 60 degree phase margin and 200 Hz bandwidth, but in this case study the phase margin is increased to 70 degree and bandwidth is also reduced to 130 HZ that is expected to get a slower system response. Figs. 13 and 14 show the dc-link voltage and active power, respectively. Although both models have more or less similar responses, the output power response of the PV system has higher overshoots and

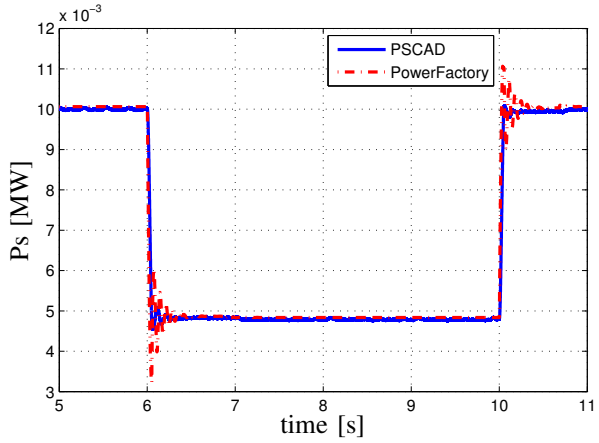

Figure 11. Active power response to irradiance variations, with MPPT.

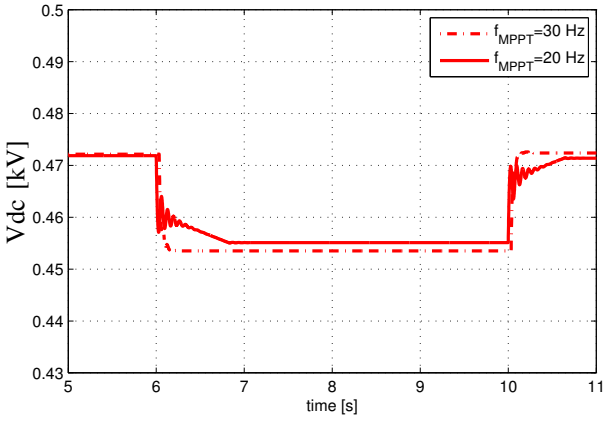

Figure 12. The dc-link voltage response to irradiance variations in PowerFactory for different MPPT frequencies.

undershoots. Apart from the models comparison, comparison of different design specifications shows that the performance of the PV system is considerably affected by changing dc-link specifications to the extent that in the second design, the PV system response becomes slower. Therefore, regarding making equivalent of PV systems in grid, one should deem this issue.

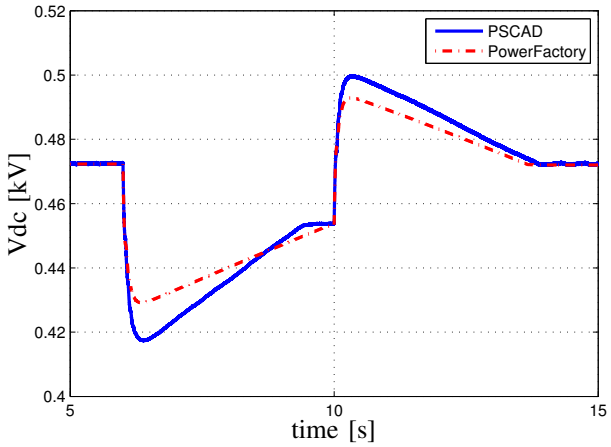

Figure 13. dc-link voltage response to irradiance variation, with MPPT.

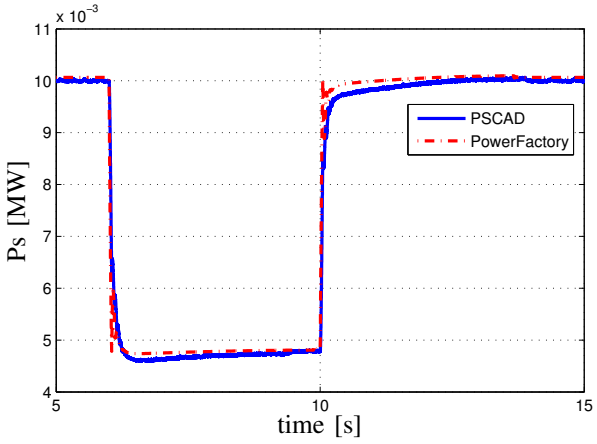

Figure 14. Active power response to irradiance variation, with MPPT.

- *Case 4: Comparison reactive power strategies with MPPT*
  In this case study, the behavior of the PV system in both models, with the last three aforementioned reactive power strategies, is taken into account. Figs. 15 and 16 show reactive power at PCC and the PCC voltage for the dynamic power factor control (strategy II). The reactive power is less oscillatory in the PowerFactory model.
  For studying the droop-based reactive power control strategy (strategy III), a grid voltage incident is created by increasing 5 % the grid voltage at t=6 sec and return to its initial value after 1 sec while the irradiance remains constant at 1000 W/m^2. The droop parameter, D, in Fig. 5 is set to 0.03. Figs. 17 and 18 show the reactive power at PCC and the PCC voltage for droop-based reactive power control strategy, respectively.
  In the voltage control method (strategy IV), the voltage of the PCC is regulated to a desired set-point. The voltage set-point for the voltage control strategy is chosen according to the voltage at PCC once the PV system is connected to the grid and works with half of the nominal power. Figs. 19 and 20 show reactive power at PCC and the PCC voltage for voltage control strategy, respectively.

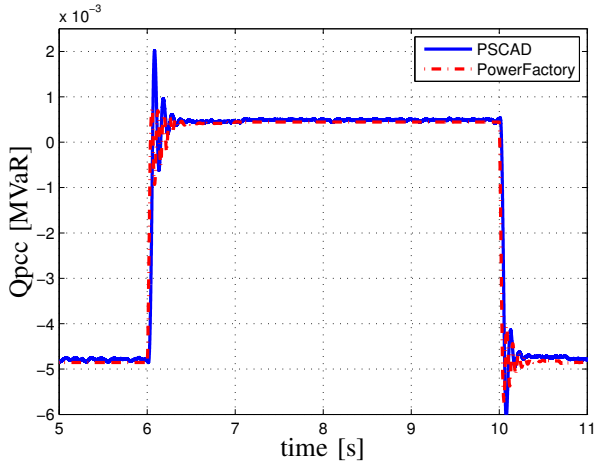

Figure 15. Reactive power at PCC, dynamic power factor strategy (II), with MPPT.

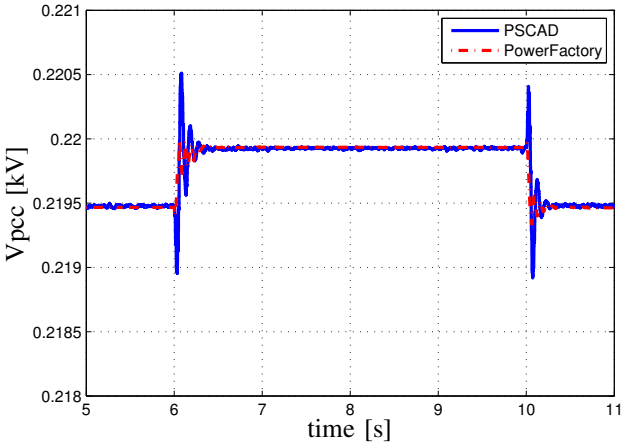

Figure 16. The PCC voltage, dynamic power factor strategy (II), with MPPT.

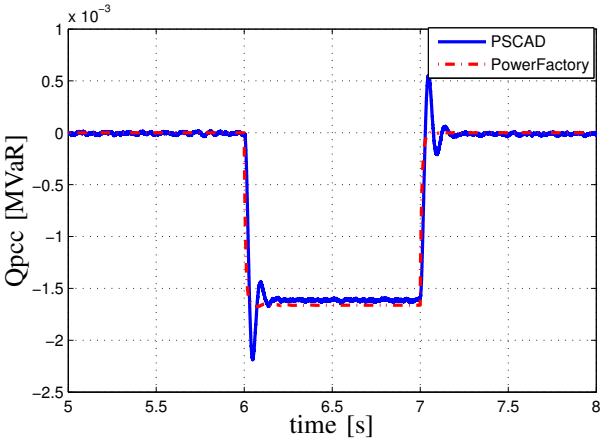

Figure 17. Reactive power at PCC, droop control strategy (III), with MPPT.

- *Case 5: Three-phase to ground fault with MPPT*
  This case study demonstrates the effect of the three-phase to ground fault on the PV system for the strategy IV. Irradiance is kept constant at 1000 W/m^2 and a fault incident is occurred at the load connection point

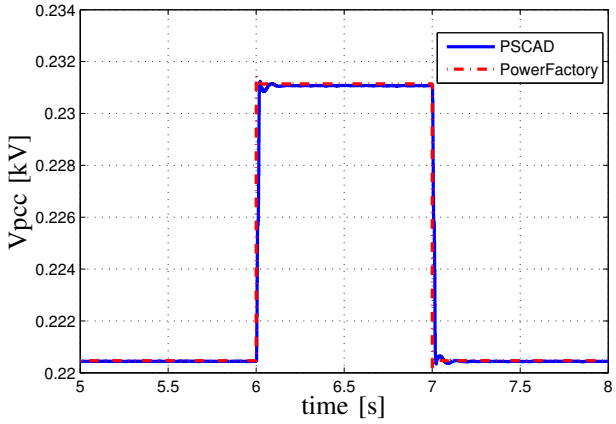

Figure 18. The PCC voltage, droop control strategy (III), with MPPT.

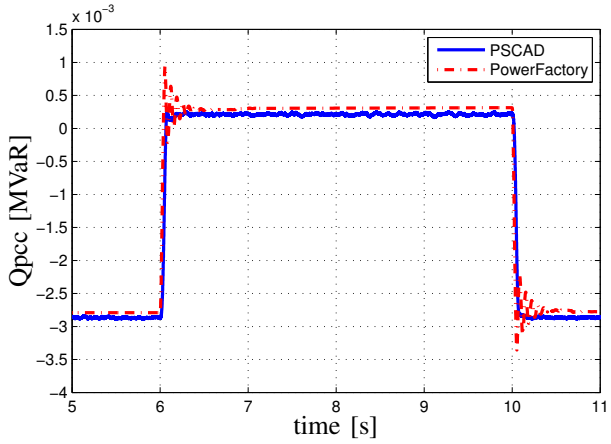

Figure 19. Reactive power at PCC, voltage control strategy (IV), with MPPT.

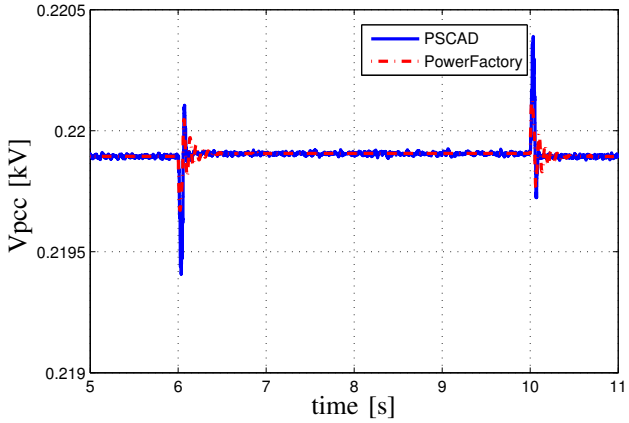

Figure 20. The PCC voltage, voltage control strategy (IV), with MPPT.

at t=6 s and cleared 100 ms later. The fault impedance is resistive and equal to 0.008 Ω. The dc-link bus voltage is shown in Fig. 21, as expected from power equation across the dc-link capacitor, the dc-link voltage is boosted. During fault interval, the transient behavior of both model are quiet similar. However, after fault clearance the transient response of both models have slight differences. Figs. 22 and 23 show active power

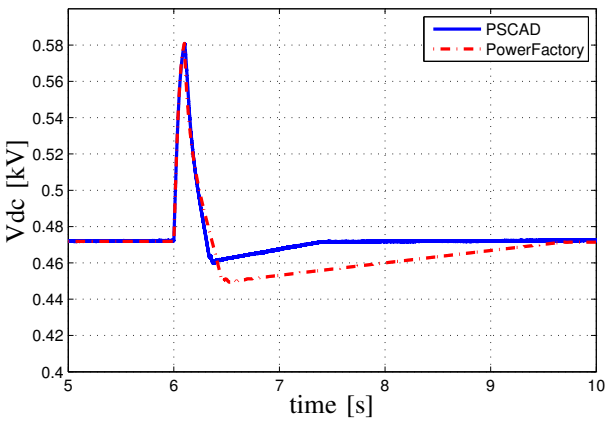

Figure 21. dc-link voltage response to three-phase to ground fault, with MPPT.

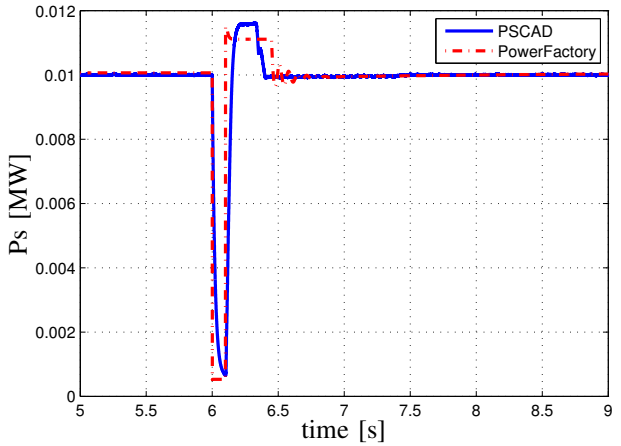

Figure 22. PV active power response to three-phase to ground fault, with MPPT.

and reactive power of the PV system, respectively. As can be seen, the general trajectory of responses is the same in both models, however there are slight differences specially after fault clearance. The reactive power contribution during fault is too small. This is because of small active power that is provided by PV array to feed dc-link capacitor and it is, in turn, due to the PV output voltage that is shifted towards the open circuit voltage where the PV output power becomes zero.

V. Conclusion

In this paper a model of a three-phase single-stage PV system was developed in PowerFactory platform. The performance of the developed was compared and confirmed with the PSCAD model, which was stemming from the previous research. The results show that both models are responding similarly to irradiance variation, although there are slight differences in the transient period subsequent to changes that might be due to MPPT function and numerical solving issues in the control system that are related to different solvers that are used in both software. Nevertheless, the results show that using rms values based simulations in PowerFactory

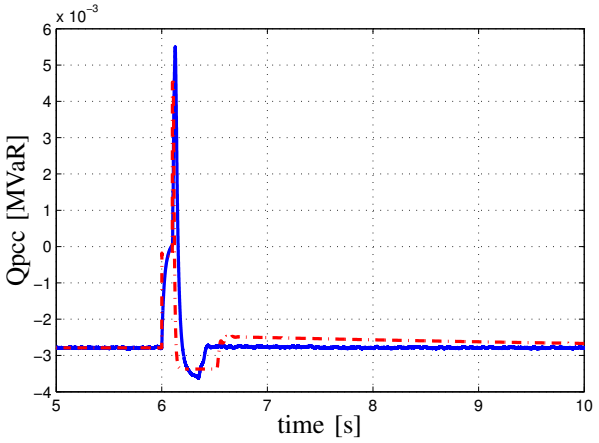

Figure 23. Reactive power at PCC, three-phase to ground fault, with MPPT.

can provide us with quite similar results using time domain instantaneous values. Therefore, the performance of large number of PV systems can be easily studied using rms simulations.

ACKNOWLEDGMENT

This project has been funded by SETS Erasmus Mundus Joint Doctorate and Smooth PV. The authors would like to express their gratitude towards all partner institutions within the programme as well as the European Commission for their support.

REFERENCES

[1] J. C. Boeme and et al, "Overview of german grid issues and retrofit of photovoltaic power plants in germany for the prevention of frequency stability problems in abnormal system conditions of the ENTSO-E region continental europe," in *1st International Workshop on Integration of Solar Power into Power Systems*, (Aarhus, Denmark), pp. 3–8, Oct. 2011.

[2] M. Braun, "Reactive power supply by distributed generators," in *2008 IEEE Power and Energy Society General Meeting - Conversion and Delivery of Electrical Energy in the 21st Century*, pp. 1 –8, July 2008.

[3] P. Sulc, K. Turitsyn, S. Backhaus, and M. Chertkov, "Options for control of reactive power by distributed photovoltaic generators," *arXiv:1008.0878*, Aug. 2010. Proceedings of the IEEE , vol.99, no.6, pp.1063-1073, June 2011.

[4] R. Tonkoski, L. Lopes, and T. EL-Fouly, "Droop-based active power curtailment for overvoltage prevention in grid connected PV inverters," in *2010 IEEE International Symposium on Industrial Electronics (ISIE)*, pp. 2388 –2393, July 2010.

[5] E. Demirok, D. Sera, R. Teodorescu, P. Rodriguez, and U. Borup, "Evaluation of the voltage support strategies for the low voltage grid connected PV generators," in *2010 IEEE Energy Conversion Congress and Exposition (ECCE)*, pp. 710 –717, Sept. 2010.

[6] A. Ellis, M. Behnke, and J. Keller, "Model makers," *IEEE Power and Energy Magazine*, vol. 9, pp. 55 –61, June 2011.

[7] A. Ellis, M. Behnke, and C. Barker, "PV system modeling for grid planning studies," in *2011 37th IEEE Photovoltaic Specialists Conference (PVSC)*, pp. 002589 –002593, June 2011.

[8] S.-K. Kim, J.-H. Jeon, C.-H. Cho, E.-S. Kim, and J.-B. Ahn, "Modeling and simulation of a grid-connected PV generation system for electromagnetic transient analysis," *Solar Energy*, vol. 83, pp. 664–678, May 2009.

[9] A. Yazdani and P. Dash, "A control methodology and characterization of dynamics for a photovoltaic (PV) system interfaced with a distribution network," *IEEE Transactions on Power Delivery*, vol. 24, pp. 1538 –1551, July 2009.

[10] A. Yazdani, A. Di Fazio, H. Ghoddami, M. Russo, M. Kazerani, J. Jatskevich, K. Strunz, S. Leva, and J. Martinez, "Modeling guidelines and a benchmark for power system simulation studies of three-phase single-stage photovoltaic systems," *IEEE Transactions on Power Delivery*, vol. 26, pp. 1247 –1264, Apr. 2011.

[11] A. Samadi, M. Ghandhari, and L. Söder, "Reactive power dynamic assessment of a PV system in a distribution grid," *Energy Procedia*, vol. 20, pp. 98–107, 2012.

[12] "Verband der elektrotechnik elektronik Informationstechnike.V. (VDN) (2010). erzeugungsanlagen am niederspannungsnetz technische mindestanforderungen für anschluss und parallelbetrieb von erzeugungsanlagen am niederspannungsnetz. draft of 07-08-2010. berlin."

[13] D. Sera, R. Teodorescu, and P. Rodriguez, "PV panel model based on datasheet values," in *IEEE International Symposium on Industrial Electronics, 2007. ISIE 2007*, pp. 2392 –2396, June 2007.

[14] A. Yazdani and R. Iravani, *Voltage-Sourced Converters in Power Systems*. Wiley, 1 ed., Feb. 2010.

[15] G. Kerber, R. Witzmann, and H. Sappl, "Voltage limitation by autonomous reactive power control of grid connected photovoltaic inverters," in *Compatibility and Power Electronics, 2009. CPE '09.*, pp. 129 –133, May 2009.

[16] K. Hussein, I. Muta, T. Hoshino, and M. Osakada, "Maximum photovoltaic power tracking: an algorithm for rapidly changing atmospheric conditions," *Generation, Transmission and Distribution, IEE Proceedings-*, vol. 142, pp. 59 –64, Jan. 1995.

P-III

Evaluation of Reactive Power Support Interactions Among PV Systems Using Sensitivity Analysis

Evaluation of Reactive Power Support Interactions Among PV Systems Using Sensitivity Analysis

Afshin Samadi, Robert Eriksson and Lennart Söder
KTH Royal Institute of Technology
School of Electrical Engineering
Department of Electric Power Systems
Stockholm, Sweden 10044
Email: afshin.samadi@ee.kth.se, robert.eriksson@ee.kth.se, lennart.soder@ee.kth.se

***Abstract*—Growing trends in generating power from distributed PhotoVoltaic (PV) systems has accommodated more and more PV systems within load pockets in distribution grid. This high penetration has brought about new challenges such as voltage profile violation, reverse load flow and etc. A few remedies have been imposed by grid codes such as reactive power contribution of PV systems and active power curtailment. This study applies two analytical methods from control science to find the possibility of controllability among the PV systems in a distribution grid for voltage profile control at specific set-points through reactive power regulation and active power curtailment. For this purpose, the voltage sensitivity matrix is used as the steady-state gain of the multi-variable system. The first method is Relative Gain Array (RGA), in which RGA of the voltage sensitivity matrix is utilized as a quantitative measure to address controllability and the level of voltage control interaction among PV systems. The second method is Condition Number (CN), in which Singular Value Decomposition (SVD) of the voltage sensitivity matrix is used as a mathematical measure to indicate the voltage control directionality among PV systems. Two radial test distribution grids with different feeder R/X ratio, overhead line and underground cable, which consist of five PV systems, are used to calculate load flow and, in turn, voltage sensitivity matrix. The results demonstrate that decentralized voltage control to specific set-points is basically impossible in the both systems. It is also shown that voltage control directionality of the both systems is increased by reactive power regulation compared to active power curtailing.**
Keyword: Photovoltaic, Voltage sensitivity matrix, RGA, SVD.

I. Introduction

Growing trends in PhotoVoltaic (PV) system installations due to encouraging feed-in-tariffs and long-term incentives have led to high penetration of PV systems in distribution grids. In Germany, for instance, there are currently 20 GW installed PV systems, of which 80% have been connected in low voltage grids [1]. Due to recent drop in costs of PV systems, especially PV panel technologies, grid-parity is not anymore unimaginable and will in near future come close to reality [2]–[4]. High penetration of PV systems without incentives is more likely to be interesting in different countries and markets rather than limited countries. For example, Italy and Spain are following Germany.

This high penetration of PV systems has also raised new challenges in the distribution grid such as voltage rise. Violation of voltage profile in some regions in Germany has led to stopping PV installation by utilities. To contrive a way to solve the unwanted problems associated with high participation of PV systems, reactive power contribution of PV systems has been proposed in recently under-codified standards, e.g. German Grid Codes [5]. Several approaches have been proposed for reactive power support [6]–[9]. One of these approaches is voltage control at the connection point of PV to grid. In the previous research [10], it was shown that this method is sensitive to adjusting set-points to the extent that improper set-points may lead to interaction among PV systems in the same vicinity. In [11], determinant of voltage sensitivity matrix from load flow calculation has been employed to study the impact of the R/X ratio on the effectiveness of using active and reactive power for regulating voltage profile. In [9], sensitivity matrix has also been used to show the difference between a system with overhead line and underground cable. However, the level of interaction and directionality among the PV systems regarding voltage control to specific set-points has not been addressed in the previous literature.

The aim of this paper is to address the possibility of controllability among PV systems for voltage profile regulation to specific set-points via two analytical control methods. For this investigation, the voltage sensitivity matrix, which can be derived via the load flow calculation, is used as the steady-state gain of the understudy system. The first method is Relative Gain Array (RGA) [12], [13] that is employed to analyze and evaluate the controllability and level of voltage control interaction among the PV systems. The second method is Condition Number (CN), in which mathematical measure of directionality is provided by Singular Value Decomposition (SVD). This method is a useful way to quantify how the range of possible gains of a multi-variable process varies for an input direction [13], [14]. Wide (or narrow) range of possible gains for a process implies large (or small) directionality.

Sub-matrices of the voltage sensitivity matrix indicate the sensitivity of the bus voltages and angels to the variation of active and reactive power at buses. The RGA and CN of the voltage sensitivity sub-matrices, in turn, indicate the degree of the interaction and directionality, respectively. The relation of feeder R/X ratio and the distance between buses in a distribution grid for voltage control is of concern. Applying the aforementioned methods provides an analytical view that how the voltage control interaction and directionality among PV systems in a distribution grid would be affected by the distance and R/X variation.

Two radial test distribution grids with different feeder R/X ratio, overhead line and underground cable, are employed as

the test platform. MATLAB environment is used to calculate the voltage sensitivity matrix and investigate it further via RGA and CN. Derived results, in conclusion, demonstrate decentralized voltage control to specific set-points through the PV systems in the distribution grid is fundamentally impossible due to the high level voltage control interaction and directionality among the PV systems.

In the following, a general overview of the voltage sensitivity will be given in section 2, basic of RGA and condition number are presented in section 3 and section 4 respectively, section 5 presents the simulation platform and section 6 deals with the results and finally the conclusion comes at section 7.

II. Voltage Sensitivity Matrix

Voltage Sensitivity matrix is a measure to quantify the sensitivity of bus voltages (|V|) and bus angles (θ) with respect to injected active and reactive power for each bus except slack bus. Sensitivity matrix is obtained through partial derivative of load flow equations, *g(|V|,θ)*, as follows [15]:

$$\begin{bmatrix} \Delta\theta \\ \Delta|V| \end{bmatrix} = \begin{bmatrix} \frac{\partial g_P(\theta,|V|)}{\partial\theta} & \frac{\partial g_P(\theta,|V|)}{\partial|V|} \\ \frac{\partial g_Q(\theta,|V|)}{\partial\theta} & \frac{\partial g_Q(\theta,|V|)}{\partial|V|} \end{bmatrix}^{-1} \begin{bmatrix} \Delta P \\ \Delta Q \end{bmatrix} =$$

$$= \begin{bmatrix} S^V_{\theta,P} & S^V_{\theta,Q} \\ S^V_{|V|,P} & S^V_{|V|,Q} \end{bmatrix} \begin{bmatrix} \Delta P \\ \Delta Q \end{bmatrix} \quad (1)$$

Voltage sensitivity matrix consists of four sub-matrices that denote the partial derivatives of bus voltage magnitude and angle with respect to active and reactive power. Due to importance of the voltage magnitude regulation by variation of active and reactive power, sub matrices that are related to variation of voltage magnitude, $S^V_{|V|,P}$ and $S^V_{|V|,Q}$, are of more interest and concern in this study. Each element of these sub matrices, e.g. S^V_{ij}, is interpreted as the variation that would happen in a voltage at bus *i* if the active power (or reactive power) at bus *j* changed 1 p.u. Voltage sensitivity matrix represents the open loop gain of the system which is later used as the steady state transfer function of the system to conduct some investigation.

Equation (1) represents a linearized form of the system equations. Keeping this in perspective, it follows from (1) that voltage magnitude variation corresponds to active and reactive power variation and consequently in order to keep the voltage magnitude theoretically constant, following is deducted which can be also employed as a measure to determine the degree of active-reactive power dependency.

$$\Delta Q = -{S^V_{|V|,Q}}^{-1} S^V_{|V|,P} \Delta P = J \Delta P. \quad (2)$$

Equation (2) is used later to compare the relation between the reactive power and active power while the voltage profile is perfectly controlled.

III. RGA Method

Although the RGA was basically introduced by Britsol [12] for pairing the input and output variables in a decentralized control system, it has also been exploited as a general measure of controllability [13], [14]. The relative gain array has been addressed in many literatures and is frequently employed as a quantitative measure of controllability and control loop interaction in decentralized control design. The RGA is originally formulated for steady state analysis and later it was extended to include the dynamics [13]. In this study, the RGA concept is used to analyze the voltage sensitivity matrix, which is calculated from system algebraic equations and therefore does not comprise dynamic.

The proposed interaction measure through RGA indicates how the apparent transfer function between manipulated or input variable (u_i) and controlled or output variable (y_j) is affected by control of other controlled variables. This measure is shown by λ_{ij} and is described by the ratio of the transfer function between a given manipulated variable and controlled variable while all other loops are open, and the transfer function between the same variables while all other outputs are closed as follows:

$$\lambda_{ij} = \frac{\left(\frac{\partial y_i}{\partial u_j}\right) \mid u_{k\neq j} constant}{\left(\frac{\partial y_i}{\partial u_j}\right) \mid y_{k\neq j} constant} \quad (3)$$

In other words, the RGA is the ratio of the open loop gain between two variables to the closed loop gain of the same variables while other outputs are perfectly controlled. For a MIMO system with *G(0)* as the steady sate transfer function, the RGA is attained as follows:

$$\Lambda(G(0)) = G(0) \times \left(G(0)^{-1}\right)^T \quad (4)$$

Where $\times$ denotes element-by-element multiplication.

Equation (3) demonstrates that the open loop gain between y_j and u_i changes by the factor λ_{ij}^{-1} while the rest of loops are closed by integral feedback control. This implies that the pairing should be preferred for RGAs that are as close to unity as possible. λ_{ij}=1 implies that there is no interaction with other control loops. Intuitively, decentralized control requires an RGA matrix close to identity [13]. In a decentralized control, the MIMO process works as several independent SISO sub-plants. If RGA elements are greater than one, the decoupling or inverse-based controller can be used to decouple interactions. However, systems with large RGA elements are basically hard to control owing to big interactions and input uncertainties; by doing so, inverse based controller should be prevented since it is not robust. Pairing with negative RGA elements must be avoided because those lead to integral instability.

Sub-matrices of the voltage sensitivity matrix in (1) are steady-state gain of the system and by doing so the RGA of $S^V_{|V|,P}$ and $S^V_{|V|,Q}$ are given as follows:

$$\Lambda(S^V_{|V|,Q}) = S^V_{|V|,P} \times \left(\left(S^V_{|V|,P}\right)^{-1}\right)^T \quad (5)$$

$$\Lambda(S^V_{|V|,Q}) = S^V_{|V|,Q} \times \left(\left(S^V_{|V|,Q}\right)^{-1}\right)^T \quad (6)$$

The RGA of $S^V_{|V|,P}$ in (5) can be used to study the possibility of controllability and interaction among voltage controllers of PV systems via power curtailing in order to regulate the voltage of buses to specific set-points. The RGA of $S^V_{|V|,Q}$ in (6) is used to investigate the possibility of controllability and interaction among voltage controllers of PV systems to

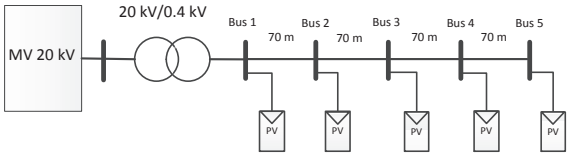

Figure 1. Test distribution grid.

regulate voltage of buses to specific set-points via regulating reactive power.

To sum up, in RGA method, the voltage sensitivity matrix must first be derived. Then, RGA of sub-matrices $S^V_{|V|,P}$ and $S^V_{|V|,Q}$ are calculated. In the next step RGA values are evaluated. RGA values close to one demonstrate a decentralized system. If the RGA values are big but less than 5, the decoupling compensators can be used to make the system decentralized. However, large RGA values, more than 5, correspond to controllability problems because of big interactions and input uncertainties [13].

IV. CN Method

Another measure to quantify the level of interaction in multi-variable systems is condition number. CN of a system is defined as the ratio between maximum and minimum singular values of the system, which are computed using SVD [13], [14]:

$$\gamma(G(0)) = \frac{\bar{\sigma}(G(0))}{\underline{\sigma}(G(0))} \tag{7}$$

A process with large CN implies high directionality and is called to be ill-conditioned [13]. The steady state gain of MIMO process varies between $\underline{\sigma}(G(0))$ and $\bar{\sigma}(G(0))$. Wide range of possible gains for a MIMO system indicates large directionality. Such a plant is often considered sensitive to uncertainty that, in turn, will lead to a poor robust performance [13]. Moreover, a large CN results in control problem. A large CN may be brought about by a small singular value that is generally undesirable.

In a nutshell, in CN method, the voltage sensitivity matrix must first be derived. Then, SVD of sub-matrices $S^V_{|V|,P}$ and $S^V_{|V|,Q}$ are computed and consequently CN is calculated. CN larger than 50 demonstrates controllability problems [13].

V. Platform of the simulation

Radial grid in Fig. 1, which consists of five houses connected through a step down transformer to a medium voltage grid, is employed as a test grid in this paper. In this study, it is assumed that all the houses have been equipped with PV systems. In this grid both overhead lines and underground cables are taken into consideration in order to study the effect of the R/X ratio. The parameters of the test radial grid have been given in Table I [9].

In the load flow calculation, the slack bus is naturally excluded from sensitivity matrix. Moreover, in the sensitivity matrix, rows and columns corresponding to buses that have no PV systems are also neglected.

Table I
Radial test grid parameters.

Grid impedance	1.4e-4 +1.4e-4i p.u.
Transformer impedance	0.0043 + 0.0067i p.u.
Over head line impedance per km	0.0516 + 0.0375i p.u.
Underground cable impedance per km	0.0400 + 0.0102i p.u.
Rated total net load	20 kW
Base Voltage	400 V
Base Power	20 kW

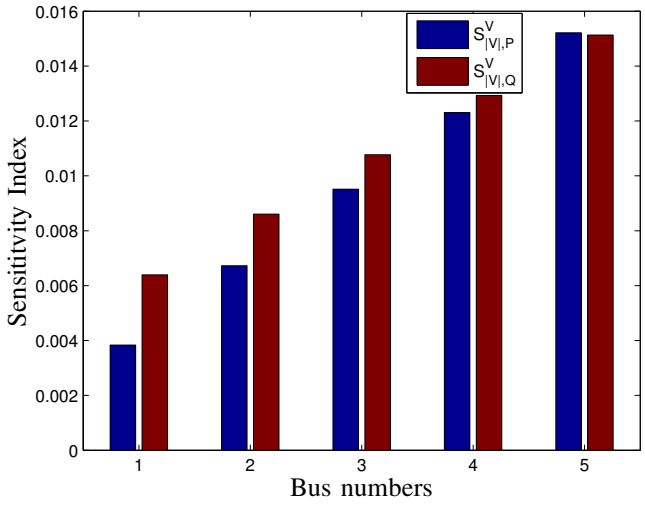

Figure 2. The sensitivity spectrum of the diagonal elements of $S^V_{|V|,P}$ and $S^V_{|V|,Q}$ for overhead lines.

VI. Results

A. Sensitivity matrix characteristic

Figs. 2 and 3 show the spectrum of the diagonal elements of $S^V_{|V|,P}$ and $S^V_{|V|,Q}$ for overhead lines and cables, respectively. As it was expected the sensitivity to reactive power in overhead line is noticeably bigger than underground cable. Nevertheless, in case of underground cable, it can be seen that at the beginning of the feeder, sensitivity to reactive power is higher compared to active power, but as approaching to the end of feeder it gets the other way around. Therefore, even though resistive part of the underground cable is dominant, controlling voltage profile by regulating reactive power at the beginning of the feeder, seems to be more effective.

B. Voltage regulation active-reactive power dependency

Irrespective of the operating point and R/X ratio, (2) yields an upper triangular matrix. Nevertheless, the diagonal elements and first row of the matrix, which are dominant elements, vary significantly between the overhead line and underground cable. Figs. 4 and 5 depict the spectrum of those elements.

The characteristics of the matrix is summarized as follows:

- The first entry in the diagonal and the first row are common and corresponds to the first bus, which can only see the impedance of the grid, and by doing so it gets same value in both systems with overhead line and underground cable.

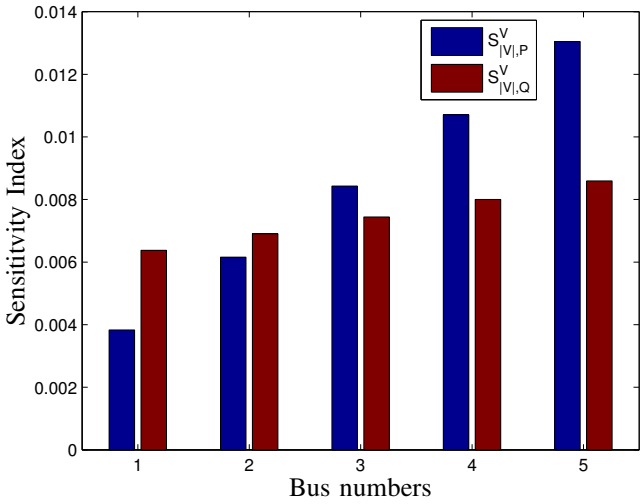

Figure 3. The sensitivity spectrum of the diagonal elements of $S^V_{|V|,P}$ and $S^V_{|V|,Q}$ for underground cable.

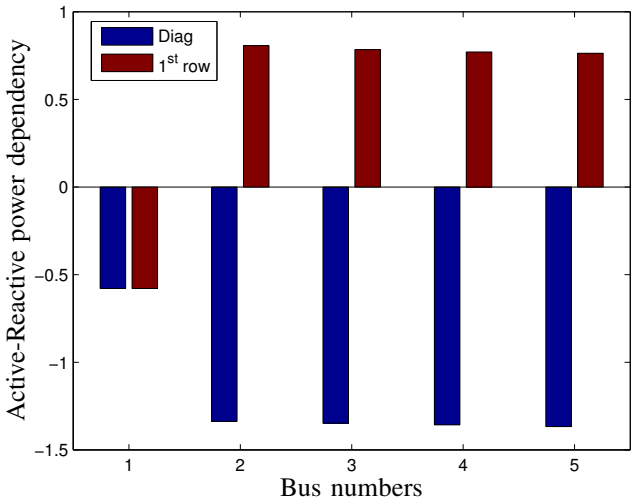

Figure 4. Spectrum of diagonal and first row elements of active-reactive power dependency for overhead line.

- Diagonal entries, except the first entry, are almost similar; first row entries, except the first entry, are also almost similar.
- The diagonal entries are almost equal to the feeder R/X ratio in both systems, overhead line and underground cable.
- The absolute difference between corresponding diagonal and first row entries, except the common entry, is almost equal to the absolute value of the common entry.
- Large elements in case of underground cables, which is in conjunction with large R/X ratio, implies that for an identical change in active power of buses, required reactive power to keep voltage profile constant varies largely. In other words, the required reactive power to keep voltage differences equal to zero ($\Delta V = 0$), is proportional to the feeder R/X ratio. By doing so, for feeders with R/X ratio more than one the required reactive power change (ΔQ) at each bus would be greater than the active power difference (ΔP) in the same bus.
- Depending upon the R/X ratio value, the sign of the first row entries except the first entry changes. In order to study the effect of the k=R/X ratio, the total amount of the overhead line impedance is taken into account, and its R/X ratio is varied. It is observed that for k smaller than 0.58 the sign of the first row entries is negative. Therefore, for small R/X ratio, if the active power difference (ΔP) in all buses are in one direction, the reactive power difference (ΔQ) at all buses will be in one direction as well. However, for large k values the sign of the first row entries are positive and opposite of the diagonal entries which means the reactive power variation at bus one is always in contrary with other buses.

Eq. (2) is used to calculate the required reactive power adjustment to compensate the voltage profile fluctuation owing to the variation of active power. Considering the initial

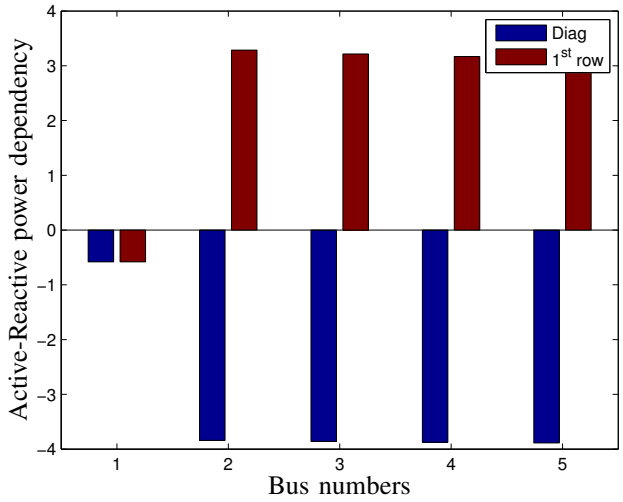

Figure 5. Spectrum of diagonal elements and first row of active-reactive power dependency for underground cable.

operating point at $P_0 = 0$ and $Q_0 = 0$ gives

$$\begin{aligned} \Delta P &= P - P_0 = P \\ \Delta Q &= Q - Q_0 = Q \\ P &= JQ \end{aligned} \tag{8}$$

Consequently, the needed power factors for the PV connected buses are calculated as follows:

$$PF = \frac{P}{\sqrt{P^2 + ((\sum J')P)^2}} \tag{9}$$

Where PF is a vector consisting of power factors at each PV installed bus. Fig. 6 depicts the power factor of each bus for differen R/X ratio while it is assumed that the total net power at each bus has been changed 1 p.u. (P=1 p.u.), as can be seen the required power factor varies drastically by increasing R/X ratio. It boils down to this fact that required reactive power to compensate voltage fluctuation depends upon R/X ratio.

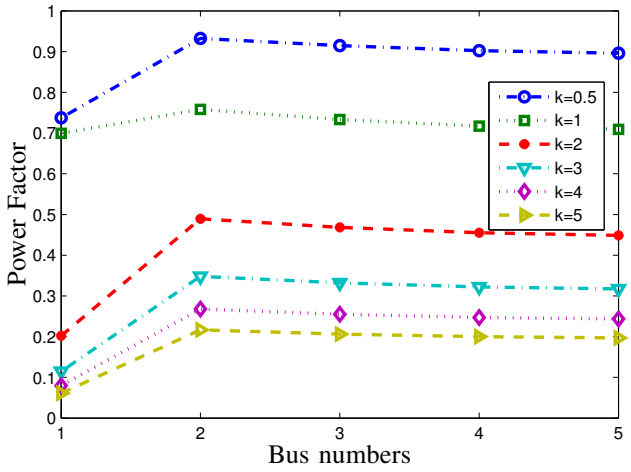

Figure 6. Required power factor for each PV system for different k=R/X ratio and $\Delta P = 1 p.u.$

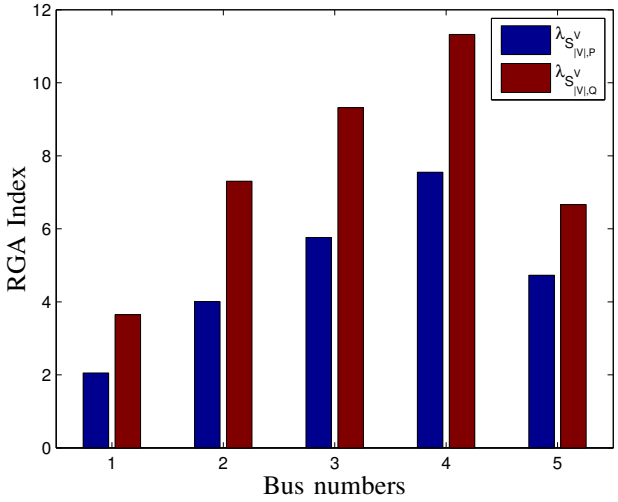

Figure 7. The RGA spectrum of the diagonal elements of $S^V_{|V|,P}$ and $S^V_{|V|,Q}$ for overhead line.

C. RGA

Subsequent to the previous section upshot, if adequate reactive power can be provided by PV systems, this question is raised whether it is possible to regulate the voltage of each bus with installed PV system to a fixed set-point through reactive power regulation or not. In this section and following, the interaction among PV systems in a radial distribution grid is quantified by RGA concept to address the possibility of controllability concerning voltage profile regulation to specific set-points.

The RGA of the $S^V_{|V|,P}$ and $S^V_{|V|,Q}$ look like a block tridiagonal matrix which positive elements are only located on the diagonal and elements on the upper diagonal and on the lower diagonal are negative. According to the RGA pairing rule, therefore, the elements on the diagonal must be paired. This block tridiagonal shape of the RGA of voltage sensitivity sub-matrices indicate that open loop gain of the system, which is the sensitivity matrix, is changed with positive sign on the diagonal and with negative sign on the upper diagonal and lower diagonal. Moreover, since the other elements of the RGA are almost zero, open loop gain of the system on these positions are changed with infinite factor which means these loops are considerably affected by other loops. Figs. 7 and 8 depict the diagonal entries spectrum of RGA of $S^V_{|V|,P}$ and $S^V_{|V|,Q}$ for overhead lines and cables while all buses are on full production, respectively. It can be seen by moving towards end of the feeder, except the last bus, the level of interaction is increasing. Since the last bus at the end of feeder is affected only by one previous neighbor bus, the level of interaction drops at this bus.

Concerning overhead line, Figs. 9 and 10 demonstrate maximum RGA of $S^V_{|V|,P}$ and $S^V_{|V|,Q}$ for different net load levels and different line distances between buses. One sees that the interaction level decreases by increasing the distance between the buses, or in turn by increasing the impedance. Moreover, it can be seen that the maximum RGA of $S^V_{|V|,P}$ declines by shifting total net load from consumption to production. Similar results, not shown here, are derived for under ground cable.

Figs. 11 and 12 show the impact of the lagging and leading power factor on the maximum RGA of $S^V_{|V|,P}$ and $S^V_{|V|,Q}$ for different loading conditions, while it is assumed that overhead line segments are 70 m. As can be seen the power factor has relatively very small effect on the maximum RGA of $S^V_{|V|,P}$ while the maximum RGA of $S^V_{|V|,Q}$ slightly increases by lagging power factor and decreases by leading power factor. The performance of the system with underground cable, not shown here, is analogues with overhead line.

The results of the maximum RGA for different k=R/X ratio are shown in Figs. 13 and 14. It is assumed that the distance between buses are 70 m and power factor is unity. It is obvious that maximum RGA of $S^V_{|V|,Q}$ increases for larger k values. It is, therefore, deducted that increasing R/X ratio would boost the interaction level among voltage controllers of PV systems regarding reactive power regulation. However, it can be seen in Fig. 13 that the maximum RGA of $S^V_{|V|,P}$ declines by large k values.

Based on the depicted results, the positive elements of the RGA of $S^V_{|V|,Q}$ are always much bigger than one irrespective of the R/X ratio, total net load and power factor. It can be, therefore, concluded that it is not possible to have decentralized voltage control in order to regulate voltage to a specific set-point at each bus even for small R/X ratio that technically adequate reactive power can be produced by PV systems [13]. Since the RGA of $S^V_{|V|,P}$ are much bigger than one, decentralized control based on the power curtailing is not also possible.

Furthermore, the results demonstrate that maximum positive elements of RGA of the voltage sensitivity matrix are large, more than 5, by doing so using decoupling controllers, in order to make a decentralized system, can fundamentally lead to control problems due to sensitivity to inputs [13]. Thus, inverse-based controllers must be avoided.

D. Condition number

At production net load level with unity power factor, CN of $S^V_{|V|,P}$ and $S^V_{|V|,Q}$ for overhead line are γ_P^{OHL}=44.2 and γ_Q^{OHL}=72.1, and for underground cable are γ_P^{UGC}=50.8 and γ_Q^{UGC}=197.2. These CNs denote that sensitivity matrix is

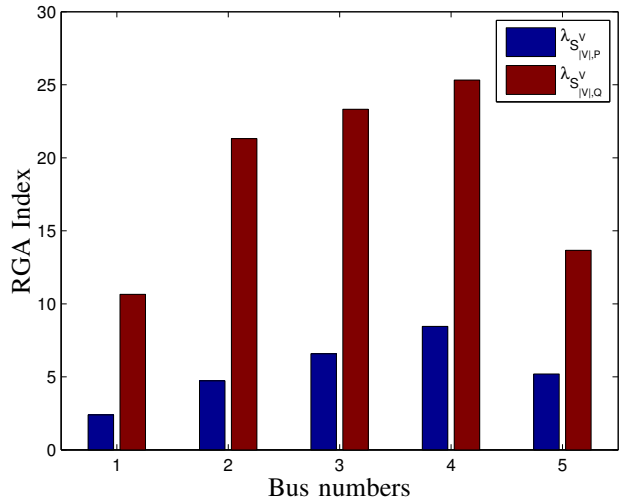

Figure 8. The RGA spectrum of the diagonal elements of $S^V_{|V|,P}$ and $S^V_{|V|,Q}$ underground cable line.

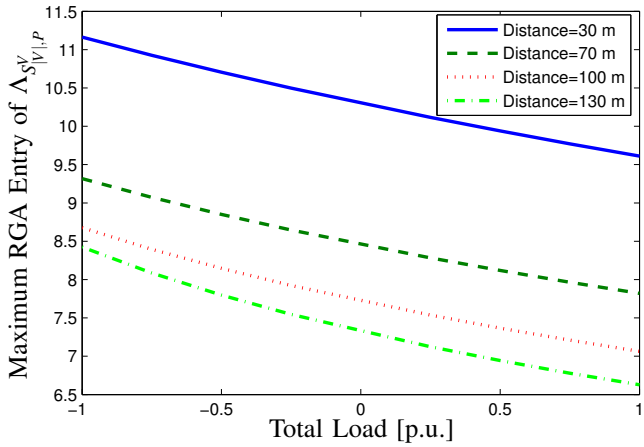

Figure 9. Maximum RGA entry of $S^V_{|V|,P}$ for different net load levels and different distances between buses, overhead line.

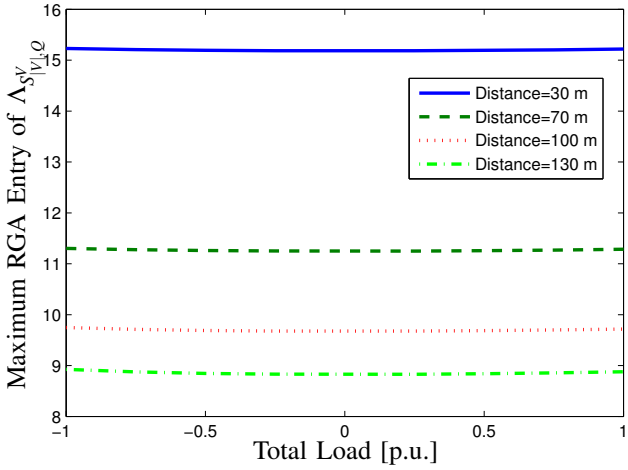

Figure 10. Maximum RGA entry of $S^V_{|V|,Q}$ for different net load levels and different distances between buses, overhead line.

ill-conditioned and the severe case is for $S^V_{|V|,Q}$. Figs. 15 and 16 illustrate the spectrum of the singular values of $S^V_{|V|,P}$ and $S^V_{|V|,Q}$, respectively. As can be seen the sensitivity matrix in both systems suffers from high directionality.

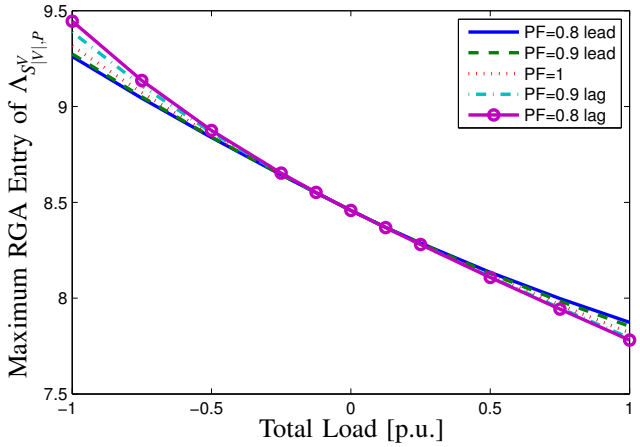

Figure 11. Maximum RGA entry of $S^V_{|V|,P}$ for different net load levels and different power factors, overhead line.

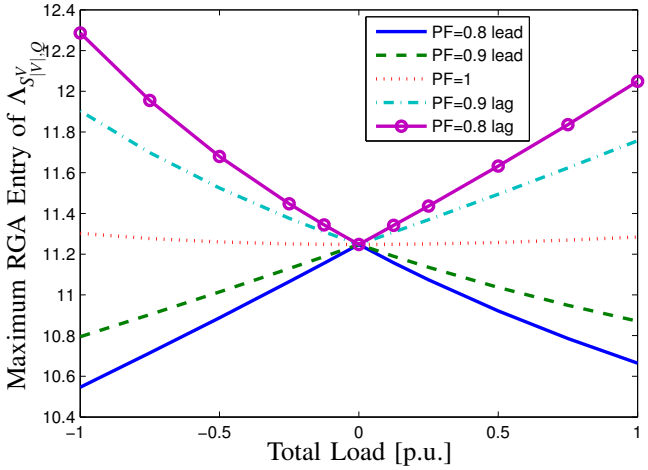

Figure 12. Maximum RGA entry of $S^V_{|V|,Q}$ for different net load levels and different power factors, overhead line.

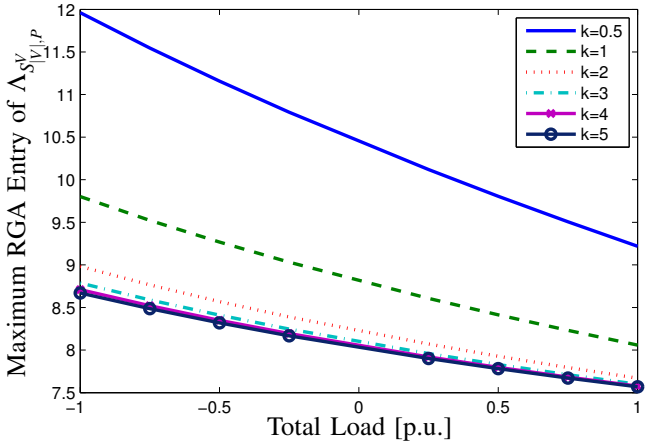

Figure 13. Maximum RGA entry of $S^V_{|V|,P}$ for different net load levels and different k=R/X ratios.

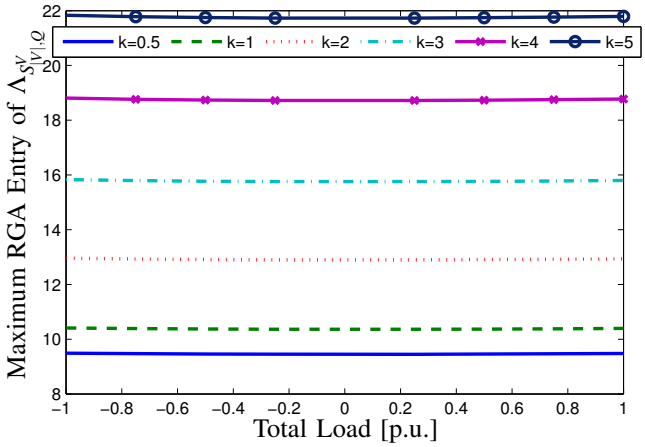

Figure 14. Maximum RGA entry of $S^V_{|V|,Q}$ for different net load levels and different k=R/X ratios.

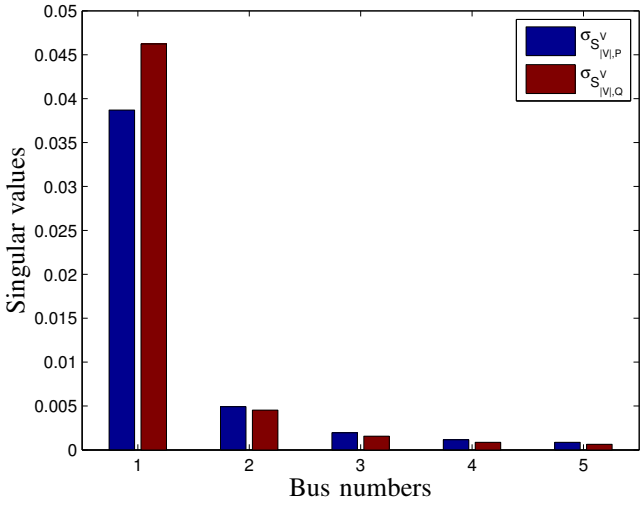

Figure 15. The singular values of $S^V_{|V|,P}$ and $S^V_{|V|,Q}$ for overhead line.

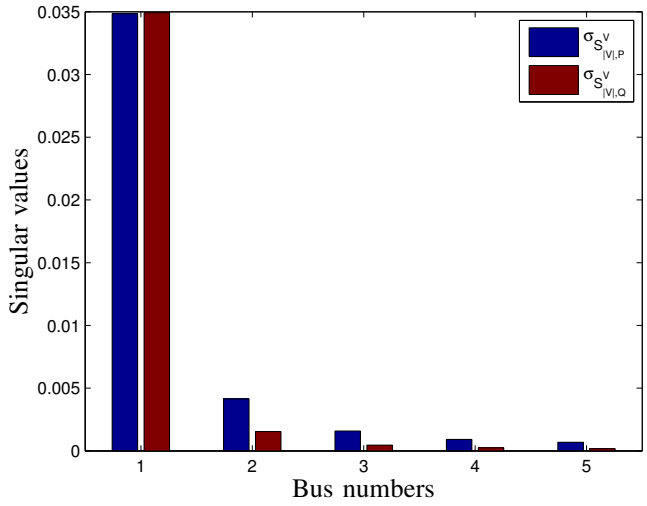

Figure 16. The singular values of $S^V_{|V|,P}$ and $S^V_{|V|,Q}$ underground cable.

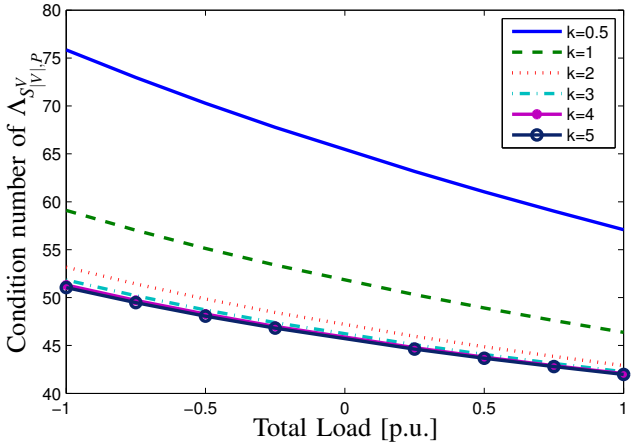

Figure 17. Condition number of $S^V_{|V|,P}$ for different net load levels and different k=R/X ratios.

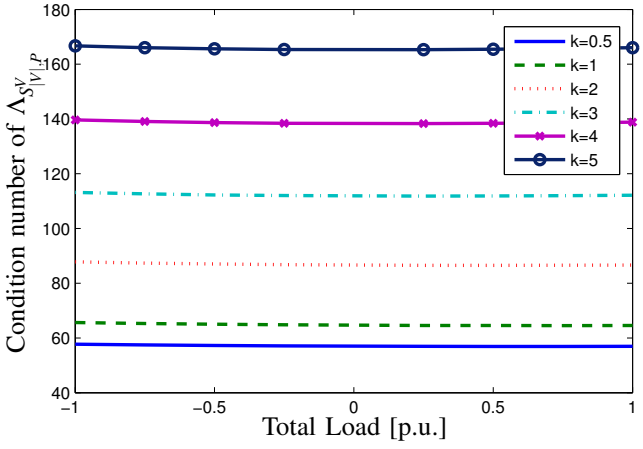

Figure 18. Condition number of $S^V_{|V|,Q}$ for different net load levels and different k=R/X ratios.

Furthermore, smallest singular value for $S^V_{|V|,Q}$ in the system with the underground cable is smaller than the system with overhead line that implies more directionality and more control problems. These results are in conjunction with RGA results.

Figs. 17 and 18 demonstrate the condition numbers of $S^V_{|V|,P}$ and $S^V_{|V|,Q}$ for different R/X ratio and different total net load levels. Regarding $S^V_{|V|,Q}$ the more increasing k the further CN goes that is along with the RGA results. Analogous with the RGA results, large R/X ratio results in relatively smaller CN for $S^V_{|V|,P}$. Changing power factor and the distance between buses yield similar results, not shown here, for CN as the RGA results in the previous section.

VII. Conclusion

This paper applies two analytical control methods, namely Relative Gain Array and Condition Number, to voltage sensitivity matrix in order to find the possibility of the controllability. RGA and CN are used to quantify the level of interaction and directionality among PV systems in distribution grids regarding voltage control, respectively. The sensitivity matrix is used as the steady-state gain of the system in this study. Moreover, the characteristic of the sensitivity matrix is employed to show the level of dependency

of reactive power to active power for voltage control. The results show that decentralized voltage control to specific set-points through reactive power regulation or active power curtailing is not possible due to large RGA elements and large CN of voltage sensitivity matrix. It is, furthermore, shown that using decoupling controllers to make system decentralized must also be avoided on the grounds that the RGA elements of the voltage sensitivity matrix are too big, larger than 5, that would result in poor control performance.

ACKNOWLEDGMENT

This project has been funded by SETS Erasmus Mundus Joint Doctorate and Smooth PV. The authors would like to express their gratitude towards all partner institutions within the programme as well as the European Commission for their support.

REFERENCES

[1] J. C. Boeme and et al, "Overview of german grid issues and retrofit of photovoltaic power plants in germany for the prevention of frequency stability problems in abnormal system conditions of the ENTSO-E region continental europe," in *1st International Workshop on Integration of Solar Power into Power Systems*, (Aarhus, Denmark), pp. 3–8, Oct. 2011.

[2] D. Verma, O. Midtgard, and T. Satre, "Review of photovoltaic status in a european (EU) perspective," in *2011 37th IEEE Photovoltaic Specialists Conference (PVSC)*, pp. 003292 –003297, June 2011.

[3] U. Schwabe and P. Jansson, "Utility-interconnected photovoltaic systems reaching grid parity in new jersey," in *2010 IEEE Power and Energy Society General Meeting*, pp. 1 –5, July 2010.

[4] J. H. Wohlgemuth, D. W. Cunningham, R. F. Clark, J. P. Posbic, J. M. Zahler, P. Garvison, D. E. Carlson, and M. Gleaton, "Reaching grid parity using BP solar crystalline silicon technology," in *33rd IEEE Photovoltaic Specialists Conference, 2008. PVSC '08*, pp. 1 –4, May 2008.

[5] "Verband der elektrotechnik elektronik Informationstechnike.V. (VDN) (2010). erzeugungsanlagen am niederspannungsnetz technische mindestanforderungen für anschluss und parallelbetrieb von erzeugungsanlagen am niederspannungsnetz. draft of 07-08-2010. berlin."

[6] M. Braun, "Reactive power supply by distributed generators," in *2008 IEEE Power and Energy Society General Meeting - Conversion and Delivery of Electrical Energy in the 21st Century*, pp. 1 –8, July 2008.

[7] P. Sulc, K. Turitsyn, S. Backhaus, and M. Chertkov, "Options for control of reactive power by distributed photovoltaic generators," *arXiv:1008.0878*, Aug. 2010. Proceedings of the IEEE , vol.99, no.6, pp.1063-1073, June 2011.

[8] R. Tonkoski, L. Lopes, and T. EL-Fouly, "Droop-based active power curtailment for overvoltage prevention in grid connected PV inverters," in *2010 IEEE International Symposium on Industrial Electronics (ISIE)*, pp. 2388 –2393, July 2010.

[9] E. Demirok, D. Sera, R. Teodorescu, P. Rodriguez, and U. Borup, "Evaluation of the voltage support strategies for the low voltage grid connected PV generators," in *2010 IEEE Energy Conversion Congress and Exposition (ECCE)*, pp. 710 –717, Sept. 2010.

[10] A. Samadi, M. Ghandhari, and L. Söder, "Reactive power dynamic assessment of a PV system in a distribution grid," *Energy Procedia*, vol. 20, pp. 98–107, 2012.

[11] R. Tonkoski and L. Lopes, "Voltage regulation in radial distribution feeders with high penetration of photovoltaic," in *IEEE Energy 2030 Conference, 2008. ENERGY 2008*, pp. 1 –7, Nov. 2008.

[12] E. Bristol, "On a new measure of interaction for multivariable process control," *IEEE Transactions on Automatic Control*, vol. 11, pp. 133 – 134, Jan. 1966.

[13] S. Skogestad and I. Postlethwaite, *Multivariable Feedback Control: Analysis and Design*. Wiley-Interscience, 2 ed., Nov. 2005.

[14] S. Skogestad and K. Havre, "The use of RGA and condition number as robustness measures," *Computers & Chemical Engineering*, vol. 20, Supplement 2, no. 0, pp. S1005–S1010, 1996.

[15] H. Saadat, *Power System Analysis Third Edition*. PSA Publishing, THIRD EDITION ed., June 2010.

P-IV

Coordinated Active Power-Dependent Voltage Regulation in Distribution Grids With PV Systems

Coordinated Active Power-Dependent Voltage Regulation in Distribution Grids With PV Systems

Afshin Samadi, *Student Member, IEEE*, Robert Eriksson, *Member, IEEE*, Lennart Söder, *Senior Member, IEEE*, Barry G. Rawn, *Member, IEEE*, and Jens C. Boemer, *Student Member, IEEE*

***Abstract*—High penetrations of photovoltaic (PV) systems in distribution grids have brought about new challenges such as reverse power flow and voltage rise. One of the proposed remedies for voltage rise is reactive power contribution by PV systems. Recent German Grid Codes (GGC) introduce an active power dependent (APD) standard characteristic curve, $\mathrm{Q(P)}$, for inverter-coupled distributed generators. This study utilizes the voltage sensitivity matrix and quasi-static analysis in order to locally and systematically develop a coordinated $\mathrm{Q(P)}$ characteristic for each PV system along a feeder. The main aim of this paper is to evaluate the technical performance of different aspects of proposed $\mathrm{Q(P)}$ characteristics. In fact, the proposed method is a systematic approach to set parameters in the GGC $\mathrm{Q(P)}$ characteristic. In the proposed APD method the reactive power is determined based on the local feed-in active power of each PV system. However, the local voltage is also indirectly taken into account. Therefore, this method regulates the voltage in order to keep it under the upper steady-state voltage limit. Moreover, several variants of the proposed method are considered and implemented in a simple grid and a complex utility grid. The results demonstrate the voltage-regulation advantages of the proposed method in contrast to the GGC standard characteristic.**

***Index Terms*—German grid codes, photovoltaic, reactive power control.**

I. Introduction

GROWING trends in photovoltaic (PV) system installations due to encouraging feed-in-tariffs and long-term incentives have led to high penetration of PV systems in distribution grids. In Germany, for instance, there are currently more than 29 GW of installed PV systems, of which 80% have been connected to low-voltage (LV) grids [1], [2]. Due to the recent drop in PV system costs, especially PV panel technologies, grid parity (defined as the moment when the cost of electricity generated by PV is competitive with the retail price) has already been reached in some residential regions [3]–[6]. High penetration of PV systems without incentives is now more likely to be interesting in a wide range of countries and markets.

Uneven distribution of PV systems within the network has caused different regional penetration levels. For instance, some regions in Germany are already facing high local penetration of more than 200 kW/km^2 in contrast to the national average, which is 39 kW/km^2 [7], [8]. This high penetration of PV systems has also raised new technical challenges in the distribution grid, such as the voltage rise due to reverse power flow during light load and high PV generation conditions [8]–[11]. Reactive power contribution by distributed generation (DG) units is one of the most commonly proposed approaches for dealing with the voltage rise [8], [11]–[16]. The recent German Grid Codes (GGC) also require reactive power contribution [17]. Reactive power variation in low-voltage (LV) grids, which normally have a large $\mathrm{R/X}$ ratio, has less influence on voltage [12], [18]. Nevertheless, from an economic point of view, the voltage profile regulation via reactive power is to be preferred over active power curtailment [8]. Voltage profile regulation based on reactive power can be performed through different ways [11], [14]–[17], [19].

The GGC proposes a $Q(P)$ characteristic curve to support the voltage profile via a PV system's reactive power [17]. In such an active power-dependent (APD) characteristic, the required reactive power is determined according to an identical $\mathrm{Q(P)}$ characteristic for each PV system, independent of its location in the grid. Though the GGC states that the distribution system operators (DSO) can use a characteristic that is different from the standard characteristic depending upon the grid configuration, the specification of such a characteristic is left with the DSO. Moreover, since the standard characteristic does not consider the voltage profile, its employment can cause unnecessary reactive power consumption. Considering the large number of PV systems in grids, unnecessary reactive power consumption by PV systems first increases the total line losses, and second, it may also jeopardize the stability of the network in the case of contingencies in conventional powerplants, which supply reactive power [20].

A method that can provide a coordinated, systematic characteristic for each PV system along a feeder is therefore needed. This paper utilizes the voltage sensitivity matrix of one operating point to determine individual $\mathrm{Q(P)}$ characteristics that use local information but provide a coordinated response without the aid of communication systems. Since the grid configuration is addressed in the voltage sensitivity matrix, the proposed method basically introduces a specific characteristic based on

Manuscript received April 04, 2013; revised October 29, 2013; accepted December 09, 2013. Date of publication January 28, 2014; date of current version May 20, 2014. This project was supported in part by SETS Erasmus Mundus Joint Doctorate and in part by Smooth PV. Paper no. TPWRD-00387-2013.

A. Samadi, R. Eriksson, and L. Söder are with the Department of Electric Power Systems, KTH Royal Institute of Technology, Stockholm SE-100 44, Sweden (e-mail: afshin.samadi@ee.kth.se).

B. G. Rawn is with the Department of Electrical Engineering (ESAT/ELECTA), University of Leuven (KU Leuven), Leuven 3001, Belgium.

J. C. Boemer is with the Department of Electrical Sustainable Energy, Delft University of Technology, Delft 2628 CD, the Netherlands.

Color versions of one or more of the figures in this paper are available online at http://ieeexplore.ieee.org.

Digital Object Identifier 10.1109/TPWRD.2014.2298614

the grid configuration for each PV system. The voltage sensitivity matrix has been widely used to compare impacts of active power curtailment and reactive power support through PV systems on the voltage profile in low-voltage (LV) grids [18] to define coordinated droop factors in the active power curtailment of PV systems [10], to demonstrate the voltage-control interaction among PV systems using control theory [21], and to eliminate the voltage variation at a target node due to the operation of a wind turbine in a microgrid via reactive power support [22]. However, to the best of the author's knowledge, locally coordinated $\mathrm{Q(P)}$ characteristics for several PV systems in distribution grids have not yet been addressed.

In this paper, the voltage sensitivity matrix is used to locally and systematically coordinate the relation between reactive power and corresponding feed-in power of each PV system in a radial grid in order to regulate either the last-bus voltage or the voltage profile. The proposed method, in fact, is a systematic approach of adjusting setting parameters of the GGC standard characteristic. The proposed APD method regulates the voltage through calculating reactive power based on the PV feed-in active power. Furthermore, the proposed method generally determines a coordinated $\mathrm{Q(P)}$ method based on the grid configuration, for example, $\mathrm{R/X}$ ratio and considering all other PV systems. Therefore, reactive power flows can be reduced and, in turn, line losses are reduced.

The results demonstrate that the proposed APD voltage regulation method can acceptably regulate the voltage under the steady-state voltage limit. Moreover, the active power loss caused by reactive power in this method is notably smaller than in the case of using the GGC standard characteristic.

The GGC objectives are explained in Section II. A general overview of the voltage sensitivity matrix is given in Section III. The theory of the proposed approach is presented in Section IV. Section V presents the concepts of loss-sensitivity analysis. The performance of the proposed method is studied on a simple test system in Section VI. A daily operation of the proposed method within a complex utility grid is investigated in Section VII. Sections VIII and IX contain a summary and conclusions.

II. German Grid Codes

The GGCs comply with the limit values of the voltage quality specified by EN 50160 [23]. According to the EN 50160, the allowable voltage range in LV grids is between 90% to 110% of the nominal voltage. Within this voltage tolerance band, DG units that deliver at least 20% of their rated power are permitted to freely change their power factor within the hatched sector represented in Fig. 1. The power factor range for units larger than 13.8 kVA is between 0.9 underexcited and overexcited while for units between 3.68 kVA and 13.8 kVA, it is 0.95 [17]. Reactive power contribution augments the integration of DG units into LV grids.

The reactive power control comes along with a considerable power loss in LV grids. Hence, in order to minimize the power loss, the GGC proposes the $Q(P)$ standard characteristic curve in Fig. 2, where P and $P_{\max}$ represent the feed-in and the maximum active power of the generator unit, respectively [17]. The objective of the standard $\mathrm{Q(P)}$ characteristic requires the generation unit to operate in an underexcited mode when the feed-in

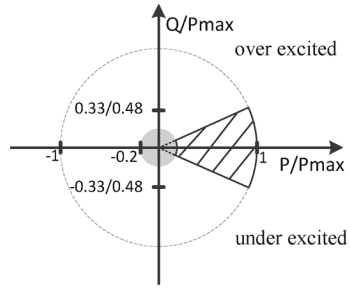

Fig. 1. Reactive power operation area for a generation unit connected to LV grids.

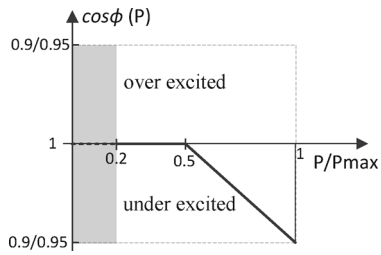

Fig. 2. Standard characteristic curve for $\cos\varphi\,(\mathrm{P})$.

active power passes over a threshold of 50% of $P_{\max}$ in order to mitigate the related voltage rise. Therefore, the GGC standard setting for PV systems is established according to Fig. 2. The proposed $\mathrm{Q(P)}$ characteristic requires inverter-based variable generation units, such as PV systems. Upon a change in active power, the generation unit should provide the required reactive power based on the setpoint on the characteristic curve within 10 s [17], which can be fulfilled by adjusting the bandwidth of the controller. The GGC mentions that depending upon different aspects, that is, grid configuration, load, and feed-in power, the DSO may need a characteristic different from the standard $Q(P)$ curve shown in Fig. 2. Nevertheless, the GGC does not address how to specify the setting parameters.

The $Q(P)$ method cannot explicitly consider grid voltage stability because the curve used is not a function of voltage.

III. Voltage Sensitivity Matrix

The voltage sensitivity matrix is a measure to quantify the sensitivity of voltage magnitudes ($|\mathrm{V}|$) and angles (θ) with respect to injected active and reactive power. The sensitivity matrix is obtained through partial derivative of power-flow equations $g(|V|,\theta)$ as follows [24]:

$$\begin{bmatrix}\Delta\theta\\ \Delta|V|\end{bmatrix}=\begin{bmatrix}\frac{\partial g_P(\theta,|V|)}{\partial\theta} & \frac{\partial g_P(\theta,|V|)}{\partial|V|}\\ \frac{\partial g_Q(\theta,|V|)}{\partial\theta} & \frac{\partial g_Q(\theta,|V|)}{\partial|V|}\end{bmatrix}^{-1}\begin{bmatrix}\Delta P\\ \Delta Q\end{bmatrix}=\underbrace{\begin{bmatrix}S_P^{\theta} & S_Q^{\theta}\\ S_P^{|V|} & S_Q^{|V|}\end{bmatrix}}_{S_V}\begin{bmatrix}\Delta P\\ \Delta Q\end{bmatrix}. \tag{1}$$

The voltage sensitivity matrix consists of four submatrices that denote the partial derivatives of bus voltage magnitude and angle with respect to active and reactive power. Due to the importance of the voltage magnitude regulation by variation of

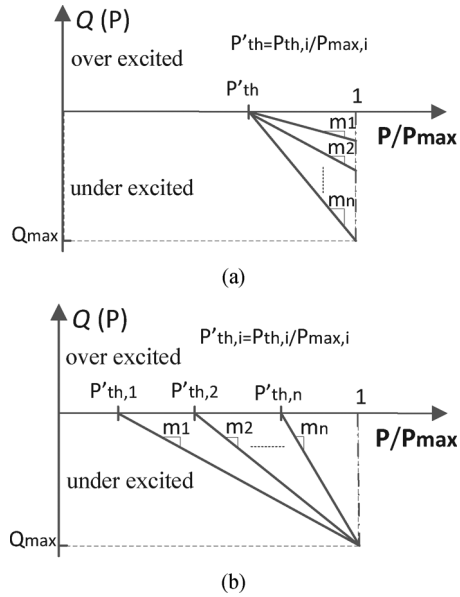

Fig. 3. Characteristic curves of the proposed APD method: (a) identical and (b) nonidentical thresholds.

active and reactive power, submatrices that are related to variation of voltage magnitude $S_P^{|V|}$ and $S_Q^{|V|}$ are of more interest and concern in this study. Each element of these submatrices is interpreted as the variation that may occur in a voltage at bus i if the active power (or reactive power) at bus j changed 1 p.u.

IV. Active Power-Dependent Voltage Regulation

In an APD voltage regulation method, the local feed-in active power of a PV system is directly employed as an input to calculate the required local reactive power to regulate the voltage. APD methods, including the proposed GGC characteristic, assume that increasing PV systems' generation would result in a voltage profile increase.

In an APD method, the general relationship between active and reactive power of a PV system is defined as follows:

$$Q = \begin{cases} m(P - P_{th}) & P > P_{th} \\ 0 & P < P_{th} \end{cases} \tag{2}$$

where m is a slope factor and P_{th} is an active power threshold above which the PV system commences consuming reactive power to regulate the voltage. Therefore, in the APD method, two parameters must be defined for each PV system.

Fig. 3 provides a comprehensive picture of characteristics of the proposed APD method that will be discussed in detail. In this method, a unique slope is designated to each PV system while active power thresholds can be either identical or nonidentical. Once the feed-in power passes the power threshold, the reactive power compensation unit kicks in to regulate the voltage to the steady-state limit based on its designated slope factor. In the proposed APD method, the voltage sensitivity matrix is employed to coordinate these two parameters among PV systems along a radial feeder by regulating either the target-bus (TB) voltage or the voltage profile (VP).

The voltage sensitivity matrix is calculated for the maximum net load/generation because that can be intuitively argued to be the critical operating point. The voltage deviation required to remain under the steady-state voltage limit is considered as a measure to find the active power thresholds. The threshold levels are adjusted in such a way to keep the target-bus voltage (the most critical voltage) under the steady-state voltage limit. Information from the voltage magnitude sensitivity submatrices is used to derive the slope factors to regulate the target-bus or the whole voltage profile, whichever case is chosen. In the following subsections, it is first discussed how to derive the slope factors and later explained how to adjust the active power thresholds.

A. Computing the Slope Factors

The proposed APD method uses the voltage sensitivity matrix to locally regulate either the TB voltage in a radial feeder or the VP of a radial feeder with several PV systems.

1) Target-Bus Voltage Regulation: Concerning the ideal voltage regulation, based on (1), it is possible to regulate reactive power of each PV system at each node in such a way to make the target-bus voltage deviation zero as follows:

$$\Delta V_n = 0 = \sum_{i=1}^{l} \left(S_{Pi,n}^{|V|} \Delta P_i + S_{Qi,n}^{|V|} \Delta Q_i \right) \tag{3}$$

where n represents the target-bus number, l is the number of PV systems, ΔV_n is the voltage deviation at the target bus, and $S_{Pi,n}^{|V|}$ and $S_{Qi,n}^{|V|}$ are, respectively, voltage magnitude sensitivity indices at the target bus with respect to active and reactive power corresponding to bus i. The controlled relation between active and reactive power variations of each PV system can be expressed as follows:

$$\begin{aligned} \Delta Q_i &= m_i \Delta P_i \\ (Q_i - Q_{th,i}) &= m_i (P_i - P_{th,i}) \end{aligned} \tag{4}$$

where m_i, the slope factor at bus i, is assigned to be the value obtained by substituting (4) into (3)

$$m_i = -\frac{S_{Pi,n}^{|V|}}{S_{Qi,n}^{|V|}}. \tag{5}$$

$P_{th,i}$ and $Q_{th,i}$ are the active and reactive power thresholds of the PV system at bus i. The threshold $P_{th,i}$ is specified as described in the next section. Since the APD voltage regulation should kick in above $P_{th,i}$, $Q_{th,i}$ is, therefore, assumed zero. The choice of (5) ensures voltage regulation by setting ΔQ to cancel the left term of (3). By doing so, analogous to (2), the required reactive power injections at each bus can be derived as follows:

$$Q_i = \begin{cases} m_i(P_i - P_{th,i}) & P_i > P_{th,i} \\ 0 & P_i < P_{th,i} \end{cases} \quad \forall i. \tag{6}$$

Equation (6) can be rearranged to express the active power threshold level as a fraction of its maximum power,

$P'_{thi} = P_{th,i}/P_{\max,i}$ which is hereafter called simply threshold, as follows:

$$Q_i = \begin{cases} m_i P_{\max,i}\left(\frac{P_i}{P_{\max,i}} - P'_{th,i}\right) & \frac{P_i}{P_{\max,i}} > P'_{th,i} \\ 0 & \frac{P_i}{P_{\max,i}} < P'_{th,i} \end{cases} \quad \forall i \tag{7}$$

where $P_{\max,i}$ is the maximum power of the ith PV system.

2) Voltage Profile Regulation: In the previous subsection, the voltage at the target bus is regulated, and the main reactive power pressure is imposed on the PV system at the target bus in the case of thresholds with equal values. It is, however, possible to regulate the voltage along the feeder by keeping the voltage profile deviations at all nodes as close as possible to zero using the following objective function:

$$\sum_{i=1}^{n} W_i \sum_{j=1}^{n} (S_{P,ij}^{|V|} + S_{Q,ij}^{|V|} m_j)^2 = 0 \tag{8}$$

where m_j is the relation between reactive and active power variation at bus j (similar to (4)), and W_i determines the importance of the voltage regulation at bus i with respect to other buses. The W_i could be set equal to each other, which, in turn, implies no priority concerning voltage regulation. However, the last-bus voltage regulation is normally more of a concern. Thus, the characteristic of $S_Q^{|V|}$ can be employed to find a weight vector. The diagonal entries of $S_Q^{|V|}$ depict the influence of the reactive power variation at one bus on the voltage at the same bus. Therefore, normalized diagonal entries of $S_Q^{|V|}$ can be used as a measure to determine the importance of voltage regulation at each bus

$$W_i = \frac{S_{Q,ii}^{|V|}}{\frac{1}{n} tr(S_Q^{|V|})}. \tag{9}$$

Computing the slope factors to minimize (8) uses all of the information of the voltage sensitivity matrix. Once the slope factors are computed, the required reactive power at each bus can be derived similar to (6).

B. Computing the Thresholds

As discussed earlier, thresholds P'_{th} are adjusted in a way to regulate the TB voltage to the steady-state voltage limit. The maximum deviation at the TB is

$$\Delta V_{\max,n} = \left(V_{\max,n} - \overline{V}\right) \tag{10}$$

where $V_{\max,n}$ is the maximum target-bus voltage that occurs at the critical operating point and $\overline{V}$ is the steady-state upper voltage limit in LV grids.

The overvoltage $\Delta V_{\max,n}$ is due to the active power injections corresponding to the left term within brackets of (1). The required underexcited reactive power to cancel the overvoltage is given by the equality

$$\Delta V_{\max,n} = -\sum_{i=1}^{n} \left(S_{Qi,n}^{|V|} \Delta Q_i\right). \tag{11}$$

The negative sign in (11) is due to underexcited nature of the required reactive power that is basically negative in the defined Q(P) plane. Thus, the negative sign is used to match both sides of the equivalence in (11).

In order to calculate the thresholds, ΔQ_i in (11) must be substituted by (4). In this regard, there are two possible options. If the thresholds are assumed to be identical, this leads to unequal reactive power sharing among PV systems according to (7) and as shown in Fig. 3(a). If equal reactive power sharing among PV systems is desired, this, at the critical operating point, means unequal thresholds as shown in Fig. 3(b). Identical thresholds force PV systems in the target bus and the nearby buses to contribute more reactive power. In doing so, those PV systems are more prone to excessive reactive power loading in their inverters. However, it is possible to equally share reactive power among PV systems at the critical operating point using nonidentical ratio values of active power thresholds. Equally distributing reactive power among PV systems can prevent excessive reactive power loading on PV inverters, but it also results in higher total reactive power consumption.

Thus, the threshold can, generally, be derived in two ways as explained below:

1) Identical Thresholds, P'_{th} Iden: By substituting (4) in (11) and assuming identical thresholds, one deduces

$$P'_{th} = 1 + \frac{\Delta V_{\max,n}}{\sum_{i=1}^{n} m_i P_{\max,i} S_{Q,ni}^{|V|}}. \tag{12}$$

2) Nonidentical Thresholds, P'_{th} Non-Iden: Considering the equal share of reactive power for each PV system at the critical operating point $\Delta Q_i = Q_{\max}$, according to (11), the required underexcited reactive power for each PV system is calculated as follows:

$$Q_{\max} = -\frac{\Delta V_{\max,n}}{\sum_{i=1}^{n} S_{Q,ni}^{|V|}}. \tag{13}$$

Then, based on (4), the thresholds for each bus are calculated as follows:

$$P'_{th,i} = 1 - \frac{Q_{\max}}{m_i P_{\max,i}} \qquad i = 1, \ldots, n. \tag{14}$$

V. Loss-Sensitivity Analysis

Based on power-flow equations of a grid, total active loss of all lines can be determined as follows:

$$P_L = \sum_{i=1}^{n} V_i \sum_{\substack{j=1 \\ j \neq i}}^{n} g_{ij} \left[V_i - V_j \cos\left(\delta_{ij}\right)\right] \tag{15}$$

where g_{ij} is the conductance of the line between bus i and j.

Total loss and power-flow equations are a function of voltage magnitude and angle. Therefore, the total loss-sensitivity coefficients with respect to active and reactive power at bus i can be derived as follows:

$$\begin{aligned} \frac{dP_L}{dP_i} &= \sum_{j=1}^{n} \frac{\partial P_L}{\partial \delta_j} \frac{\partial \delta_j}{\partial P_i} + \sum_{j=1}^{n} \frac{\partial P_L}{\partial |V_j|} \frac{\partial |V_j|}{\partial P_i} \\ \frac{dP_L}{dQ_i} &= \sum_{j=1}^{n} \frac{\partial P_L}{\partial \delta_j} \frac{\partial \delta_j}{\partial Q_i} + \sum_{j=1}^{n} \frac{\partial P_L}{\partial |V_j|} \frac{\partial |V_j|}{\partial Q_i}. \end{aligned} \tag{16}$$

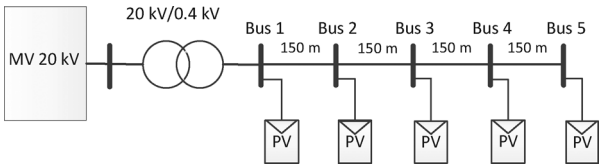

Fig. 4. Test distribution grid. All PV systems have a rating of 30 kW.

TABLE I
RADIAL TEST GRID PARAMETERS [25]

Grid impedance	2.828+2.828j Ω
Transformer impedance	0.0191+0.0351j Ω
Cable impedance per km	0.346+0.0754j Ω/*km*

Equation (16) can be rearranged in a matrix form with the help of the voltage sensitivity matrix S_V as follows:

$$\begin{bmatrix} \frac{dP_L}{dP} \\ \frac{dP_L}{dQ} \end{bmatrix} = S_V^T \begin{bmatrix} \frac{\partial P_L}{\partial \delta} \\ \frac{\partial P_L}{\partial |V|} \end{bmatrix} \tag{17}$$

where $\partial P_L/\partial\delta$ and $\partial P_L/\partial|V|$ can also be derived from (15).

VI. SIMPLE TEST SYSTEM

In order to easily observe the performance of the proposed methods, first, a simple test grid is taken into consideration. Fig. 4 depicts the simple radial test grid used in this part of study, which consists of five buses in an LV feeder connected through a step-down transformer to a medium-voltage grid. In this study, all of the buses on the LV feeder are equipped with an identical 30-kW PV system. The parameters of the test radial grid have been given in Table I [25].

Since voltage regulation through DG must operate within one to a few seconds, quasistatic analysis is appropriate. In this paper, therefore, quasistatic power-flow calculation is employed.

Normally speaking, the voltage violation occurs during maximum PV production, which is during sunny, clear-sky days, and minimum demand. Therefore, it is assumed that all five PV systems present identical generation characteristics and, for the sake of clarity, in this part of the study, loads are neglected. Fig. 5 illustrates the voltage profile by varying the net generation from 0 to 150 kW without reactive power support. It is evident from Fig. 5 that when all PV systems deliver full power at unity power factor, voltages of the two last buses are above the steady-state voltage limit, which is considered 110% of the nominal voltage according to EN 50160 [23]. Moreover, it is obvious that the PV system at the last bus on the feeder experiences higher voltage, and so it is considered as the target bus.

For designing the Q(P) parameters (slope and threshold), the voltage sensitivity matrix is computed for the extreme operating point, where production of PV systems is maximum and there is no load.

A. Slope Factors

Computed slope factors for the proposed APD methods are shown in Table II. Equation (9) is used to calculate the weight factors for the APD-VP method in Table III. Comparing absolute value of slope factors indicates that the APD-TB voltage

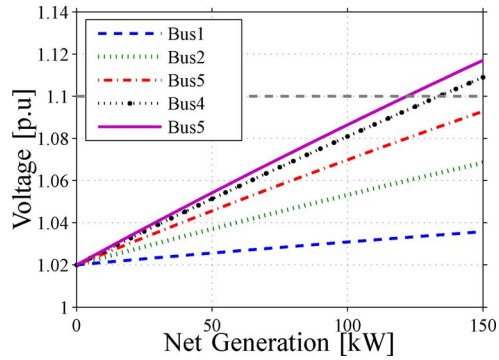

Fig. 5. Voltage profile of the simple LV grid.

TABLE II
SLOPE FACTORS IN THE APD METHOD

Method	m_1	m_2	m_3	m_4	m_5
APD-TB	-0.521	-1.345	-1.802	-2.104	-2.334
APD-VP	-0.521	-1.263	-1.646	-1.854	-1.964

TABLE III
WEIGHT FACTORS BASED ON (9)

W_1	W_2	W_3	W_4	W_5
0.645	0.827	1.000	1.173	1.355

TABLE IV
CALCULATED THRESHOLDS

APD	*Threshold*	$P'_{th,1}$	$P'_{th,2}$	$P'_{th,3}$	$P'_{th,4}$	$P'_{th,5}$
TB	iden	0.787	0.787	0.787	0.787	0.787
	non-iden	0.264	0.714	0.772	0.817	0.835
VP	iden	0.759	0.759	0.759	0.759	0.759
	non-iden	0.263	0.696	0.767	0.793	0.804

regulation has steeper slope factors in contrast to APD-VP voltage regulation. According to (12) and (14), the larger the absolute value of m, the higher the threshold, which can also be seen in Table IV. Larger thresholds reduce the total reactive power consumption by PV systems for an identical generation profile.

B. Identical Thresholds

A larger absolute value of m factors can, however, impose larger reactive power loading on PV inverters at the end of the feeder in the case of using P'_{th} *iden*. Table V depicts the minimum power factor operation of each PV system at the critical operating point. As shown in Table V, in the case of P'_{th} *iden*, the APD-TB method imposes smaller power factor on the last bus. For instance, the power factor of the PV system at the target bus in the presence of the APD-TB voltage regulation is 0.895, which is below the GGC power factor limit. The power factor in the presence of the APD-VP method is augmented to 0.904, which is within the GGC standard power factor band.

In the proposed APD methods there is, therefore, a tradeoff between total reactive power consumption and reactive power loading of PV inverters. If the inverter loading is a challenge, using the APD-VP method and attributing larger weight factors to the nodes at the beginning of the feeder, compared to those at the end, can mitigate the inverter loading. However, it

TABLE V
MINIMUM OPERATING POWER FACTOR OF EACH PV SYSTEM IN THE APD METHOD

APD	P_{th}	$cos\phi_1$	$cos\phi_2$	$cos\phi_3$	$cos\phi_4$	$cos\phi_5$
TB	iden	0.994	0.961	0.934	0.913	0.895
	non-iden	0.933	0.933	0.933	0.933	0.933
VP	iden	0.992	0.957	0.930	0.913	0.904
	non-iden	0.933	0.933	0.933	0.933	0.933

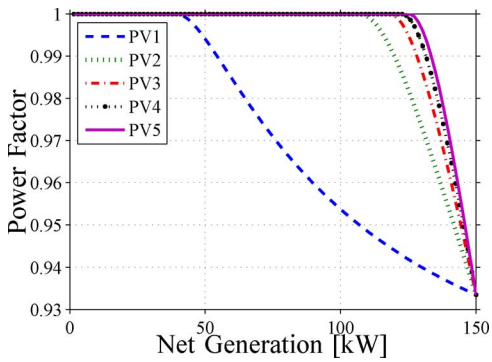

Fig. 6. Power factor of PV systems for the APD-VP method with the nonidentical thresholds.

leads to a lower threshold that, in turn, implies higher total reactive power consumption. Considering high PV penetration, total reactive power consumption may be a major criterion for the power system stability in the case of conventional power-plants contingency [20]. Thus, if APD-TB does not impose any reactive power loading beyond the limit of the PV system at the target bus and PV systems located in the same vicinity, it may be preferred over APD-VP to design $\mathrm{Q(P)}$ parameters in order to reduce reactive power consumption. Otherwise, APD-VP may be used to remove the reactive power loading at the expense of more total reactive power consumption.

C. Nonidentical Thresholds

When nonidentical thresholds are used, the minimum power factors of PV systems are equal for APD-TB and APD-VB methods due to the equal reactive power sharing among PV systems at the critical operating point according to (13). By doing so, the level of the inverter reactive power loading is irrespective of TB or VP methods for the nonidentical thresholds. For instance, the minimum power factor of all PV systems, which occurs at the critical operating point, is 0.933. Hence, the reactive power loading of PV inverters, in contrast to the identical thresholds, is significantly reduced. Nevertheless, equal reactive power sharing only occurs at the critical operating point and, thus, power factors of PV systems are not similar for the remaining operating conditions, as shown in Fig. 6, because PV systems kick in at different thresholds. For instance, in the presence of the APD-VP method, the reactive power compensation of the first PV system has to kick in at $P'_{th,1} = 0.263$ ($P_{th,1} = 7.89$ kW), while the last PV system kicks in at $P'_{th,5} = 0.804$ ($P_{th,5} = 24.13$ kW). Entering the lower thresholds for PV systems at the beginning of the feeder, however, leads to higher total reactive power consumption.

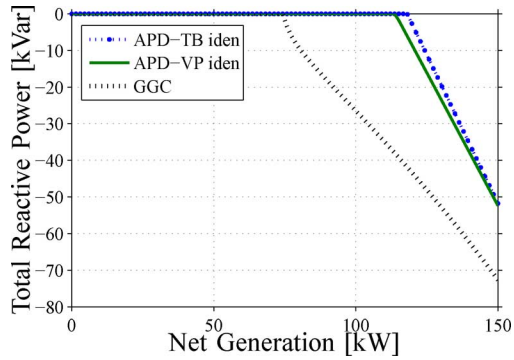

Fig. 7. Total reactive power consumption by PV systems for APD-TB and APD-VP methods with identical thresholds and the GGC standard characteristic.

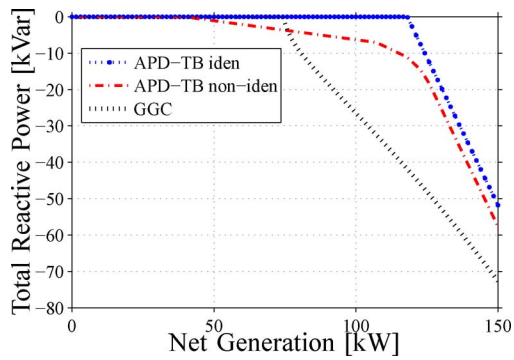

Fig. 8. Total reactive power consumption by PV systems for the APD-TB method with identical and nonidentical thresholds and the GGC standard characteristic.

Therefore, nonidentical thresholds improve the inverter loading problem at the expense of consuming more total reactive power. In this regard, one should go for the nonidentical thresholds if the inverter loading is a restriction; otherwise, the identical thresholds are a better option from a less total reactive power consumption perspective.

D. Reactive Power Consumption

In conjunction with the previous discussion, Fig. 7 demonstrates that APD-VP, in contrast to APD-TB, consumes more total reactive power in the presence of the identical thresholds. In the case of non-identical thresholds, not shown here, the same scenario happens and the VP method needs trivially higher total reactive power as well.

Moreover, Fig. 8 shows that the TB method with the nonidentical thresholds demands more reactive power in contrast to the identical thresholds. It is also worth mentioning that at the critical operating point, the nonidentical thresholds require slightly more reactive power in comparison with the identical thresholds. It is due to the line impedance that is also consuming some reactive power and, thus, regulating the last-bus voltage via PV systems at the beginning of the feeder takes more reactive power. The same results, not shown here, are seen in the case of the VP method.

From Figs. 7 and 8, it is obvious that the total consumed reactive power by GGC is considerably higher than the proposed APD methods.

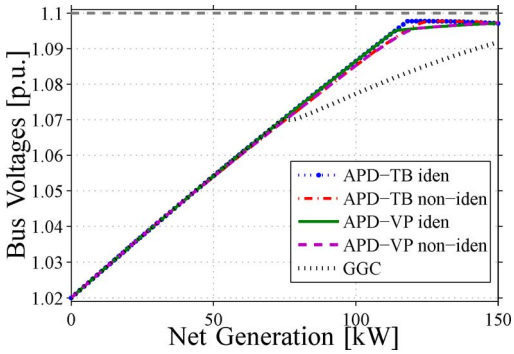

Fig. 9. Last-bus voltage for APD methods and the GGC standard characteristic.

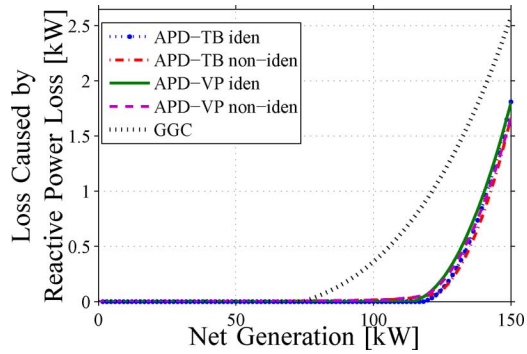

Fig. 10. Total loss caused by reactive power consumption through PV systems for APD methods and the GGC.

E. Voltage Regulation

The regulated last-bus voltage through APD methods is shown in Fig. 9. The regulated last-bus voltage is flatter in the case of APD-TB on the grounds that the regulation target is only the last bus. When calculated power levels are above the threshold of the last bus, the voltage regulation performance of each APD-TB and APD-VP becomes similar for identical and nonidentical thresholds. Therefore, above the threshold of the last bus, the difference in the thresholds calculation does not affect the general behavior of the voltage trajectory. Nevertheless, below the threshold of the last bus, the voltage profile of nonidentical thresholds is below the case of identical thresholds due to the early reactive power contribution. This issue, therefore, implies more total reactive power consumption in the case of P_{th} *non – iden*, which is also expected from the last section.

The final value of the last-bus voltage is similar in TB and VP methods due to the primary objective of the thresholds calculation that makes the last-bus voltage deviation zero. The final voltage value lays slightly below the exact steady-state voltage limit due to the linearizing approximation in (1).

The GGC leads to the lower last-bus voltage because the voltage regulation is not considered, which, in turn, results in more reactive power consumption.

F. Total Active Power Loss

Fig. 10 shows the total active power loss created by reactive power consumption through PV systems. Though the caused loss by the proposed approach is significantly less than the created loss by the GGC, the difference of loss in the proposed methods is trivial. Nevertheless, the APD-TB *non – iden* creates smallest total loss among APD methods. In general, dP_L/dQ coefficients increase for farther PV systems in the feeder. Therefore, high reactive power contribution at the end of the feeder leads to more losses. For instance, though P'_{th} *iden* requires less total reactive power in comparison with P'_{th} *non – iden*, it results in slightly larger total loss due to the aforementioned reason. Moreover, the APD-TB trivially creates less total loss in comparison with the APD-VP, owing to lower total reactive power.

VII. Complex Test System

It is important to verify the generality of the proposed methods regarding voltage regulation and reactive power consumption in complex grids during one-day operation. Therefore, a utility grid located in Northern Jutland, Denmark, as shown in Fig. 11 is used as the LV complex test grid [26]. This complex grid consists of eight feeders and 35 buses. The information of this grid is summarized in Table VI [26]. As a future scenario in this grid, it is assumed that 24 PV systems with four different nameplate powers are unevenly distributed among 35 buses as can be seen in Table VII and Fig. 11.

In order to evaluate a full day of operation, 15-min average power production and demand are employed, which is appropriate for a quasistatic study focused on steady-state conditions. In this regard, Fig. 12 shows a 9-kW Sunny Boy SMA PV system power production in a clear-sky summer day. Due to the clear sky, an assumption of equal solar irradiance availability

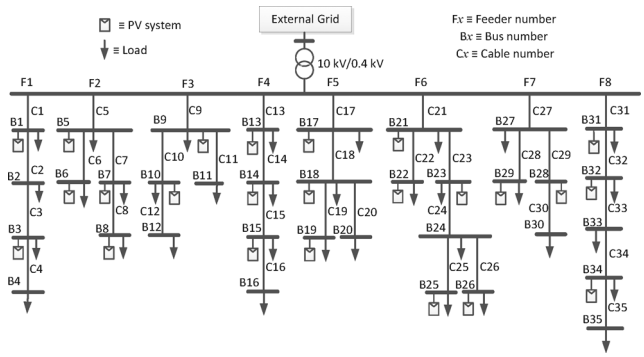

Fig. 11. Complex test utility distribution grid.

TABLE VI
Parameters of the Complex Grid [26]

		Impedance Ω/km
Cables	C_x x=1,5,9,13,17,21,27-31	0.21 + 0.086j
	C_x x=2-4,6-8,10-12,14-16,18-20,22-26	0.32 + 0.086j
	C_x x=32-35	0.6 + 0.09j
Transformer	630 kVA, 10/0.4 kV, Dyn5, U_k=4.66%, P_{cu}=6.5 kW	

TABLE VII
Location and Nameplate Power of PVs in the Complex Grid

PV system nameplate power	Bus number of installed PV
15 kW	B13, B26, B31
20 kW	B6, B8, B10, B16, B21, B23, B29, B34
25 kW	B3, B5, B7, B9, B15, B17, B18, B26, B28
30 kW	B1, B19, B32

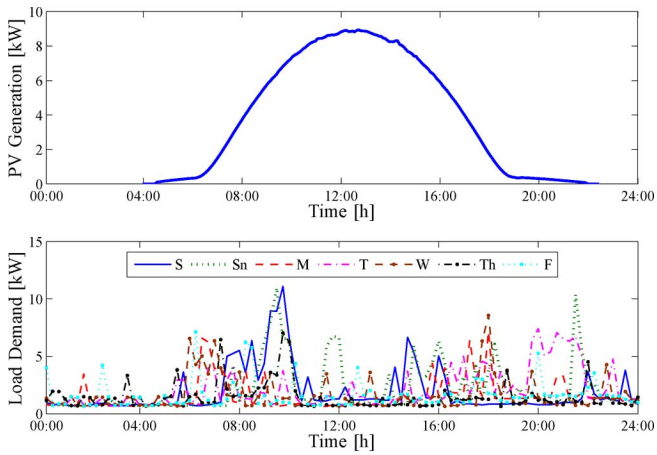

Fig. 12. The 15-min measured PV production and load demand profile during the summer.

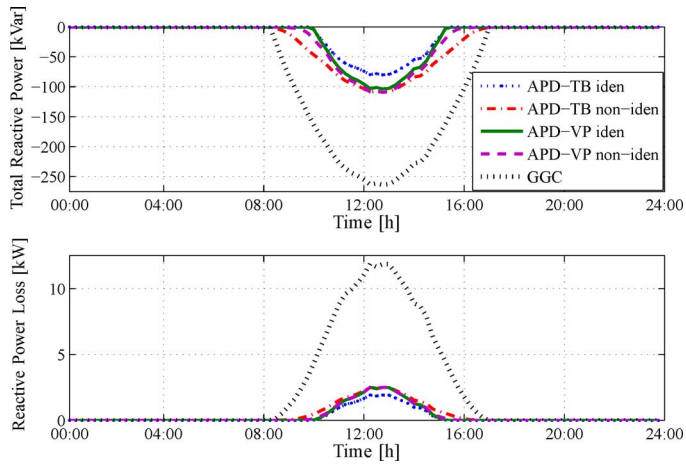

Fig. 13. Daily total reactive power consumptions by PV systems and their associated losses in the presence of APD methods and the GGC standard characteristic.

for all PV systems in the grid is reasonable. Therefore, the production profile is scaled up according to the nameplate power of each PV system in the grid.

Moreover, 15-min average load demand of a villa house is employed to simulate the load in this study. Fig. 12 also demonstrates the demand profile of the house for one week in the summer. In order to consider the load diversity, these seven load profiles are randomly distributed among all 35 buses in the grid. Although the power factor of loads is not available, according to the Swedish DSO, the power factor in distribution grids is close to one. Hence, it seems reasonable to assume that loads operate with 0.98 inductive power factor.

As mentioned earlier, the design of $\mathrm{Q(P)}$ parameters (slope factor and threshold) is carried out by calculating the voltage sensitivity matrix and the critical voltage for the extreme operating point, when PV systems generate their maximum power and loads are at the lowest demand. In the summer, during sunny, clear-sky days, PV systems normally produce their maximum power. Minimum loads may vary from one node to another, and according to the load profiles in this case study, it is assumed that there is always a minimum of 600-W consumption at each node.

For designing the $\mathrm{Q(P)}$ parameters via proposed APD methods, the following steps must be followed:

1) running load flow for the extreme operating point;
2) determining the most critical bus voltage as the target bus;
3) computing the sensitivity $S_P^{|V|}$ and $S_Q^{|V|}$ submatrices;
4) eliminating the rows and columns of $S_P^{|V|}$ and $S_Q^{|V|}$ that correspond to nonequipped PV system buses;
5) calculating slope factors of APD-TB and APD-VP methods according to (5) and (8);
6) calculating identical and nonidentical thresholds according to (12) and (14).

For the selected extreme operating point, voltages at B19, B25, B26 and B34 located, respectively, on F5, F6, F6, and F8 pass the upper steady-state voltage limit. However, the most critical voltage occurs at B26 located on F6 with the magnitude of 1.1206. Hence, this bus and its associated critical voltage value are considered as the target bus.

A. Total Reactive Power Consumption and its Associated Active Power Loss

Fig. 13 demonstrates the daily total reactive power consumption and its associated active power loss for the proposed APD methods as well as the GGC standard characteristic. Along with the results of the simple test system, the APD-VP, compared to APD-TB, consumes more total reactive power in the presence of the identical thresholds. Moreover, the nonidentical thresholds similarly lead to a wider range of reactive power consumption compared to the identical thresholds. However, APD-TB non-iden demands slightly higher total reactive power in contrast to APD-VP. Nevertheless, it is obvious that the total consumed reactive power by the GGC standard characteristic is considerably higher than the proposed APD methods.

Analogous to the simple test system, the loss difference among proposed APD methods is also trivial in the complex system. However, the APD-TB leads to lower losses due to the lower total reactive power consumption. In addition, nonidentical thresholds result in slightly higher losses due to a wider range of reactive power consumption. Nevertheless, the proposed methods significantly reduce losses compared to the GGC standard characteristic.

B. Voltage Regulation and Power Factors

During the daily operation, without reactive power support, voltages at B19 on F5, B25 and B26 on F6, and B34 on F8 hit the upper steady-state voltage limit. The proposed APD methods can successfully regulate all voltages under the steady-state limit. For instance, Fig. 14 shows unsupported voltages and supported voltages via APD methods and GGC at B26 on F6, the most critical one, and B19 on F5. Analogous to the simple test grid, the voltage regulation performance at B26 for all APD methods is similar at higher production levels. Furthermore, it is obvious that the GGC standard characteristic pushes the voltage down to a lower level because, as mentioned earlier, the voltage regulation is not addressed in it.

Though all critical voltages are well regulated via proposed APD methods, APD-TB iden causes slightly smaller error in regulating bus voltages to the steady-state limit as can also be

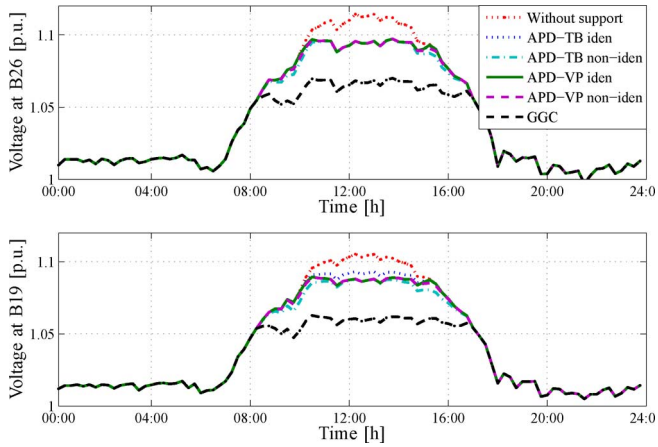

Fig. 14. Daily voltage profile of B19 and B26 without reactive power support and with support via APD methods and the GGC standard characteristic.

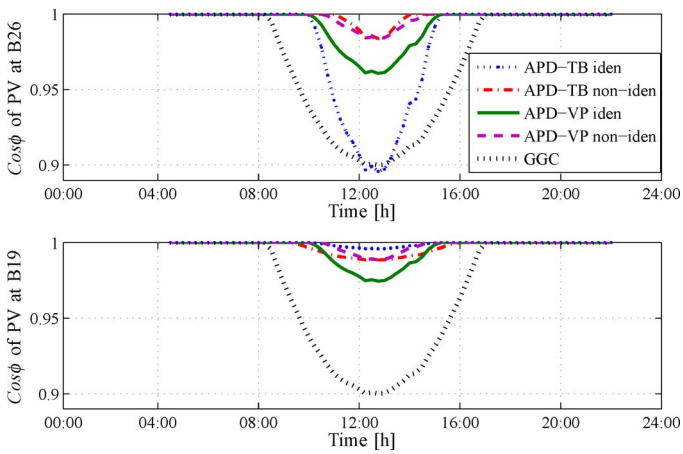

Fig. 15. Daily power factor of PV systems located at B19 and B26 in the presence of APD methods and the GGC standard characteristic.

seen for the voltage at B19. This is due to considerable lower reactive power consumption via APD-TB iden (Fig. 13), that is, in turn, because of putting the reactive power consumption pressure on the TB. It can also be seen in Fig. 15 that in APD-TB, the PV system power factor at B26 is much lower than the PV system power factor at B19. It is also clear that the APD-VP removes the pressure from the PV system at the TB. Furthermore, it can be observed that nonidentical thresholds lead to higher and more uniform power factors among PV systems.

VIII. Summary

A qualitative comparison of the proposed methods with the state of the art, which is the GGC method, is provided in Table VIII. The pros and cons of the proposed methods can be summarized as follows.

- APD-TB needs less total reactive power in contrast to APD-VP. Nevertheless, the proposed APD methods consume much less total reactive power than the GGC.
- In the case of identical thresholds, APD-VP decreases the reactive power loading in inverters in comparison with APD-TB.
- Concerning the voltage regulation fulfilment, APD-TB and APD-VP have no notable advantage over each other. Nevertheless, regulating voltage to the steady-state limit through the proposed APD approach, in contrast to the GGC, is superior.
- Though using nonidentical thresholds alleviates reactive power loading in inverters, the total required reactive power is increased.
- Compared to the GGC, the proposed method considerably decreases active power losses caused by reactive power injections. Within the variants of proposed APD methods, the difference between losses is trivial. With that being said, the APD-TB *iden* may create lower total loss due to lower reactive power consumption.

TABLE VIII
Qualitative Comparison

Method	Voltage Regulation[1]	Reactive Power[2]	Inverter Loading[3]	Total Loss[4]
TB iden	+++	+++	o	+++
TB non-iden	+++	+	+++	+++
VP iden	+++	++	++	+++
VP non-iden	+++	+	+++	+++
GGC	-	-	++	-

*+++ superior, ++ very good, + good, o average, - inferior

[1] Regulate the voltage to steady-state limit
[2] Causing less reactive power consumption
[3] Decreasing reactive power loading in PV inverters
[4] Causing less active power loss by reactive power

IX. Conclusion

This paper demonstrates how the advantages of the voltage sensitivity matrix allow systematic coordination of PV inverters while still using local measurements. Two main parameters of the $Q(P)$ characteristic for each PV system in a distribution grid, namely, the slope factor and the threshold, are specified based on analysis of the voltage sensitivity matrix. The proposed approach regulates either the target-bus voltage or the voltage profile. Therefore, the slope factors are derived in two different methods. Moreover, the thresholds are also calculated via two different methods, namely, identical threshold and equal reactive power sharing. The results demonstrate that the proposed methods are able to regulate the voltage to the steady-sate voltage limit, while the voltage regulation in the GGC method is not addressed. Since the proposed methods explicitly include voltage limits, they can decrease the total required reactive power as well as active power loss caused by reactive power in comparison with the GGC.

It is also shown that the proposed TB and VP methods have no advantage over each other with respect to regulation of the target bus or losses. Nevertheless, the TB method, in contrast to the VP method, consumes less total reactive power. The advantage of VP over TB is decreasing the inverter reactive power loading in the case of identical thresholds. Moreover, if loading is a restriction, using nonidentical thresholds can alleviate the reactive power loading with inverters at the expense of larger total reactive power.

The comparison has shown the substantial advantages that the proposed methods have over the GGC in terms of voltage maintenance and loss reduction in distribution feeders. Their application may be regarded as cumbersome since an adjustment of pa-

rameters, following the connection of any additional PV system to the feeder, would be required by the DSO in order to use the proposed methods to their full capability. A more practical approach, however, is an implementation of the proposed methods in the DSO's long-term (strategic, that is, 10-year ahead) network planning process. The DSO would predefine the threshold and slope values for PV systems in certain grid locations based on an expected future PV integration level and distribution in the grid. While this may result in suboptimal performance in the transitional period, an optimal choice of parameters with regard to the finally expected grid stage would be achieved.

ACKNOWLEDGMENT

The authors would like to express their gratitude towards all partner institutions within the program as well as the European Commission for their support. The authors would like to thank O. Hansson, of Fortum, for providing load data.

REFERENCES

[1] J. C. Boemer, K. Burges, P. Zolotarev, J. Lehner, P. Wajant, M. Fürst, R. Brohm, and T. Kumm, "Overview of German grid issues and retrofit of photovoltaic power plants in Germany for the prevention of frequency stability problems in abnormal system conditions of the ENTSO-E region continental europe," presented at the 1st Int. Workshop Integration of Solar Power into Power Syst., Aarhus, Denmark.

[2] A. Jaeger-Waldau, "PV status report 2012—research, solar cell production and market implementation of photovoltaics," European Commission, DG Joint Research Center, Institute for Energy and Transport, Renewable Energy Unit, Ispra, Italy, Tech. rep. EUR 25749 EN, 2012.

[3] D. Verma, O. Midtgard, and T. Satre, "Review of photovoltaic status in a european (EU) perspective," in *Proc. 37th IEEE Photovoltaic Specialists Conf.*, Jun. 2011, pp. 003292–003297.

[4] U. Schwabe and P. Jansson, "Utility-interconnected photovoltaic systems reaching grid parity in New Jersey," in *Proc. IEEE Power Energy Soc. Gen. Meeting*, Jul. 2010, pp. 1–5.

[5] J. H. Wohlgemuth, D. W. Cunningham, R. F. Clark, J. P. Posbic, J. M. Zahler, P. Garvison, D. E. Carlson, and M. Gleaton, "Reaching grid parity using BP solar crystalline silicon technology," in *Proc. 33rd IEEE Photovoltaic Specialists Conf.*, May 2008, pp. 1–4.

[6] D. Pérez, V. Cervantes, M. J. Báez, and J. González-Puelles, "PV grid parity monitor," ECLAREON, Tech. rep., 2012.

[7] Y.-M. Saint-Drenan, S. Bofinger, B. Ernst, T. Landgraf, and K. Rohrig, "Regional nowcasting of the solar power production with PV-plant measurements and satellite images," presented at the ISES SolarWorld Congr., Kassel, Germany, 2011.

[8] T. Stetz, F. Marten, and M. Braun, "Improved low voltage grid-integration of photovoltaic systems in Germany," *IEEE Trans. Sustain. Energy*, vol. PP, no. 99, pp. 1–9, 2012.

[9] R. Shayani and M. de Oliveira, "Photovoltaic generation penetration limits in radial distribution systems," *IEEE Trans. Power Syst.*, vol. 26, no. 3, pp. 1625–1631, Aug. 2011.

[10] R. Tonkoski, L. Lopes, and T. El-Fouly, "Coordinated active power curtailment of grid connected PV inverters for overvoltage prevention," *IEEE Trans. Sustain. Energy*, vol. 2, no. 2, pp. 139–147, Apr. 2011.

[11] E. Demirok, P. C. Gonzalez, K. Frederiksen, D. Sera, P. Rodriguez, and R. Teodorescu, "Local reactive power control methods for overvoltage prevention of distributed solar inverters in low-voltage grids," *IEEE J. Photovoltaics*, vol. 1, no. 2, pp. 174–182, Oct. 2011.

[12] A. Engler and N. Soultanis, "Droop control in LV-grids," in *Proc. Int. Conf. Future Power Syst.*, Nov. 2005, p. 6.

[13] M. Braun, "Reactive power supply by distributed generators," in *Proc. IEEE Power Energy Soc. Gen. Meeting –Convers. Del. Elect. Energy 21st Century*, Jul. 2008, pp. 1–8.

[14] P. Sulc, K. Turitsyn, S. Backhaus, and M. Chertkov, Options for control of reactive power by distributed photovoltaic generators, 2010. [Online]. Available: arXiv:1008.0878

[15] A. Yazdani, A. Di Fazio, H. Ghoddami, M. Russo, M. Kazerani, J. Jatskevich, K. Strunz, S. Leva, and J. Martinez, "Modeling guidelines and a benchmark for power system simulation studies of three-phase single-stage photovoltaic systems," *IEEE Trans. Power Del.*, vol. 26, no. 2, pp. 1247–1264, Apr. 2011.

[16] A. Samadi, M. Ghandhari, and L. Söder, "Reactive power dynamic assessment of a PV system in a distribution grid," *Energy Procedia*, vol. 20, pp. 98–107, 2012.

[17] *Power Generation Systems Connected to the Low/Voltage Dstribution Network*, VDE-AR-N 4105:2011-08, Forum Netztechnik/Netzbetrieb im VDE (FNN), Berlin, Germany, 2011.

[18] R. Tonkoski and L. Lopes, "Voltage regulation in radial distribution feeders with high penetration of photovoltaic," in *Proc. IEEE Energy 2030 Conf.*, Nov. 2008, pp. 1–7.

[19] A. Cagnano, E. De Tuglie, M. Liserre, and R. Mastromauro, "Online optimal reactive power control strategy of PV inverters," *IEEE Trans. Ind. Electron.*, vol. 58, no. 10, pp. 4549–4558, Oct. 2011.

[20] "Studie zur Ermittlung der Technischen Mindesterzeugung des Konventionellen Kraftwerksparks zur Gewährleistung der Systemstabilität in den Deutschen Übertragungsnetzen bei Hoher Einspeisung aus Erneuerbaren Energien," Tech. Rep. Studie im Auftrag der deutschen Übertragungsnetzbetreiber, 2012.

[21] A. Samadi, R. Eriksson, and L. Söder, "Evaluation of reactive power support interactions among PV systems using sensitivity analysis," in *Proc. 2nd Int. Workshop Integr. Solar Power into Power Syst.*, Lisbon, Portugal, pp. 245–252.

[22] R. Aghatehrani and R. Kavasseri, "Reactive power management of a DFIG wind system in microgrids based on voltage sensitivity analysis," *IEEE Trans. Sustain. Energy*, vol. 2, no. 4, pp. 451–458, Oct. 2011.

[23] CENELEC, "Voltage characteristics of electricity supplied by public distribution networks, " Brussels, Belgium, EN 50160.

[24] H. Saadat*, Power System Analysis*, 3rd ed. Alexandria, VA, USA: PSA, 2010.

[25] E. Demirok, D. Sera, R. Teodorescu, P. Rodriguez, and U. Borup, "Evaluation of the voltage support strategies for the low voltage grid connected PV generators," in *Proc. IEEE Energy Convers. Congr. Expo.*, 2010, Sep. 2010, pp. 710–717.

[26] J. Pillai, P. Thogersen, J. Moller, and B. Bak-Jensen, "Integration of electric vehicles in low voltage danish distribution grids," in *Proc. IEEE Power Energy Soc. Gen. Meeting*, 2012, pp. 1–8.

Afshin Samadi (S'12) was born in Hamedan, Iran. He received the B.Sc. degree in electrical engineering from Bu-Ali Sina University, Hamedan, Iran, in 2004, the M.Sc. degree in electrical engineering from the University of Tehran, Tehran, Iran, in 2008, and is currently pursuing the Ph.D. degree in electric power systems at the KTH Royal Institute of Technology, Stockholm, Sweden.

His research interest is control strategies for photovoltaic system integration in power grids.

Robert Eriksson (M'11) received the M.Sc. and Ph.D. degrees in electrical engineering from the KTH Royal Institute of Technology, Stockholm, Sweden, in 2005 and 2011, respectively.

Currently, he is Associate Professor with the Center for Electric Power and Energy, Technical University of Denmark. He is also Part-Time Researcher at the Department of Electric Power Systems, KTH Royal Institute of Technology. His research interests include power system dynamics and stability, HVDC systems, dc grids, and automatic control.

Lennart Söder (SM'10) was born in Solna, Sweden, in 1956. He received the M.Sc. and Ph.D. degrees in electrical engineering from the KTH Royal Institute of Technology, Stockholm, Sweden, in 1982 and 1988, respectively.

Currently, he is a Professor and Head of the Department of Electric Power Systems, Royal Institute of Technology (KTH). He works with projects concerning electricity markets and integration of wind power, solar power, and electric vehicles.

Barry G. Rawn (M'10) received the B.A.Sc. and M.A.Sc. degrees in engineering science and electrical engineering and the Ph.D. degree in electrical engineering from the University of Toronto, Toronto, ON, Canada, in 2002, 2004, and 2010, respectively.

His research interests include sustainable energy infrastructure and nonlinear dynamics. He is a Postdoctoral Researcher in the Electra division of the ESAT Department, the University of Leuven, Leuven, Belgium.

Jens C. Boemer (S'13) received the Dipl.-Ing. degree in electrical engineering from Technical University of Dortmund, Dortmund, Germany, in 2005 and is currently pursuing the Ph.D. degree in stability of sustainable power systems (with a focus on the network fault response of transmission systems with very high penetration of distributed generation) at the Delft University of Technology, Delft, the Netherlands.

He specialized in power systems and renewable energies. He supported the German Environment Ministry in the drafting of the Ancillary Services Ordinance for wind powerplants (SDLWindV) and developed an operational strategy for the Irish transmission system operator EirGrid/SONI with regard to very high instantaneous shares of wind power in the All Island Power System. He is Senior Consultant at the Power Systems and Markets Group at the Ecofys premises, Berlin, Germany. Currently, he is on a temporary research stay with the Intelligent Electrical Power Grids section at the Electrical Sustainable Energy Department, Delft University of Technology.

Mr. Boemer is a member of VDE.

P-V

Optimal Coordination of Q(P) Characteristics for PV Systems in Distribution Grids for Minimizing Reactive Power Consumption

http : //www.cigre.org

AORC Technical meeting 2014

"No.1046."

Optimal Coordination of Q(P) Characteristics for PV Systems in Distribution Grids for Minimizing Reactive Power Consumption

A.SAMADI **E.SHAYESTEH** **L.SÖDER**

Electric Power System
KTH Royal Institute of Technology
Sweden

SUMMARY

Accommodating more and more photovoltaic (PV) systems within load pockets in distribution grids due to encouraging feed-in-tariffs has raised new technical challenges such as voltage rise. Different remedies have been proposed to deal with the voltage violation. The most common remedy is supporting the voltage profile via reactive power contribution of PV systems. The German Grid Codes (GGC) also requires reactive power contribution of PV systems. The GGC also proposes an active power dependent (APD) power factor standard characteristic $cos\phi(P)$. However, the standard characteristic lacks a systematic approach to set the $cos\phi(P)$ parameters according to the location of PV systems within the grid. A systematic APD voltage regulation Q(P) with four design variants has been proposed in the literature to coordinate the Q(P) characteristics among PV systems. This paper proposes an alternative approach to optimally coordinate Q(P) parameters among PV systems without the aid of any communication systems. The contribution of the proposed APD method, in contrast to its predecessor, is being an optimization-based procedure; thus, Q(P) characteristics are optimally designed and coordinated among PV systems. In other words, the main objective of this study is to deploy the voltage sensitivity matrix to optimally coordinate the Q(P) parameters among PV systems within the grid. The performance of the proposed optimal APD is compared with its predecessor; the results show that the proposed method can considerably reduce the total reactive power consumption and the corresponding losses in comparison with the predecessor APD method.

KEYWORDS

Photovoltaic - Reactive power control - German Grid Codes - Voltage support scheme

afshin.samadi@ee.kth.se

1. Introduction

Growing trends in photovoltaic system installations due to encouraging feed-in-tariffs have led to high penetration of PV systems in distribution grids. In Germany, for instance, there are currently more than 32 GW installed PV systems, of which 80% have been connected in low voltage grids [1-2]. These high penetrations of PV systems have raised new challenges in the distribution grid such as reverse power flow and voltage rise.

Reactive power contribution via PV systems is one of the proposed remedies to cope with the unwanted overvoltage associated with high participation of PV systems [3-5]. Nevertheless, considering high penetration of PV systems, unnecessary reactive power consumption increases the line losses; furthermore, it may jeopardize the stability of power system in the case of contingency in conventional power plants supplying reactive power [6]. Therefore, it is important to reduce the total reactive power consumption. Several approaches have been proposed for reactive power support: constant power factor [3]; active power dependent (APD) power factor *cosϕ(P)* [3-4], [7]; a combination of *cosϕ(P)* and droop-based voltage regulation *Q(V)* characteristic *cosϕ(P,V)* [3]; and APD reactive power characteristic Q(P) [5]. Constant power factor may cause unnecessary reactive power consumption and line losses because it always contributes reactive power even in occasions when there is no voltage violation. In order to decrease reactive power consumption, the recent German Grid Codes (GGC) proposed a standard *cosϕ(P)* characteristic for distributed generation (DG) units to support the voltage profile [7]. Nevertheless, the GGC does not clarify how to set the parameters of the standard characteristic among PV systems at different locations within a grid. Though the GGC states PV systems may need a different characteristic than the standard characteristic, the specification of such a characteristic is left to the distribution system operators (DSO). Though the *cosϕ(P)* and Q(V) characteristics are combined in [3] to take the advantage of both methods, no systematic approach was introduced to design the parameters of the presented *cosϕ(P,V)* characteristic. The main concept of *cosϕ(P)* and Q(P) characteristics are the same, which both of them are active power dependent characteristics and the feed-in active power of the PV system is used as a feedforward signal to calculate the required reactive power. Therefore, the developed APD voltage regulation method in [5] introduces a systematic approach to design and coordinate the parameters of the Q(P) characteristic among PV systems using only the information of the voltage sensitivity matrix and without any communication aid. This method can design the parameters of the Q(P) characteristic via four variants. Though [5] provides a detailed discussion regarding the advantages and disadvantages of each variant, the final optimal choice of the variant is left to the user.

The goal of this paper is to develop a new optimization formulation to optimally coordinate the APD Q(P) parameters among PV systems. The objective of the optimization is minimizing the total reactive power consumption of individual PV systems over their power production profile. To design the Q(P) parameters in the proposed method, only the information of the voltage sensitivity matrix is employed and there is no need for any communication system. The quality of the proposed optimal APD method is evaluated against the predecessor APD method. The results demonstrate the superior performance of the proposed method.

2. German Grid Codes

According to the GGC in the low voltage grids, distributed generation (DG) units that deliver at least 20% of their rated power are allowed to change their power factor between 1 lower to 0.95 or 0.9 depending upon the size of the DG [7]. The lower limit of power factor for DGs larger than 13.8 kVA is 0.9 while for DGs between 3.68 kVA and 13.8 kVA it is 0.95 [7].

As mentioned earlier, on the one hand reactive power contribution of PV systems alleviates the voltage violation, but on the other hand causes the power loss. Accordingly, the GGC proposes the standard *cosϕ(P)* characteristic curve in Fig. 1, where P and P_{max} represent the feed-in and the maximum active power of the generator unit, respectively [7]. The objective of the standard *cosϕ(P)* characteristic is requiring the DGs to operate in an under-excited mode when the feed-in active power passes over a threshold of 50% of P_{max}, above which the voltage rise is more likely, in order to alleviate the related voltage rise. The GGC states that depending upon different aspects, i.e. grid configuration, load and feed-in power, distribution network operators may need a characteristic

different from the proposed standard *cosϕ(P)* characteristic shown in Fig. 1. Nevertheless, the GGC does not address how to specify the setting parameters. Using the unique standard characteristic for all PV systems within a grid can result in the unnecessary reactive power consumptions [5].

Figure 1. Standard *cosϕ(P)* characteristic

Figure 2. Q(P) characteristic for APD

3. The Previous APD Voltage Regulation Presented in [5]

The GGC standard characteristic lacks a systematic approach to properly design and coordinate its parameters, namely the slope and the threshold, for individual PV systems within the grid. Therefore, [5] proposes the APD voltage regulation Q(P) as a systematic approach to design and coordinate the slope and the active power threshold in Fig. 2. The APD method can explicitly consider the voltage and regulates it under the steady-state voltage limit. The APD method does not need any communication system and only uses the voltage sensitivity matrix in (1) at the extreme operating point, in which all PV systems are at the full production and loads are at the minimum level, as follows

$$\begin{bmatrix}\Delta\theta\\ \Delta V\end{bmatrix}=\begin{bmatrix}\partial\theta/\partial P & \partial\theta/\partial Q\\ \partial V/\partial P & \partial V/\partial Q\end{bmatrix}\begin{bmatrix}\Delta P\\ \Delta Q\end{bmatrix}=\begin{bmatrix}S_P^{\theta} & S_V^{\theta}\\ S_P^{V} & S_Q^{V}\end{bmatrix}\begin{bmatrix}\Delta P\\ \Delta Q\end{bmatrix} \quad (1)$$

where θ and V represent angle and magnitude of voltages of buses, respectively; P and Q are the net active and reactive power of buses within the grid [8].

For the APD method presented in [5], first the target bus (TB), where the maximum overvoltage at the extreme operating point occurs, is determined, and then the information of voltage sensitivity matrix is used to find the slope and the threshold of individual PV systems. The slopes are derived in two different ways:

1. Regulating the TB voltage;
2. Regulating the voltage profile within the entire feeder.

The threshold of the Q(P) characteristic can also be calculated via two different ways:

1. Having an identical threshold while maximum reactive powers of PVs at the extreme operating point become non-identical;
2. Having non-identical thresholds while maximum reactive powers of PVs at the extreme operating point become identical.

Figs. 3 show the schematic of the APD Q(P) characteristic. Therefore, the APD method introduces four different variants to design the Q(P) parameters. The pros and cons of each variant were discussed in detail in [5]; however, the choice is left to the DSOs to adopt the one that suits to the corresponding grid and specifications of the PV systems in it.

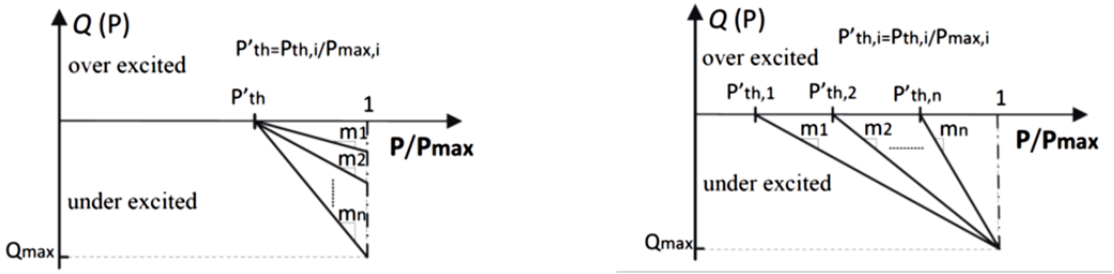

Figure 3: Curves of the APD Q(P) characteristics, (left) identical and (right) non-identical thresholds.

4. Set-up of the proposed optimal APD

The aim of this paper, as mentioned earlier, is to develop a new optimization formulation that can streamline the deployment of the APD concept to optimally coordinate the Q(P) parameters among PV systems within the grid. The objective of the proposed method is to design the slope and the threshold of Q(P) characteristics in such a way to minimize the sum of the hatched areas in Fig. 2. The total area is related to the total reactive power consumption, but not exactly since the probability of different consumption levels is not constant. In this regard, the following objective function is proposed

$$\min_{(P_{th,i},\Delta Q_i)} \quad \left(\sum_{i=1}^{n} (P_{\max pv,i} - P_{th,i}) \Delta Q_{\max,i} \right) \tag{2}$$

where $P_{th,i}$ and $\Delta Q_{max,i}$ are optimization variables and, respectively, are the threshold and the maximum required reactive power of the *i-th* PV system Q(P) characteristic at the critical operating point. According to Fig. 2, the slope m_i is the by-product of the $P_{th,i}$ and $\Delta Q_{max,i}$.

The theoretical concept behind the APD method in addition to some new concepts is employed to figure out the constraints of the proposed objective function. Accordingly, the proposed objective function must be subjected to the following constraints:

I. Voltage regulation

The goal of using Q(P) characteristics is to cancel the TB overvoltage, which is defined as follows

$$\Delta V_{max,TB} = V_{max,TB} - \overline{V} \tag{3}$$

where $V_{max,TB}$ is the maximum voltage at the TB and $\overline{V}$ is the steady-state voltage limit, which is 1.1 p.u according to the EN 50160 [9].

Based on (1), the required reactive power to compensate the TB overvoltage at the extreme operating point is

$$\Delta V_{\max,TB} = \sum_{i=1}^{n} S^{V}_{QTB,\mathrm{i}} \Delta Q_{\max,i} \tag{4}$$

where n is the number of buses.

II. Maximum reactive power contribution

The reactive power contribution of PV systems is limited according to the GGC regulation; thus, to comply with the GGC standard the $\Delta Q_{max,i}$ is subjected to

$$0 \le \Delta Q_{\max,i} \le P_{\max,\mathrm{i}} \sqrt{\frac{1}{\cos \varphi^2_{\max}} - 1} \tag{5}$$

III. The slope limit

The rate of reactive power changes versus active power variations depends on the slope. Therefore, the slope factor of the Q(P) characteristic must also be limited. Hence, in order to find a proper range for the slope factor, the specification of the *Q(P)* characteristic and the information of the voltage sensitivity matrix is employed. According to the *Q(P)* characteristic in Fig. 2, the relation between reactive power and the feed-in power of the PV system is

$$\begin{aligned} \Delta Q_i &= m_i (P_i - P_{th,\mathrm{i}}) \\ &= m_i \Delta P_i \end{aligned} \tag{6}$$

Based on (1) , the voltage deviations of buses within the grid can also be represented by

$$\begin{bmatrix} \Delta V_1 \\ \vdots \\ \Delta V_{TB} \\ \vdots \\ \Delta V_n \end{bmatrix} = \begin{bmatrix} S^{V}_{P1,1} & \cdots & S^{V}_{P1,n} & S^{V}_{Q1,1} & \cdots & S^{V}_{Q1,n} \\ \vdots & \ddots & \vdots & \vdots & \ddots & \ddots \\ S^{V}_{PTB,1} & . & S^{V}_{PTB,n} & S^{V}_{QTB,1} & \cdots & S^{V}_{QTB,n} \\ \vdots & \ddots & \vdots & \vdots & \ddots & . \\ S^{V}_{Pn,1} & \cdots & S^{V}_{Pn,n} & S^{V}_{Qn,1} & \cdots & S^{V}_{Qn,n} \end{bmatrix} \begin{bmatrix} \Delta P_1 \\ \vdots \\ \Delta P_n \\ \Delta Q_1 \\ \vdots \\ \Delta Q_n \end{bmatrix} \tag{7}$$

Replacing (6) in (7) gives

$$\begin{bmatrix} \Delta V_1 \\ \vdots \\ \Delta V_n \end{bmatrix} = \begin{bmatrix} \alpha_{11} & \cdots & \alpha_{1n} \\ \vdots & \ddots & \vdots \\ \alpha_{n1} & \cdots & \alpha_{nn} \end{bmatrix} \begin{bmatrix} \Delta P_1 \\ \vdots \\ \Delta P_n \end{bmatrix} \tag{8}$$

where α_{ji} is defined as follows:

$$\alpha_{ji} = S^{V}_{Pj,\mathrm{i}} + m_i S^{V}_{Qj,\mathrm{i}} \tag{9}$$

The zero and negative values of α lead to zero and negative values in ΔV and, therefore, by an increase in the production of PV systems, the voltage variation will be suppressed. In other words, m_i should be

$$m_i \le -\frac{S^{V}_{Pj,\mathrm{i}}}{S^{V}_{Qj,\mathrm{i}}} \qquad \forall j \tag{10}$$

So, the m_i is selected as the minimum value in (10).

5. Case Study

In order to implement the proposed method following steps must be taken

a) finding the worst case scenario, which is the extreme operating point at full PV power production and light load condition while there is no reactive power support;
b) deriving the voltage sensitivity matrix for the worst case scenario;
c) solving the optimization problem formulated in (2) for the worst case scenario;
d) applying the Q(P) parameters according to the optimization result for all cases .

A similar simulation platform as described in [5] is also employed in this study to first verify the performance of the proposed method regarding voltage regulation and reactive power consumption, and second evaluate its quality against the APD method. Therefore, the test grid is a utility grid located at Northern Jutland in Denmark as shown in Fig. 4. This grid consists of eight feeders and thirty five buses. The information of this grid is given in Table I [10]. As a future scenario in this grid, it is assumed that 24 PV systems with four different nameplate powers are unevenly distributed among 35 buses as can be seen in Table. II and Fig. 4.

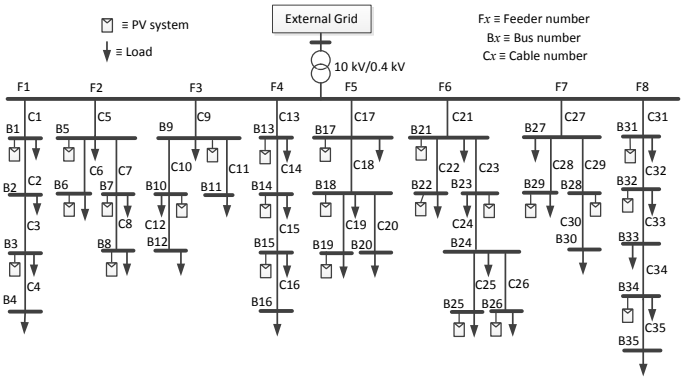

Figure 4: Test utility distribution grid [10].

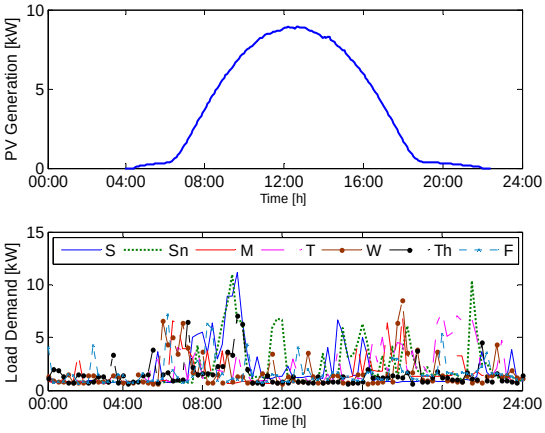

Figure 5: 15-min measured PV production and load profile during the summer.

In this study a quasi-static analysis is employed. Therefore, 15-minutes average PV power production and load demand within a full day are deployed to carry out the investigation. Fig. 5 shows a 9 kW PV system power production in a clear sky summer day. Owing to the clear sky, one can simply assume an equal solar irradiance for all PV systems in the grid. Accordingly, the production profile is scaled up based on the nameplate power of each PV system in the grid.

Moreover, 15-minutes average load demand of a villa house is used to simulate the load in this study. Fig. 5 depicts the load profile of the house for one week in summer. These seven load profiles are randomly distributed among all 35 buses in the grid to consider the load diversity. It is assumed that loads operate with the similar 0.98 inductive power factor.

Table I: Parameters of the test utility grid [10].

		Impedance Ω/km
Cables	Cx x=1,5,9,13,17,21,27-31	0.21 + 0.086j
	Cx x=2-4,6-8,10-12,14-16,18-20,22-26	0.32 + 0.086j
	Cx x=32-35	0.6 + 0.09j
Transformer	630 kVA, 10/0.4 kV, Dyn5, Uk=4.66%, Pcu=6.5 kW	

Table II: Location and size of installed PV systems.

PV system size	Bus number of installed PV
15 kW	B13, B26, B31
20 kW	B6, B8, B10, B16, B21, B23, B29, B34
25 kW	B3, B5, B7, B9, B15, B17, B18, B26, B28
30 kW	B1, B19, B32

The extreme operating point is at the maximum PV systems' production, which is normally at the sunny, clear-sky days, and minimum loads. The minimum load may vary from one node to another, according to the given load profiles it can be seen there is always a minimum of 600 W consumption at each node.

Under the selected extreme operating point conditions, bus voltages located at B19, B25, B26 and B34 experience a voltage above the steady-state voltage limit. However, the most critical voltage occurs at B26 with the magnitude of 1.1206. Accordingly, this bus is considered as the target bus.

5.1 Total reactive power consumption and associated losses and power factors

The quality of the proposed optimal APD method is evaluated against the predecessor APD with identical thresholds and the TB voltage regulation APD TB-Iden, which according to [5] resulted in the lowest reactive power consumption and losses but largest inverter loading among all the four variants of PV systems. Fig. 6 illustrates the daily total reactive power consumption via PV systems and corresponding losses caused by it. Though the maximum total reactive power consumption of the optimal APD method is slightly larger at the peak day, the overall daily reactive power profile of it is tangibly under the APD TB-Iden. So, the proposed optimal APD method, in contrast to the APD TB-Iden, reduces 29% of total reactive power consumption and, in turn, decreases losses by 24% during daily operation.

The daily power factors of the PV systems located at B19 and B26 are given in Fig. 7. The PV system power factor at the B26 in the case of APD TB-Iden hits the GGC limit (0.9 inductive) while APD optimal stays under the GGC limit. Therefore, the proposed approach not only reduces the total reactive power consumption and loses but also prevents the inverter loading at the TB.

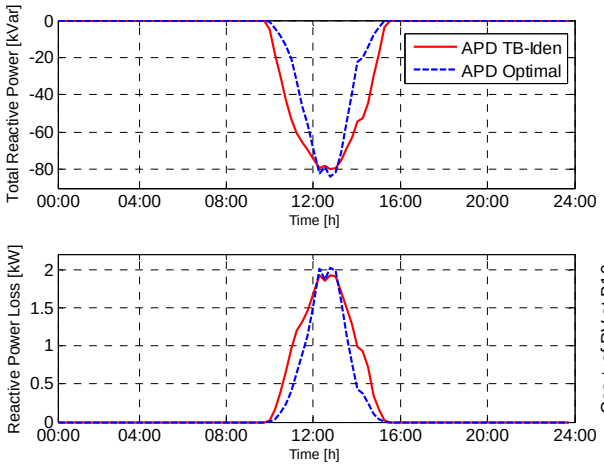

Figure 6: Daily total reactive power consumptions by PV systems and their associated losses in the presence of the APD optimal and APD TB-Iden.

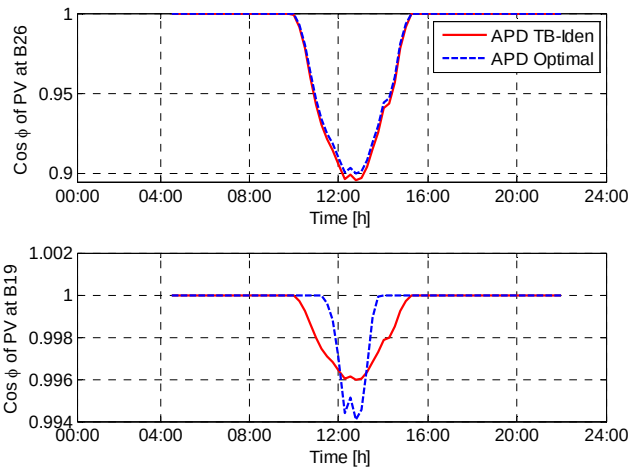

Figure 7: Daily power factor of PV systems located at B19 and B26 in the presence of the APD optimal and APD TB-Iden.

Fig. 8 shows the performance of the proposed optimal APD method and APD TB-Iden. As can be seen, the optimal APD can successfully regulate the voltage under steady-state limit.

6. Conclusion

This paper shows how the information of the voltage sensitivity matrix can be employed to develop an optimal and systematic method to support the voltage profile of distribution grids during high penetration of PV systems. The voltage support scheme is basically the active power dependent reactive power characteristic Q(P). The proposed method formulates an optimization problem to reduce the sum of reactive power consumption of individual PV systems over their production profile. Parameters of the Q(P) characteristics, namely the slope and the threshold, are then calculated through solving the optimization problem. The results demonstrate that the proposed optimal APD method considerably reduces the total reactive power consumption and corresponding losses while the voltage is successfully regulated under the steady-state limit. Besides, the quality comparison shows the superiority of the proposed optimal APD method against the predecessor APD method.

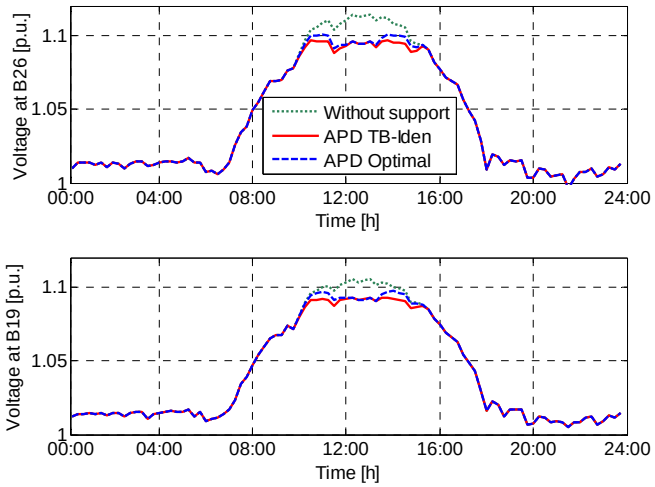

Figure 7: Daily voltage profile of B19 and B26 without reactive power support and with support via APD TB- Iden and optimal APD methods.

References

[1] J. C. Boemer,K.Burges, P. Zolotarev, J.Lehner,P.Wajant,M. Fürst, R. Brohm, and T. Kumm, "Overview of German grid issues and retrofit of photovoltaic power plants in Germany for the prevention of frequency stability problems in abnormal system conditions of the ENTSO-E region continental europe," presented at the 1st Int.Workshop Integration of Solar Power into Power Syst., Aarhus, Denmark.

[2] A. Jaeger-Waldau, "PV status report 2012—research, solar cell production and market implementation of photovoltaics," European Commission, DG Joint Research Center, Institute for Energy and Transport, Renewable Energy Unit, Ispra, Italy, Tech. rep. EUR 25749 EN, 2012.

[3] E. Demirok, P. C. Gonzalez, K. Frederiksen, D. Sera, P. Rodriguez, and R. Teodorescu, "Local reactive power control methods for overvoltage prevention of distributed solar inverters in low-voltage grids," *IEEE J. Photovoltaics*, vol. 1, no. 2, pp. 174–182, Oct. 2011.

[4] A. Samadi, M. Ghandhari, and L. Söder, "Reactive power dynamic assessment of a PV system in a distribution grid," *Energy Procedia*, vol. 20, pp. 98–107, 2012.

[5] A. Samadi, R. Eriksson, L. Söder, B. Rawn, J. C. Boemer " Coordinated Active Power-Dependent Voltage Regulation in Distribution Grids With PV Systems" Accepted for publication in the *IEEE Transaction on Power Delivery*.

[6]"Studie zur Ermittlung der Technischen Mindesterzeugung des Konventionellen Kraftwerksparks zur Gewährleistung der Systemstabilität in den Deutschen Übertragungsnetzen bei Hoher Einspeisung aus Erneuerbaren Energien," Tech. Rep. Studie im Auftrag der deutschen Übertragungsnetzbetreiber, 2012.

[7] VDE "Power generation systems connected to the low/voltage distribution network," in *VDE application rule VDE-AR-N 4105:2011-08*, 2011.

[8] H. Saadat*, Power System Analysis*, 3rd ed. Alexandria, VA, USA: PSA, 2010.

[9] CENELEC, "Voltage characteristics of electricity supplied by public distribution networks, " Brussels, Belgium, EN 50160.

[10] J. Pillai, P. Thogersen, J. Moller, and B. Bak-Jensen, "Integration of electric vehicles in low voltage danish distribution grids," in Proc. IEEE Power Energy Soc. Gen. Meeting, 2012, pp. 1–8.

P-VI

Multi-objective coordinated droop-based voltage regulation in distribution grids with PV systems

Renewable Energy 71 (2014) 315–323

Contents lists available at ScienceDirect

Renewable Energy

journal homepage: www.elsevier.com/locate/renene

Multi-objective coordinated droop-based voltage regulation in distribution grids with PV systems

Afshin Samadi [a, *], Ebrahim Shayesteh [a], Robert Eriksson [a], Barry Rawn [b], Lennart Söder [a]

[a] Department of Electric Power Systems, KTH Royal Institute of Technology, Teknikringen 33, 10044 Stockholm, Sweden
[b] Department of Electrical Engineering (ESAT/ELECTA), University of Leuven (KU Leuven), Leuven, Belgium

ARTICLE INFO

Article history:
Received 10 September 2013
Accepted 20 May 2014
Available online 12 June 2014

Keywords:
Photovoltaic
Reactive power control
Droop control
German grid codes

ABSTRACT

High penetrations of photovoltaic (PV) systems in distribution grids have caused new challenges such as reverse power flow and voltage rise. Reactive power contribution by PV systems has been proposed by grid codes and literature as one of the remedies for voltage profile violation. Recent German Grid Codes (GGC), for instance, introduce a standard active power dependent reactive power characteristic, $Q(P)$, for inverter-coupled distributed generators. Nevertheless, the GGC recommends a voltage dependent reactive power characteristic $Q(V)$ for the near future, recognizing that the $Q(P)$ characteristic cannot explicitly address voltage limits. This study utilizes the voltage sensitivity matrix and quasi-static analysis in order to develop a coordinated $Q(V)$ characteristic for each PV system along a radial feeder using only the local measurement and drooping technique concepts. The aim of this paper is using a multi-objective design to adjust the parameters of the $Q(V)$ characteristic in the proposed droop-based voltage regulation in order to minimize the reactive power consumption and line losses. On the other hand, it is also possible to adjust the parameters in order to reach equal reactive power sharing among all PV systems. A radial test distribution grid, which consist of five PV systems, is used to calculate power flow and, in turn, the voltage sensitivity matrix. The comparison of results demonstrates that both approaches in the proposed droop-based voltage regulation can successfully regulate the voltage to the steady-state limit. Moreover, it is shown that the profile of reactive power consumption and line losses are considerably reduced by the multi-objective design.

1. Introduction

Long term supporting schemes for photovoltaic (PV) system installation have accommodated large numbers of PV systems within load pockets in distribution grids [1–4]. In Germany, for instance, there are currently more than 29 GW installed PV systems, of which 80% have been connected to low voltage grids [5,6]. Grid-parity (defined as the moment when the cost of electricity generated by PV is competitive with the retail price) has already been met in some residential regions owing to the sharp drop in costs of PV system manufacturing, especially PV panel technologies [1,3,7–9]. Therefore, PV system integration without the feed-in tariff support mechanism is now more likely to be attractive in a wide range of countries and markets. For instance, Italy has recently boosted its PV installed capacity to 17 GW and holds the second big market in Europe. China has also set a new target of 50 GW by 2020 [6].

Large numbers of PV system installations in distribution grids have come along with new technical challenges, such as voltage rise due to reverse power flow during light load and high PV generation conditions [3,4,10–15]. Uneven distribution of PV systems within the network has led to different regional penetration levels and has accelerated the technical challenges. Some regions in Germany, for example, have already encountered high local penetration of more than 200 kW/km^2 compared to the national average, which is 39 kW/km^2 [11,16]. Hence, remedial actions in PV system performance and integration must be taken into consideration.

The most common proposed remedy to mitigate the imposed voltage rise challenge and in the mean time increasing the hosting capacity without grid reinforcement is reactive power contribution by PV systems [11,14,17–21]. The recent German Grid Codes (GGC) also require reactive power contribution [22]. Normally due to large R/X ratios in low voltage (LV) grids, the reactive power variation has

* Corresponding author. Tel.: +46 76 206 11 54; fax: +46 8 790 6510.
E-mail addresses: afshins@kth.se, afshin.samadi@gmail.com (A. Samadi).

http://dx.doi.org/10.1016/j.renene.2014.05.046
0960-1481/

less effect on voltage regulation in comparison to the active power variation [17,23]. Nevertheless, from an economic point of view, the voltage profile regulation via reactive power is to be preferred over active power curtailment [11]. Reactive power control to support the voltage profile can be performed via different ways such as: constant power factor, active power dependent reactive power regulation $Q(P)$ and voltage dependent reactive power regulation $Q(V)$ [14,19–22,24,25]. Constant power factor can cause unnecessary line losses and reactive power consumption since it always contributes reactive power even in occasions when there is no voltage violation. Considering high penetration of PV systems, unnecessary reactive power consumption firstly increases the line losses as well as the congestion possibility and secondly may jeopardize the stability of power system in the case of contingency in conventional power plants supplying reactive power [26]. Therefore, the GGC proposes a standard $Q(P)$ characteristic for inverter-based distributed generation (DG) units like PV systems to reduce the reactive power consumption and line losses in which basically power factor varies dynamically based on the feed-in active power variation of the DG. Nevertheless, the GGC admits that the active power dependent method cannot explicitly address voltage limits and, thus, recommends network voltage dependent reactive power regulation methods, $Q(V)$, in the near future. Nevertheless, the GGC does not propose any specific $Q(V)$ characteristic. A grid impedance-adaptive $Q(V)$ approach has been proposed in Ref. [27] that requires the PV inverter to measure the grid impedance. In the case of multiple PV systems, the lack of a synchronized injection signal contributes to a low accuracy of impedance measuring [28,29] and the performance of the $Q(V)$ can negatively be affected. It was shown in Ref. [30] that for different LV grid classes a set of static parameters can be found by trial and error for grid impedance based $Q(V)$ characteristic to get sub-optimal but still acceptable performance. An improved $Q(V)$ algorithm is proposed in Refs. [4,31]; however, it needs a communication infrastructure to transmit all nodal information to a centralized controller in order to dispatch the minimum reactive power among PV systems. Investing for a communication infrastructure may be costly and there may be reliability challenges, so there is a need of an alternative approach.

There is a need to develop $Q(V)$ characteristics that are based on local information, but still take account of the system's structure and dependencies, and minimize reactive power consumption and line losses. Information about the effects of a local injection on power flow are described by the voltage sensitivity matrix. The voltage sensitivity matrix has been widely employed to compare impacts of active power curtailment and reactive power support through PV systems on the voltage profile in low voltage grids [23], to define coordinated droop factors in the active power curtailment of PV systems [13], to demonstrate the voltage control interaction among PV systems using control theories [32], and to eliminate the voltage variation at a target node due to the operation of a wind turbine in a microgrid via reactive power support [33]. The droop control concept has been primarily utilized in power systems with multiple generators and converters to droop frequency of each source with its delivered active power in order to share the load among them [34,35]. However, it can also be employed to share the reactive power by drooping the voltage.

The contribution of this paper is utilizing the voltage sensitivity matrix and the droop control concept to systematically coordinate and optimize the $Q(V)$ characteristic of each PV system in a radial grid using only local measurements in order to regulate the voltage profile under the upper steady-state voltage limit. A multi-objective design is taken into consideration to optimally adjust the settings of individual droop-based $Q(V)$ characteristics of PV systems such that the reactive power consumption profile and line losses profile are minimized. It is shown that the proposed droop-based voltage (DBV) regulation characteristic can be adjusted for equal reactive power sharing to equally treat owners of PV household systems if there is any associated reactive power penalty imposed by distribution grid operators. Nevertheless, it can considerably lead to sub-optimal operation from reactive power consumption and line losses perspectives.

The results demonstrate that the proposed DBV method can successfully regulate the voltage under the upper steady-state voltage limit. Moreover, using the optimization can considerably reduce the profiles of reactive power consumption as well as line losses, though it leads to an uneven reactive power distribution among PV systems.

The problem setup is explained in Section 2. Formulation of droop-based voltage regulation is given in Section 3. The system under study and simulation platform is introduced in Section 4. Section 5 and Section 6 contain results and conclusions.

2. Problem setup

Germany, as the pioneer of integrating PV systems into LV grids, has experienced variety of technical challenges such as overvoltage and has been trying to update its standard for DG connection to LV grids. The background and state-of-the-art of the recent GGC regarding voltage regulation, and their associated challenges, as well as the principle of a drooping technique as a remedy for voltage regulation are now discussed.

2.1. German grid codes

Analogous to high voltage grids, power generation systems in LV grids must contribute to static voltage stability during their normal operation in the future [22]. The GGC comply with the limit values of voltage quality specified by DIN EN 50160 [36]. According to the DIN EN 50160, the allowable voltage range in LV grids is between 90% and 110% of the nominal voltage [36]. According to the GGC, within this voltage tolerance band, DG units that are larger than 13.8 kVA and delivering at least 20% of their rated power, are permitted to freely change their power factor within the hatched sector represented in Fig. 1, between 0.9 under-excited and over-excited. For DG units smaller than 13.8 kVA but still bigger than 3.68 kVA, the power factor range is 0.95 [22].

Though the reactive power control can support the voltage and augment the integration of DG units into LV grids, it comes along with a considerable active power loss in LV grids. Hence, the GGC proposes a standard $Q(P)$ characteristic curve represented in Fig. 2 to minimize the line losses, where P and P_{max} represent the feed-in and the maximum active power of the generator, respectively [22]. The standard $Q(P)$ characteristic is only applicable to inverter-based

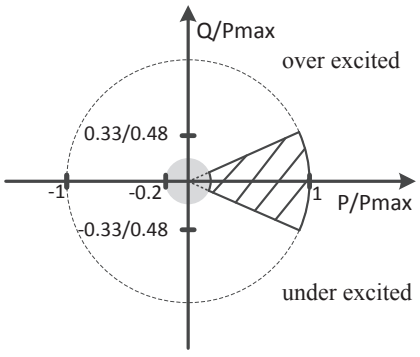

Fig. 1. Reactive power operation area for a generation unit connected to LV grids.

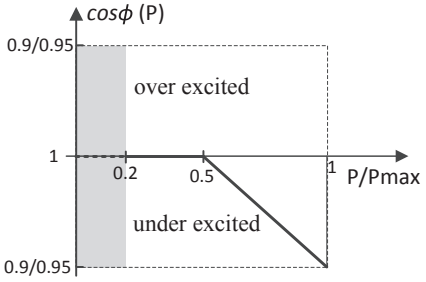

Fig. 2. Standard characteristic curve for cosφ (P).

variable generation units such as PV systems. The objective of the standard $Q(P)$ characteristic is requiring the generation unit to operate in an under-excited mode when the feed-in active power passes over a threshold of 50% of P_{max} in order to mitigate the related voltage rise. Upon a change in active power, the generation unit should provide the required reactive power based on the set-point on the characteristic curve within 10 s [22], which can be fulfilled by adjusting the band-width of the controller.

The $Q(P)$ method functions irrespective of the voltage and cannot explicitly address voltage regulation. The GGC, therefore, recommends using network voltage dependent methods in the near future scenarios such as $Q(V)$ characteristics known in high voltage (HV) grids. Nevertheless, the GGC does not introduce any specific $Q(V)$ characteristic.

2.2. Drooping technique background

Droop control is a well-known concept in conventional power systems used primarily for the load sharing among multiple generation units [34,35]. In this method, the frequency of each generation unit is allowed to droop in accordance with its delivered active power in order to share the system load. Analogous with the frequency droop control, drooping voltage magnitude via reactive power can provide the possibility of sharing reactive power among generation units. Power flow concept between two generation sources can basically demonstrate the theory of load and reactive power sharing methods. For instance, active and reactive power flow between two voltage sources, V_1 and V_2, can be derived as follows:

$$P = V_1 \frac{R(V_1 - V_2\cos(\delta_1 - \delta_2)) + XV_2\sin(\delta_1 - \delta_2)}{R^2 + X^2} \tag{1}$$

$$Q = V_1 \frac{X(V_1 - V_2\cos(\delta_1 - \delta_2)) - RV_2\sin(\delta_1 - \delta_2)}{R^2 + X^2} \tag{2}$$

Assuming that the resistance is negligible, which is the case in HV grids, and the difference between δ_1 and δ_2 is small, one can easily see that active and reactive power are predominately controlled by power angle, which in turn related to the frequency, and voltage magnitude, respectively. In LV feeders, however, the R/X ratios are generally large and thus the reactance term (X) becomes much smaller than resistance. By doing so, the voltage magnitude and angle in LV grids are mainly affected by active power and reactive power, respectively. Nevertheless [17], shows the conventional droop approaches in interconnected HV systems can be applied in the same manner in LV grids. However, with regard to the line losses and the inverter loading, voltage regulation through reactive power in LV grids may be less effective for feeders with high R/X ratios. Therefore, it is necessary to develop a method to be able to maximize the reactive power consumption required for voltage support.

3. Formulation of DBV regulation

In the DBV regulation method, the local voltage of the connection point of a PV system is directly employed as an input to calculate the required local reactive power to regulate the voltage. Therefore, the consumption of reactive power can be explicitly managed by severity of the voltage violation. Therefore, using the $Q(V)$ method can prevent unnecessary reactive power consumption in contrast to $Q(P)$ method, which employs the delivered power of the generation unit as an input.

In the DBV method, the general relation between reactive power of a PV system and the local grid voltage is defined as follows:

$$Q = \begin{cases} m(V - V_{th}) & V > V_{th} \\ 0 & V < V_{th} \end{cases} \tag{3}$$

where m is the slope factor (kVar/V) and V_{th} is the voltage threshold above which the PV system must absorb reactive power to mitigate the voltage. Therefore, the DBV characteristic has two parameters that must be defined for each PV system.

Fig. 3 provides a general picture of the DBV characteristic. V_d is the drooped voltage at the critical operating point, which occurs for maximum net load/generation, and ΔQ is the required reactive power to push the critical voltage value back under the steady-state voltage limit. Thus, m can be calculated as follows:

$$m = \frac{\Delta Q}{V_d - V_{th}} \tag{4}$$

In the proposed DBV method, the voltage sensitivity matrix is employed to coordinate the slope factor and the voltage threshold of each PV system along a radial feeder by considering the maximum critical voltage deviation at the last-bus on the feeder. This worst case deviation occurs for the maximum net load/generation point. The maximum voltage deviation with respect to the upper steady-state voltage limit has to be cancelled, hence, the ΔQ required in (4) is computed using the voltage sensitivity matrix computed at the maximum net load/generation operating point.

3.1. Sensitivity analysis

The concept of the voltage sensitivity matrix and the loss sensitivity matrix are now examined more closely to support design of the characteristic and minimization of losses.

3.1.1. Voltage sensitivity matrix

The voltage sensitivity matrix is a measure to quantify the sensitivity of voltage magnitudes ($|V|$) and angles (δ) with respect to injected active and reactive power. The sensitivity matrix is obtained through partial derivative of power flow equations, $g(|V|,\delta)$, as follows [37]:

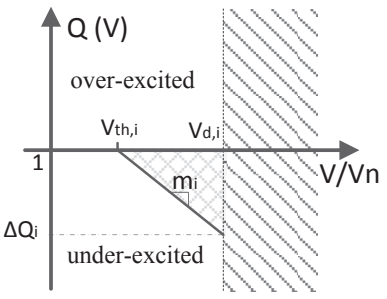

Fig. 3. Characteristic curve of reactive power droop with voltage level.

$$\begin{bmatrix}\Delta\delta\\ \Delta|V|\end{bmatrix}=\begin{bmatrix}\frac{\partial g_P(\delta,|V|)}{\partial\delta} & \frac{\partial g_P(\delta,|V|)}{\partial|V|}\\ \frac{\partial g_Q(\delta,|V|)}{\partial\delta} & \frac{\partial g_Q(\delta,|V|)}{\partial|V|}\end{bmatrix}^{-1}\begin{bmatrix}\Delta P\\ \Delta Q\end{bmatrix}=\underbrace{\begin{bmatrix}S_P^{\delta} & S_Q^{\delta}\\ S_P^{|V|} & S_Q^{|V|}\end{bmatrix}}_{S_V}\begin{bmatrix}\Delta P\\ \Delta Q\end{bmatrix} \tag{5}$$

The voltage sensitivity matrix consists of four sub-matrices that contain the partial derivatives of bus voltage magnitude and angle with respect to active and reactive power. Due to the importance of the voltage magnitude regulation by variation of active and reactive power, the sub matrices that are related to variation of voltage magnitude, $S_P^{|V|}$ and $S_Q^{|V|}$, are of more interest and concern in this study. Each element of these sub matrices is interpreted as the variation that may happen in a voltage at bus i if the active power (or reactive power) at bus j changed 1 p.u.

3.1.2. Loss sensitivity analysis

Based on power flow equations of a grid [37], total active loss of all lines, P_L, can be determined as follows:

$$P_L=\sum_{i=1}^{n}V_i\sum_{\substack{j=1\\ j\neq i}}^{n}g_{ij}\left[V_i-V_j\cos(\delta_{ij})\right] \tag{6}$$

where g_{ij} and δ_{ij} are the conductance of the line and the voltage angle difference between bus i and j, respectively.

Total line losses and power flow equations are function of voltage magnitude and angle. Therefore, the sensitivity coefficients of P_L with respect to active and reactive power at bus i can be derived as follows:

$$\begin{aligned}\frac{dP_L}{dP_i}&=\sum_{j=1}^{n}\frac{\partial P_L}{\partial\delta_j}\frac{\partial\delta_j}{\partial P_i}+\sum_{j=1}^{n}\frac{\partial P_L}{\partial|V_j|}\frac{\partial|V_j|}{\partial P_i}\\ \frac{dP_L}{dQ_i}&=\sum_{j=1}^{n}\frac{\partial P_L}{\partial\delta_j}\frac{\partial\delta_j}{\partial Q_i}+\sum_{j=1}^{n}\frac{\partial P_L}{\partial|V_j|}\frac{\partial|V_j|}{\partial Q_i}\end{aligned} \tag{7}$$

Eq. (7) can be rearranged in a matrix form with the help of the voltage sensitivity matrix, S_V, as follows:

$$\begin{bmatrix}\frac{dP_L}{dP}\\ \frac{dP_L}{dQ}\end{bmatrix}=S_V^T\begin{bmatrix}\frac{\partial P_L}{\partial\delta}\\ \frac{\partial P_L}{\partial|V|}\end{bmatrix}=\begin{bmatrix}S_P^L\\ S_Q^L\end{bmatrix} \tag{8}$$

where $\partial P_L/\partial\delta$ and $\partial P_L/\partial|V|$ can also be derived from (6).

3.2. Computing the parameters of Q(V) characteristic

The maximum voltage deviation from the upper steady-state voltage limit occurs at the last bus and at the presence of the critical operating point, based on (5) it is possible to regulate reactive power of each PV system at each node in such a way to compensate the last-bus voltage deviation. The maximum voltage deviation at the last bus is

$$\Delta V_{\max,n}=(V_{\max,n}-\overline{V}) \tag{9}$$

where n represents the last-bus number, $V_{\max,n}$ is the maximum last-bus voltage that occurs at the critical operating point and $\overline{V}$ is the steady-state upper voltage limit in LV grids. The overvoltage $\Delta V_{\max,n}$ is due to the active power injections corresponding to the left term within brackets of (5). The required under-excited reactive power of each PV system at each node to compensate the overvoltage must comply with the following equality

$$\Delta V_{\max,n}=-\sum_{i=1}^{n}\left(S_{Qn,i}^{|V|}\Delta Q_i\right) \tag{10}$$

The negative sign in (10) is due to the under-excited nature of the required reactive power that is basically negative in the defined $Q(V)$ plane. Thus, the negative sign is used to match both sides of the equivalence in (10).

The challenge is how to associate the ΔQ with individual PV systems in order to properly distribute the required reactive power of each PV system along the feeder.

Obviously, the drooped voltage of the last-bus, $V_{d,n}$, must be equal to $\overline{V}$; once the required reactive power of each PV is known, the drooped voltage for the rest of buses can be calculated by the following equation

$$V_{d,i}=V_{\mathrm{cri},i}-\sum_{j=1}^{n}\left(S_{Q,ij}^{|V|}\Delta Q_j\right) \tag{11}$$

where $V_{\mathrm{cri},i}$ is the critical voltage at the bus i at the presence of the critical operating point. As can be seen in Fig. 3, the $V_{d,i}$ should be higher than the corresponding $V_{\mathrm{th},i}$. Thus, if the calculated $V_{d,i}$ is lower, the corresponding ΔQ_i in (10) must be set to zero because the corresponding PV should not contribute reactive power according to (3) and the other injections (ΔQ_j, $i\neq j$) must be recalculated.

By having the value of the voltage threshold and the required reactive power of each PV system, the corresponding slope factor is calculated based on (4).

The voltage threshold and ΔQ of each PV system is determined through two approaches, namely multi-objective DBV design and equal reactive power sharing, that will be explained in the following sections.

3.3. Approach I: multi-objective DBV design

The slope factor and the voltage threshold of the DBV characteristic for each PV system can be determined through an optimization that will be explained in the following subsections.

3.3.1. Objective function

In the proposed multi-objective approach, three different target objectives are minimized, namely maximum reactive power consumption, maximum line losses caused by reactive power, and overall profile of reactive power consumption. The general form of the proposed objective function is:

$$\max_{(\Delta Q,V_{\mathrm{th}})}\begin{pmatrix}w_1\times f_1(\Delta Q)+\\ w_2\times f_2(\Delta Q,V_{\mathrm{th}})-\\ w_3\times f_3(\Delta Q)\end{pmatrix} \tag{12}$$

where target objectives are weighted by factors w_1-w_3.

- Target Objective 1:

The required reactive power for PV systems can be chosen in such a way to minimize the sum of individual reactive power consumption of each PV system at the critical operating point in (10). Thus, the first objective target is formulated as follows:

$$f_1 = \sum_{i=1}^{n} \Delta Q_i \tag{13}$$

Since the nature of under-excited reactive power is assumed to be negative, the objective target is considered by positive sign in the objective function (12).

- Target Objective 2:

The first objective target only minimizes the total reactive power consumption at the critical operating point. However, since the system's operating points vary, it is required to minimize the reactive power usage over the range of voltages experienced, represented by the hatched triangle in Fig. 3. The hatched area is related to the reactive power consumption, but not exactly since the probability of different voltage levels is not constant. Nevertheless, minimizing the sum of hatched areas of all $Q(V)$ characteristics can reduce the total reactive power consumption. Therefore, the voltage threshold in the DBV characteristic can be adjusted in such a way to minimize the reactive power profile over the voltage profile through the following objective target:

$$f_2 = \sum_{i=1}^{n} \Delta Q_i (V_{d,i} - V_{\mathrm{th},i}) \tag{14}$$

Similar to the previous objective target, due to the negative nature of under-excited reactive power, this objective target is also considered with positive sign in (12).

- Target Objective 3:

Since consumption profile of reactive power is minimized in (14), the profile of line losses is, in turn, supposed to be minimized. Nevertheless, the active power loss caused by reactive power at the critical point can also be minimized. According to (7), the variation of total line losses caused by reactive power variation is:

$$\Delta P_L = \sum_{i=1}^{n} S_{Qi}^{L} \Delta Q_i \tag{15}$$

Therefore, in order to minimize the line losses one should minimize the right hand side of (15).

$$f_3 = \sum_{i=1}^{n} S_{Qi}^{L} \Delta Q_i \tag{16}$$

Since both multiplying terms in (16) are negative, this objective target must be considered with negative sign in (12).

3.3.2. Optimization variables

In the proposed optimization, the decision variables are reactive power consumption, ΔQ, and threshold voltage, V_{th}, at the critical operating point.

3.3.3. Constraints

In order to find a proper, feasible set of candidate solutions following constraints must be fulfilled:

- Constraint 1:

The main goal of the DBV method is to eliminate the maximum overvoltage at the worst case operating point; hence, the set of candidate reactive power values has to fulfil this criterion by satisfying the equality in (10).

- Constraint 2:

Reactive power consumption imposes extra loading on PV inverters as well as the grid transformers. In this regard, as also mentioned earlier, the GGC limit the amount of reactive power to a specific value based on the size of PV systems. Therefore, reactive power of each PV system should stay within the following band

$$-P_{\max,i}\sqrt{\left(\frac{1}{cos^2\phi_{\max,i}} - 1\right)} \le \Delta Q_i \le 0 \tag{17}$$

where $P_{\max,i}$ and $cos\phi_{\max,i}$ are the maximum generation power and the minimum allowable power factor of the PV system at the bus i.

- Constraint 3:

The analysis of unit characteristics is based on the assumption that they contribute appropriately to limit the voltage of the last bus, which is also assumed to be highest. This need not in general be true but always occurs in the worst case of light load and full PV production conditions. In this case voltages will increase monotonically along a radial feeder. Hence to preserve the analysis intended in (10), the voltage thresholds

$$1 < V_{\mathrm{th},1} < V_{\mathrm{th},2} < \ldots < V_{\mathrm{th},n} < V_{d,n} = \overline{V} \tag{18}$$

- Constraint 4:

Each PV system on the feeder can contribute reactive power if and only if its corresponding drooped voltage in (11) drops below its corresponding voltage threshold. Therefore, according to the negative nature of under-excited reactive power, $\Delta Q_i \le 0$, the following constraint must be satisfied for all PV systems:

$$\Delta Q_i (V_{d,i} - V_{\mathrm{th},i}) \le 0 \tag{19}$$

which is met when first there is a need for under-exited reactive power contribution (non-positive ΔQ_i) at the i–th PV system, and second the drooped voltage of the same PV system is greater than the corresponding voltage threshold.

- Constraint 5:

The slope factor in the $Q(V)$ characteristic shown in Fig. 3 is a dependent variable, which is a byproduct of the decision variables and the drooped voltage derived in (4). Since one does not want to have rapid changes in reactive power support just because of a small change in load and/or solar irradiance, the slope factor has to be limited. This limit is defined by use of the sensitivities. According to Fig. 3, for a voltage variation at the bus i above the voltage threshold, the required reactive power variation at the same bus is given by

$$\Delta Q_i = m_i \Delta V_i \tag{20}$$

According to (5), the relation between the voltage variation at the bus i and the reactive power variation at the same bus can be related by

$$\Delta V_i \geq -S_{Qi,i}^{|V|}\Delta Q_i \tag{21}$$

By substituting (20) in (21), one can get

$$m_i \geq -\frac{1}{S_{Qi,i}^{|V|}} \tag{22}$$

3.4. Approach II: Equal reactive power sharing

The general tendency in the DBV method is that PV systems at the beginning of the feeder contribute less reactive power for the voltage regulation than PV systems at the end. Therefore, one possible option is to set ΔQ_i in (10) equal to each other in order to take the advantage of all PV systems in the grid and, moreover, to prevent disparity between PV owners. Then, the equal required reactive power, $\Delta Q_i = q$, can be easily calculated from (10). Nevertheless, as it will be demonstrated later, this causes more overall reactive power consumption and line losses.

Apart from the ΔQ setting in the DBV characteristics, the voltage thresholds must also be adjusted to provide the possibility of equal reactive power sharing among all PV systems. Therefore, it is important to find a set of voltage thresholds that can guarantee the participation of the nearer upstream PV systems on the feeder. Hence, since the first PV system on the feeder has the least participation tendency, the maximum possible voltage threshold of the first PV system that allows its participation is considered as a criterion to find the rest of voltage thresholds. The maximum voltage threshold of the first PV system coincides with its corresponding minimum slope factor. Therefore, the maximum voltage threshold of the first PV system on the feeder can easily be calculated as follows

$$V_{\mathrm{th},1} = V_{d,1} - \frac{q}{m_{\mathrm{min}1}} \tag{23}$$

In order to determine the rest of voltage thresholds, the net load/generation of all PV systems is monotonically and simultaneously increased and in the mean time the first-bus voltage is tracked; once the maximum voltage threshold appears at the first bus, the voltages of other buses represent the rest of voltage thresholds.

4. Platform of the simulation

Fig. 4 depicts the radial test grid used in this study, which consists of five buses in an LV feeder connected through a step-down transformer to a medium voltage grid. In this study the load demand is assumed to be negligible compared to PV production. The parameters of the test radial grid have been given in Table 1 [38].

Since voltage regulation via DG units should function within 10 s, a quasi-static analysis is appropriate and employed in this study using MATLAB R2010b. Moreover, GAMS23.6 is employed for solving the optimization problem (12), assuming equal weights for all target objectives, subjected to constraints 1–5. Assuming no load condition, Fig. 5 depicts the voltage profile of the feeder concerning different net generations with the unity power factor. It is evident from Fig. 5 that when all PV systems deliver full power at unity power factor, voltage of two last-buses is above the upper steady-state voltage limit, which is considered 110% of the nominal voltage according to the EN DIN 50160 [36].

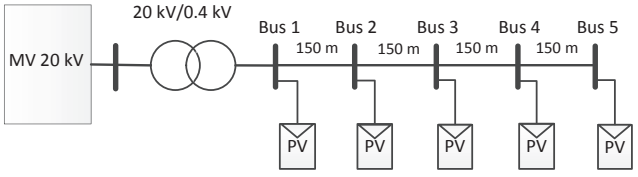

Fig. 4. Test distribution grid. All PV systems have a rating of 30 kW.

Table 1
Radial test grid parameters 38.

Grid impedance	2.828 + 2.828i Ω
Transformer impedance	0.0191 + 0.0351i Ω
Line impedance per km	0.346 + 0.0754i Ω/km

5. Results

The nominal power of each PV system is 30 kW and, therefore, according to the GGC power factor range, the reactive power is limited to 14.5 kVar. The voltage sensitivity matrix is calculated at the critical operating point, which here is 150 kW at the unity power factor (the maximum total net load/generation). The sensitivity coefficient of total line losses for each bus is calculated at the presence of the maximum total net load/generation and the maximum under-excited reactive power at the corresponding bus. As Table 2 presents, the absolute value of calculated sensitivity coefficients of total lines losses are increased farther downstream the feeder that means the reactive power consumption by PV systems located at the end of the feeder causes more line losses, which would be expected from the radial grid topology.

5.1. DBV characteristics parameters

Table 3 shows ΔQ, voltage threshold, drooped voltage and slope factor of the DBV characteristic for the both multi-objective approach and equal reactive power sharing approach. Fig. 6 demonstrates the $Q(V)$ characteristic of PV5 that results from each approach.

5.1.1. ΔQ

In the case of the equal reactive power sharing, all the PV systems participate and have the similar ΔQ. However, in the case of multi-objective approach, the last three PV systems on the feeder fully contribute reactive power, PV2 contributes only 43% of its permissible reactive power capacity, and PV1 does not contribute at

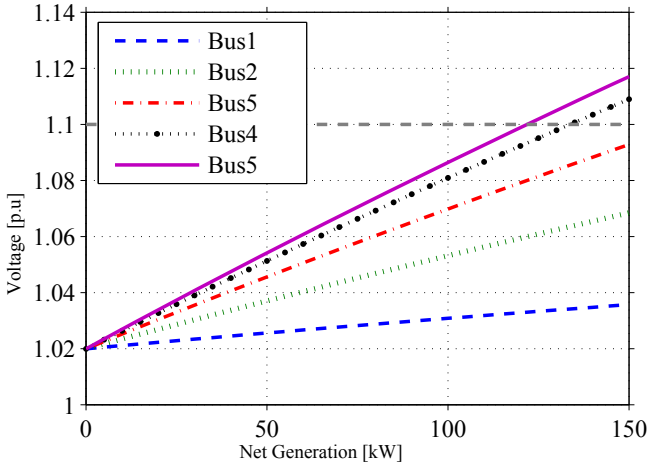

Fig. 5. Voltage profile of the LV feeder without reactive power support.

Table 2
Sensitivity coefficients of P_L.

S^L_{Q1}	S^L_{Q2}	S^L_{Q3}	S^L_{Q4}	S^L_{Q5}
−0.009	−0.019	−0.027	−0.035	−0.041

all. Based on the $S^V_{Qn,i}$ coefficients in (10), reactive power variations at nodes located farther downstream on the feeder have more effect on the last-bus voltage regulation [32] and, therefore, fully utilizing PV systems farther on the feeder can decrease the total reactive power consumption. Nevertheless, objective 1 in a compromise with two other objectives guarantees the best candidate of ΔQ to reduce not only maximum total reactive power consumption at the critical operating point but also the total line losses at the same point as well as the overall reactive power consumption profile.

5.1.2. Voltage threshold

Equally reactive power sharing among PV systems requires notably lower voltage thresholds as represented in Table 3. In contrast, in the case of the optimized approach, the target objective 2 to optimize the reactive power consumption profile results in a shift of the voltage thresholds towards the drooped voltages (6 and 7th rows of Table 3). A narrower activation range of the DBV characteristic results, as can be seen in Fig. 6.

5.2. Voltage profile

The regulated voltages of the first and the last buses on the feeder for the both multi-objective approach and equal reactive power sharing approach are shown in Fig. 7. Both cases can regulate the voltage under the upper steady-state voltage limit, and this demonstrates the effectiveness of the proposed DBV method. However Fig. 7 shows that in the case of the equal reactive power sharing approach, the PV systems have to commence reactive power consumption at a small fraction of the net load/generation, which implies more reactive power consumption.

5.3. Reactive power consumption

Figs. 8 and 9 show the individual reactive power consumption of each PV system along the feeder for the equal reactive power sharing approach and the optimized approach, respectively. As it was expected, all PV systems approximately consume the same amount of reactive power in the equal reactive power sharing approach. In comparison, the pattern of reactive power distribution is uneven in the case of multi-objective approach in a way that follows logically for this case from its target objectives. From overall reactive power consumption perspective, it is most effective to use reactive power from end of feeder. The optimization should maximize contributions starting from the end of the feeder. It can also be seen in Table 3 that the last three PV systems have the same

Table 3
DBV parameters for each PV system.

Method	Par. [p.u.]	PV_1	PV_2	PV_3	PV_4	PV_5
Equal sharing	ΔQ	0.384	0.384	0.384	0.384	0.384
	V_{th}	1.022	1.026	1.029	1.031	1.032
	V_d	1.024	1.054	1.077	1.092	1.1
	m	166.2	13.4	7.9	6.2	5.6
Multi objective	ΔQ	0	0.207	0.484	0.484	0.484
	V_{th}	1.023	1.054	1.073	1.087	1.094
	V_d	1.026	1.056	1.078	1.093	1.1
	m	0	130.2	107.6	91.7	79.4

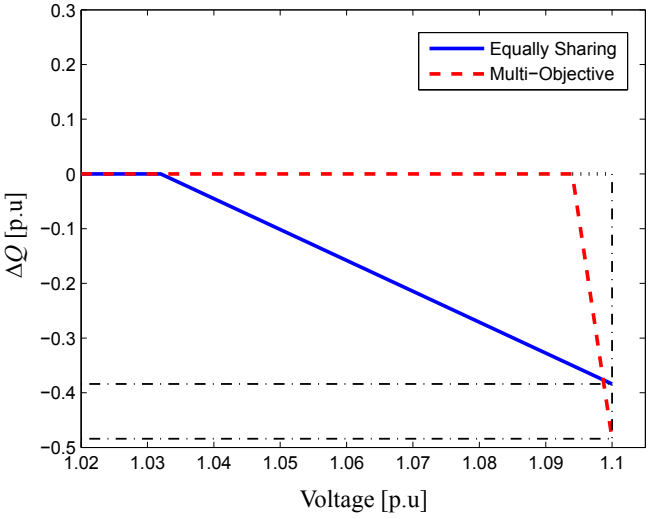

Fig. 6. DBV characteristic of PV5.

value of ΔQ limited to the power factor 0.9 at the maximum net load/generation point and the ΔQ for PV2 is a lesser value that is equal to the residual additional amount needed to provide enough reactive power from all units to cancel the last bus voltage deviation. It deserves mentioning that slight differences between final reactive power values in Table 3 and Fig. 9 are owing to the linearizing approximation in (5).

Fig. 10 illustrates the total reactive power consumption profile for the both approaches and as can be seen, the total consumption profile is significantly lower in the optimized approach. Moreover, it is obvious that the maximum reactive power consumption at the critical operating point is much lower in the case of the optimized approach. In fact, requiring all PV systems to equally contribute reactive power leads to the larger reactive power consumption profile. The first PV system on the feeder, in contrast to other PV systems, sees only the R/X ratio of the grid Thevenin impedance that is very different from the feeder R/X ratio. Therefore, requiring the first PV system to contribute same amount as other PV systems has especially worsened the reactive power consumption profile in the equal reactive power sharing approach, for almost no gain in voltage correction. The contribution of the first PV system could be

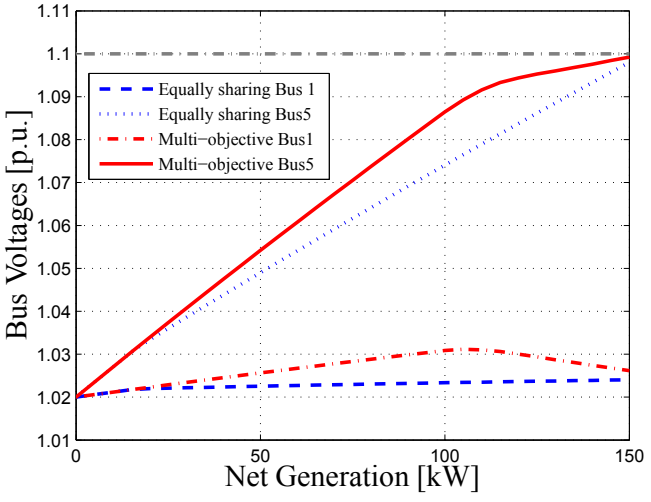

Fig. 7. First-bus and last-bus voltage profiles.

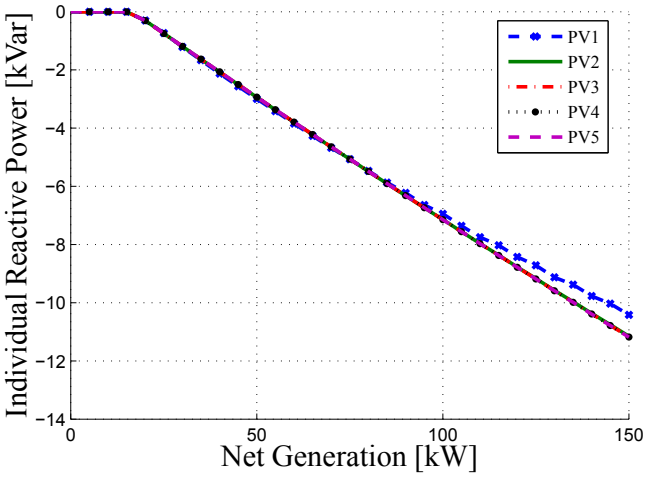

Fig. 8. Individual reactive power consumption by PV systems in the case of the equal reactive power sharing.

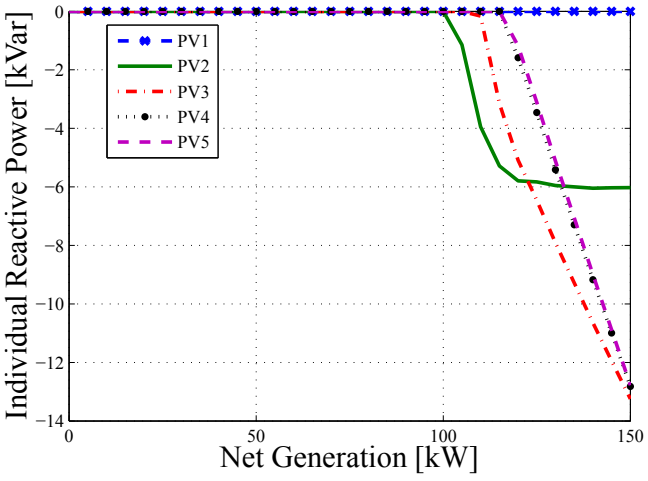

Fig. 9. Individual reactive power consumption by PV systems at the presence of the multi-objective approach.

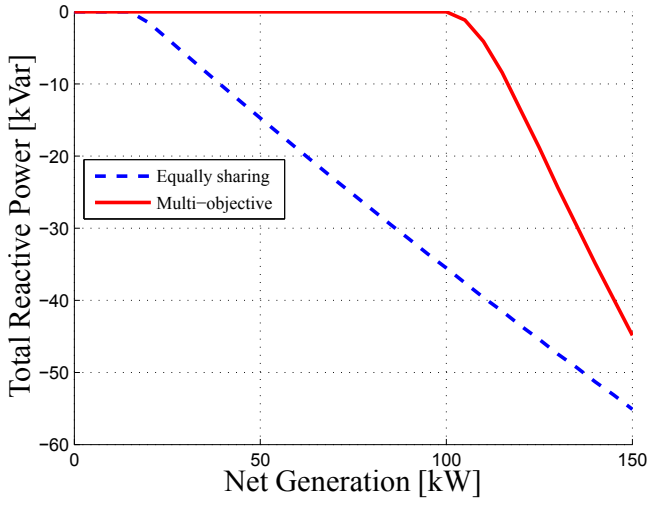

Fig. 10. Total reactive power consumption by PV systems.

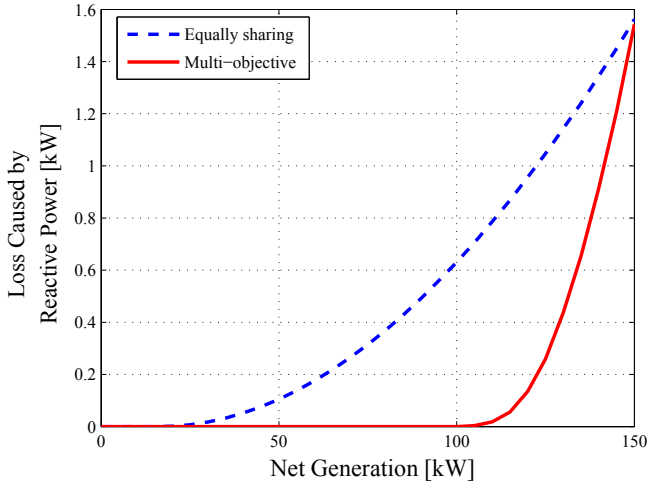

Fig. 11. Total line losses caused only by reactive power consumption through PV systems.

removed, significantly improving the reactive power consumption profile in the equal reactive power sharing approach. However, total reactive power consumption is still lower in the multi-objective approach, which also finds better combinations of V_{th} and ΔQ to not only reduce maximum reactive power consumption and line losses at the critical operating point but also decline the reactive power consumption profile.

5.4. Total line losses

Fig. 11 depicts the total line losses caused solely by reactive power flow for the both equal reactive power sharing and optimized approaches. The optimized approach decreases the overall reactive power consumption profile and consequently the line losses profile is supposed to decline, which is evident from Fig. 11. As mentioned earlier, coefficients of S_Q^L increase for farther buses downstream on the feeder. Therefore, on the one hand reactive power contribution by PV systems nearer upstream on the feeder can decrease the total line losses, but on the other hand, as explained earlier, using PV systems located farther downstream on the feeder reduces the maximum total reactive power consumption, which in turn can also decrease the losses. The objective 3 in a compromise with the objective 1 and represented constraints introduce a set of ΔQ to decline the total line losses and the maximum reactive power consumption.

6. Conclusion

This paper demonstrates that the features of the voltage sensitivity matrix in association with a multi-objective design can be used to optimally coordinate characteristics of the droop-based voltage regulation among PV systems in the radial feeders. Each characteristic is specified by two main parameters, namely the voltage threshold and the slope factor, which are determined based on the voltage sensitivity analysis and the multi-objective approach in order to balance the individual reactive power distribution against total reactive power consumption and line losses. It was shown in the test case that a characteristic minimizing reactive power consumption and line losses has higher and narrower ranges of activation for each PV, and a large slope, with the effect that voltage deviations are compensated only when they approach the highest allowable value. At the other extreme, a characteristic that instead results in equal sharing by PVs was shown to require wider

activation ranges and lower gains, but to also incur the penalty of higher losses and reactive power consumption. If the narrow activation range is considered as a problem then possible extension is adding additional constraints on activation range and other parameters to accommodate practical issues. Moreover, in the future scenarios if consuming reactive power by household PV systems come along with the cost penalties, finding a mechanism to equally share the penalty of reactive power may be more efficient than equally distributing reactive power among household PV systems.

Acknowledgement

This project has been funded by SETS Erasmus Mundus Joint Doctorate. The authors would like to express their gratitude towards all partner institutions within the programme as well as the European Commission for their support.

References

[1] Bazilian M, Onyeji I, Liebreich M, MacGill I, Chase J, Shah J, et al. Re-considering the economics of photovoltaic power. Renew Energy 2013;53:329–38.
[2] Cherrington R, Goodship V, Longfield A, Kirwan K. The feed-in tariff in the UK: a case study focus on domestic photovoltaic systems. Renew Energy 2013;50:421–6.
[3] Pinto A, Zilles R. Reactive power excess charging in grid-connected PV systems in brazil. Renew Energy 2014;62:47–52.
[4] Cagnano A, Torelli F, Alfonzetti F, De Tuglie E. Can PV plants provide a reactive power ancillary service? a treat offered by an on-line controller. Renew Energy 2011;36:1047–52.
[5] Boemer JC, et al. Overview of German grid issues and retrofit of photovoltaic power plants in Germany for the prevention of frequency stability problems in abnormal system conditions of the ENTSO-E region continental Europe. In: 1st international workshop on integration of solar power into power systems, Aarhus, Denmark.
[6] Jaeger-Waldau A. PV status report 2012-research, solar cell production and market implementation of photovoltaics. Technical report. European Commission, DG Joint Research Center, Institute for Energy and Transport, Renew Energy Unit; 2012.
[7] Schwabe U, Jansson P. Utility-interconnected photovoltaic systems reaching grid parity in new jersey. In: IEEE power and energy society general meeting; 2010. pp. 1–5.
[8] Wohlgemuth JH, Cunningham DW, Clark RF, Posbic JP, Zahler JM, Garvison P, et al. Reaching grid parity using BP solar crystalline silicon technology. In: 33rd IEEE photovoltaic specialists conference. PVSC '08; 2008. pp. 1–4.
[9] Pérez D, Cervantes V, Báez MJ, González-Puelles J. PV grid parity monitor. Technical Report, ECLAREON; 2012.
[10] Tonkoski R, Lopes LA. Impact of active power curtailment on overvoltage prevention and energy production of PV inverters connected to low voltage residential feeders. Renew Energy 2011;36:3566–74.
[11] Stetz T, Marten F, Braun M. Improved low voltage grid-integration of photovoltaic systems in Germany. IEEE Trans Sustain Energy; 2012:1–9.
[12] Shayani R, de Oliveira M. Photovoltaic generation penetration limits in radial distribution systems. IEEE Trans Power Syst 2011;26:1625–31.
[13] Tonkoski R, Lopes L, El-Fouly T. Coordinated active power curtailment of grid connected PV inverters for overvoltage prevention. IEEE Trans Sustain Energy 2011;2:139–47.
[14] Demirok E, Casado Gonzalez P, Frederiksen K, Sera D, Rodriguez P, Teodorescu R. Local reactive power control methods for overvoltage prevention of distributed solar inverters in low-voltage grids. IEEE J Photovolt 2011;1:174–82.
[15] El Halabi N, GarcÃa-Gracia M, Borroy J, Villa J. Current phase comparison pilot scheme for distributed generation networks protection. Appl Energy 2011;88:4563–9.
[16] Saint-Drenan Yves-Marie, Bofinger S, Ernst B, Landgraf T, Rohrig K. Regional now casting of the solar power production with pv-plant measurements and satellite images. In: ISES SolarWorld Congress.
[17] Engler A, Soultanis N. Droop control in LV-grids. In: International conference on future power systems; 2005. p. 6.
[18] Braun M. Reactive power supply by distributed generators. In: IEEE power and energy society general meeting – conversion and delivery of electrical energy in the 21st century; 2008. pp. 1–8.
[19] Sulc P, Turitsyn K, Backhaus S, Chertkov M. Options for control of reactive power by distributed photovoltaic generators, arXiv:1008.0878. Proc IEEE 2010;99(6):1063–73. June 2011.
[20] Yazdani A, Di Fazio A, Ghoddami H, Russo M, Kazerani M, Jatskevich J, et al. Modeling guidelines and a benchmark for power system simulation studies of three-phase single-stage photovoltaic systems. IEEE Trans Power Deliv 2011;26:1247–64.
[21] Samadi A, Ghandhari M, Söder L. Reactive power dynamic assessment of a PV system in a distribution grid. Energy Procedia 2012;20:98–107.
[22] Power generation systems connected to the low/voltage distribution network. In: VDE application rule VDE-AR-N 4105:2011-08.
[23] Tonkoski R, Lopes L. Voltage regulation in radial distribution feeders with high penetration of photovoltaic. In: IEEE energy 2030 conference, 2008, ENERGY; 2008. pp. 1–7.
[24] Cagnano A, De Tuglie E, Liserre M, Mastromauro R. Online optimal reactive power control strategy of PV inverters. IEEE Trans Industrial Electron 2011;58:4549–58.
[25] Samadi A, Eriksson R, Soder L, Rawn B, Boemer J. Coordinated active power-dependent voltage regulation in distribution grids with PV systems. IEEE Trans Power Deliv Early; Access Online 2014.
[26] Technical Report Studie zur Ermittlung der technischen Mindesterzeugung des konventionellen Kraftwerksparks zur Gewährleistung der Systemstabilität in den deutschen Übertragungsnetzen bei hoher Einspeisung aus erneuerbaren Energien. Studie im Auftrag der deutschen Übertragungsnetzbetreiber; 2012.
[27] Kerber, Georg. Konzept für eine autonome blindleistungsregelung von umrichteranlagen; 2008.
[28] Timbus A, Teodorescu R, Blaabjerg F, Borup U. Online grid impedance measurement suitable for multiple PV inverters running in parallel. In: Twenty-first annual IEEE applied power electronics conference and exposition. APEC '06; 2006. p. 5.
[29] Balaguer I, Kim H-G, Peng F, Ortiz E. Survey of photovoltaic power systems islanding detection methods. In: 34th annual conference of IEEE industrial electronics. IECON 2008; 2008. pp. 2247–52.
[30] Kerber G, Witzmann R, Sappl H. Voltage limitation by autonomous reactive power control of grid connected photovoltaic inverters. In: Compatibility and power electronics. CPE '09; 2009. pp. 129–33.
[31] Craciun B-I, Man E, Muresan V, Sera D, Kerekes T, Teodorescu R. Improved voltage regulation strategies by PV inverters in LV rural networks. In: 3rd IEEE international symposium on power electronics for distributed generation systems (PEDG); 2012. pp. 775–81.
[32] Samadi A, Eriksson R, Söder L. Evaluation of reactive power support interactions among PV systems using sensitivity analysis. In: 2nd international workshop on integration of solar power into power systems, Lisbon, Portugal. p. 245–52.
[33] Aghatehrani R, Kavasseri R. Reactive power management of a DFIG wind system in microgrids based on voltage sensitivity analysis. IEEE Trans Sustain Energy 2011;2:451–8.
[34] Chandorkar M, Divan D, Adapa R. Control of parallel connected inverters in stand alone AC supply systems. IEEE Trans Industry Appl 1993;29:136–43.
[35] Marwali M, Jung J-W, Keyhani A. Control of distributed generation systems – part II: load sharing control. IEEE Trans Power Electron 2004;19:1551–61.
[36] Voltage characteristics of electricity supplied by public distribution systems. In: DIN EN 50160.
[37] Saadat H. Power system analysis. 3rd ed. PSA Publishing; 2010.
[38] Demirok E, Sera D, Teodorescu R, Rodriguez P, Borup U. Evaluation of the voltage support strategies for the low voltage grid connected PV generators. In: IEEE energy conversion congress and exposition (ECCE); 2010. pp. 710–7.

P-VII

Static Equivalent of Distribution Grids with High Penetration of PV Systems

Static Equivalent of Distribution Grids with High Penetration of PV Systems

Afshin Samadi, *Student Member, IEEE,* Lennart Söder, *Senior Member, IEEE,* Ebrahim Shayesteh, and Robert Eriksson, *Member, IEEE*

***Abstract*—High penetrations of PV systems within load pockets in distribution grids have changed pure consumers to prosumers. This can cause technical challenges in distribution and transmission grids such as overvoltage and reverse power flow. Embedding voltage support schemes into PVs such as standard $Cos\phi(P)$ characteristic proposed by the German Grid Codes, may cause more changes in the steady-state behavior of distribution grids and, in turn, the transmission side. Accordingly, it is important to properly model active distribution grids to analyze the system impacts of these changes, to plan and operate future smart power grids. However, due to the high dimension of distribution grids, considering a detailed distribution grid to study the transmission side or a fraction of the distribution grid, is either cumbersome or impractical. Therefore, it is required to develop a reasonable equivalent that can fairly capture the dominant behavior of the distribution grids. The aim of this paper is to use gray-box modeling concepts to develop a static equivalent of distribution grids comprising large number of PV systems embedded with voltage support schemes. In the proposed model, the PV systems are aggregated as a separate entity, and not as a negative load, which is traditionally done. The results demonstrate the superior quality of the proposed model compared to the model with PV systems as the negative load.**

***Index Terms*—Photovoltaic systems, load modeling, system identification, reactive power control.**

I. Introduction

LONG term supporting schemes for photovoltaic (PV) system installation have accommodated large numbers of PV systems within load pockets in distribution grids [1]–[5]. In Germany, for instance, there were more than 32 GW installed PV systems by the end of 2012, of which 70% have been connected to low voltage grids [1], [2]. Grid-parity (defined as the moment when the cost of electricity generated by PV is competitive with the retail price) has already been met in some residential regions owing to the sharp drop in costs of PV system manufacturing, especially PV panel technologies [1], [6], [7]. Therefore, PV system integration without the feed-in tariff support mechanism is now more likely to be attractive in a wide range of countries and markets. For instance, Italy has boosted its PV installed capacity to 17 GW and holds the second biggest market in Europe. China has also set a new target of 50 GW by 2020 [1].

Generally speaking, traditional power systems feed power via transmission lines to distribution grids, where the majority of power system loads are installed. In today's power system, this, however, may not be the case because the integration of distributed generations such as PV systems into distribution grids has resulted in pumping power to transmission lines in light load conditions. Therefore, a different response behavior of distribution grids in terms of active and reactive power variations versus voltage variations on the transmission side can be expected. Moreover, high penetration of PV systems into distribution grids can cause local problems such as overvoltage [2]–[5], [8]–[19]. Different remedies have been proposed in literature to cope with overvoltage such as grid reinforcement [2], [5]; on load tap changers for distribution transformers [5], [8], [9]; active power curtailment [5], [10], [11]; and reactive power control [5], [12]–[21]. Nevertheless, from an economic point of view, the voltage profile regulation via reactive power is more effective than other aforementioned remedies [5]. Voltage profile regulation based on reactive power can be performed through different ways [12]–[21]. Employing reactive power-based schemes to support voltage may even change more the power-voltage characteristics of distribution grids. Hence, with a rapid transformation of pure consumers to prosumers, reasonable modelling of active distribution grids plays an influential role in 1) analyzing the system impacts of this change, 2) planning, and 3) the secure operation of future smart power grids.

Normally, the dimension of distribution grids is large due to large number of sections, branches and load points in contrast to a power transmission system with generation and transmission lines [22]. The real size of a power transmission system can basically be quite big and, therefore, considering a detailed distribution grid to study the power transmission system is neither practical nor necessary. Running a power system simulation including a complex, detailed distribution grid is cumbersome and, hence, it is important to have a simple model that can encapsulate the general behavior of the complex distribution grid in order to facilitate the investigation of power systems. In other words, if the area of investigation is the higher-level power grid, considering the distribution grid with its all dimension is inefficient. Besides, even considering the whole dimension of the distribution grid to only study one part of it, is not appropriate. Hence, there is a need to find a simple equivalent of the distribution grid that still can provide reasonable precision.

Furthermore, distribution grids are normally owned and operated by distribution system operators (DSOs) as autonomous systems in which grid information such as loads, generators, and line specifications are usually considered commercially

Afshin Samadi, Lennart Söder and Ebrahim Shayesteh are with the Department of Electric Power Systems, KTH Royal Institute of Technology, Stockholm SE-10044, Sweden, e-mail:afshin.samadi@ee.kth.se.

Robert Eriksson is with the Department of Electrical Engineering, DTU Technical University of Denmark, 2800 Kgs. Lyngby, Denmark.

sensitive [23]. On the other hand, a power system is composed of several autonomous distribution and transmission systems owned by DSOs and transmission system operators (TSOs) that must collaborate together in order to operate in a secure, stable and cost effective manner. In this regard, grid operators need to share their grids information to ensure a desired operation of the power system. However, as discussed above, there are two main challenges associated with sharing distribution grids information: 1) huge volume of grid information size 2) commercially sensitive information. Consequently, a reasonable aggregation approach can be a great asset for DSOs to tackle aforementioned challenges and exchange the characteristics of their grids with TSOs and/or other DSOs. An accurate equivalent of distribution grids ensures the secure analysis of the power system that in turn assists to keep a healthy status of the power system.

Developing an equivalent load model is mathematically an identification problem. Depending upon the available physical information and insight of the true system, there are three choices for the model structure, namely black box, gray box and white box [24]. In the black-box model, the topology of the true system is not known and merely the input and output data of the true system are available, which the aim is to map the input data set to the output data set by adjusting free parameters such that the output of the equivalent model becomes as similar as possible to the true system. In the white-box model, as the other extreme case, not only the topology of the true system is known, but also the physical components and their associated composition rates are also available. Thus, the task in the white-box model is to find an exact mathematical model of the true system. In many cases developing such a model can be complex and may deviate from the purpose of developing a simple load equivalent model. The gray-box modeling is something in between, in which the topology of the true system is available but not the exact components and their composition rate. Hence, there are still number of free parameters that must be estimated via the system identification. In this regard, the aim in the gray-box model is to identify the free parameters similar to the black-box model based on the observed data behavior.

The physical structure of distribution grids is known; however, physical components of demand and their composition rates are not available. Therefore, one can select a gray-box model to develop a load equivalent. The dominant physical behavior of the true grid is represented via a set of equations in the described gray-box model, and the mismatch between the model and the true grid is left to an optimization process to estimate the free parameters of the gray-box model.

The gray-box load modeling has been addressed in the previous literature [25]–[28]. A dynamic equivalent of a MicroGrid, which consists of only solid oxide fuel cells and high speed single shaft microturbines, was developed using the gray-box model along with evolutionary particle swarm optimization algorithm for identifying equivalent parameters in [25]. The dynamic equivalent of an active distributed network was developed using gray-box model and MATLAB System Identification Toolbox for parameter estimation purpose [26]–[28]. However, equivalents of distribution grids comprising large amount of PV systems embedded with voltage control scheme have not been addressed in the literature yet.

The aggregated static model of a distribution grid is normally represented by the constant impedance, constant current and constant power load model (ZIP load model) [26]–[31]. Distributed renewable energy sources such as PV systems are traditionally addressed as a negative load in the aggregation of loads and PV systems [32]–[37]. Nevertheless, as mentioned earlier, high penetrations of PV systems in distribution grids can change the behaviour of distribution grids. Equipping PV systems with voltage support schemes such as the standard $Cos\phi(P)$ characteristic required by German Grid Codes (GGC) [12] may even cause more changes in the behavior of distribution grids. For instance, the feed-in power of PV systems in the $Cos\phi(P)$ characteristic is directly imported as a feedforward signal to estimate the required reactive power. Therefore, PV systems not only change the behaviour of the grid in terms of active power but also in terms of reactive power. Accordingly, it is needed to develop a new equivalent model of distribution grids that can capture the dominant behavior of PV systems embedded with voltage support schemes.

The aim of this paper is using the gray-box modelling concept in the system identification to develop a static equivalent of the distribution grid consisting of large number of PV systems equipped with voltage support schemes. In the proposed model, distributed PV systems within the grid are represented as a separate entity in the aggregation, and loads are also aggregated as a separate ZIP equivalent. In the proposed procedure, all the inputs and outputs are measured at the feeding point, where is the boundary point between the distribution level and a higher level grid. The voltage at the feeding point serves as the input, while the outputs are the net generation/consumption active and reactive power of the ZIP/PV equivalent.

The proposed static equivalent model of the distribution grid is formulated for load-flow studies that can simply be integrated into load-flow programs and replace the true distribution grid, while still can keep the overall accuracy high. As mentioned earlier, the proposed aggregation approach can be used by DSOs to develop a characteristic behavior model of their grid and freely share it with other DSOs and TSOs, which may need this model to evaluate their grid in order to operate in a secure and economic manner. The accuracy of the static equivalent is the backbone of many other studies such as evaluation of operation, voltage stability, design and implementation of controllers, developing new standards (e.g. voltage). The proposed approach in this paper results in much better accuracy as compared to the traditional approach (modeling PVs as negative load). The poor accuracy in the traditional approach can lead to under or over estimation of power and voltage. This can negatively affect the proper evaluation of the power system exposure to changes happened in distribution grids that, in turn, may jeopardize the stable and secure operation of power systems.

The set-up of the equivalent procedure is explained in Section 2. The structure of the proposed equivalent, *Model I*: ZIP/PV equivalent is given in Section 3. *Model II*: PV as the negative load is presented in Section 4. The performance of

the proposed procedure is studied on a utility test grid as a case study in Section 5. Section 6 contains conclusions.

II. Set-up

In order to develop an equivalent model of a target distribution grid as a true system via the gray-box model, the following steps must be carried out:

- selecting a proper equivalent topology that could capture the dominant behavior of the true system;
- formulating the corresponding equations of the selected topology;
- determining the inputs and outputs;
- estimating free parameters through the identification process;
- validating the performance of the identified free parameters of the equivalent model.

A. True System

The main objective of this study is to develop a static equivalent model of a true distribution grid with a high penetration of PV systems embedded with voltage support schemes that can be integrated into load-flow programs. Therefore, the true system, in this study, is a distribution grid that consists of one feeding point; distribution transformers and lines; individual loads at different nodes within the grid; and individual PV systems. The feeding point is the boundary point between the distribution level and a higher level grid, where the equivalent of the distribution grid is to be obtained.

Active and reactive power of loads in the true grid are represented by constant impedance, constant current, and constant power load model (ZIP model)

$$P_L = P_{L0}\left(\alpha_z V^2 + \alpha_i V + \alpha_p\right) \tag{1}$$

$$Q_L = Q_{L0}\left(\beta_z V^2 + \beta_i V + \beta_p\right) \tag{2}$$

where P_{L0} and Q_{L0} are the load active and reactive power at the base voltage. α_z, α_i and α_p are the ZIP coefficient for active power that their sum must be equal to one. Besides, β_z, β_i and β_p are the ZIP coefficients for reactive power that also must have a sum equal to one. Though simulated results using ZIP load model may deviate from the actual field test results, the ZIP load model has been widely recommended and utilized in majority of system studies [26]–[31]. Therefore, in this study the ZIP load model is employed to represent the behavior of the actual load model in the true system.

Furthermore, PV systems are assumed embedded with the required GGC standard characteristic $cos\phi(P)$ represented in Fig. 1 [12]. The objective of the GGC standard characteristic is requiring the generation unit to operate in an under-excited mode when the feed-in active power passes over a threshold of 50% of P_{max} in order to mitigate the related voltage rise. According to the GGC, distributed generations are allowed to contribute reactive power while operating above 20% of their nominal power [12].

In order to roughly simulate field test results, quasi-static analysis of the true grid is deployed to provide the simulated data of active power and reactive power versus the voltage variation at the feeding-point of the grid.

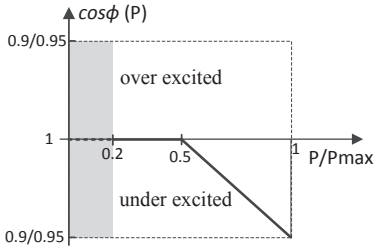

Fig. 1. Standard characteristic curve for *cosφ* (P).

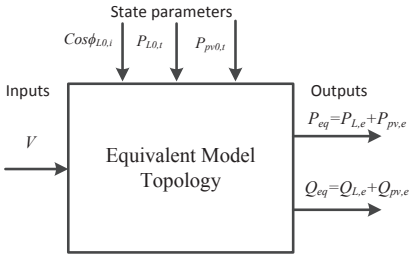

Fig. 2. Schematic of the equivalent model set-up.

In order to consider variations of solar and demand, different scenarios are investigated for developing the equivalent load model. In each scenario, state parameters of the grid, which represent the status of the grid, are assumed known. The state parameters of the grid are

1) the total load active power consumption within the grid at the base voltage $P_{L0,t}$, which is the sum of all individual loads at the base voltage

$$P_{L0,tot} = \sum_{i=1}^{L} P_{L0,i} \tag{3}$$

where L is the number of loads within the grid;
2) power factor of individual loads $cos\phi_{L0,i}$ that in turn yields the total load reactive power;
3) the total PV production $P_{pv,tot}$, which is the sum of all individual PV systems.

B. General Layout of the Equivalent

The general layout of the equivalent is depicted in Fig. 2. As can be seen, the input of the equivalent model is the bus voltage at the feeding point (V). State parameters of the grid are also imported to the equivalent model to determine the status of the equivalent model. The values of state parameters and the voltage can vary within specific ranges. Thus, the free parameters of the equivalent model must be estimated such that the output of the equivalent model can demonstrate similar behavior as the output of the true system within the same ranges of variations in the state parameters and the voltage. The outputs of the proposed equivalent model are the net active and reactive power of the equivalent PV model and the equivalent load model.

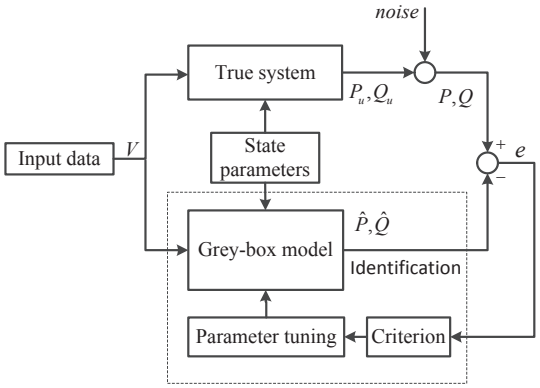

Fig. 3. Free parameter estimation process in the gray-box model.

C. Estimating Free Parameters

The flowchart of free parameters estimation process is illustrated in Fig. 3, where the bus voltage at the feeding point serves as the input. The variation of V triggers the corresponding variations in load characteristics at each node in the true system. The larger variation of the V provides a better insight into the load characteristics. Generally, voltage variations bigger than 0.1 p.u. can demonstrate the voltage dependency behavior of the load [30]. Under the V variations and grid state variables, the noise-free outputs of the true system P_u and Q_u are obtained. In real case applications, however, there are always some noise and disturbance associated with measurements as well as uncertainty at the load level and its composition rate at each node. In other words, the noise is an inherited part of any measurement-based load modelling approach. Therefore, in this study, the noise-free simulated results are polluted with a Gaussian noise to resemble P and Q characteristics as a real case application.

The V variations along with corresponding grid state parameters are also imported to the gray-box model to estimate $\hat{P}$ and $\hat{Q}$. The difference between output of the true system and the gray-box model e is fed back to the parameters tuning algorithm to estimate the free parameters by minimizing the sum of squared errors ($\sum e^2$), which represents the model error at the end.

D. Model Error

Any model identification method introduces a model error composed of two components, namely bias error and the variance error [24]:

$$(Model\ error)^2 = (Bias\ error)^2 + Variance\ error \tag{4}$$

The bias error is related to the structure inflexibility of the model and basically demonstrates the systematic deviation between the true system and the model structure. In other words, the bias error is a part of the model error that represents the limited flexibility of the model. The flexibility of a model is equivalent to its complexity. Normally, modelling a nonlinear process leaves a bias error. Bias error in aggregation of a distribution grid consisting of various load components is unavoidable. Generally, increasing the flexibility of the model by increasing the number of free parameters will lead to a lower bias error. Nevertheless, the bias error and the variance error are in conflict and choosing a complex model results in a larger variance error. The variance error describes the deviation between estimated free parameters and their optimal values that happens due to using a finite and noisy data set. In other words, the variance error depicts that part of the model error that represents uncertainties in estimated free parameters. It is shown in [24] that the variance error increases by increasing the number of free parameters. Moreover, it can be shown that regardless of the model, for a large training data set (data set that is employed to estimate the free parameters), the variance error approximately has a linear relation with the number of free parameters n as follows:

$$variance\ error \sim \sigma \frac{n}{N} \tag{5}$$

where σ is the noise variance and N is the number of training data samples [24]. It is obvious that a large training data set can cancel out the noise impact and lower the variance error. Moreover, the fewer the free parameters (lower complexity), the more accurate the estimation and the lower the variance error would be that is contrary to the bias error concept. In regard to this fact, it can be shown that among all models that describe a process accurately, the simplest one is the best [24].

With that being said, due to the bias/variance error dilemma, the model should be neither too simple nor too complex and instead somewhere in between.

E. Optimization Problem

Identification task is an optimization problem and so an objective function must be formulated. The root mean square error (RMSE) is a frequently used measure to evaluate residuals between the predicted model values and actual values observed in the true system. As discussed earlier, the number of training data sets plays a key role in the accuracy of the model identification. Thus, assuming M as the number of the data sets, the RMSEs of active and reactive power associated with ith data set are represented as follows:

$$E_{pi} = \sqrt{\frac{\sum_{i=1}^{N} \left(P_i - \hat{P}_i\right)^2}{N}} \tag{6}$$

$$E_{qi} = \sqrt{\frac{\sum_{i=1}^{N} \left(Q_i - \hat{Q}_i\right)^2}{N}} \tag{7}$$

since the value of P and Q can vary significantly in different data sets, the relative RMSEs of E_{pi} and E_{qi} are employed

$$e_{pi} = \frac{E_{pi}}{\overline{P}_i} \tag{8}$$

$$e_{qi} = \frac{E_{qi}}{\overline{Q}_i} \tag{9}$$

where $\overline{P}_i$ and $\overline{Q}_i$ are the average active and reactive power of the ith data set, respectively. Therefore, the proposed objective function for the model identification is

$$min\left(\sum_{i=1}^{M}\left(e_{pi}^2 + e_{qi}^2\right)\right) \tag{10}$$

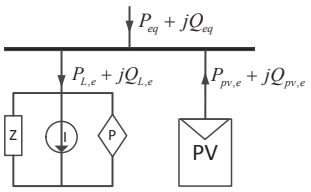

Fig. 4. Equivalent ZIP/PV model.

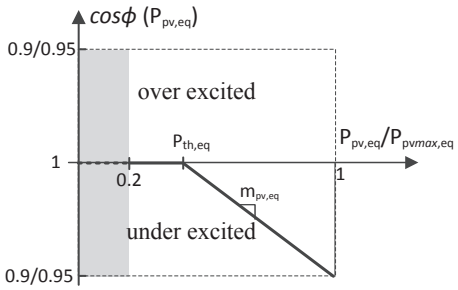

Fig. 5. *cosφ* (P) characteristic curve of the equivalent PV model.

It will be shown in the next section that the formulated optimization problem in this study is non-linear. Generally, there are two types of non-linear optimization techniques, namely local optimization techniques and global optimization techniques. As it stems from the name of non-linear local optimization techniques, the found optimum via these techniques is a local optimum located in the vicinity of the initial guess without searching other parameter space and, therefore, the performance of them heavily depends upon the starting point guess. Nevertheless, the convergence speed in local optimization techniques are relatively higher than global techniques. Global techniques, on the one hand, try to escape from being trapped in a local optimum by searching through the entire parameter space, but on the other hand the convergence speed to any optimum is likely slow. Thus, it is a good idea to employ a hybrid procedure using a global optimization technique to reach near the region of parameter space that the optimum may lie and then feeding the estimated free parameters to a local optimization technique to find the optimum [24]. In this study, the genetic algorithm is employed to find the region and sequential quadratic programming is used to find the optimum.

III. Model I: ZIP/PV Equivalent

The schematic of the proposed equivalent ZIP/PV model is shown in Fig. 4. The equivalent model consists of 1) an equivalent ZIP load model; 2) an equivalent PV model associated with an equivalent $cos\phi(P)$ characteristic.

The equivalent ZIP load model is described by the following set of equations

$$P_{L,eq} = P_{L0,tot}\left(\alpha_Z V^2 + \alpha_I V + \alpha_P\right) \tag{11}$$
$$Q_{L,eq} = Q_{L0,tot}\left(\beta_Z V^2 + \beta_I V + \beta_P\right) \tag{12}$$

where $P_{L,eq}$ and $Q_{L,eq}$ are the active and reactive power of the equivalent ZIP load, respectively. $P_{L0,tot}$ and $Q_{L0,tot}$ are total load active and reactive power at the base voltage, respectively. α_Z, α_I and α_P are, respectively, constant impedance part, constant current part and constant power part of active power of the equivalent ZIP load that must satisfy the constraint in (13). In the same way, β_Z, β_I and β_P are, respectively, constant impedance part, constant current part and constant power part of reactive power of the equivalent ZIP load that are subjected to the constraint in (14).

$$\alpha_Z + \alpha_I + \alpha_P = 1 \tag{13}$$
$$\beta_Z + \beta_I + \beta_P = 1 \tag{14}$$

The equivalent PV in the proposed gray-box model is depicted by the following equations:

$$P_{pv,eq} = \alpha_{pv} P_{pv,tot} \tag{15}$$
$$cos\phi_{pv,eq} = m_{pv,eq}\left(P_{pv,eq} - P_{th,eq}\right) + 1 \tag{16}$$
$$Q_{pv,eq} = P_{pv,eq}\sqrt{\frac{1}{\left(cos\phi_{pv,eq}\right)^2} - 1} \tag{17}$$

where $P_{pv,eq}$ and $Q_{pv,eq}$ are active and reactive power of the equivalent PV model. $P_{pv,tot}$ is the total generated active power by PV units in the true system. α_{pv} represents the mismatch of losses via lines. The voltage support characteristic of the equal PV system shown in Fig. 5 is assumed to be similar to the GGC standard characteristic. Nevertheless, in the proposed ZIP/PV equivalent model, the slope $m_{pv,eq}$ and the threshold power $P_{th,eq}$ of the equivalent $cos\phi(P)$ characteristic are free parameters and their tuning is left to the identification process.

Based on (11), (12), (15) and (17), the equivalent active and reactive power at the feeding point can be stated as follows:

$$P_{eq} = P_{L,eq} - P_{pv,eq} \tag{18}$$
$$Q_{eq} = Q_{L,eq} - Q_{pv,eq} \tag{19}$$

Therefore, there exists, as demonstrated in the following vector, nine free parameters in the proposed ZIP/PV model, which must be estimated via the proposed optimization process.

$$\begin{bmatrix}\alpha_Z & \alpha_I & \alpha_P & \beta_Z & \beta_I & \beta_P & \alpha_{pv} & m_{pv,e} & P_{th,e}\end{bmatrix} \tag{20}$$

IV. Model II: PV System as the Negative Load

Non-dispatchable renewable generations such as solar power productions are often addressed as negative loads [32]–[37]. Hence, PV systems are not considered as a separate entity. The following set of equations represent PV systems as a negative load within the ZIP load equivalent model:

$$P_{eq} = \left(P_{L0,tot} - P_{pv,tot}\right)\left(\alpha_Z V^2 + \alpha_I V + \alpha_P\right) \tag{21}$$
$$Q_{eq} = \left(Q_{L0,tot} - Q_{pv,tot}\right)\left(\beta_Z V^2 + \beta_I V + \beta_P\right) \tag{22}$$

where $Q_{pv,tot}$ is the total reactive power consumptions by PV systems and calculated based on the GGC characteristic in Fig. 1 and the total active power production of PV systems.

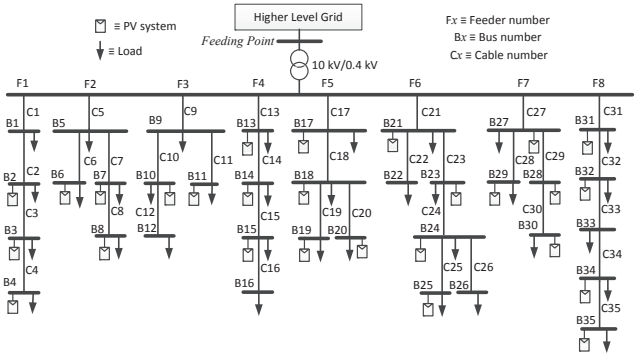

Fig. 6. Test utility distribution grid.

TABLE I
PARAMETERS OF THE TRUE GRID [38].

		Impedance Ω/km
Cables	C_x x=1,5,9,13,17,21,27-31	0.21 + 0.086j
	C_x x=2-4,6-8,10-12,14-16,18-20,22-26	0.32 + 0.086j
	C_x x=32-35	0.6 + 0.09j
Transformer	630 kVA, 10/0.4 kV, Dyn5, U_k=4.66%, P_{cu}=6.5 kW	

As depicted in the following vector, there are therefore only six free parameters in this equivalent model:

$$\begin{bmatrix}\alpha_Z & \alpha_I & \alpha_P & \beta_Z & \beta_I & \beta_P\end{bmatrix} \tag{23}$$

The number of free parameters in the *Model II* is less than the *Model I*, which means less flexibility in the *Model II*. Hence, one can expect a higher bias error in the *Model II* as compared to the *Model I*, irrespective of number of training data samples.

V. CASE STUDY

In this study, the test true system is a utility grid located at Northern Jutland in Denmark as shown in Fig. 6 [38]. This distribution grid consists of eight feeders and thirty five buses. The information of this grid is summarized in Table I [38].

Maximum load active power of different buses within the grid is given in Table II; the total maximum load active power is therefore $P_{L0,tot}^{max}$=515 kW. It is worth mentioning that the load amount at each bus is assumed to be an aggregation of all connected loads to the same bus. It is shown in [31] that the ZIP coefficients of residential customer loads can be classified into 6 classes given in Table III. Thus, these 6 load classes are deployed in this study.

As a future scenario in this grid, it is assumed that all buses in this grid have the potential of PV system installation. In this case study, however, only 27 buses out of 35 are considered

TABLE II
LOCATION AND NAMEPLATE POWER OF LOADS WITHIN THE GRID.

Load power	Bus number
10 kW	B_x x= 1,3,6-7,10,12,14,19-20,23,25-28,30,33,35
15 kW	B_x x= 2,8,10,11,16-17,22,32
20 kW	B_x x= 4,9,13,15,18,24,34
25 kW	B_x x= 5,21,29,30

TABLE III
ACTIVE AND REACTIVE ZIP COEFFICIENTS PER RESIDENTIAL LOAD CLASS [31].

Load class	α_z	α_i	α_p	β_z	β_i	β_p
Class A	1.5	-2.31	1.81	7.41	-11.97	5.55
Class B	1.57	-2.48	1.91	9.28	-15.29	7.01
Class C	1.56	-2.49	1.93	10.1	-16.75	7.65
Class D	1.31	-1.94	1.63	9.2	-15.27	7.07
Class E	0.96	-1.17	1.21	6.28	-10.16	4.88
Class F	1.18	-1.64	1.47	8.29	-13.67	6.38
Average	1.34	-2	1.66	8.43	-13.85	6.42

TABLE IV
LOCATION OF BUSES WHERE THERE ARE NO INSTALLED PVS.

Bus numbers
B_x x= 1, 5, 9, 12, 16, 22, 26, 33

equipped with PV systems; Table IV specifies buses without PV system. PV systems at each bus are considered to be an aggregated amount of several rooftop PV systems connected to the same bus. The nameplate power of aggregated installed PV systems at each bus is equal to the maximum aggregated load power at the same bus. The total maximum capacity of installed PVs is therefore $P_{pv,tot}^{max}$=400 kW. In this case study, the penetration level of PV systems, which is here defined as peak installed PV capacity to peak demand of the feeder, is 77%. Moreover, PV systems are assumed embedded with the proposed GGC standard characteristic $cos\phi(P)$ represented in Fig. 1.

In this study, a symmetrical three-phase load-flow analysis in MATLAB is used to simulate required sets of training and test data, which will be discussed in the following subsections. The proposed methodology in this study is, therefore, examined based on simulated data sets. Nevertheless, the proposed methodology can simply be adapted to work based on measurements when they are available. However, one must keep in mind that normally providing measured data sets can be challenging. Because, first, voltage at the feeding point must be varied within an acceptable range around the base voltage (the larger the variation, the more accurate the model). There might, however, be some limitations and/or regulations that may prevent or limit voltage variations. Second, if total production of PV systems is not available, it must be forecasted based on solar irradiation. Moreover, load and solar production may vary within the voltage variation interval (e.g. instant turn on/off of fridges, and passing clouds); this can add more uncertainty in the modeling. It is worth mentioning that in the proposed procedure based on simulated data sets, measurement disturbances, load and PV uncertainties are considered as an added noise to a noise-free simulated data set in order to resemble a more realistic case.

A. Generating Training Data Sets

In order to generate scenarios, following assumptions and calculation steps are taken:

A1 Assuming a similar load class within all buses in the grid for each scenario;

A2 Assuming a similar constant power factor, 0.95 inductive, for individual loads within the grid for all scenarios (according to the Swedish DSO the power factor in distribution grids is close to one; thus 0.95 seems reasonable);

A3 Considering three scenarios (low, medium and high) for the total load active power $P_{L0,tot}$ at the base voltage: 20%, 50% and 90% of the maximum total load active power $P^{max}_{L0,tot}$;

A4 Assuming that all individual PV systems are functioning above at least 50% of their maximum power in which all $cos\phi(P)$ characteristics are active;

A5 Assuming three scenarios for the total PV production, 55%, 80% and 100% of the maximum total PV production $P^{max}_{pv,tot}$;

A6 Assuming a Gaussian noise with zero mean value and 0.01 standard deviation to simulate the measurement noise and uncertainties;

C1 Distributing the total load active power among individuals load such that satisfies (3) at the base voltage;

C2 Varying the feeding point voltage between 0.92 and 1.08 for each scenario and performing the quasi steady-state analysis to record the noise-free active and reactive power at the feeding point;

C3 Adding the simulated noise to the noise-free active and reactive power at the feeding point.

where A and C stand for assumption and calculation, respectively. Combinations of six different load classes, three different load scenarios, and three different PV production scenarios provide 54 scenarios in total. These scenarios are imported to the proposed gray-box model identification process to estimate the free parameters. The objective function of the optimization problem in the identification process is developed according to (10) and subjected to the equality constraints in (13) and (14) as well as the following inequality constraint to limit reactive power variations of PV systems, which are also limited according to the GGC standard characteristic.

$$0.9 \leq cos\phi_{pv,eq} \leq 1 \tag{24}$$

The optimization variables are the same as the free parameters given in (20) and (23). The optimization set-up is solved using *Global Optimization Toolbox* of MATLAB in which the built-in hybrid scheme in the genetic algorithm (GA) is employed. As discussed earlier, the GA can reach a parameter space region near an optimum relatively fast, but it takes longer time to achieve convergence. So the GA with small number of generations is used to reach the region, and then, its solution is fed as an initial point to the sequential quadratic programming optimization, which is faster and more efficient for the local search.

The estimated free parameters of the both equivalent models are given in Table V. It is worth mentioning that the obtained ZIP equivalent coefficients in the both models differ from the average of ZIP coefficients of six load classes in Table III. It is also important to note that since specifications of each distribution grid (e.g. line impedances, transformers, loads, PV size, voltage control type of PV systems and etc.) differ from other distribution grids, free parameters of the equivalent model and their values would be different for each distribution grid. Nevertheless, the proposed methodology can be applied to any network to derive its appropriate equivalent.

TABLE V
ESTIMATED FREE PARAMETERS OF THE BOTH EQUIVALENT MODELS.

Equivalent	α_Z	α_I	α_P	β_Z	β_I	β_P	α_{pv}	$m_{pv,eq}$ [1]	$P_{th,eq}$ [2]
Model I	1.16	-1.68	1.52	5.25	-7.72	3.47	1.002	-5.6e-4	209.4
Model II	-0.95	2.92	-0.97	-3.12	7.45	-3.33	-	-	-

[1] $[kW]^{-1}$
[2] [kW]

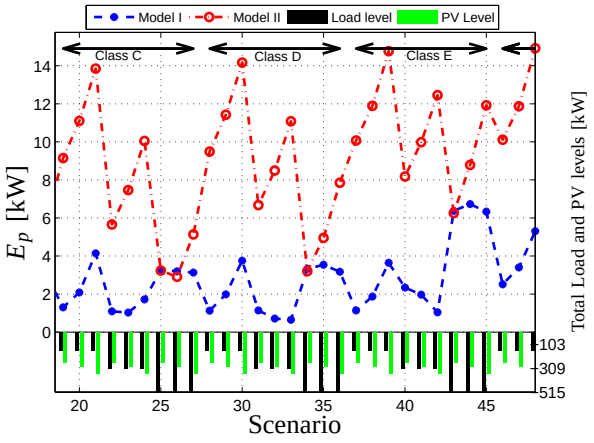

Fig. 7. Active power errors between the true grid and the corresponding equivalent models.

B. Generating Test Data Sets

The performance of the developed models must be evaluated on a fresh, different data sets to estimate the quality of the models. In this regard, in contrast to the training data sets, the total load levels and the total PV production levels are respectively varied to 30%, 60% and 100% of $P^{max}_{L0,tot}$ and 65%, 75% and 90% of $P^{max}_{pv,tot}$.

C. Results

The generated test data sets are employed to examine the performance of the both equivalent models. Fig. 7 shows the active power error of the both models according to (6). For the sake of better depiction, only the load classes of C, D, E, and partly F are demonstrated in Fig. 7. Besides, A, B and C load classes have more or less similar ZIP coefficients and so the performance of each model is comparatively similar within these load classes. The total load active power and the total PV production in each scenario are also presented at the bottom of the figure to provide a better illustrative evaluation. It is obvious in the figure that the active power errors are significantly reduced in the *Model I* compared to the *Model II*. Furthermore, one can observe that the active power errors in the *Model II* generally become larger when the total PV production is above the total load consumption.

Fig. 8 demonstrates the reactive power errors based on (7) between the true grid and the equivalent models. In general,

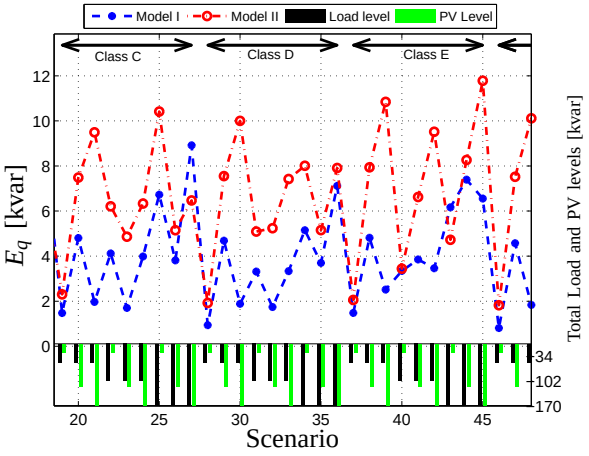

Fig. 8. Reactive power errors between the true grid and the corresponding equivalent models.

reactive power errors are tangibly reduced in the *Model I* in comparison with the *Model II*. Furthermore, it can generally be observed when the total reactive power consumption via the PV systems raise over the total load reactive power consumption, the *Model II* causes larger errors.

Therefore, the *Model II* in general leads to larger errors especially when the total PV power contribution goes beyond the total load power consumption. Hence, one can notice better the importance of having the separate PV equivalent in the case of high PV penetration.

Within all scenarios, the average of active power errors $\overline{E_p}$ and reactive power errors $\overline{E_q}$ are given in Table VI. Statistically speaking, the $\overline{E_p}$ and $\overline{E_q}$ in the *Model I* are respectively reduced by 72% and 41% compared to the *Model II*. Moreover, these average error values are taken as measures to evaluate the performance of the equivalent active and reactive power curves versus the voltage at the feeding point. As can be seen in Fig. 7, the active power error levels of the both models in scenario 40 are roughly close to their corresponding average errors. Similarly, one can see that the both models at the scenario 41 have roughly similar reactive power error levels as their average error values. Fig. 9 illustrates active and reactive power variations versus the voltage variation at the feeding point for the scenarios 40 and 41, respectively. It is worth mentioning that the total load active power at the base voltage $P_{L0,tot}$ and the total generated power by PV systems $P_{pv,tot}$ are remained constant while the voltage as the input is varied. In both models, it is obvious that increasing the voltage increases the equivalent active and reactive power as it is expected from the voltage dependency characteristic of the load. However, comparing $P_{eq}(V)$ and $Q_{eq}(V)$ in the both equivalent models reveals that the *Model I* not only introduces lower error but also follows the similar trajectory as the true grid; on the other hand, the general behavior of the *Model II* to a large extent is far from the true grid.

The scenarios associated with the exterma of E_p and E_q for the *Model I* are taken as an another measure to compare the quality of this model with regard to the *Model II*. The minimum and the maximum E_p values of *Model I* occur in

TABLE VI
AVERAGE ERRORS WITHIN ALL SCENARIOS.

Equivalent	$\overline{E_p}$ [kW]	$\overline{E_q}$ [kvar]
Model I	2.44	3.84
Model II	8.61	6.55

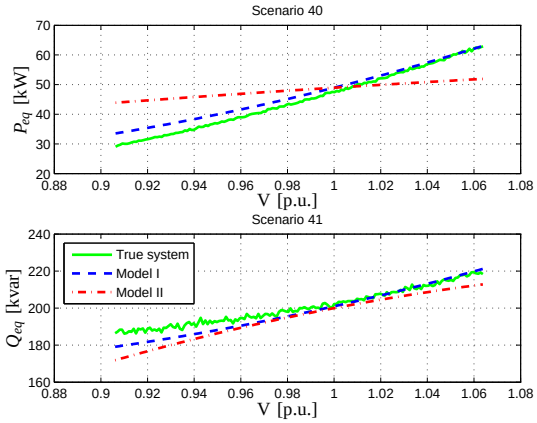

Fig. 9. The response of the true grid and the both equivalent models at the average error values of the both equivalents.

scenarios 33 and 44 respectively. Fig. 10 shows the $P_{eq}(V)$ curves for the both equivalent models and the true grid at the exterma of E_p. It is obvious that in the case of minimum error, which the associated E_p with *Model II* is around its average value, the behavior of the *Model I* is significantly better. Moreover, it is evident from the upper graph in Fig. 10 that in the scenario 33 (minimum E_p in the *Model I*), in which the total PV production is higher than the total load consumption at the base voltage $P_{L0,tot} = 309$ kW and $P_{pv,tot} = 360$ kW, the general voltage-dependency behavior of the *Model II* completely deviates from what is seen in the true system. In this scenario an increase in the voltage would lead to a decrease in the equivalent active power, which is tantamount to a decline in the load. This opposite active power-voltage behavior is because of fewer free parameters in the *Model II* (i.e. lower flexibility) that causes a poor setting of free parameters, and along with, voltage dependant parameters α_Z and α_I are remained independent of generation and consumption power patterns. In other words, in the *Model II*, identified free parameters cannot be a proper representative of loads and PV systems for different possible combinations of active power production and consumption levels; e.g. in this case study when production is higher than consumption, the *Model II* exhibits an opposite behavior than the true system. In the scenario 44 (maximum E_p in the *Model I*), the total PV production is less than the total load consumption at the base voltage $P_{L0,tot} = 515$ kW and $P_{pv,tot} = 300$ kW. The E_p of scenario 44 in the *Model II* is slightly higher than the maximum E_p of the *Model I*. Thus, even at the maximum E_p of the *Model I* in scenario 44, one can intuitively expect a better response for the *Model I* compared to the the *Model II*. Moreover, the trajectory of *Model I* still lies on the same trajectory as the true grid. Though the *Model II* in scenario

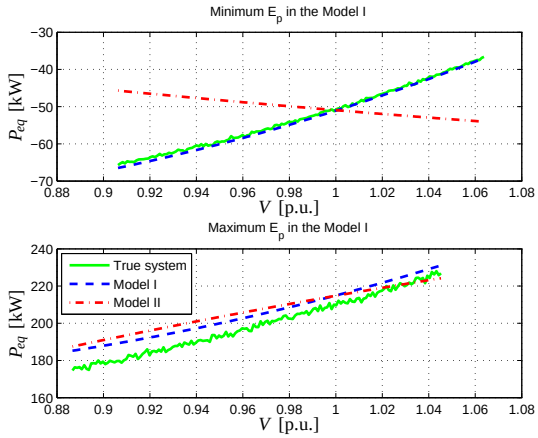

Fig. 10. Equivalent active power at the feeing point in the presence of the E_p exterma.

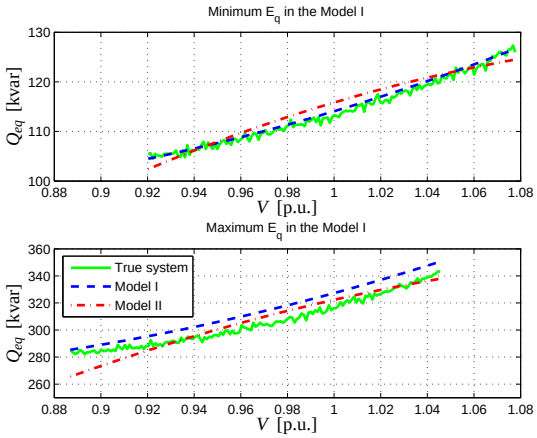

Fig. 11. Equivalent reactive power at the feeing point in the presence of the E_q exterma.

44 does not show an opposite active power-voltage behavior, its trajectory still follows a different pattern than the true grid.

The minimum and the maximum E_q values of the *Model I* occur in scenarios 46 and 27, respectively. Fig. 11 depicts the $Q_{eq}(V)$ curves for the both equivalent models and the true grid at the exterma of E_q. It is worth mentioning that in all scenarios of this case study, both PV systems and loads consume reactive power. Thus, the equivalent reactive power remains in consumption mode for any combination of PVs and loads reactive power. This means less stress on free parameters associated with reactive power aggregation. In the *Model II*, therefore, one can expect a better reactive power-voltage behavior in contrast to the active power-voltage behavior presented in Fig. 10. In the scenario 44, the E_q of the *Model II* is slightly higher than the minimum E_q of the *Model I*. Accordingly, it is obvious that the behavior of the *Model I* is much more close to the true system as compared to the *Model II*. In the scenario 27, the E_q value of the *Model II* is slightly lower than the maximum E_q of the *Model I*. Nevertheless, it is still clear that the trajectory of the *Model I* is following the same trajectory as the true grid, while the trajectory of the *Model II* obviously differs from the true grid.

In addition to causing lower errors, it can be concluded that, first, the trajectory behavior of the *Model I* is superior than the *Model II*. Second, the general active power-voltage behavior of the *Model II* and the true system can be diametrically opposed depending on active power production and consumption levels. Hence, it is necessary to address PV system as a separate entity. Otherwise using the *Model II* with the wrong behavior in power system studies can lead to under or over estimation of power and voltage, which can negatively affect the secure operation and planning of the power system. For instance, if one employs the traditional *Model II* to design a voltage controller in the vicinity of the feeding point, then the controller will not act correctly in the true system.

D. Further Application

As stated earlier, reactive power support via PV systems can be done via different methods such as: constant power factor, active power dependent reactive power regulation Q(P) and droop-based voltage (DBV) regulation Q(V) [12]–[21]. In the DBV regulation method, as shown in Fig. 12, local voltage at a PV system connection point is imported as an input to calculate the required local reactive power to regulate the voltage. Since voltage is explicitly addressed in the DBV method, reactive power consumption can be managed by severity of the voltage violation. Therefore, using the Q(V) method can prevent unnecessary reactive power consumption in contrast to Q(P) method, which employs the delivered power of a PV system as the input. The GGC also recommends using DBV regulation method in the near future scenarios [12].

To further evaluate the performance and the generality of the proposed static equivalencing methodology, it is assumed that PV systems are equipped with DBV characteristics. Parameters of the Q(V) characteristic, namely slope and voltage threshold, for PV systems in the true systems are set according to the proposed multi-objective coordinated DBV approach in [19] to minimize reactive power consumption. So, with the use of the Q(V) characteristic, one can expect a lower share of reactive power as compared to the GGC standard characteristic employed in the previous subsection.

Training and test data sets are generated very similar to the subsections V-A and V-B; the only difference is that PV systems are embedded with Q(V) characteristics. Besides, in the proposed equivalent ZIP/PV model, *Model I*, it is assumed that the equivalent PV is associated with an equivalent Q(V) characteristic; hence, equations corresponding to reactive power of the equivalent PV system (16) and (17) in the *Model I* must be replaced by the following equation

$$Q_{pv,eq} = m_{pv,eq}\left(V - V_{th,eq}\right) \tag{25}$$

where $m_{pv,eq}$ and $V_{th,eq}$ are respectively the slope and the voltage threshold of the equivalent Q(V) characteristic, which their identified values via the proposed gray-box model identification process become $m_{pv,e} = 233\ p.u.$ and $V_{th,e} = 1.051\ p.u.$

TABLE VII
ESTIMATED FREE PARAMETERS OF THE BOTH EQUIVALENT MODELS IN THE CASE OF THE DBV CHARACTERISTIC.

Equivalent	α_Z	α_I	α_P	β_Z	β_I	β_P	α_{pv}	$m_{pv,eq}$ [1]	$V_{th,eq}$ [1]
Model I	0.92	-1.2	1.27	-8.2	17.9	-8.8	1.004	233	1.051
Model II	-1.06	3	-0.93	11.9	-18	7.08	-	-	-

[1] [p.u.]

for this case study, respectively. The identified free parameters are given in Table VII. The average of active power errors $\overline{E_p}$ of *Model I* and *Model II* becomes 2.6 kW and 9 kW, respectively, which are roughly close to the $\overline{E_p}$ of both models at the scenario 46. The average of reactive power errors $\overline{E_q}$ of *Model I* and *Model II* are 8.3 *kvar* and 21.2 *kvar*, respectively, which are roughly close to the $\overline{E_q}$ of both models at the scenario 28. These results show that average values of active and reactive power errors in the *Model I* are respectively reduced by 71% and 61% in comparison with the *Model II*. In contrast to the results of the previous subsection, i.e. PV systems with the GGC characteristic, the average values of reactive power errors in the *Model I* is reduced more in the case of the DBV characteristic that will be reasoned in the following.

The performance of both models is evaluated at the aforementioned scenarios corresponding to average active and reactive power errors of both models. Fig. 13 depicts equivalent active and reactive power variations versus the voltage variation at the feeding point for the scenarios 46 and 28, respectively. In the scenario 46, in which the total PV production is higher than the total demand, the active power-voltage behavior of the *Model II* and the true system are diametrically opposed. The similar course of discussion given in the previous subsection justifies this wrong behavior. Moreover, it is similarly clear that the active power-voltage behavior of the *Model I* is very close to the true system. The reactive power-voltage characteristic curve of the true system in the lower graph of Fig. 13 illustrates a sudden rise almost after the voltage of 1.05 *p.u.*. This lies in the fact that the DBV reactive power control mechanism in PV systems operates based on a feedforward signal of the voltage, and so, when the voltage goes beyond thresholds of PV systems, reactive power consumption is commenced. Furthermore, the multi-objective coordinated DBV method tries to minimize reactive power consumption; this leads to a narrower range of activation band with high steep slopes for Q(V) characteristics [19]. In this regard, reactive power compensation units of PV systems kick in at relatively higher voltages with a steep rise. Hence, due to aforementioned reasons, the reactive power-voltage trajectory of the true system looks like a piecewise curve, which can reason the higher average reactive power error associated with the *Model II* in comparison with the GGC characteristic-based PV systems. Fig. 13 also illustrates that the reactive power-voltage behavior of the *Model II* cannot track down the reactive power variations associated with PV systems due to the lack of flexibility in the model. On the other hand, the *Model I* behaves in a similar manner as the true system due to a higher flexibility that stems from extra

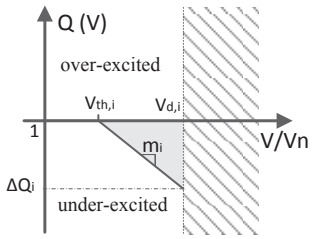

Fig. 12. Characteristic curve of reactive power droop with voltage level.

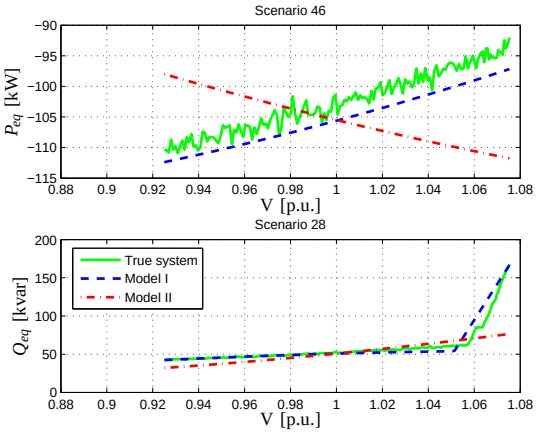

Fig. 13. The response of the true grid and the both equivalent models at the average error values of the both equivalents while PV systems are equipped with Q(V) characteristics.

independent free parameters used to model PV systems as a separate entity. Therefore, the piecewise behavior of the DBV-based reactive power control mechanism calls even more for addressing PV systems as a separate entity in the aggregation of future distribution grids.

VI. CONCLUSION

This paper deploys the gray-box modelling concept to propose a new static equivalent model of distribution grids with a high level penetration of PV systems embedded with voltage support schemes such as the GGC standard characteristic $Cos\phi(P)$ and droop-based voltage regulation characteristic Q(V). In the proposed model, PV systems within the grid are aggregated as a separate entity in addition to the ZIP equivalent load. So, the proposed structure of the equivalent consists of an equivalent ZIP load and an equivalent PV embedded with an equivalent of the corresponding voltage support scheme utilized in the grid. The paper also considers the traditional way of addressing PV systems as the negative load in the grid to investigate the quality of the proposed method. A utility grid was used as the test true system; in this system with maximum active and reactive demand of 515 kW and 170 kVar, the active and reactive power errors of the proposed ZIP/PV equivalent in the presence of the GGC characteristic were in the range of 2.44 *kW* (0.5%) and 3.84 *kvar* (2.2%), respectively; and in the presence of the DBV characteristics were in the range of 2.6 *kW* (0.5%) and 8.3 *kvar* (4.9%), respectively. The results demonstrate that the proposed equivalent model not only

reduces active and reactive errors compared to the traditional way but also represents a similar trajectory behavior in $P_{eq}(V)$ and $Q_{eq}(V)$ at the feeding point as the true distribution grid does. Furthermore, it is shown that the active power-voltage behavior of the traditional model cannot be a proper representative of the true system for different possible scenarios of consumption and production levels (e.g. in this case study when the total production of PV systems goes beyond the total load consumption level) due to inflexibility of the model that causes a bad parameter setting. It is also demonstrated that in the case of PV systems equipped with DBV characteristics, the reactive power-voltage characteristic of the traditional model cannot capture the piecewise functioning behavior of DBV characteristics embedded in PV systems.

Thus, in the current and future distribution grids with high level PV penetrations, it is beneficial to address PV systems as a separate entity in the aggregation as demonstrated in the proposed ZIP/PV equivalent.

REFERENCES

[1] A. Jaeger-Waldau, "PV status report 2013," tech. rep., European Commission, DG Joint Research Center, Institute for Energy and Transport, Renewable Energy Unit, Sept. 2013.

[2] M. Vandenbergh, D. Craciun, V. Helmbrecht, R. Hermes, R. Lama, P. Michele Sonvilla, M. Rekinger, and G. Concas, "Prioritisation of technical solutions available for the integration of pv into the distribution grid," tech. rep., DERlab, European Distributed Energy Resources Laboratories e. V., June 2013.

[3] S. Steffel, P. R. Caroselli, A. M. Dinkel, J. Q. Liu, R. N. Sackey, and N. R. Vadhar, "Integrating solar generation on the electric distribution grid," *IEEE Transactions on Smart Grid*, vol. 3, pp. 878–886, June 2012.

[4] M. Baran, H. Hooshyar, Z. Shen, and A. Huang, "Accommodating high PV penetration on distribution feeders," *IEEE Transactions on Smart Grid*, vol. 3, pp. 1039–1046, June 2012.

[5] T. Stetz, F. Marten, and M. Braun, "Improved low voltage grid-integration of photovoltaic systems in Germany," *IEEE Transactions on Sustainable Energy*, vol. PP, no. 99, pp. 1 –9, 2012.

[6] M. Bazilian, I. Onyeji, M. Liebreich, I. MacGill, J. Chase, J. Shah, D. Gielen, D. Arent, D. Landfear, and S. Zhengrong, "Re-considering the economics of photovoltaic power," *Renewable Energy*, vol. 53, pp. 329–338, May 2013.

[7] D. Pérez, V. Cervantes, M. J. Báez, and J. González-Puelles, "PV grid parity monitor," tech. rep., ECLAREON, Oct. 2012.

[8] Y. Liu, J. Bebic, B. Kroposki, J. De Bedout, and W. Ren, "Distribution system voltage performance analysis for high-penetration PV," in *IEEE Energy 2030 Conference, 2008. ENERGY 2008*, pp. 1–8, Nov. 2008.

[9] X. Liu, A. Aichhorn, L. Liu, and H. Li, "Coordinated control of distributed energy storage system with tap changer transformers for voltage rise mitigation under high photovoltaic penetration," *IEEE Transactions on Smart Grid*, vol. 3, pp. 897 –906, June 2012.

[10] R. Tonkoski, L. Lopes, and T. El-Fouly, "Coordinated active power curtailment of grid connected PV inverters for overvoltage prevention," *IEEE Transactions on Sustainable Energy*, vol. 2, pp. 139 –147, Apr. 2011.

[11] R. Tonkoski and L. A. Lopes, "Impact of active power curtailment on overvoltage prevention and energy production of PV inverters connected to low voltage residential feeders," *Renewable Energy*, vol. 36, pp. 3566–3574, Dec. 2011.

[12] "Power generation systems connected to the low/voltage distribution network," in *VDE application rule VDE-AR-N 4105:2011-08*, 2011.

[13] A. Cagnano, E. De Tuglie, M. Liserre, and R. Mastromauro, "Online optimal reactive power control strategy of PV inverters," *IEEE Transactions on Industrial Electronics*, vol. 58, pp. 4549 –4558, Oct. 2011.

[14] P. Sulc, K. Turitsyn, S. Backhaus, and M. Chertkov, "Options for control of reactive power by distributed photovoltaic generators," *arXiv:1008.0878*, Aug. 2010. Proceedings of the IEEE , vol.99, no.6, pp.1063-1073, June 2011.

[15] E. Demirok, P. Casado Gonzalez, K. Frederiksen, D. Sera, P. Rodriguez, and R. Teodorescu, "Local reactive power control methods for overvoltage prevention of distributed solar inverters in low-voltage grids," *IEEE Journal of Photovoltaics*, vol. 1, pp. 174 –182, Oct. 2011.

[16] A. Yazdani, A. Di Fazio, H. Ghoddami, M. Russo, M. Kazerani, J. Jatskevich, K. Strunz, S. Leva, and J. Martinez, "Modeling guidelines and a benchmark for power system simulation studies of three-phase single-stage photovoltaic systems," *IEEE Transactions on Power Delivery*, vol. 26, pp. 1247 –1264, Apr. 2011.

[17] A. Samadi, M. Ghandhari, and L. Söder, "Reactive power dynamic assessment of a PV system in a distribution grid," *Energy Procedia*, vol. 20, pp. 98–107, 2012.

[18] A. Samadi, R. Eriksson, L. Soder, B. Rawn, and J. Boemer, "Coordinated active power-dependent voltage regulation in distribution grids with PV systems," *IEEE Transactions on Power Delivery*, vol. 29, pp. 1454–1464, June 2014.

[19] A. Samadi, E. Shayesteh, R. Eriksson, B. Rawn, and L. Söder, "Multi-objective coordinated droop-based voltage regulation in distribution grids with PV systems," *Renewable Energy*, vol. 71, pp. 315–323, Nov. 2014.

[20] A. Engler and N. Soultanis, "Droop control in LV-grids," in *2005 International Conference on Future Power Systems*, pp. 6 pp. –6, Nov. 2005.

[21] M. Braun, "Reactive power supply by distributed generators," in *2008 IEEE Power and Energy Society General Meeting - Conversion and Delivery of Electrical Energy in the 21st Century*, pp. 1 –8, July 2008.

[22] A. Neto, A. Rodrigues, R. Prada, and M. Da Guia da Silva, "External equivalent for electric power distribution networks with radial topology," *IEEE Transactions on Power Systems*, vol. 23, no. 3, pp. 889–895, 2008.

[23] A. Marvasti, Y. Fu, S. DorMohammadi, and M. Rais-Rohani, "Optimal operation of active distribution grids: A system of systems framework," *IEEE Transactions on Smart Grid*, vol. 5, pp. 1228–1237, May 2014.

[24] O. Nelles, *Nonlinear System Identification: From Classical Approaches to Neural Networks and Fuzzy Models*. Springer, 2001.

[25] F. O. Resende and J. Peas Lopes, "Development of dynamic equivalents for MicroGrids using system identification theory," in *Power Tech, 2007 IEEE Lausanne*, pp. 1033–1038.

[26] S. M. Zali and J. Milanovic, "Modelling of distribution network cell based on grey-box approach," in *7th Mediterranean Conference and Exhibition on Power Generation, Transmission, Distribution and Energy Conversion (MedPower 2010)*, pp. 1–6.

[27] S. Zali and J. Milanovic, "Generic model of active distribution network for large power system stability studies," vol. 28, no. 3, pp. 3126–3133.

[28] J. Milanovic and S. Mat Zali, "Validation of equivalent dynamic model of active distribution network cell," vol. 28, no. 3, pp. 2101–2110.

[29] "Standard load models for power flow and dynamic performance simulation," vol. 10, no. 3, pp. 1302–1313.

[30] H. Renmu, M. Jin, and D. Hill, "Composite load modeling via measurement approach," vol. 21, no. 2, pp. 663–672.

[31] A. Bokhari, A. Alkan, R. Dogan, M. Diaz-Aguilo, F. de Leon, D. Czarkowski, Z. Zabar, L. Birenbaum, A. Noel, and R. Uosef, "Experimental determination of the ZIP coefficients for modern residential, commercial, and industrial loads," *IEEE Transactions on Power Delivery*, vol. 29, pp. 1372–1381, June 2014.

[32] T. Kato, T. Inoue, and Y. Suzuoki, "Impact of large-scale penetration of photovoltaic power generation systems on fluctuation property of electricity load," in *Transmission and Distribution Conference and Exposition, 2010 IEEE PES*, pp. 1–6.

[33] D. Halamay, T. Brekken, A. Simmons, and S. McArthur, "Reserve requirement impacts of large-scale integration of wind, solar, and ocean wave power generation," in *2010 IEEE Power and Energy Society General Meeting*, pp. 1–7.

[34] Warsono, D. King, C. Ozveren, and D. Bradley, "Economic load dispatch optimization of renewable energy in power system using genetic algorithm," in *Power Tech, 2007 IEEE Lausanne*, pp. 2174–2179.

[35] A. Marinopoulos, A. Bouhouras, G. Peltekis, A. Makrygiannis, and D. Labridis, "PV systems penetration and allocation to an urban distribution network: A power loss reduction approach," in *PowerTech, 2009 IEEE Bucharest*, pp. 1–6, June 2009.

[36] A. Ellis, M. Behnke, and C. Barker, "PV system modeling for grid planning studies," in *2011 37th IEEE Photovoltaic Specialists Conference (PVSC)*, pp. 002589–002593, June 2011.

[37] B. Tamimi, C. Canizares, and K. Bhattacharya, "System stability impact of large-scale and distributed solar photovoltaic generation: The case of ontario, canada," vol. 4, no. 3, pp. 680–688.

[38] J. Pillai, P. Thogersen, J. Moller, and B. Bak-Jensen, "Integration of electric vehicles in low voltage danish distribution grids," in *2012 IEEE Power and Energy Society General Meeting*, pp. 1–8, 2012.

For KTH Royal Institute of Technology:
DOCTORAL THESIS IN ELECTRICAL ENGINEERING
TRITA-EE 2014:050
www.kth.se

ISSN 1653-5146
ISBN 978-91-7595-303-8